REMOTE SENSING OF LARCH DISEASE AND ACUTE OAK DECLINE OUTBREAKS IN BRITAIN

Thesis submitted for the degree of

Doctor of Philosophy

at the University of Leicester

by

Chloe Barnes

School of Geography, Geology and Environment

University of Leicester

May, 2018

Abstract

Remote Sensing of Larch Disease and Acute Oak Decline Outbreaks in Britain

Chloe Barnes

In UK forest environments, infection from phytopathogens presents a significant risk to tree health and an increasingly pressing concern for forest management. This thesis has considered *Phytophthora ramorum*, the causal agent of larch disease, and the most recent episode of acute oak decline (AOD) resulting from multiple bacterial agents. The specific focus of the research project concerned the automated isolation of individual tree crowns (ITCs) in forests subject to phytopathogen infection, which facilitated an ITC-scale assessment of tree disease from remotely sensed datasets. The potential applications of airborne laser scanning (ALS) and unmanned aerial vehicle (UAV) based multispectral imagery were assessed in relation to *P. ramorum* and AOD outbreaks respectively. The ITC segmentation results demonstrated the successful isolation of partially and wholly defoliated larch crowns (>70%) from ALS through the application of a pit-free canopy height model generation methodology. However, the photogrammetrically-derived surface elevation from the UAV-based imagery facilitated a poor overall segmentation of individual oak crowns for all severities of crown decline (<30%). The disease detection capabilities of the two remote sensing technologies reported significant results in the case of both studies. The application of ALS for the assessment of *P. ramorum* infection reported significant isolation ($p < 0.01$) of moderate and severely infected individual trees. Larch disease presence/absence and severity was also classified at the ITC-scale with overall accuracies of 72% and 65% respectively. In the application of UAV-based multispectral imagery for AOD assessment, significant differences ($p < 0.10$) were observed between all five categories of crown decline. The crown decline severity classification at the ITC-scale yielded accuracies of 91% and 55% for the three and five severity classes respectively. Overall, the research results demonstrate the capabilities of remote sensing in the targeted assessment of phytopathogens, adding value to both scientific understanding and the management of forest environments.

Acknowledgements

I would firstly like to thank my PhD supervisory team Prof. Heiko Balzter, Dr Kirsten Barrett (University of Leicester), Dr Juan Suárez (Forest Research) and James Eddy (Bluesky) for their continued hard work throughout the entire course of my PhD studies. I am extremely grateful for all the time, energy, knowledge, experience and wisdom you have provided. I also wish to take the opportunity to thank Natural Resources Wales and Geo-4D who have provided significant assistance to the research. More specifically, Sam Milner and James Fleming the representatives from the two respective organisations who have provided prompt responses to my many emails and enquiries. I would also like to thank all my colleagues at the University of Leicester for their friendly and continued support. A special thank you to Charlotte Langley who always has an answer to every question no matter how big or small.

I also owe a huge debt of gratitude to my family, who have provided me with unwavering support, love and guidance, especially my parents Ian and Clare Barnes and my better half Joe Pugsley. Also a special thanks to my fieldwork assistants Clare Barnes, Ian Barnes, Joe Pugsley, Nicholas Williams and Benson Williams for joining and assisting me on soggy days in the forest. You all made spending days surveying trees out in the rain a lot more fun and enjoyable. I would also like to thank Bill Barritt, Emma Pugsley, Roger Pugsley, Andy Williams and Kate Williams for providing a place to stay during all my fieldwork excursions to Wales.

Table of Contents

List of Figures

List of Tables

List of Acronyms and Abbreviations

A1	Highest percentage overlap value for automated crown
A2	Second highest percentage overlap value for automated crown
AI	Aggregation Index
ALS	Airborne Laser Scanning
ANOVA	Analysis of Variance
AOD	Acute Oak Decline
ARI	Anthocyanin Reflectance Index
B[X]	Bicentiles calculated using X% of maximum tree height. (X = 10 to 90)
BI	Birch
BE	Beech
C	Commission error
CART	Classification and Regression Trees
CC	Canopy Cover
CD	Canopy Density
CDZ	Core Disease Zone
CHM	Canopy Height Model
$CHM_{standard}$	Canopy Height Model constructed via the subtraction of the digital terrain model from the digital surface model.
$CHM_{pitfree}$	Canopy Height Model constructed using a pit-free generation methodology
cm	Centimetres
COD	Chronic Oak Decline
CoH	Cut-off Height

COHESION	Patch Cohesion Index
CORE_AM	Core Area (Area Weighted Mean)
DA	Delineation Accuracy
DBH	Diameter Breast Height
DCAD	Disjunct Core Area Density
DIVISION	Landscape Division Index
DLZ	Disease Limitation Zone
DSI	Digital Stereo Imagery
DSM	Digital Surface Model
DTM	Digital Terrain Model
EL	European Larch
ENN_AM	Euclidean Nearest Neighbour (Area Weighted Mean)
GCP	Ground Control Point
GIS	Geographical Information System
GPS	Global Positioning System
GRVI	Green Red Vegetation Index
GNDVI	Green Normalised Difference Vegetation Index
ha	Hectares
HL	Hybrid Larch
Hz	Hertz
IN	Infected
ITC	Individual Tree Crown
JL	Japanese Larch
κ	Kappa value

K	The *K* value represents the number of samples considered for the classification of each feature in the k-nearest neighbour classification
kHz	Kilohertz
km	Kilometres
k-NN	k-Nearest Neighbour
LFD	Lateral Flow Device
LiDAR	Light Detection and Ranging
LM	Local Maxima
LPI	Landscape Patch Index
LQ	Lower Quartile
LSI	Landscape Shape Index
m	Metres
MB	Mixed Broadleaves
MC	Mixed Conifers
Mean_20	The mean value from the brightest 20% of pixels situated within the individual tree crown outline
Mean_80	The mean value from the brightest 80% of pixels situated within the individual tree crown outline
Mean_All	The mean value from all pixels situated within the individual tree crown outline
MLC	Maximum Likelihood Classification
mm	Millimetres
mrad	Milliradians
MTCI	MERIS Terrestrial Chlorophyll Index
m_{try}	In the random forest classification this is the number of input variables at each split in the tree building process

NDVI	Normalised Difference Vegetation Index
NDVI-RE	Normalised Difference Vegetation Index Red Edge
NI	Not Infected
NIR	Near-Infrared
nm	Nanometres
NP	Number of Patches
n_{tree}	Number of trees in the random forest classification
O	Omission error
OA	Overall Accuracy
p value	Calculated probability
P05	Fifth Percentile
P20	Twentieth Percentile
PD	Patch Density
PLADJ	Percentage of Like Adjacencies
PPC	Photogrammetric Point Cloud
PRD	Patch Richness Density
PA	Producer's Accuracy
R	Reflectance
R1	Highest percentage overlap value for reference crown
R2	Second highest percentage overlap value for reference crown
RBF	Radial Basis Function
RF	Random Forest
RG	Region Growing
RQ	Research Question

RTK	Real-Time Kinetic
SFIM	Smoothing Filter-Based Intensity Modulation
SHIDI	Shannon's Diversity Index
SIDI	Simpson's Diversity Index
SS	Sitka Spruce
SVM	Support Vector Machine
TCA	Total Core Area
TIN	Triangulated Irregular Network
μm	Micrometre
VI	Vegetation Index
UA	User's Accuracy
UAV	Unmanned Aerial Vehicle
UK	United Kingdom
UQ	Upper Quartile
WGWE	Welsh Government Woodland Estate
WICS	Window Independent Context Segmentation
WS	Watershed

Chapter 1: Introduction

1.1 Research Context

Phytopathogens are defined as organisms which cause decline and deterioration in plant health and condition (Bigler *et al*., 2006). Anthropogenic activities have increased the threat from both native and exotic phytopathogens in forest environments via climatic change, environmental stress and increased movement of plant material (Brasier, 2008). In the United Kingdom (UK), forestry has experienced several notable introductions of phytopathogens in recent years (Brasier, 2008; Mitchell *et al*., 2014; Baral *et al*., 2014). These have included the introduction of *Phytophthora ramorum* (larch disease) (Lane *et al*., 2003), which resulted in significant infections of commercial larch (*Larix* spp.) in forests across Southwest England, South Wales and Southwest Scotland (Brasier and Webber, 2010; Harris and Webber, 2016). In addition, mature native oak species (*Quercus* spp.) have been affected by rapid deterioration and mortality as a result of the latest acute oak decline (AOD) outbreak (Denman and Webber, 2009; Denman *et al*., 2010) caused by bacterial pathogens including *Gibbsiella quercinecans* and *Brenneria goodwinii* (Brady *et al*., 2010; Denman *et al*., 2012; Brady *et al*., 2016; Denman *et al*., 2016). The geographic areas of greatest concern with regard to AOD extend across southern and midland England and into Wales (Denman and Webber, 2009). Both larch disease (*P. ramorum*) and AOD present major challenges for forest and woodland management in the UK, with additional difficulties resulting from the complexities and uncertainties surrounding the specific phytopathogen-host interactions (Brasier and Webber, 2010; Denman *et al*., 2010; Denman *et al*., 2016; Harris and Webber, 2016).

The monitoring of forest environments is a key strategic activity for the management of phytopathogens and insect pests (Sturrock *et al*., 2011). Landscape level monitoring of areas susceptible to known phytopathogens is traditionally conducted manually via sketch maps during aerial surveys (Leckie *et al*., 2005). This approach is currently employed for *P. ramorum* monitoring in England, Wales, Scotland and Northern Ireland (Medcalf *et al*., 2011; National Assembly for Wales, 2016). However, such surveys are labour intensive (Coops *et al*., 2003) and subject to a range of limitations including reliance on human judgement and interpretation (Leckie *et al*., 2005), coarse spatial scales and low positional accuracies (Foster *et al*., 2017). Informed data regarding the spatial extent and

severity of phytopathogen infections is paramount for the management, planning and modelling of disease outbreaks in forest environments (Hall *et al*., 2016).

Remote sensing technologies present a standardised and objective approach to the assessment and characterisation of forest health (Reid *et al.*, 2016). Passive and active sensors have previously been documented to successfully assess vegetation condition and decline across a variety of platforms including satellite, aircraft, and unmanned aerial vehicles (UAVs), providing datasets across a range of spatial scales (Vastaranta *et al*., 2013a; Lehmann *et al*., 2015; Näsi *et al*., 2015; Wang *et al*., 2015; Michez *et al*., 2016). Spectral and structural changes in vegetation following phytopathogen infection can be identified from remote sensors (Blackburn, 2007; Stone *et al*., 2008; Coops *et al*., 2009; Kwak *et al*., 2010). Metrics and indices derived from airborne laser scanning (ALS) and optical imagery respectively, have previously been applied in the detection and severity categorisation of insect pests and phytopathogens in a range of vegetated environments (Vastaranta *et al*., 2013a; Lehmann *et al*., 2015; Näsi *et al*., 2015). However, due to the specificity of phytopathogen-host interactions and symptom expression, data collection and analysis is required to determine relationships between remotely sensed values and a particular phytopathogen infection in a certain host species (Lovett *et al*., 2006; Barry *et al*., 2008; Mahlein *et al*., 2010).

High-resolution datasets associated with airborne and UAV platforms facilitate the assessment of forest characteristics and condition at the individual tree crown (ITC) scale (Reid *et al*., 2016; Shendryk *et al*., 2016). Fine scale segmentations can be utilised to group tree crowns or crown sections for analysis, based on the presence of homogenous characteristics within the dataset (Ke *et al*., 2010), alternatively, established segmentation algorithms can be applied to surface elevation inputs to automatically delineate ITC boundaries (Wang *et al*., 2004; Chen *et al*., 2006; Nevalainen *et al*., 2017). This crown-based approach combined with high levels of geographic precision presents a range of advantages for disease management and phytosanitary interventions including the isolation of initial infections (Wulder *et al*., 2006; Wulder *et al*., 2012), targeted assessment of susceptible tree species (Stone and Coops, 2004; Michez *et al*., 2016), identification of disease resistant individuals (Sniezko, 2006) and the study of heterogeneous patterns of infection across forest landscapes (Stone and Coops, 2004). Nevertheless, the automated segmentation of ITCs subject to decline can be complicated

due to the increased structural variability of diseased tree crowns (Holdenrieder *et al*., 2004; Larsen *et al*., 2011; Näsi *et al*., 2015; Barnes *et al*., 2017b).

In order to consider the practical applications of high resolution remote sensing for the assessment of *P. ramorum* and AOD in ITCs across forest landscapes, several key gaps in the scientific literature must firstly be addressed. For example, fundamental questions concerning the performance of established methodologies for the segmentation of diseased tree crowns in coniferous plantation and deciduous woodland environments require consideration. In addition, relationships between remotely sensed metrics and the deterioration of individual larch and oak tree crowns affected by *P. ramorum* and AOD respectively, must also be established and quantified. To provide a scientific and methodological approach to address these research questions, this thesis has considered the performance of two different remote sensing platforms and sensors in two contrasting forest environments. In the case of *P. ramorum* and larch disease, the performance and potential contributions of ALS for the isolation and disease assessment of ITCs was tested in the context of a coniferous plantation environment. In relation to AOD, the application of UAV-based multispectral imagery was considered for the identification of ITCs, in addition to the discrimination and classification of crown decline severity categories in an oak-dominated mature woodland. Overall, the results from the research project provide an array of data and conclusions for more informed decision making regarding the applications of remote sensing in the management of phytopathogens in UK forests.

1.2 Thesis Structure

The overall structure of the thesis can be considered in three main sections (Figure 1.1). The first three chapters of the thesis provide an introduction to the research themes, outline the principal research questions, present an in-depth review of the current state of scientific knowledge in the field of study and provide geographical context regarding the selected study areas. The second section of the thesis, which presents the methods, results, analyses and initial discussions can be considered in two main work-streams. Chapters 4 and 5 consider the application of ALS in *P. ramorum* infected larch stands. In particular, Chapter 4 presents the research regarding the automated isolation of ITCs, whilst Chapter 5 utilises these results to conduct disease assessments at the ITC-scale. The second work-stream continues the themes of the first but considers the application of UAV-based multispectral imagery in an AOD affected woodland. More specifically, Chapter 6

documents the research concerning the identification and segmentation of ITCs, whilst Chapter 7 presents the applications of the UAV multispectral imagery for the assessment of crown decline associated with AOD at the ITC-scale. The final section of the thesis

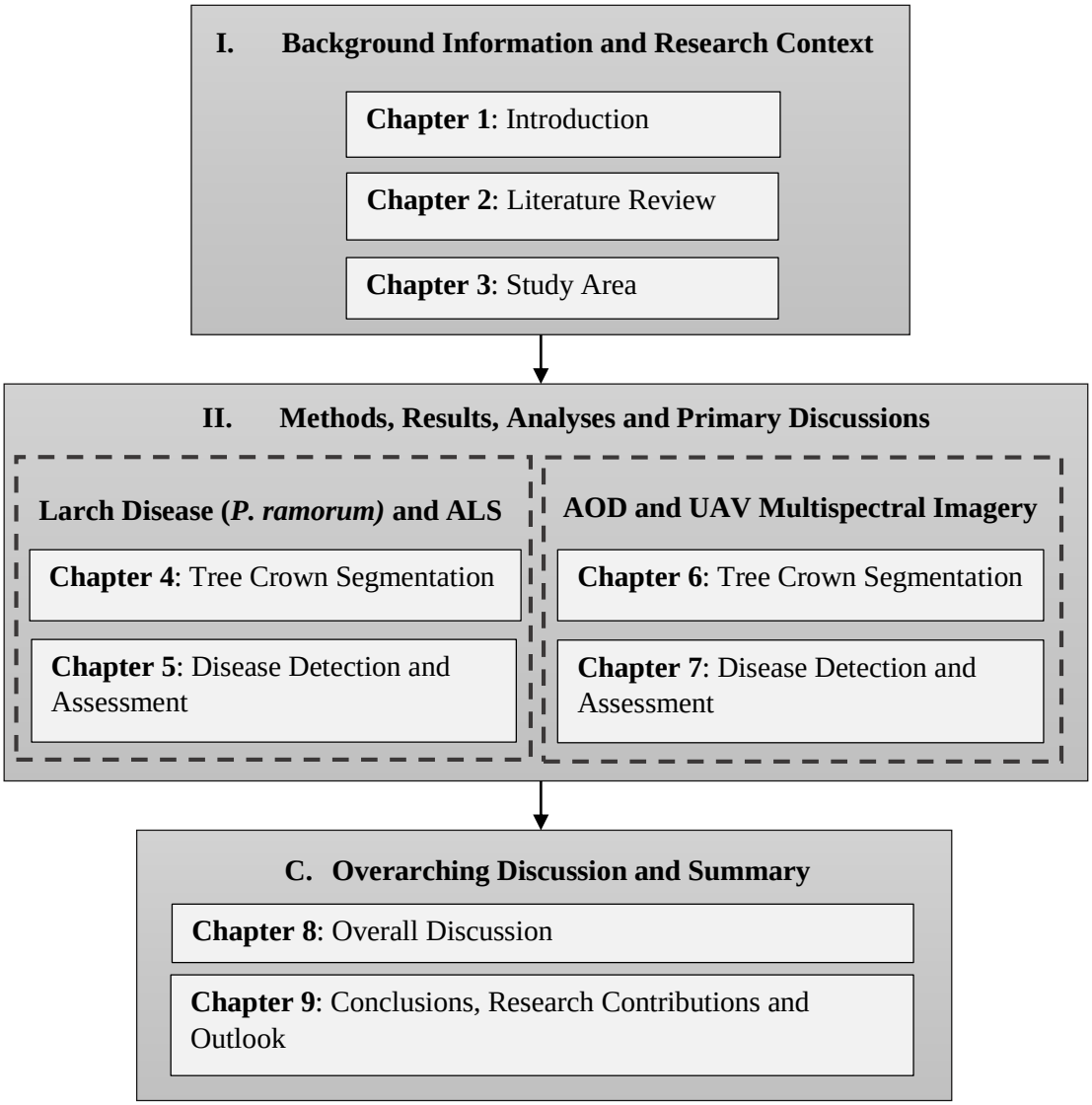

Figure 1.1 – Structure of thesis chapters.

comprising of Chapters 8 and 9 provides a synopsis of the research and considers the context of the research outcomes for the application of remote sensing in the assessment and management of phytopathogens in forestry.

1.3 Research Questions and Objectives

In relation to the key themes of the research outlined earlier in the chapter (Section 1.1) and the research gaps identified in Chapter 2 (Section 2.4.2), a series of research

questions (RQs) were constructed to be addressed within the thesis to fulfil the overarching science question (SQ) of the research:

SQ: How can high resolution remotely sensed datasets be applied to the detection and assessment of phytopathogens in UK forests?

Chapters 4 to 7 present the methods, results and analyses for the research conducted and each is associated with a particular selection of related research questions. Chapter 4 concerns the segmentation of individual larch tree crowns infected with *P. ramorum* from ALS-derived canopy height models (CHMs). This research addresses a key research gap with regard to the isolation of partially (> 20% defoliation) and wholly defoliated ITCs in diseased forest environments. In addition, the chapter also considers the application of a novel automated method for the assessment of ITC segmentation accuracy. The specific emphasis of the chapter concerns the influence of segmentation method, CHM resolution and data pit removal on the overall ITC delineation success in larch stands subject to varying severities of *P. ramorum* infection. In particular Chapter 4 address the following research questions:

RQ1: *How does the removal of data pits during canopy height model generation influence the segmentation of individual tree crowns in P. ramorum infected plantation larch stands?*

RQ2: *What is the influence of canopy height model pixel size on the performance of individual tree crown segmentation in P. ramorum infected plantation larch stands?*

RQ3: *How do the marker-controlled watershed and region growing algorithms compare for individual tree crown segmentation in P. ramorum infected plantation larch stands?*

Applying the findings from Chapter 4, Chapter 5 considers the application of ALS datasets for the assessment and detection of *P. ramorum* infection in individual larch crowns. In particular, the chapter addresses the application of height-based metrics derived from ALS point clouds and fragmentation metrics derived from CHMs for the assessment of disease presence and severity at the ITC-scale. This research addresses vital gaps within the current extent of scientific research concerning the application of ALS point cloud metrics for the assessment of phytopathogens in forestry. In addition, the

research also presents the novel application of landscape fragmentation metrics, from the field of ecology, to quantify the patchiness of CHMs for ITCs subject to defoliation. The key research questions addressed in Chapter 5 include:

RQ4: *Does tree height influence the airborne laser scanning point cloud height value metrics and canopy height model fragmentation metrics derived from healthy trees in plantation larch forest?*

RQ5: *Can airborne laser scanning point cloud height value metrics and canopy height model fragmentation metrics extracted from individual larch tree crowns discriminate between four P. ramorum disease severity categories?*

RQ6: *Can automated individual larch tree crowns be correctly classified into disease presence and severity categories using airborne laser scanning point cloud height value metrics and canopy height model fragmentation metrics?*

In comparison to the previous two chapters, Chapters 6 and 7 concern a different remote sensing approach and another series of bacterial phytopathogens in a contrasting forest environment. More specifically, the focus of these two chapters concerns the application of multispectral imagery acquired via UAV for the assessment of AOD in a mature oak-dominated woodland. Chapter 6 presents the research relating to the segmentation of individual oak trees subject to varying severities of crown decline as a result of AOD. The analysis conducted in the chapter aims to provide an improved understanding of the overall performance of photogrammetrically-derived DSMs from UAV imagery for the detection of treetops and the isolation of ITCs in a heterogeneous deciduous forest affected by AOD. In particular, the chapter considers the influence of treetop extraction method and DSM pixel size on the identification and segmentation of oak trees across five stages of crown decline. The specific research questions addressed in this chapter include:

RQ7: *Can photogrammetry-derived digital surface models acquired via unmanned aerial vehicle be applied to the successful identification of treetops and crown boundaries in oak trees at five stages of crown decline?*

RQ8: *How do the local maxima and contour methods of treetop extraction compare in a mature oak-dominated deciduous woodland affected by acute oak decline?*

RQ9: *What is the influence of photogrammetry-derived digital surface model pixel size on the performance of treetop detection and individual tree crown segmentation in a mature oak-dominated woodland affected by acute oak decline?*

The final research questions addressed in Chapter 7 concern the application of UAV-based multispectral imagery for the assessment of crown decline associated with AOD in a mature oak-dominated woodland environment. In particular, the chapter considers the application of six vegetation indices (VIs) (NDVI, NDVI-RE, GRVI, GNDVI, MTCI, ARI), utilising bands across the visible and near-infrared (NIR) regions of the electromagnetic spectrum, to discriminate at the ITC-scale between five categories of crown decline severity. In addition, the chapter also considers the method of VI extraction from ITCs and its influence on the discrimination of five crown decline severity categories. The three methods tested include the mean of all values in ITCs (Mean_All), mean of the brightest 80% of pixels in ITCs (Mean_80) and mean of the brightest 20% of pixels in ITCs (Mean_20). The chapter addresses several research gaps with regard to the assessment of AOD from UAVs and the influence of VI extraction method on the application of very high resolution multispectral imagery for the assessment of tree crown decline. The specific research questions addressed by this chapter include:

RQ10: *Can the mean NDVI, NDVI-RE, GRVI, GNDVI, MTCI and ARI values extracted from individual oak crowns discriminate between five crown decline severity categories in a mature oak-dominated woodland affected by acute oak decline?*

RQ11: *Does the calculation of mean vegetation indices from all pixels, the brightest 80% of pixels and the brightest 20% of pixels in individual tree crowns influence the discrimination of five crown decline severity categories in oak tree crowns affected by acute oak decline?*

RQ12: *Can oak trees be correctly classified into three and five crown decline severity categories using vegetation indices extracted from unmanned aerial vehicle-based multispectral imagery?*

Chapter 2: Literature Review

This chapter presents some of the key challenges for the assessment and management of phytopathogens in forest environments, with a particular focus on the UK. In addition, the content of the chapter also addresses the fundamental concepts concerning the acquisition and processing of remotely sensed data for the evaluation of vegetation health. Previous research concerning the application of remote sensing for the assessment of diseased and or stressed vegetation will also be considered, drawing on examples from the fields of forestry and agronomy. The chapter will also highlight ideas and findings from the current scientific literature and identify the challenges and knowledge gaps within the field that require further research.

2.1 Forest Environments and Phytopathogens

2.1.1 Introduction

Forests provide a vital function in the earth's biogeochemical systems, supporting a range of terrestrial biodiversity (Sturrock *et al*., 2011). Within forest environments, pathogens such as fungi, oomycetes, bacteria, viruses, nematodes and parasitic higher plants, are considered an integral component of the ecosystem (Hansen and Goheen, 2000; Winder and Shamoun, 2006). When situated within their native ranges, pathogens present minimal risk to natural ecosystems, unless vegetation is subject extreme environmental stress or disturbance (Hansen and Goheen, 2000; Hyun and Choi, 2014; Cobb and Metz, 2017). In contrast, pathogens introduced into exotic environments often pose a significant risk to plant health, due to the absence of natural resistance in host species (Brasier, 2008).

The term phytopathogen is used to describe an organism, which causes decline and deterioration in plant health and condition (Bigler *et al*., 2006). Anthropogenic activities have increased the threat from both native and exotic phytopathogens via climatic change and increased movement of plant material (Brasier, 2008). The biosecurity threat posed by invasive phytopathogens to native plants and trees has caused international concerns with regard to the health of terrestrial ecosystems (Potter *et al*., 2011). In addition to the threats posed by phytopathogens, forest environments can also be subject to mortality and dieback events as a result of insect pests, with defoliators and

borers typically resulting in the greatest damages (Boyd *et al*., 2013). In many instances, the decline in tree health incurred subsequent to infection from phytopathogens, increases the likelihood of colonisation by opportunistic insect pests (Bigler *et al*., 2006; Boyd *et al*., 2013). Forest environments often sustain the most significant losses when the dominant tree species is also the primary host of the introduced phytopathogen or insect pest (Loo, 2009). The nature of damage in these environments is also dependent upon the symptoms presented by affected vegetation and virulence of the infection (Lovett *et al*., 2006). Nevertheless, many phytopathogens have previously caused high levels of tree mortality and significant changes to forest function and structure (Needham *et al*., 2016), resulting in enduring socio-economic and environmental consequences (Liebhold *et al*., 1995; Condeso and Meentemeyer, 2007; Sheremet *et al*., 2017).

2.1.2 Phytopathogens in the Context of UK Forestry

UK forestry has experienced several notable introductions of phytopathogens in recent years including *Phytophthora alni* (alder dieback), *Phytophthora ramorum* (larch disease), *Pseudomonas syringae* (horse chestnut bleeding canker) (Brasier, 2008) and *Hymenoscyphus fraxineus* (ash dieback) (Mitchell *et al*., 2014; Baral *et al*., 2014). Table 2.1 highlights the potential threats of these introduced phytopathogens to UK forestry based on the DEFRA assessment of the UK Plant Health Risk Register (DEFRA, 2016). Across the board for all sectors (agriculture, horticulture and forestry) no significant variation in the rate or frequency of phytopathogen introductions into the UK was observed in the period between 1970 and 2004, despite notable increases in plant imports. This may be as the result of the improved health of plant imports and enhanced biosecurity at borders (Jones and Baker, 2007). Nevertheless, with minimal research regarding the trends of phytopathogen introductions, there is insufficient evidence to evaluate a causal relationship between increased trade of plants and plant products and elevated levels of introduction events (Waage and Mumford, 2008; MacLeod *et al*., 2010). Despite this, the expanding global trade of plants and plant products still poses the greatest threat to the biosecurity of native UK forests and woodlands (Sutherland *et al*., 2008; Potter *et al*., 2011).

Table 2.1 – A selection of phytopathogens threatening UK forestry and the risks posed based on the DEFRA assessment for the UK Plant Health Risk Register (DEFRA, 2016).

Phytopathogen	Major Tree Host	Likelihood*		Impact*		Value of Host*	Relative Risk Rating[$]	
		U	M	U	M		U	M
Phytophthora alni	Alder spp. (*Alnus*)	4	4	4	4	3	48	48
Phytophthora ramorum	Larch spp. (*Larix*)	5	4	5	4	5	125	80
Pseudomonas syringae	Horse Chestnut (*Aesculus hippocastanum*)	5	5	4	4	2	40	40
Hymenoscyphus fraxineus	Ash (*Fraxinus excelsior*)	4	4	5	4	5	100	80

*Scored between 1 (lowest) and 5 (highest). [$]Calculated via the multiplication of likelihood, impact and value of host. Abbreviations: U – unmitigated; M – mitigated.

2.1.3 *Phytophthora ramorum* and Larch Disease

The oomycete *P. ramorum* (Werres *et al*., 2001), considered to have originated from the Asian continent (Ivors *et al*., 2004; Brasier *et al*., 2010), has been recognised as the causal agent of two significant landscape-scale dieback events in exotic forest environments including 'sudden oak death' on the west coast of the USA (Rizzo *et al*., 2002) and larch disease in the UK (Webber *et al*., 2010; Harris and Webber, 2016). Biochemical analysis indicates that the *P. ramorum* populations in North America and Europe are biological distinct (Ivors *et al*., 2006; Van Poucke *et al*., 2012), nevertheless similarities in the phytopathogens behaviour and dispersal mechanisms have been observed. Transmission between hosts primarily results from the dispersal of inoculum in moist conditions, via rainsplash and wind driven rain (Davidson *et al*., 2005; Harris and Webber, 2016).

P. ramorum was first identified in the UK in 2002 on *Rhododendron ponticum* (Lane *et al*., 2003). The establishment of the exotic phytopathogen is thought to have occurred as the result of a single introduction from infected nursery stock imported from within the European Union (Webber, 2008). Following its introduction into the UK, *P. ramorum* was subsequently confirmed to have infected a Southern Red Oak (*Quercus falcata*) in the Southeast of England (Brasier *et al*., 2004). The first indications of the phytopathogens potential implications for larch tree species were acknowledged in 2009,

following multiple reports of *P. ramorum* infections on Japanese larch (*Larix kaempferi*) across Southwest England. Infected individuals presented symptoms including resin bleeds, gingering foliage and defoliation. This represented a major shift in the epidemiological behaviour of *P. ramorum* and marked the beginning of the first landscape-scale disease outbreak from the phytopathogen in commercial conifers (Brasier and Webber, 2010; Harris and Webber, 2016). As of 2013, *P. ramorum* had resulted in the felling of 16, 000 ha of larch across the UK, including Japanese (*Larix kaempferi*), European (*Larix decidua*) and hybrid *(Larix x eurolepis*) species (Forestry Commission, 2014). The significant spread of *P. ramorum* during this period was attributed to the cooler and wetter summer conditions experienced in 2012, which favoured the sporulation and dispersal of the phytopathogen (King *et al*., 2015). In addition, the dense monoculture planting (2,500- 3000 stems per ha) of commercial larch was also acknowledged as a causal factor (Harris and Webber, 2016).

Current distributions of *P. ramorum* in natural and nursery environments extend across all 68 counties in England and Wales (Chadfield and Pautasso, 2012). However, when considered in the context of forest environments the distribution of *P. ramorum* demonstrates a heterogeneous pattern, with infections concentrated in Southwest England, South Wales and Southwest Scotland. The concentration of *P. ramorum* outbreaks in these regions has been primality influenced by the geographical location of susceptible host species (Conyers *et al*., 2011). Additionally, precipitation (mean monthly rainfall) (Chadfield and Pautasso, 2012) and proximity to garden centres and nurseries (Xu *et al*., 2009) have also been significantly correlated with *P. ramorum* distribution. Present approaches employed to monitor the spread of *P. ramorum* at the landscape-scale in the UK are primarily focused on the application of annual surveys conducted manually by tree-health surveyors via helicopter (Medcalf *et al*., 2011). In the context of the spatial extent of forests required for survey, of the 1.54 million ha of productive conifer forest in the UK (Ferris *et al*., 2000), approximately 10% of this is occupied by larch tree species (Brasier and Webber, 2010; Webber *et al*., 2010; Potter and Urquhart, 2017). Due to the deciduous nature of larch species (Gower and Richards, 1990), surveys are conducted in spring following the flush of larch needles. In circumstances whereby *P. ramorum* is suspected, infections are confirmed through a combination of visual inspections in addition to field and laboratory based testing **(**Tracy, 2009). Following the verification of a positive *P. ramorum* infection, a statutory plant health notice is issued under the Plant

Heath Order 2004 (Statutory Instrument 2004 No 3213), requiring infected stock and a surrounding buffer zone to be felled (Tracy, 2009; Harris and Webber, 2016).

2.1.4 Acute Oak Decline

A series of oak declines have previously been reported in the UK and across Europe over the last century. Despite the widespread occurrence and longevity of declines in oak tree species, causal factors and symptoms presented by affected individuals have varied considerably (Thomas *et al*., 2002; Denman and Webber, 2009). In the UK recurring periods of decline in native oaks including English oak (*Quercus robur*) and Sessile oak (*Quercus petraea*) have been attributed to a range of biotic and abiotic factors such as drought, air quality, high levels of soil nitrogen, root disease and insect defoliation following episodes of mildew. Based on the epidemiological characteristics of oak declines the resulting deterioration can be separated into two broad categories, acute oak decline (AOD) and chronic oak decline (COD). AODs are typically episodic events with rapid appearance over a five- to ten-year period, resulting in high levels of tree mortality before stabilising and tailing off. In contrast, CODs are characterised by a slower progression of symptom development, longer persistence in the environment and lower levels of tree mortality (Denman and Webber, 2009).

In the UK, the latest episode of AOD resulting from bacterial phytopathogens, has caused particular concern as a result of the rapid deterioration and high levels of mortality in affected oak trees (Denman and Webber, 2009; Denman *et al*., 2010). The exact identity of the casual bacteria has been an area of uncertainty, however it is presently understood that AOD has a polymicrobial cause, with bacteria including *Gibbsiella quercinecans* and *Brenneria goodwinii* exhibiting an important role in symptom development (Brady *et al*., 2010; Denman *et al*., 2012; Brady *et al*., 2016; Denman *et al*., 2016). AOD has been documented in native oak species including English oak (*Q. robur*) and Sessile oak (*Q. petraea*) as well as the non-native Turkey Oak (*Quercus cerris*) (Denman *et al*., 2014). AOD affects mature trees, causing the death of infected individuals within as little as 3 years, following the appearance of initial symptoms (Denman and Webber, 2009). The most distinctive symptom associated with AOD is the presence of dark stem bleeds from lesions or vertical cracks between the bark plates. Crown condition also deteriorates as a result of AOD (Brady *et al*., 2010; Denman *et al*., 2010), however the relationship between stem and foliar symptom severities are still unclear (Denman *et*

al., 2014). Stems in the later stages of AOD may also present D-shaped exit holes caused by the opportunistic colonisation by the buprestid beetle *Agrilus biguttatus* (Denman *et al.*, 2010; Brown *et al*., 2015).

At present, the geographic distribution of AOD in the UK extends across southern and midland England and into Wales (Denman and Webber, 2009). As a result of the insufficient scientific evidence regarding the biological causes and spread of AOD, management guidelines offer generic advice reflecting conventional practise for containing phytopathogens and unspecific recommendations for biosecurity. Felling of infected individuals is not currently recommended, unless immediate safety concerns are noted. However, landowners are advised to prevent access to affected trees and minimise contact with stem bleeds to reduce infection transmission (Denman *et al*., 2010).

2.1.5 Management of Phytopathogens in UK Forestry

The contrasts present in the two examples highlighted above (larch disease and AOD) demonstrate the complexities faced when managing the threats posed by phytopathogens to forest and woodland environments in the UK. One of the greatest challenges with regard to preparation for new outbreaks, arises from the fact that many potential invasive phytopathogens are at present unknown to science, as was the case with *P. ramorum* prior to its introduction to the USA (Potter *et al*., 2011) and the bacteria associated with the latest episode of AOD (Denman *et al*., 2016). Resultantly, scientific understanding regarding phytopathogen-host interactions evolves following a new outbreak, via both field observations and laboratory analyses (Potter *et al*., 2011). The example of the AOD outbreak in the UK, illustrates the difficulties in implementing a targeted phytosanitary response when scientific understating is limited (Denman *et al*., 2010).

The monitoring of forest environments is a key strategic activity with regard to the management of exotic phytopathogens and insect pests (Sturrock *et al*., 2011). However, the identification of new infections within the landscape can be problematic given that forests and woodlands account for 13% of total land cover in the UK (Riutta *et al*., 2014). In addition, trees within urban landscapes, which arguable exhibit a greater risk to new phytopathogens due to their proximity to anthropogenic activity, also require monitoring for new infections (Tubby and Webber, 2010). Present approaches employed for the identification of new outbreaks of phytopathogens and insect pests in the UK

typically rely on reports from the general public or landowners (Forestry Commission, 2014), in addition to information captured by an increasingly stretched workforce of tree-heath surveyors and plant pathologists (Jones and Baker, 2007). Landscape level monitoring of areas susceptible to known phytopathogens is traditionally conducted manually via sketch maps and photographs collected during aerial surveys (Leckie *et al*., 2005). This approach is currently employed with regard to *P. ramorum* monitoring in England, Wales, Scotland and Northern Ireland (Medcalf *et al*., 2011; National Assembly for Wales, 2016). Nevertheless, such surveys are labour intensive (Coops *et al*., 2003) and rely on human judgement and interpretation which can be hindered by a range of factors including light conditions, angle of view, topography, surveyor training and experience, fragmentation of landscapes, patterns of defoliation and surveyor fatigue (Leckie *et al*., 2005). In addition, surveys are typically of low positional accuracies and coarse spatial scales (Foster *et al*., 2017). Furthermore, in newly affected areas the establishment of phytopathogens and symptom expression is often below the threshold levels for identification in these landscape-level surveys (Alexander and Lee, 2010; Filipe *et al*., 2012).

Subsequent to the regional escalation of a new phytopathogen or insect pest outbreak in the natural environment, management can become complex with many parties and stakeholders required to provide a collective and coherent response (Potter and Urquhart, 2017). Particular difficulties can arise with regard to the definition of financial and institutional responsibilities (Potter *et al*., 2011). In the case of *P. ramorum*, the Welsh Government recognised the high financial and resource inputs required for total eradication of the phytopathogen. Resultantly the preferred strategy focused on slowing the spread of *P. ramorum* in the disease limitation zone (DLZ) outside of the heavily affected core disease zone (CDZ) centred in South Wales (National Assembly for Wales, 2016). The difficulties implementing and enforcing management strategies for phytopathogens can also be highlighted in the case of *P. ramorum*. For example, in relation to the completion rates of felling on time under Statutory Plant Health Notice (Table 2.2), the private sector fell below the percentages achieved in the public sector (WGWE), especially for the DLZ. Nevertheless, co-operation between stakeholders is essential for successful development of effective management strategies for invasive phytopathogens (Pautasso *et al*., 2012).

Table 2.2 - Completion of felling on time under Statutory Plant Health Notice in Wales up to April 2015 (National Assembly for Wales, 2016).

Ownership	Completed (%)	
	CDZ	DLZ
WGWE	52	85
Private	47	39

Abbreviations: CDZ – Core Disease Zone, DLZ – Disease Limitation Zone, WGWE – Welsh Government Woodland Estate.

Non-native species of plant, insect, bacteria and fungi are estimated to result in a cost of ~ £2billion year^{-1} to the UK economy (Tubby and Webber, 2010). Planning for the future risk posed by exotic phytopathogens and insect pests is an important component of their overall management (Sturrock *et al*., 2011). Whilst efforts should be focused on preventing the introduction of exotic phytopathogens via stricter biosecurity protocols and harsher penalties on biosecurity breaches, the introduction of new phytopathogens is inevitable (Brasier, 2008). Resultantly, future management of phytopathogens in UK forests and woodlands, requires a collaborative approach from all stakeholders (Pautasso *et al*., 2012), utilising technical and organisational innovations to ensure the early detection of new outbreaks and the minimisation of economic and ecological consequences (Lawrence and Labus, 2003; Boyd *et al*., 2013).

2.2 Remote Sensing for Forest Environments

2.2.1 Principles of Remote Sensing

In the broadest sense, the term remote sensing denotes the acquisition of data regarding objects via sensors, which require no direct contact with the specific target or entity (Nutter *et al*., 2010). Remote sensing techniques encompass a range of passive and active sensors mounted on satellite, aircraft and UAV platforms, which have all previously been applied to the assessment and monitoring of vegetation (Huete, 2012). Recent developments in the application of remote sensing for the study of forest environments have facilitated a shift in the emphasis of research from data preparation to the extraction of information (Wulder and Franklin, 2003). Present applications for remote sensing in forest environments cover a vast variety of disciplines including forest inventory development (Ørka *et al*., 2013), conservation monitoring (Nagendra *et al*., 2013), forest ecology (Lefsky *et al*., 2002), fire monitoring (Lentile *et al*., 2006), biomass

estimation (Koch, 2010), and forest health assessment (Lausch *et al*., 2016). The potential capabilities of a particular remotely sensed dataset will be dependent on the sensor and platform used for data collection, in addition to the datasets temporal and spatial resolutions (Turner *et al*., 2003; Lausch *et al*., 2016).

2.2.2 Sensors

Remote sensors can be categorised as passive or active, based on the nature or origin of the radiation measured. Once distinguished in this way, sensors can be further characterised by the wavelength interval of the electromagnetic spectrum detected by the sensor (Turner *et al*., 2003). Passive sensors measure reflected radiation, without the requirement of an emitted pulse from the sensor itself. Optical sensors are the most common example of passive remote sensing, measuring reflected radiation from the earth's surface, across the visible and infrared regions (0.4 – 14 μm) of the electromagnetic spectrum (Turner *et al*., 2003). These sensors have the longest history in the field of remote sensing (Song, 2012) and are the most widely used system for the assessment of terrestrial ecosystems (Dash and Ogutu, 2016). Optical sensors are often distinguished as multispectral or hyperspectral, in reference to the number and bandwidth of individual channels (Goetz, 2009).

In contrast, active sensors emit a pulse of radiation towards a surface and measure the energy reflected back to the sensor (Turner *et al*., 2003). Light detection and ranging (LiDAR) is an active sensor, using pulses of laser light to record the distance between target and sensor. Additional parameters regarding the position and altitude of the sensor, allow the absolute three-dimensional position of the target to be recorded (Lefsky *et al*., 2002). Based on the inherent characteristics of the LiDAR, two broad categories of the system including discrete-return and full-waveform, are currently in operation from the airborne platform. Discrete-return sensors provide vertical information via series of return intervals (up to 5), whilst in comparison, full-waveform LiDAR provides sub-metre vertical profiles via digitized vertical sampling (Lim *et al*., 2003). The three-dimensional nature of remotely sensed datasets derived from LiDAR, facilitates the extraction of structural parameters for forest environments (Popescu *et al*., 2003). Radio detection and ranging (radar) is also another example of an active sensor previously applied to the remote assessment of forests (Boyd and Danson, 2005). In this instance, microwave radiation is emitted from the sensor, with the timing and character of the backscatter received applied in the assessment of forest character and condition (Turner *et al*., 2003).

2.2.3 Platforms

Three main platforms can be considered for the remote sensing of forest environments, these include satellite, aircraft and UAV (Berni *et al*., 2009). Whilst space and airborne mounted sensors can be considered more traditional platforms (Richards and Jia, 2006), recent technical advancements and market-demand have perpetuated the application of UAVs for the collection of remotely sensed data (Colomina and Molina, 2014). In relation to the assessment of forest landscapes, each remote sensing platform presents its own advantages and limitations (Wang *et al*., 2015).

The expansion and development of satellite remote sensing began following the launch of Landsat 1 in 1972 (Schowengerdt, 2007). Subsequently, more than 50 satellites have been launched, contributing to the remote monitoring and assessment of terrestrial ecosystems (Dash and Ogutu, 2016). The global nature of satellite remote sensing facilitates the extraction of information regarding forest areas at regional, national and international scales (Hyyppä *et al*. 2000; Dash and Ogutu, 2016). The repetitive data collection provided by satellites also facilitates the acquisition of datasets with comparatively high temporal resolution (Dash and Ogutu, 2016). The satellite platform for remote sensing at present, offers a range of sensors for monitoring forest landscapes including optical (multispectral and hyperspectral) (Schowengerdt, 2007), LiDAR (ICEsat/GLAS) (Zwally *et al*., 2002) and radar (synthetic aperture radar) (Koch, 2010). The greatest limitation regarding the application of satellite data for the assessment of forest environments concerns the spatial resolution of the acquired datasets (Poona and Ismail, 2013). For example, limitations are incurred when pixels from course resolution optical imagery provide a combined reflectance signature from trees, understorey, leaf litter and bare-earth (Wulder, 1998). Additional limitations associated with satellite remote sensing also concern the modification of reflectance signatures by the atmosphere (Schowengerdt, 2007). For example, cloud cover can be particularly problematic with regard to the optical remote sensing of some regions of the world (Turner *et al*., 2003).

Airborne remote sensing has been employed since the 1940s, in the form of aerial photographs, for the assessment of forests (Carleer and Wolff, 2004). Current airborne sensors encompass a range of active and passive remote sensing (Lefsky *et al*., 2002), with typical spatial resolutions of 0.2 to 2 m and fields of view between 2 and 5 km (Nebiker *et al*., 2008). Whilst airborne sensors typically result in the acquisition of higher

resolution datasets, in comparison to those acquired via satellite, a trade-off in the area of ground covered is resultantly incurred (Wulder *et al*., 2004). Temporal resolution of airborne datasets is achieved by the commission of multiple flights for data acquisition, which can prove expensive for many organisations (Suárez *et al*., 2005). Resultantly, data acquisition costs are one of the greatest limitations associated with airborne remotely sensed data. Additional limitations associated with the platform also include the effects of cloud cover (Suárez *et al*., 2005) and geometric artefacts in datasets due to sensor optics (Wulder *et al*., 2004).

In comparison to space and airborne platforms, UAVs provide a low-cost alternative for the remote assessment of forests and woodlands. The centimetre resolutions associated with UAV datasets, provide the highest spatial resolutions of the three platforms (Di Gennaro *et al*., 2016). These systems can be easily mounted with a variety of spectral sensors including multispectral and hyperspectral cameras, in addition to light-weight LiDAR units (Torresan *et al*., 2016). The very high spatial resolutions associated with optical datasets gathered from UAVs have also facilitated the expansion of photogrammetric point clouds (PPCs) as a means of characterising surface elevation (Michez *et al*., 2016). Furthermore, the low costs associated with data acquisition facilitate the opportunity for affordable repeat surveys, providing high temporal resolutions (Grenzdörffer *et al*., 2008). These particular features make UAVs an attractive platform for the collection of remotely sensed datasets for forest and woodland environments. Nevertheless, the trade-off for very high spatial resolution comes via significant reductions in spatial coverage, with data capture confined to local scales (Lehmann *et al*., 2015). Whilst UAVs have become an increasingly utilised remote sensing platform in environmental science since the late 2000s (Michez *et al*., 2016), the operational application of UAVs in the forestry sector at present is typically experimental (Tang and Shao, 2015; Gambella *et al*., 2016).

In many situations the application of a holistic remote sensing approach, which combines an array of sensors and or platforms is often preferable for the assessment of forest environments (Coops *et al*., 2006; Wang *et al*., 2015). Whilst remote sensing offers a range of sensors and platforms with potential benefits to forestry, the application of these remote sensing resources across the sector requires their operationalisation in forest management (Boyd and Danson, 2005). Traditionally, the forestry sector in the UK has been slow to make operational use of technological development in remote sensing,

largely due to financial costs and lack of specialist staff. Remotely sensed datasets, such as optical imagery and LiDAR, are typically acquired via an airborne platform for applications in the UK forestry sector (Suárez *et al*., 2005).

2.3 Processing Remotely Sensed Data for the Assessment of Phytopathogens in Forestry

This section will consider processing techniques for the utilisation of remotely sensed datasets in the assessment of disease in forest environments, with particular focus on very high resolution optical datasets and ALS. Processing techniques will be reviewed broadly across the discipline of forestry with additional directed emphasis on methodologies for the assessment of forest phytopathogens and insect pests.

2.3.1 Field Data Collection

Prior to the utilisation of remotely sensed datasets for forest assessment, information regarding a series of biophysical forest parameters must firstly be acquired from field surveys (Popescu *et al*., 2003). To determine the relationship between remotely sensed data and insect pest or phytopathogen occurrence in vegetation, ground based quantification of disease presence and severity must first be undertaken for validation to be conducted (Stone and Coops, 2004; Reid *et al*., 2016; Shendryk *et al*., 2016). In some instances, established standard tree health metrics can be used to characterise the degree of damage sustained by diseased vegetation (Reid *et al*., 2016) such as crown vigour (Millers *et al*., 1991), canopy closure (Reid *et al*., 2016) and crown condition classification guides (Schomaker *et al*., 2007; Wang *et al*., 2015). Nevertheless, as a result of the variability in symptom expression following infection from a particular phytopathogen or insect pest in a certain host tree species (Lovett *et al*., 2006), specific metrics or measures of stem and foliage deterioration may also be collected (Brown *et al*., 2016). Due to the subjective nature of visually determined metrics, consistency can be maintained when observations are recorded by the same surveyor (Nutter *et al*., 2010). Locations selected for field-based measurements and observations should also capture the tree health variability of the particular study site (Shendryk *et al*., 2016).

2.3.2 Spectral Reflectance and Vegetation Indices

Optical remotely sensed datasets span the visible and infrared regions of the electromagnetic spectrum (Turner *et al*., 2003). Certain sections or bands of the spectrum

in these regions are of particular use for the assessment of vegetation. The selection of useful reflectance bands for the study of forest environments is informed by a basic understanding of the general spectral reflectance characteristics of vegetation. Figure 2.1 presents the typical spectral reflectance exhibited by a green leaf, highlighting the slight peak in reflectance at 550 nm, in addition to a dominant and rapid rise in reflectance at the red-edge region (690-740nm) (Curran *et al*., 1990; Blackburn, 2007). This red-edge phenomenon is the result of contrasting low and high reflectance in the red and NIR regions of the electromagnetic spectrum, caused by chlorophyll absorption and internal leaf scattering respectively (Nilsson, 1995). As a collective, leaf pigments such as chlorophylls, exert a dominant influence on the wavelengths of light that are absorbed and reflected, particularly in the visible region (Thomas and Gausman, 1977). However, each specific pigment exhibits unique properties of spectral absorption, which manifests into the overall spectral reflectance (Figure 2.2) (Blackburn, 2007). With limited pigment absorption in the NIR, water content within plant leaves exhibits a dominant control on reflectance within this region of the spectrum. Furthermore, the structural composition of plant leaves including hairs, waxes, tissue density and airspaces, also influence the spectral reflectance signature of vegetation (Jones and Vaughan, 2010). Variability in all these influencing factors with regard to genera, species, season and environmental change all result in slight variation in the spectral properties of vegetation (Sims and Gamon, 2002).

As a result of infection by phytopathogens, the biophysical properties of vegetation are altered, influencing spectral characteristics with quantifiable reflectance changes (Blackburn, 2007; Pu *et al*., 2008). When such changes are explicitly understood, they can be exploited for the purpose of disease detection (Stone *et al*., 2008). In some instances, such changes can facilitate the detection of phytopathogens or insect pests prior to the onset of visible symptoms (Carter *et al*., 1996; Pontius *et al*., 2008). In the context of spectral reflectance, knowledge regarding the most sensitive wavelengths to a particular phytopathogen or insect pest in a specified host can inform disease detection via remote sensing (Foster *et al*., 2017). Nevertheless, optical remote sensing in forestry typically involves the assessment of entire canopies rather than individual leaves. As a result, consideration has to be given to the dynamics and characteristics of the entire vegetated environment (Jones and Vaughan, 2010; Waser *et al*., 2014).

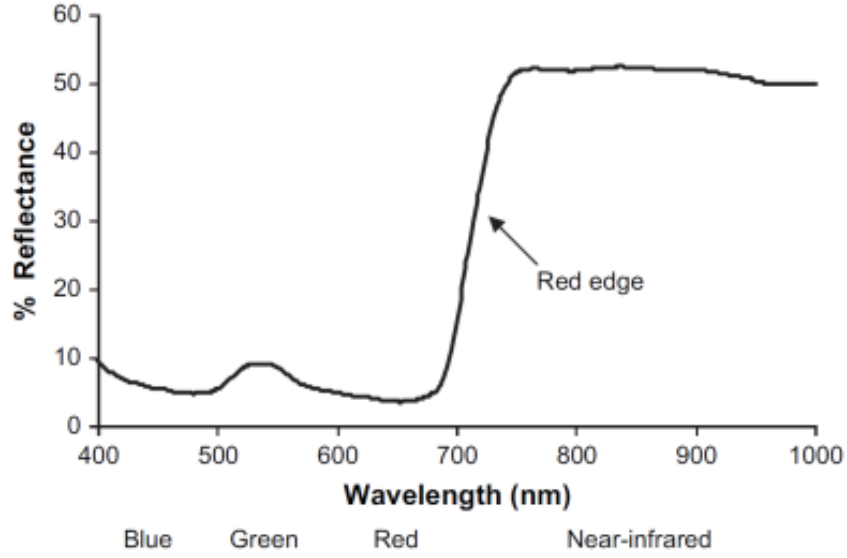

Figure 2.1 – The characteristic reflectance spectrum of a typical green leaf across the visible (400-700nm) and NIR wavelengths (700-1000nm) (Blackburn, 2007).

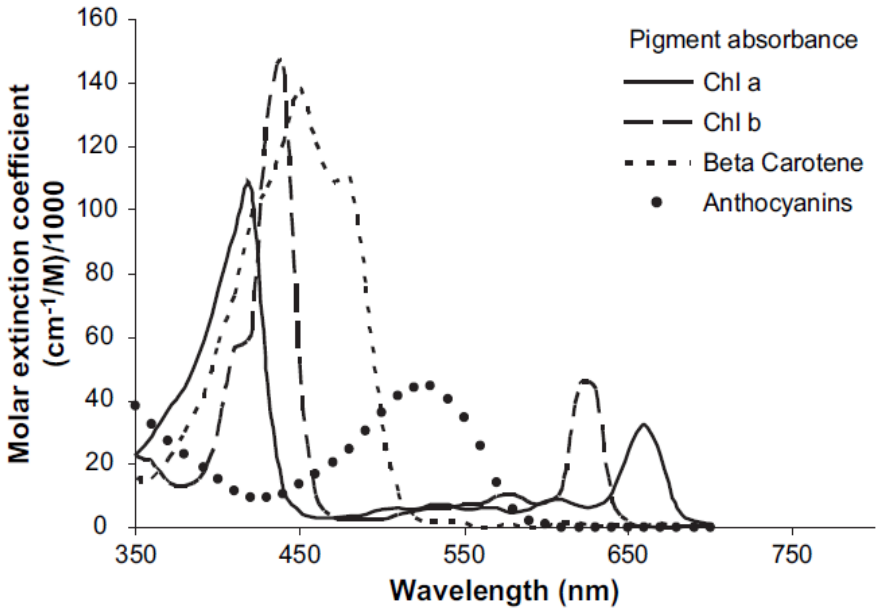

Figure 2.2 – Absorption spectra of the major pigments of plant tissue (Blackburn, 2007).

Vegetation indices (VIs) are often employed in the assessment of vegetation to isolate reflectance bands of interest in optical datasets (Reid *et al.*, 2016). VIs are mathematical combinations of narrow-band optical reflectance (Devadas *et al.*, 2009). The most commonly employed vegetation index (VI) for the assessment of vegetation is the normalised difference vegetation index (NDVI), which utilises the red and NIR wavelengths of the electromagnetic spectrum. In the case of close range optical datasets,

VIs that utilise the visible spectrum have been noted to outperform NDVI for the assessment of plant condition (Nijland *et al*., 2014).

For the assessment of disease, VIs which use wavelengths of reflectance subject to alteration as the result of infection are selected for disease detection (Lévesque and King, 2003). Previous studies have noted the particular sensitivity of wavelengths in the green, red and NIR regions of the electromagnetic spectrum, to infection by phytopathogens and insect pests (Coops *et al*., 2003; Lawrence and Labus, 2003; Leckie *et al*., 2005; Wulder *et al*., 2006). To demonstrate the range of VIs available, Table 2.3 highlights a selection which have previously been applied for disease detection in vegetation. The suitability of a particular VI for the assessment of disease, will be dependent upon a range of factors, principally regarding the specific symptoms expressed by infected vegetation (Barry *et al*., 2008; Mirik *et al*., 2012; Yuan *et al*., 2014). In addition, the availability of specific bands for the calculation of VIs is also a predominant influence in the selection of VIs for the study of phytopathogens and insect pests in vegetated environments. Bandwidth is also of particular importance, with hyperspectral remote sensing providing greater specificity to regions of the electromagnetic spectrum in comparison to more traditional multispectral sensors, which are limited to a smaller number of broader bands (Pu *et al*., 2008; Devadas *et al*., 2009; Adelabu *et al*., 2014).

The extraction of unique spectral signatures at the ITC-scale also requires careful consideration of spectral variability within ITCs, especially in relation to very high resolution optical datasets (Nielsen *et al*., 2014; Lehmann *et al*., 2015). For example, in the case of UAV-based imagery, thousands of pixels can represent one individual tree canopy (Garcia-Ruiz *et al.*, 2013) resulting in serious challenges for the extraction of relevant data and the elimination of noise, such as pixels associated with shadow (Näsi *et al*., 2015). Methodologies employed to minimise the extraction of noise related pixels from tree crowns have previously included the selection of the brightest pixels within ITCs (Näsi *et al*., 2015), the selection of sunlight portions of the canopy (Leckie *et al*., 1992) and a halo approach which ignores the brightest central pixels associated with the treetop (Coops *et al*., 2003). Nevertheless, no methodology has been consistently reported to provide the optimal extraction of spectral information and VIs from ITCs, especially for the assessment of phytopathogens and insect pests in forest environments.

Optical imagery acquired via all remote sensing platforms has previously been applied for forest health assessment (Fraser and Latifovic, 2005; de Beurs and Townsend, 2008; Nielsen *et al*., 2014; Näsi *et al*., 2015; Nainanayake *et al*., 2016; Pasquarella *et al*., 2017), however in the context of this thesis, specific emphasis is placed on data acquired via aircraft and UAVs. By comparison, aircraft demonstrate a longer history in the application of optical remote sensing for phytopathogen and insect pest assessment (Everitt *et al*. 1999; Coops *et al*., 2003) than UAVs (Näsi *et al*., 2015). Nevertheless, both present feasible options for the acquisition of high resolution optical imagery with the selected platform largely influenced by the spatial extent of the study area and available financial resources. Operational applications of optical sensors from these two platforms for the remote assessment of phytopathogens in forestry require consideration of several key factors. Firstly, the date of data acquisition is of particular importance, especially in the case of deciduous tree species. For example in the case of oak trees, early immature leaves exhibit a depressed reflectance in the NIR even when the tree appears green (Liu *et al*., 2006). In addition, phytopathogen-host interactions may also vary seasonally, as a result certain periods of the year will facilitate the optimal spectral distinction between healthy and infected vegetation (Stone and Coops, 2004; Liu *et al*., 2006; Johnson *et al*., 2013). Acknowledgment should also be given to potential complications arising in situations whereby multiple causes of disease and or stress occur within the same landscape (Hatala *et al*., 2010). These variables ultimately require attention prior to and during the acquisition and analysis of optical datasets for the assessment of phytopathogens in forest environments.

Table 2.3 – Vegetation indices previously applied to the assessment of phytopathogens and insect pests in vegetation (* previously applied in forestry).

Index	Equation	Index Reference	Disease Assessment Examples
ARI: Anthocyanin Reflectance Index*	$(1/R_{550}) – (1/R_{700})$	Gitelson *et al*. (2001)	Stress in Eucalypts *(Eucalyptus globulus, E. grandis, E. pilularis*) (Barry *et al*., 2008); Rust infection (*Puccinia striiformis, P. graminis, P. triticina*) in wheat leaves (*Triticum aestivum*) (Devadas *et al*., 2009); Fungal pathogens (*Cercospora beticola, Erysiphe betae, Uromyces betae*) in sugar beet (*Beta vulgaris*) (Mahlein *et al*., 2010).
DVI: Difference Vegetation Index	NIR - Red	Tucker (1979)	Leaf spot (*Cercospora beticola*) in sugar beet (*Beta vulgaris*) (Steddom *et al*., 2003); *Verticilium wilt* in cotton (Chen *et al*., 2011).
ExG: Excess Greenness*	2*Green – (Red + Blue)	Nijland *et al*. (2014)	Tree and plot health metrics in Lodgepole pine (*Pinus contorta*) (Reid *et al*., 2016).
GCC: Green Chromatic Coordinate*	Green/(Red + Blue + Green)	Nijland *et al*. (2014)	Tree and plot health metrics in Lodgepole pine (*Pinus contorta*) (Reid *et al*., 2016).
GNDVI: Green Normalised Difference Vegetation Index*	(NIR – Green)/(NIR + Green)	Gitelson *et al*. (1996)	Russian wheat aphid (*Diuraphis noxia*) damage (Mirik *et al*., 2012); Bark beetle (*Ips typographus*) detection in Norway spruce (*Picea abies*) (Ortiz *et al*., 2013); Disease (*Pseudomonas syringae*) in kiwifruit (*Actinidia* spp.) (Taylor *et al*., 2014).
GRVI: Green-Red Vegetation Index	(Green - Red)/(Green + Red)	Tucker (1979)	Thrips (*Thrips tabaci*) damage in cotton (Ranjitha *et al*., 2014).
GI: Greenness Index	R_{554}/R_{677}	Zarco-Tejada *et al*. (2005)	Yellow rust (*Puccinia striiformis*), powdery mildew (*Blumeria graminis*) and wheat aphid (*Sitobion avenae*) in wheat (Yuan *et al*., 2014).
MTCI: MERIS terrestrial chlorophyll index	(NIR - Red-edge)*(Red-edge - Red)	Dash and Curran (2004)	Disease (*Pseudomonas syringae*) in kiwifruit (*Actinidia* spp.) (Taylor *et al*., 2014).
NDVI: Normalized Difference Vegetation Index*	(NIR – Red)/(NIR + Red)	Rouse *et al*. (1974)	Eurasian woodwasp (*Sirex noctilio*) in pine (*Pinus patula*) (Ismail *et al*., 2007); Bark beetle (*Ips typographus*) detection in Norway spruce (*Picea abies*) (Ortiz *et al*., 2013); Emerald ash borer (*Agrilus planipennis*) in ash trees (*Fraxinus* spp.) (Murfitt *et al*., 2016).
NDVI-RE: Normalized Difference Index Red Edge*	(NIR – Red-edge)/(NIR + Red-edge)	Gitelson and Merzlyak (1994)	Bark beetle (*Ips typographus*) detection in Norway spruce (*Picea abies*) (Ortiz *et al*., 2013); Insect defoliation (mopane worm) in mopane woodland (Adelabu *et al*., 2014); Disease (*Pseudomonas syringae*) in kiwifruit (*Actinidia* spp.) (Taylor *et al*., 2014).
Normalised Red*	R/(R + G + NIR)	Sripada *et al*. (2006)	Health of Black Alder (*Alnus glutinosa*) (Michez *et al*., 2016).
RGI: Red Green Index*	Red/Green	Coops *et al*. (2006)	Stress in Eucalypts *(E. grandis, E. pilularis*) (Barry *et al*., 2008); Spruce beetle (*Dendroctonus rufipennis*) in Engelmann spruce (*Picea engelmannii*) (Foster *et al*., 2017).
SR: Simple Ratio	R_{745}/R_{675}	Birth and McVey (1968)	Laurel wilt (*Raffaelea lauricola*) in avocado trees (*Persea americana*) (Sankaran *et al*., 2012); Hemlock woolly adelgid (*Adelges tsugae*) in Hemlock (*Tsuga* spp.) (Hanavan *et al*., 2015).

2.3.3 Airborne Laser Scanning Point Clouds and Forestry Metrics

ALS produces three-dimensional point clouds, which in the case of discrete return sensors, exhibit the height values of the first and last return laser pulses across the sampling area (Lim *et al*., 2003). These point clouds are typically subject to a height normalisation process, which ensures each point represents the relative height above ground (Khosravipour *et al*., 2014). To extract useful information regarding forest structure from these point clouds, metrics utilising various characteristics of laser returns can be calculated (Kwak *et al*., 2010). Broadly speaking, metrics derived from ALS point cloud height values for the assessment of forest structure can be separated into three overarching categories, these include height-based metrics and percentiles, distributional metrics and cover metrics. Height-based metrics and percentiles summarise patterns regarding the height of ALS returns. Distributional metrics concern the distribution of returns through the canopy profile, whilst cover metrics typically compare two subsets of points to produce a variety of indices (Coops *et al*., 2009; Kantola *et al*., 2010). In order to remove the influence of understorey vegetation, a cut-off height, typically between 1 and 2 m, is applied during the calculation of metrics (Andersen, 2009; Hopkinson *et al*., 2016; Zellweger *et al*., 2016). ALS point cloud metrics from all three categories have previously been applied across a variety of forest environments to establish a range of biophysical parameters including tree height, foliage profiles, canopy structure (Coops *et al*., 2007), canopy health and crown defoliation (Coops *et al*., 2009; Kantola *et al*., 2010).

In diseased trees, defoliation and crown dieback are common symptoms of infections by phytopathogens and insect pests, which result in structural changes to the vegetation (Coops *et al*., 2009). Sensors such as ALS, which provide high resolution information regarding the three-dimensional character of vegetation can be utilised to assess structural changes in forest environments (Kwak *et al*., 2010). In the case of disease detection, metrics derived from ALS point cloud height values to assess defoliation and dieback utilise the theory that laser pulses will increasingly intercept the forest canopy when foliage is lost (Coops *et al*., 2009; Kwak *et al*., 2010; Bright *et al*., 2013). Table 2.4 summarises the metrics derived from ALS point cloud height values that have previously been applied in the assessment of insect pest defoliation in forested environments. However, none of the examples were noted in relation to the assessment of phytopathogens.

Table 2.4 – Metrics derived from ALS point cloud height values previously applied to the assessment of defoliation and decline in forest environments.

Metric	Equation	Disease Assessment Examples
Maximum Height	Maximum height of LiDAR returns from the crown	Green and grey attack phases of mountain pine beetle (*Dendroctonus ponderosae*) in Lodgepole pine (*Pinus contorta*) at individual tree level (Coops *et al*., 2009).
Mean Height	$\bar{x} = \frac{\sum x}{N}$	Green and red attack phases of mountain pine beetle (*Dendroctonus ponderosae*) in Lodgepole pine (*Pinus contorta*) at individual tree level (Coops *et al*., 2009).
Standard Deviation of Height	$\sigma = \sqrt{\frac{1}{N}\,(x_i - u)^2}$	Green and grey attack phases of mountain pine beetle (*Dendroctonus ponderosae*) in Lodgepole pine (*Pinus contorta*) at individual tree level (Coops *et al*., 2009).
Percentiles	Height of the [X]th percentile of total tree height	Common pine sawfly (*Diprion pini*) defoliation in Scots pine (*Pinus sylvestris*) (70th percentile) (Kantola *et al*., 2010).
Bicentiles	Proportion of returns below [X]% of total height	Common pine sawfly (*Diprion pini*) defoliation in Scots pine (*Pinus sylvestris*) at the plot level (B80 and B90) (Vastaranta *et al*., 2013a) and individual tree level (B10, B20, B30, B40, B50, B60) (Kantola *et al*., 2010).
Number of Canopy Returns	Number of returns from the canopy	Red and grey attack phases of mountain pine beetle (*Dendroctonus ponderosae*) in Lodgepole pine (*Pinus contorta*) at individual tree level (Coops *et al*., 2009).
Ground Return Ratio	Ground returns / Total returns	Damage from forest fire (Kwak *et al*., 2010).
Cover	First returns (<2m) / Total returns	Plot scale assessment of mountain pine beetle (*Dendroctonus ponderosae*) in Lodgepole pine (*Pinus contorta*) (Coops *et al*., 2009).
Crown Area	Crown area as a convex hull	Common pine sawfly (*Diprion pini*) defoliation in Scots pine (*Pinus sylvestris*) at the individual tree level (Kantola *et al*., 2010).

A range of challenges and limitations should also be acknowledged with regard to the operational applications of ALS for phytopathogen and insect pest assessment in forestry. For example, structural variations in canopy architecture as a result of stand age, species and composition will all alter the ALS point clouds acquired for healthy tree crowns (Ørka *et al*., 2009). In specific relation to tree height, limited attention in the

scientific literature has at present, concerned the application of metrics derived from ALS point cloud height values for disease detection across a range of stand ages. Additional limitations can also be acknowledged in the case of infections which begin in the mid- to lower-canopy. In these instances, disease detection may be hindered, especially in the case of discrete return ALS, which biases the resulting datasets against foliage located in these regions of the crown (Lovell *et al*., 2003). The identification of dead trees can also be complicated due to the minimal interaction of ALS pulses with dead limbs and stems (Lovell *et al*., 2003). Further difficulties have also been noted in circumstances where dead individuals are located in clusters or underneath leafy canopies (Lee and Lucas, 2007). In addition, the potential impacts of ALS point density should also be considered (Kantola *et al*., 2010). However, Vastaranta *et al*. (2013a) noted little sensitivity to point cloud density with regard to the assessment of the common pine sawfly (*Diprion pini*) and the defoliation of Scots pine (*Pinus sylvestris*).

2.3.4 Canopy Height Models

In the remote assessment of forest environments, ALS point clouds are commonly interpolated to produce two dimensional raster datasets. Products typically generated include digital terrain models (DTMs) and digital surface models (DSMs) calculated using the last and first ALS returns respectively (Jakubowski *et al*., 2013). Subsequently, canopy height models (CHMs) representing the relative height of above-ground vegetation, can be constructed by the subtraction of the DTM from the DSM (Koch *et al*., 2006). The output cell size of ALS-derived raster products is informed by both the point density (points/m^2) and the proposed application of ALS datasets (Khosravipour *et al*., 2014).

CHMs constructed using the DSM minus DTM methodology ($CHM_{standard}$) have been widely applied across forest environments (Van Leeuwen *et al*., 2010; Jakubowski *et al*., 2013). Nevertheless, these products are subject to surface irregularities, often referred to as data pits or holes. The presence of these data pits can present difficulties in the extraction of forest parameters, especially at the ITC-level (Ben-Arie *et al*., 2009; Van Leeuwen *et al*., 2010; Khosravipour *et al*., 2014). Despite the uncertainty surrounding the specific origin of these pits, cited causal factors have been acknowledged during the acquisition and processing of ALS datasets (Ben-Arie *et al*., 2009; Véga and Durrieu, 2011), these include the penetration of laser beams through the canopy, merging of ALS flight lines (Leckie *et al*., 2003), classification of ground and non-ground points (Kraus

and Pfeifer, 1998) and interpolation of point clouds to raster datasets (Axelsson, 1999). Furthermore, in forest environments subject to defoliation and dieback, the more complex canopy structure results in larger elevation irregularities across the canopy surface and an increased presence of data pits in CHMs (Holdenrieder *et al*., 2004; Larsen *et al*., 2011; Barnes *et al*., 2017b). To address the problem of data pits, many studies have used image smoothing techniques such as Gaussian filtering, to remove intra-canopy elevation artefacts (Brandtberg *et al*., 2003; Koch *et al*., 2006; Jing *et al*., 2012). More recent solutions have introduced the use of pit-filling algorithms (Ben-Arie *et al*., 2009; Zhao *et al*., 2013) and the application of pit-free CHM generation methodologies (Khosravipour *et al*., 2014).

Despite the difficulties incurred in CHM feature extraction as a result of data pits, the increased irregularities in surface elevation across ITCs can also be applied for disease detection purposes (Holdenrieder *et al*., 2004; Barnes *et al*., 2017a). As a result of increased penetration of ALS pulses through defoliated canopies, crowns subject to disease typically exhibit a patchy appearance when viewed as CHMs (Holdenrieder *et al*., 2004; Barnes *et al*., 2017a). Whilst ALS point clouds have been successfully applied to disease detection in forest environments (Table 2.4), the value of raster products derived from ALS for the assessment of phytopathogens and insect pests has been poorly addressed in the current scientific literature. One example presented by Vastaranta *et al*. (2012) highlighted the potential applications of bitemporal CHM contrasts to monitor snow-induced damage in pine (*Pinus sylvestris*) dominated forest in Southern Finland. Nevertheless, further research is required to determine the potential contributions of CHM datasets for the assessment of disease at the ITC-scale within forest environments.

2.3.5 Individual Tree Crown Segmentation

Traditional approaches in forest management have adopted a stand (2 – 20 ha) (Reid *et al*., 2016) and plot scale (Coops *et al*., 2006) assessment of forest condition. These methods typically employ a pixel-based approach to the description and mapping of forest health. One benefit of high resolution remotely sensed datasets for the study of forested areas is the isolation of ITCs within the forest canopy. By considering single crowns, as opposed to single pixels, the overall character of each tree canopy can be assessed (Shendryk *et al*., 2016) and the influence of background noise created by understorey vegetation and ground cover minimised (Reid *et al*., 2016). Object-based approaches which define segments of the canopy based on homogenous characteristics in

spectral reflectance or structure can also be employed as opposed to isolated ITCs for fine-scale assessment of crown condition (Ke *et al*., 2010). Nevertheless, an ITC-based approach allows ground based metrics collected for individual trees in the field to be directly analysed in relation to the structural and spectral characteristics of these individuals observed from remote sensing (Barry *et al*., 2008; Wulder *et al*., 2012).

Remotely sensed datasets representing canopy height can be employed as inputs for automated ITC segmentation, which exploits structural differences present between treetops, canopy boundaries and canopy spaces to isolate ITCs (Wang *et al*., 2004; Chen *et al*., 2006). In the application of ALS for ITC segmentation, datasets are typically provided in a raster format as CHMs (Richardson and Moskal, 2011; Hu *et al*., 2014). Nevertheless, methods utilising ALS point clouds have also been developed and successfully applied to the isolation of ITCs (Li *et al*., 2012). In addition, surface elevation derived from very high resolution imagery using photogrammetry techniques has also been utilised for ITC delineation (St-Onge *et al*., 2015). However, these datasets have less commonly been applied than ALS to ITC segmentation (Rahlf *et al*., 2015) and typically provide a poorer characterisation of forest canopies due to the inability of optical sensors to penetrate through the canopy surface (Tanhuanpää *et al*., 2016).

A range of established segmentation algorithms can be applied to the automated delineation of ITCs (Table 2.5) (Wang *et al*., 2004; Chen *et al*., 2006; Bunting and Lucas, 2006). Commonly applied algorithms including the region growing (Erikson, 2003; Tiede *et al*., 2005) and watershed segmentations (Soille, 1999; Chen *et al*., 2006) often require the prior identification of treetops as seed inputs. Treetops are typically located via the detection and filtering of local maxima (Kwak *et al*., 2007; Zhen *et al*., 2014), representing points where neighbouring pixels present equal or lower values in height (Koch *et al*., 2006). Alternative approaches have also applied contouring methods to extract treetops from forest canopies (Koukoulas and Blackburn, 2005). The marker-controlled watershed segmentation applies treetops as nodes from which the inverted input raster of "valleys" is "flooded". The respective boundaries for each tree crown are then delineated by establishing the "watershed" for each individual "valley" (Wang *et al*., 2004). In contrast, the region growing algorithm applies the treetop seed inputs to compare and merge neighbouring pixels until a specified threshold criteria are reached (Tiede *et al*., 2005; Böhner *et al*., 2006; Ke and Quakenbush, 2011). The performance of a particular ITC delineation algorithm is dependent on the characteristics of both tree

canopies and input datasets, and the subsequent suitability of methods for a specific study should be considered (Pouliot *et al*., 2002; Jing *et al*., 2012; Kaartinen *et al*., 2012).

Table 2.5 – The ITC segmentation success rates of previous studies using surface elevation inputs with information about the different data inputs, segmentation algorithms and forest environments.

	Input Dataset	Pixel Size (m)	Segmentation Algorithm	Forest Environment	Success (%)	Reference
ALS	CHM	0.2	Watershed	Savanna woodland	64	Chen *et al*. (2006)
	CHM	N/S	Pouring (similar to watershed)	Douglas fir stand	87	Koch *et al*. (2006)
				Mixed broadleaved forest	50	
	Point Cloud	N/A	Top-to-bottom Region Growing	Mixed conifer forest	86	Li *et al*. (2012)
Optical	CHM	0.2	Watershed	Norway spruce	74	Nasi *et al*. (2015)
	DSI	0.5	Watershed	Pine dominated stand	97	Tanhuanpää *et al*. (2016)
				Spruce dominated stand	89	

Abbreviations: DSI = Digital Stereo Imagery; N/A = Not Applicable; N/S = Not Stated.

The pixel size of the surface elevation input is an important factor with regard to the overall success rates of ITC segmentations (Pouliot *et al*., 2002; Chen *et al*., 2006; Ene *et al*., 2012). In cases where the resolution is too coarse, the ability to distinguish between the boundaries of neighbouring tree crowns can be lost where pixels contain multiple overlapping tree crowns. Conversely, when spatial resolution is too fine, excessive intra-crown height variability may cause an over-segmentation of canopies. Pouliot *et al*. (2002) described the ratio between crown diameter and pixel size in order to address this point, suggesting a lower and upper limit of 3:1 and 9:1 respectively. The optimum ratio will vary with data inputs and in accordance with the sensitivity of segmentation algorithms to intra-crown irregularity and the distinction of crown boundaries, but can provide a useful tool in considering the influence of pixel size on ITC delineation success (Ke and Quakenbush, 2011; Barnes *et al*., 2017b). Nevertheless, the insufficient availability of data regarding the relationship between pixel size and tree crown dimensions makes it difficult to determine specific recommendations for raster input resolution (Ke and Quakenbush, 2011).

In addition to pixel size, the application of smoothing filters can also influence the quantity of intra-crown variation in input datasets (Vauhkonen *et al*., 2012). In the case

of ALS-derived CHMs the application of these filters can also reduce the influence of data pits in tree crown detection (Chapter 2; Section 2.3.4) (Brandtberg *et al*., 2003; Koch *et al*., 2006; Jing *et al*., 2012). Gaussian filtering is frequently applied to provide a smooth input for ITC delineation and reduce over-segmentation (Ke and Quakenbush, 2011; Koch *et al*., 2006). In this instance the degree of smoothing can be largely controlled by the specified kernel size (Dralle and Rudemo, 1996; Chen *et al*., 2006). Previous studies have informed Gaussian filter size using the dimensions of the smallest crown in the canopy of interest (Chen *et al*., 2006). The final smoothing of the raster input is also altered by the number of Gaussian runs employed (Solberg *et al*., 2006).

Forest structure is an important influencing factor for the success of ITC segmentation (Vauhkonen *et al*., 2012). A large number of ITC delineation studies have focused on the isolation of individuals in homogenous coniferous plantation forest (Ke and Quakenbush, 2011; Richardson and Moskal, 2011). These environments are more favourable to ITC segmentation as a result of the conical shape of conifers and the regularity of planting and tree spacing (Ke and Quakenbush, 2011), especially when stands consist of single species. Fewer studies have considered the application of ITC segmentation in heterogeneous forest environments, especially those comprised of deciduous broadleaved tree species (Richardson and Moskal, 2011). ITC segmentation in these environments is complicated by a number of factors. Firstly, midstorey layers within the canopy shaded by dominant tree crowns may go undetected (van Leeuwen and Nieuwenhuis, 2010; Richardson and Moskal, 2011). In addition, the more complex nature of the canopy surface makes the identification of a single treetop or peak for each individual more difficult (Lucas and Lee, 2007; Richardson and Moskal, 2011). Table 2.5 provides an overview of some of forest types previously considered for ITC segmentation. Those applied in deciduous broadleaved environments (Koch *et al*., 2006) provided poorer ITC segmentation success rates than those reported in coniferous forests.

The performance of established ITC segmentation methodologies in ALS-derived CHMs for tree crowns subject to varying severities of disease and decline has not been directly or explicitly analysed in the scientific literature. In forests subject to defoliation and dieback as a result of phytopathogens or insect pests, canopy structures are typically more complex and exhibit larger elevation irregularities across the canopy surface (Holdenrieder *et al*., 2004; Larsen *et al*., 2011), causing an increased presence of data pits in ALS-derived CHMs (Barnes *et al*., 2017b). Such characteristics, whilst useful in

disease detection (Coops *et al*., 2009; Bright *et al*., 2013) provide an added complication with regard to the isolation of ITCs for the assessment of crown deterioration. In relation to photogrammetry-derived DSMs and CHMs, minimal research has at present been directed to assess the performance of ITC segmentation approaches in diseased canopies across a range of crown decline severities (Näsi *et al*., 2015). Consequently, the methodologies employed for ITC delineation from surface elevation in canopies affected by disease requires consideration of the increased presence of data pits and height variability across a range of disease severities, in addition to a robust assessment of their implications for segmentation accuracy.

The assessment of segmentation accuracy is also an important stage in the ITC delineation process (Zhen *et al.*, 2016). The rigorous assessment of automated ITC boundaries is essential to highlight the strengths and weaknesses of segmentation approaches in different forest environments and facilitate robust comparisons between previous studies (Chen *et al*., 2006; Richardson and Moskal, 2011), such as those presented in Table 2.5. One approach to accuracy assessment for ITC detection is the reporting of omission and commission errors, which has typically been applied with regard to treetop detection success (Khosravipour *et al*., 2014). Commission errors (C) are reported when multiple treetops are detected for one ITC, whilst omission errors (O) represent instances where no treetop is generated for an ITC. Using both these errors and the total number of tree crowns (*n*) in the study area the overall accuracy (OA) can be calculated (Pouliot *et al*., 2002):

$$\mathrm{OA}\% = ((n - \mathrm{O} + \mathrm{C})/n) * 100$$

However, when ITC segmentations aim to represent the entire tree crown for parameter extraction, such as diameter and area calculations, a simple detection rate does not provide sufficient information regarding the ability of automated polygons to represent actual tree crowns. In these circumstances the assessment of segmentation accuracy is based on the agreement or overlap between automated and manually delineated reference crowns (Koch *et al*., 2006; Fang *et al*., 2016). Previous studies have applied a categorical assessment (Table 2.6) of overlap to establish detailed information about ITC segmentation accuracy. The assignment of these categories has previously been conducted via visual inspection of reference and automated crowns (Leckie *et al*., 2003; Koch *et al*., 2006; Kwak *et al*., 2007; Jing *et al*., 2012; Hu *et al*., 2014; Fang *et al*., 2016).

Nevertheless, to provide a more robust means of establishing the crown delineation accuracy categories the assessment of overlap between reference and automated ITCs requires an approach less open to individual interpretation.

Table 2.6 – Assessment categories for individual tree crown delineation accuracy analysis (Leckie *et al*., 2003; Hu *et al*., 2014; Fang *et al*., 2016).

Categories	Description
Correct delineation	Exact match between reference tree crown and automatically delineated tree crown
Satisfactory delineation	Automatically delineated tree crown corresponds to reference tree but boundaries are slightly larger or smaller (at least 50% overlap)
Merged tree	More than one reference tree crown lies within automatically delineated tree crown
Split	More than one automatically delineated tree crown lies within reference tree crown
Not found	Reference tree crown has no corresponding automatically delineated tree crown or overlap with the automatically delineated tree crown is less than 50%

In the case of operational phytopathological assessments from remotely sensed datasets, the application of an ITC approach presents several advantages for targeting specific locations that require phytosanitary interventions (Leckie *et al*., 2016). For example, in the early stages of the disease establishment in forest stands, the isolation of ITCs that initially succumb to infection can enable a rapid response to phytopathogens and insect pests presenting new risks to forest areas (Wulder *et al*., 2006; Wulder *et al*., 2012). In the study of diseased forest landscapes, ITC-based approaches also facilitate the detailed evaluation of heterogeneous patterns of infection (Stone and Coops, 2004). In addition, the use of ITC delineation techniques alongside species identification (Persson *et al*., 2004; Li *et al*., 2013) can facilitate a targeted assessment of susceptible tree species (Stone *et al*., 2004; Michez *et al*., 2016). This combined approach also presents the potential for the identification of disease resistant individuals, which may prove particularly useful with regard to the breeding of resistant genotypes and the development of resilience in forest stock (Sniezko, 2006). Tree health maps created using an ITC-based approach provide a powerful description of forest canopy condition, difficult to replicate with field-based studies without significant investments in time and resources (Shendryk *et al*., 2016).

2.3.6 Classification for Mapping Phytopathogens in Forest Environments

Utilising the relationships between remotely sensed and ground based metrics, classifications can be undertaken to provide a spatial representation of disease or decline across forest environments (Shendryk *et al*., 2016). In the case of remotely sensed optical images, classification provides a means of summarising and consolidating large complex datasets (Xie *et al*., 2008; Blaschke, 2010) and is commonly applied using one of two distinct approaches. A traditional pixel-based approach considers the characteristics of each image pixel and classifies these individually via a set of pre-defined criteria (Blaschke, 2010). Whilst this method has been commonly applied across the field of remote sensing, increasing critique has mounted in recent decades with regard to the limitations of this approach (Liu *et al*., 2006; Blaschke, 2010). One of the biggest drawbacks, particularly in relation to high resolution datasets, is the speckling or "salt and pepper" effect resulting from small sale intra-class variability between individual pixels (Castillejo-González *et al*., 2009).

In contrast, object-based classifications concern the assessment and categorisation of groups of continuous pixels (Yu *et al*., 2006), where objects possess an intrinsic size and shape, and are defined as basic entities of pixel groups comprised of similar digital values (Hay *et al*., 2001). Objects applied to classification can however span across a variety of spatial scales such as forest plots (Vastaranta *et al*., 2013a), ITCs (Näsi *et al*., 2015) and intra-crown segments (Michez *et al*., 2016). The application of an object-based approach in forestry can aid the reduction of local variation and overcome heterogeneity resulting from shadow, texture and shape (Castillejo-González *et al*., 2009; Heurich *et al*., 2010). Through the application of an ITC segmentation, individual crowns can be employed as objects for disease presence or severity classifications, with the characteristics from the whole crown considered for the assignment of a particular category or class (Immitzer *et al*., 2012; Murfitt *et al*., 2016; Reid *et al*., 2016; Shendryk *et al*., 2016). For phytopathogen and insect pest assessment in forestry an object-based approach to classification is often preferable, especially for high resolution datasets (Table 2.7) (Nielsen *et al*., 2014; Lehmann *et al*., 2015; Michez *et al*., 2016).

A large number of classifiers have been established and documented for the categorisation of vegetation characteristics such as structure, health and species (Melgani and Bruzzone, 2004; McInerney and Nieuwenhuis, 2009; Kantola *et al*., 2010; Rumpf *et al*., 2010; Bright *et al*., 2013; Ortiz *et al*., 2013; Adelabu *et al*., 2014; Murfitt *et al*., 2016).

When remotely sensed datasets have been acquired alongside ground surveys, labelled training datasets are typically established to facilitate the application of supervised classification methods for a particular set of predictor variables (Xie *et al*., 2008). In the case of disease presence and severity assessment in forestry Table 2.7 provides a summary of previous classifications, highlighting the variety in classification approaches and remotely sensed input variables.

Support vector machines (SVMs) are one example of an established supervised classifier (Rumpf *et al*., 2010). The basic principle of SVM, isolates classes by determining an optimal separating hyperplane, which maximises the distance between the hyperplane and the margin (nearest point of both classes). The support vectors represent the samples exhibiting the minimal distance to the hyperplane. The resulting separation is therefore robust to outliers (Vapnik, 1998; Rumpf *et al.,* 2010). In instances where datasets are not linearly separable, kernel functions can be employed. One common kernel applied in SVM is the radial basis function (RBF), which is parametrised using a simple parameter (σ), determining the decision boundary smoothness. An additional parameter (*C*) handles noise and error caused by the expectation that some training and validation samples may be assigned to the wrong class (Rumpf *et al*., 2010). At present, the scientific literature offers minimal guidance regarding the selection of kernel-specific parameters (Petropoulos *et al*., 2012), however, a cross validation grid search of the training dataset can be applied to optimise the σ and *C* input parameters (Hsu *et al*., 2003).

The k-Nearest Neighbour (k-NN) is a non-parametric pattern recognition classifier (Collins *et al*., 2004; Melgani and Bruzzone, 2004) underpinned by the principle that instances within a dataset are typically located in close proximity to other instances that have similar properties (Cover and Hart, 1967; Kotsiantis, 2007). Using this theory, k-NN identifies the *K* nearest samples to the query and assigns the category based on the most frequent class label (Kotsiantis, 2007). The selection of the number of neighbours (*K*) can be optimised prior to classification via experimental selection and preliminary testing (Collins *et al*., 2004) or using the training dataset to apply a cross validated grid search (Melgani and Bruzzone, 2004; Hsu *et al*., 2003). The overall performance of the k-NN can be highly dependable on the selection of the *K* variable and training data with overlapping classes may not be suitable for this type of classification (Samaniego *et al*., 2008).

The random forest (RF) classification method (Breiman, 2001), is a non-parametric classification approach which generates a series of classification and regression trees (CART). Each tree is generated using a bootstrapped set of training samples, with the split at each regression tree governed by a randomised subset of input variables for each node (Hudak *et al*., 2008; Oliveira *et al*., 2012). The final classification result is subsequently determined based of the highest mean probability estimate across all trees (Belgiu and Drăguţ, 2016). Two important input parameters for the RF classification include the number of regression trees (n_{tree}) and the number of input variables at each split in the tree building process (m_{try}). In relation to tree species classification, Immitzer *et al*. (2012) noted that overall classification accuracy increased for increasing n_{tree} values until a plateau was reached at a value of 250. In the case of m_{try}, Immitzer *et al*. (2012) also reported better classification accuracies for 1 or 2 variables per node compared to 3, 4, or 5 variables. The relative insensitivity of RF to small samples sizes or "Hughes effect" merits the selection of the classifier in instances where the number of training samples per class is limited (Immitzer *et al*., 2012).

All of the established classifiers previously employed across the field of remote sensing each present a series of advantages and limitations. In many cases, suitability is largely dependent on input data characteristics such as the quantity of training data and class separability (Huang *et al*., 2002; Samaniego *et al*., 2008; Immitzer *et al*., 2012). The selection of an appropriate classifier for a particular dataset is important as the application of different methods can yield significantly different classification results (Ortiz *et al*., 2013). To review the performance of selected classifiers, overall accuracy percentage (OA) and Cohen's κ coefficient (Cohen, 1960) can be calculated. For a more detailed overview, a confusion matrix in addition to user's (UA) and producer's accuracies (PA) for individual classes can also be computed and analysed (Congalton and Green, 1999).

The selection of disease severity category boundaries is also particularly important for the classification of infection severity (Coops *et al*., 2003). For instance, classifications which make a simple distinction between living and dead trees typically exhibit higher overall accuracies (Garrity *et al*., 2013; Fassnacht *et al*., 2014), than those which distinguish between multiple disease severity categories (Kelly and Liu, 2004; Waser *et al*., 2014) (Table 2.7). The specified category boundaries, range of severities within categories and distinction between categories can all influence classification performance (Coops *et al*., 2003; Waser *et al*., 2014). For example, previous studies have

noted difficulties in the differentiation between classes across the spectrum of moderate disease severity for forest insect pests using VI input variables (Coops *et al.*, 2003; Leckie *et al*., 2005). Further complications have also been documented with regard to the separation of healthy trees and those in the early stages of infection progression (Bater *et al*., 2010; Kantola *et al*., 2010). As a result, the selection of disease severity categories should consider the potential discrimination capabilities of remotely sensed input variables and the operational requirements of data regarding disease occurrence and severity.

Routine assessment of phytopathogen and insect pest outbreaks across large areas continues to remain a challenge for forest management (Bater *et al*., 2010). Whilst remote sensing can be applied to assess the symptomatic expression of infection by a phytopathogen or insect pest, the technology at present has limited capability to differentiate or determine the exact cause of decline in crown condition (Liu *et al*., 2006). Nevertheless, the mapping of deterioration in tree health provides forest managers with information and precise locations to target ground based management practises and testing. The compatibility of remotely sensed mapping products with geographical information systems (GIS) also facilitates the combination of information regarding forest health with existing datasets such as forest inventories. Thus allowing a more informed decision making process and allocation of resources (Lehmann *et al*., 2015).

2.3.7 Remote Sensing for Operational Management of Disease in Forestry

Informed data regarding the spatial extent and severity of phytopathogens is paramount for the management, planning and modelling of disease in forest environments across the globe (Fassnacht *et al*., 2014; Hall *et al*., 2016). Remote sensing approaches present a standardised and objective approach to the assessment and characterisation of forest health across a range of scales (Lausch *et al*., 2016; Reid *et al.,* 2016). Nevertheless, in many instances manual surveys (field and aerial) still dominate in the operational management of phytopathogens and insect pests in the forestry sector (Hall *et al*., 2016; Lausch *et al*., 2017), as is the case with *P. ramorum* and larch disease in the UK (Medcalf *et al*., 2011). Commonly cited reasoning for the limited application of remote sensing for the assessment of forest health and disease has included the perceived insufficient resolution associated with optical data and costs associated with data acquisition and processing (Suárez *et al*., 2005; Rullan-Silva *et al*., 2013; Hall *et al*., 2016).

Table 2.7 – Previous applications of remote sensing for the classification of disease or decline in forest environments.

Classification Approach	Classification Method	No. Classes	Platform	Input Variables	Classification Accuracy (%)	Disease Assessment Example	Reference
Pixel-Based	Gaussian Mixture Model	2	Satellite	Imagery (VIs)	97.9 – 98.5	Tree mortality in piñon-juniper (*Pinus edulis-Juniperus monosperma*) woodlands.	Garrity *et al.* (2013)
Object-Based	SVM	2	Satellite	Imagery (SFIM pansharpened imagery)	96	Japanese pine wilt disease and Japanese oak wilt disease.	Johnson *et al.* (2013)
Object-Based	RF	2	Aircraft	ALS (height percentiles 80 and 90)	84.3	Common pine sawfly (*Diprion pini*) defoliation in Scots pine (*Pinus sylvestris*).	Vastaranta *et al.* (2013a)
Object-Based	WICS	2	Aircraft	Imagery (colour infrared)	88 - 90	Deadwood areas from the spruce bark beetle (*Ips typographus*) in Norway spruce (*Picea abies*).	Nielsen *et al.* (2014)
Object-Based	Multinomial Logistic Regression	4	Satellite	Imagery (bands and VIs)	73	Ash (*Fraxinus excelsior*) dieback caused by *Hymenoscyphus pseudoalbidus*.	Waser *et al.* (2014)
Object-Based	Nearest Neighbour	5	UAV	Imagery (modified NDVI)	82.5 - 85	Oak splendour beetle (*Agrilus biguttatus*) in oak (*Quercus* spp.) trees.	Lehmann *et al.* (2015)
Object-Based	k-NN	2[$] and 3[¥]	UAV	Imagery (NDVI, red-edge, green and red hyperspectral bands)	90[$] and 76[¥]	Spruce bark beetle (*Ips typographus*) in Norway spruce (*Picea abies*).	Näsi *et al.* (2015)
Pixel-Based	MLC	3	Satellite	Imagery (texture)	88 - 96	Health of deciduous *Robinia pseudoacacia* forests.	Wang *et al.* (2015)
Object-Based	RF	2	UAV	Imagery (normalised red)	90.6	Health of Black Alder (*Alnus glutinosa*).	Michez *et al.* (2016)

Abbreviations: k-NN = k Nearest-Neighbour; MLC = Maximum Likelihood Classification; RF = Random Forest; SFIM = Smoothing Filter-based Intensity Modulation; SVM = Support Vector Machine; WICS = Window Independent Context Segmentation

Remote sensing techniques offer the potential to capture symptom expression in vegetation at an earlier stage of disease establishment than manual aircraft surveys. In addition, the operational adoption of early disease detection via remote sensing could also facilitate a shift from reactionary to proactive management of phytopathogens and insect pests in forestry (Reid *et al*., 2016). Furthermore, a remote sensing approach also presents additional advantages such as compatibility with digital forest inventories, automatic processing algorithms and greater consistency between different dates and areas of acquisition (Fassnacht *et al*., 2014). In order to highlight the practical and operational capabilities of remote sensing for effective disease detection and assessment, clear examples of success with reproducible and robust results are required.

2.4 Literature Review Summary

2.4.1 Present Extent of Current Knowledge

The review of the literature presented in this chapter demonstrates at the board scale, the presence of a solid foundation of scientific understanding with regard to the processing and utilisation of remotely sensed datasets for the assessment of disease in forest environments. Numerous examples have demonstrated the capabilities of both active and passive sensors across a variety of platforms for the assessment of tree diseases in particular forest environments, especially with regard to those resulting from insect pests. Nevertheless, due to the complexities and specificity of phytopathogen-host interaction and the range of variables surrounding the acquisition and processing of remotely sensed data, at the smaller scale, specific questions and uncertainties still remain within the scientific literature.

2.4.2 Research Gaps

One key outcome of the literature review concerns the current absence of remote sensing in the operational assessment of phytopathogens in UK forestry. In the case of current *P. ramorum* management, heavy reliance on visual aerial surveys for landscape-level assessment of outbreaks is subject to a number of limitations. Given the previous success of remote sensing for the detection of disease in other coniferous plantation environments, research concerning the particular applications of remote sensing in this case would facilitate a more informed decision making process for future *P. ramorum* management. With regard to AOD, the absence of a designated campaign for disease detection monitoring highlights the potential for remote sensing technologies to be

considered in AOD management. Previous studies presented in the scientific literature can be applied as analogues for this research, however due to the specificity of phytopathogen-host interactions, different types of remotely sensed data require assessment for a particular phytopathogen in a specific forest environment.

In relation to the remote sensing platforms and sensors, several key research gaps were also identified in relation to phytopathogen assessment in forest environments. For example, it was noted that a limited number of studies within the literature had previously considered the application of ALS to assess structural forest change resulting from insect pests, with no reference relating to the use of the technology for phytopathogens. In the case of remote sensing platforms, it was acknowledged that the current use of UAVs in the forestry sector is considered experimental, with limited reference to the applications of this particular platform to phytopathogen assessment. Resultantly, further research would provide a more informed conclusion to the significance of ALS and the UAV platform for the assessment of phytopathogens in forest environments.

With regard to the processing of remotely sensed datasets in preparation for disease assessment, several key areas of uncertainty were noted in relation to the automated segmentation of ITCs. For example, forest areas subject to defoliation and dieback as a result of disease exhibit increased surface elevation irregularities and data pits across the canopy, adding potential complications to the segmentation of ITCs. Present research has yet to directly address this issue in order to suggest appropriate techniques for the application of ALS and photogrammetry-derived DSMs and CHMs in diseased forest stands. In addition, further uncertainties were also acknowledged in relation to the optimal pixel size of raster surface elevation inputs for ITC segmentation, with limited reference or guidance for informed pixel size selection under different forest conditions. It was also noted that only a small number of ITC segmentation studies have previously been conducted in heterogeneous deciduous forests. Research conducted within these environments has also reported limited success, with delineation difficulties typically cited as a result of increased surface elevation variability.

Whilst previous examples from the literature have highlighted the benefits of an ITC-based approach for the assessment of tree disease from optical datasets, uncertainties were acknowledged in relation to minimising the influence of noise-related pixels. For example, several methodologies have previously been referenced and tested, however no

clear or optimal method has at present been determined, especially in relation to very high resolution imagery obtained from UAVs. Resultantly, further research is required to determine the influence of the method applied to spectral information extraction at the ITC-scale on the applications of UAV-based imagery for the assessment of phytopathogens.

A number of research gaps were also noted in relation to the extraction of structural parameters from ALS for the assessment of tree crown condition. For example, the disease detection capabilities of CHMs has not previously been considered in the scientific literature. Whilst the increased variability of surface elevation in CHMs subject to defoliation and decline has been acknowledged, this characteristic has not been tested in relation to the detection or severity discrimination of phytopathogen infection in forest environments. In addition, ALS point cloud metrics have not previously been applied in relation to the assessment of disease resulting from phytopathogen infection. Furthermore, the application of these metrics for disease assessment across a range of stand ages has also been poorly addressed.

Overall, this chapter has highlighted several research gaps within the scientific literature. The specific research questions constructed to address these in relation to *P. ramorum* and AOD in the UK have previously been outlined in Chapter 1, Section 1.3. It is imperative that the research undertaken to address these gaps demonstrates a clear focus on challenging these present uncertainties and provides conclusions in a manner that facilitates an ease of understanding for decision making and adoption in operational forestry management practise.

Chapter 3: Study Areas

This chapter provides an overview of the study areas selected for the research presented in the thesis. The two environments selected for the research concerning larch disease (*P. ramorum*) and AOD exhibit an array of contrasts including size, species composition, planting, and management, providing two juxtaposed examples regarding the applications of remote sensing for phytopathogen assessment in UK forests.

3.1 *P. ramorum* and Larch Disease in Wales

The research concerning *P. ramorum* in larch forest stands was conducted in Wales, UK. The two selected study areas were situated at Ogmore Forest in South Wales (51.5954°N, -3.5320°W) and Radnor Forest in Mid Wales (52.2708°N, -3.1503°W) (Figure 3.1), both managed by Natural Resources Wales. Ogmore Forest is situated within the core *P. ramorum* disease zone in Wales and has been subject to the infection since 2011 (Figure 3.2). Due to the spread of the *P. ramorum* across the Ogmore site, a second site, Radnor Forest, comprising of healthy larch stands was also selected outside of the core *P. ramorum* disease zone. Figure 3.3 provides an overview of landscape at the two study sites.

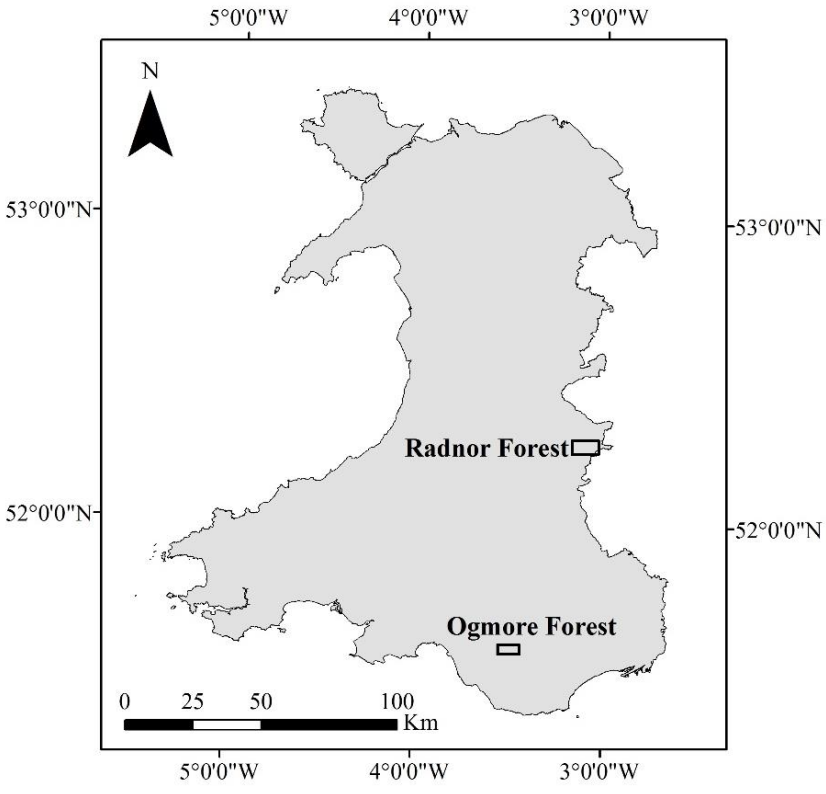

Figure 3.1 – Location of *P. ramorum* study areas in Wales (grey area).

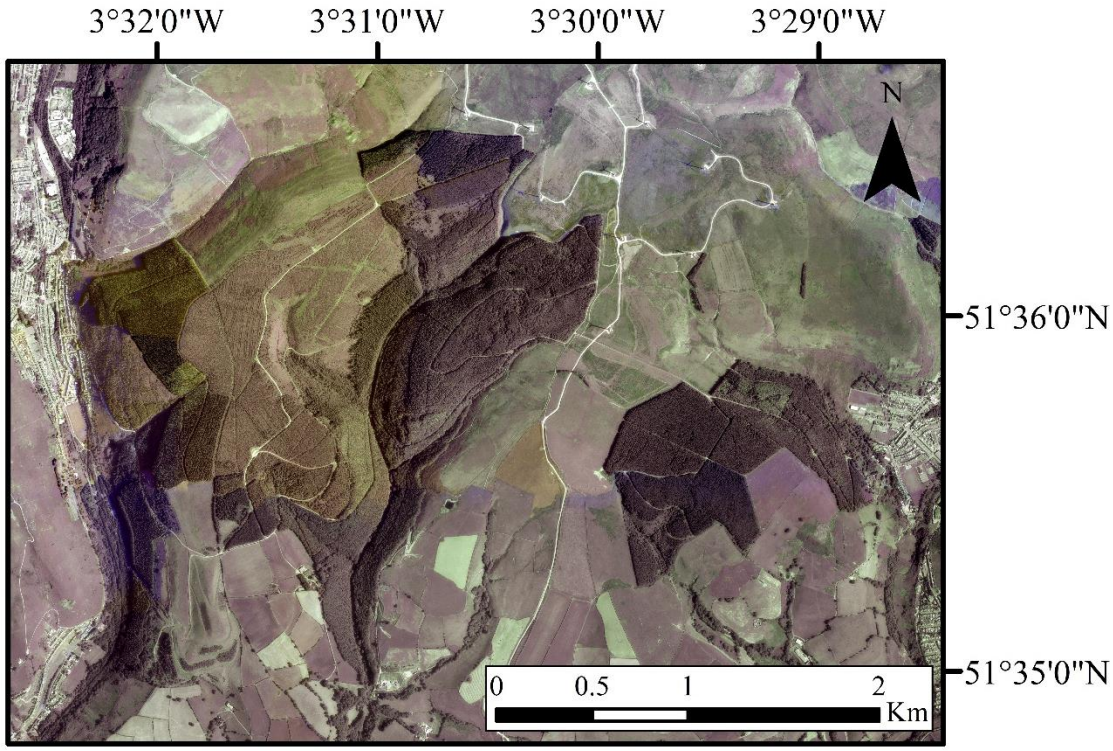

Figure 3.2 – Aerial photography for the Ogmore Forest (2010) provided by the Welsh Assembly Government.

Figure 3.3 – Photographs representing the landscape at A) Ogmore Forest in South Wales and B) Radnor Forest in Mid-Wales.

The two study sites (Ogmore and Radnor Forests) were both applied in the research concerning the segmentation of ITCs (Chapter 4) and the assessment of *P. ramorum* infection from ALS (Chapter 5). However, the location and size of sampling areas applied in these two sections of research (Figure 3.4) varied slightly due different requirements for plot size and ground sampling. Detailed information regarding the characteristics of sample plots is provided in the respective research chapters.

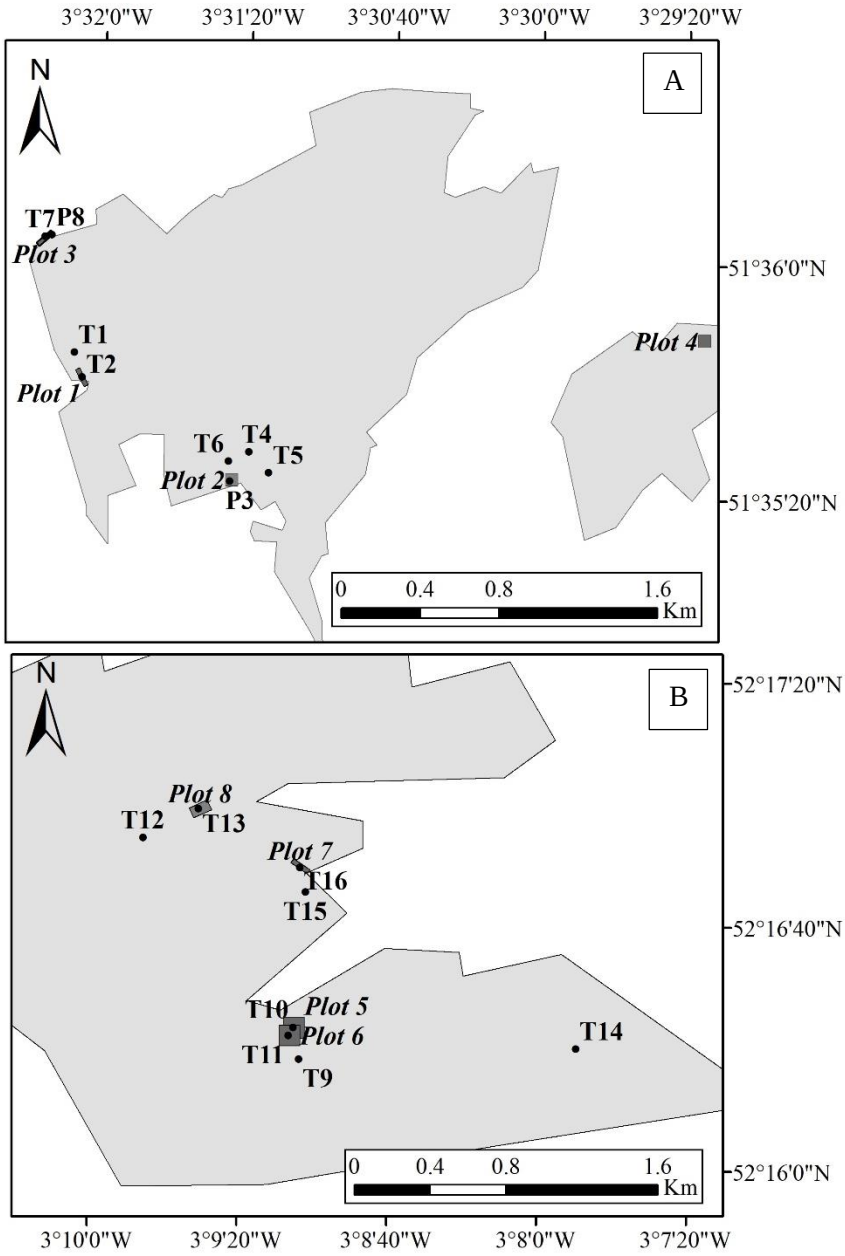

Figure 3.4 – Location of sample plots and transects established for the *P. ramorum* research at the Ogmore (A) and Radnor (B) Forests. Sample plots (1 - 8) applied in Chapter 4 are displayed in dark grey and labelled in italics. The sample transects and plots (T1 - 16 and P3) used in Chapter 5 are displayed as a black dot. The light grey in the figures represents forested area.

3.2 AOD in Oxfordshire

The research undertaken concerning AOD was located at the Stratfield Brake woodland, which situated in Kidlington, Oxfordshire in the UK (51.8053°N, -1.2825°W) (Figure 3.5) and is managed by the Woodland Trust. The site consists of a mature and young woodland as well as a wetland area (Figure 3.6). The mature woodland, which was the focus of the research, is dominated by English oak (*Quercus robur*) interspersed with ash (*Fraxinus excelsior*). AOD has been noted within the mature woodland and previously studied in epidemiologically focused research (Sapp *et al*., 2016). The mature woodland, which covers an area of 3 ha, was split into two sections, to provide a training and validation dataset for the study (Figure 3.7), comprising of 90 and 99 individual trees respectively.

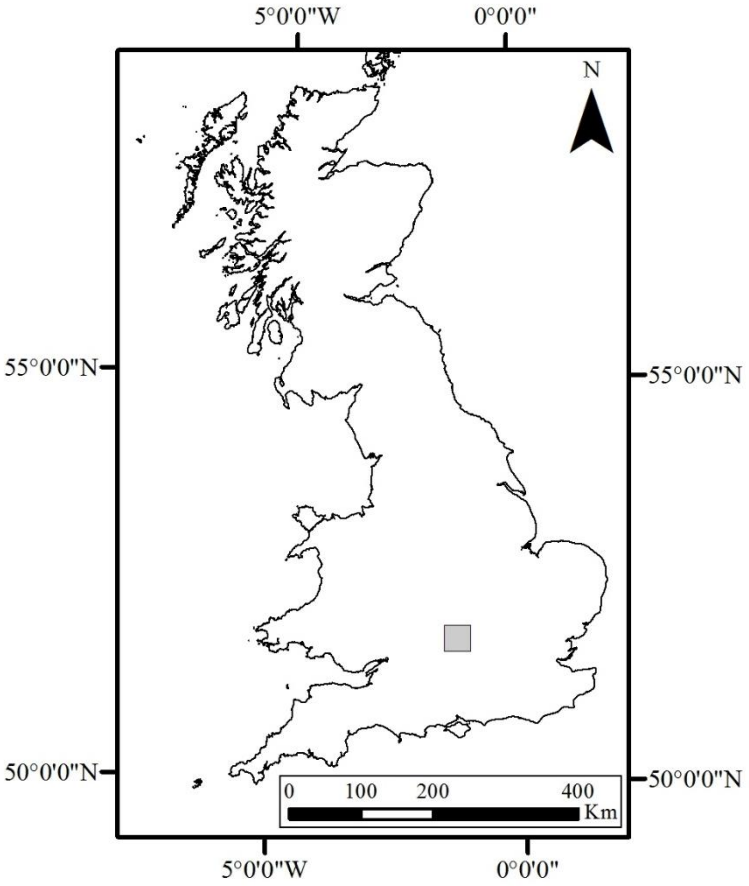

Figure 3.5 – Location of the Stratfield Brake study site (grey square) in the context of Great Britain.

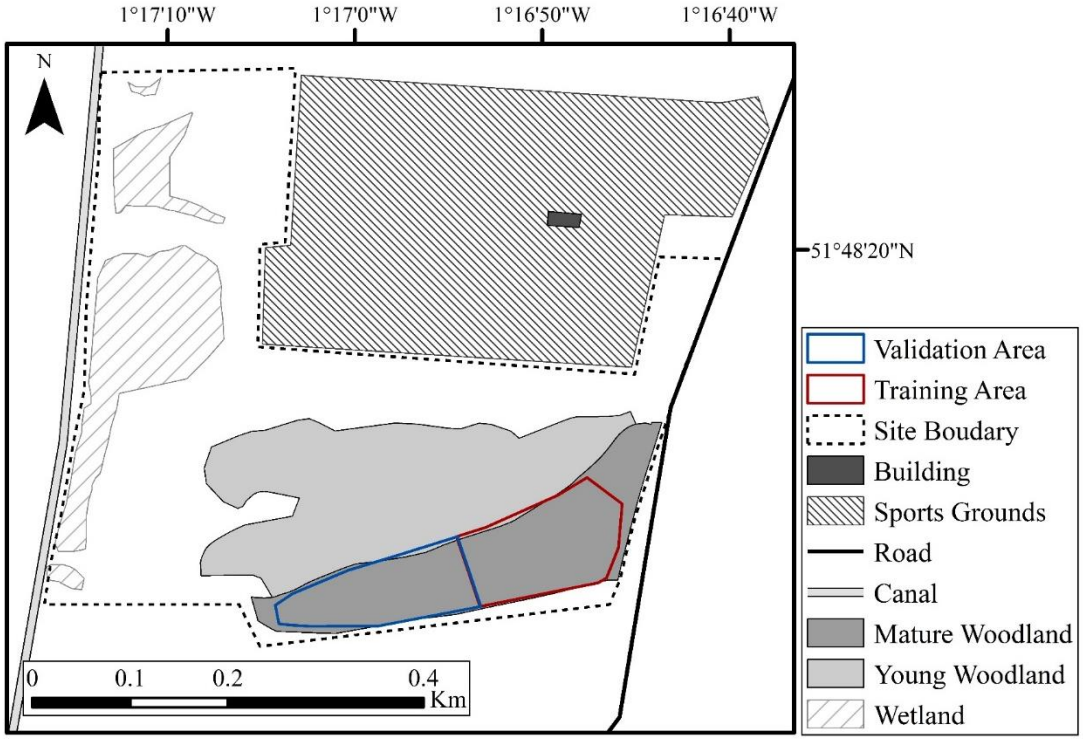

Figure 3.6 – Stratfield Brake site characteristics and key features.

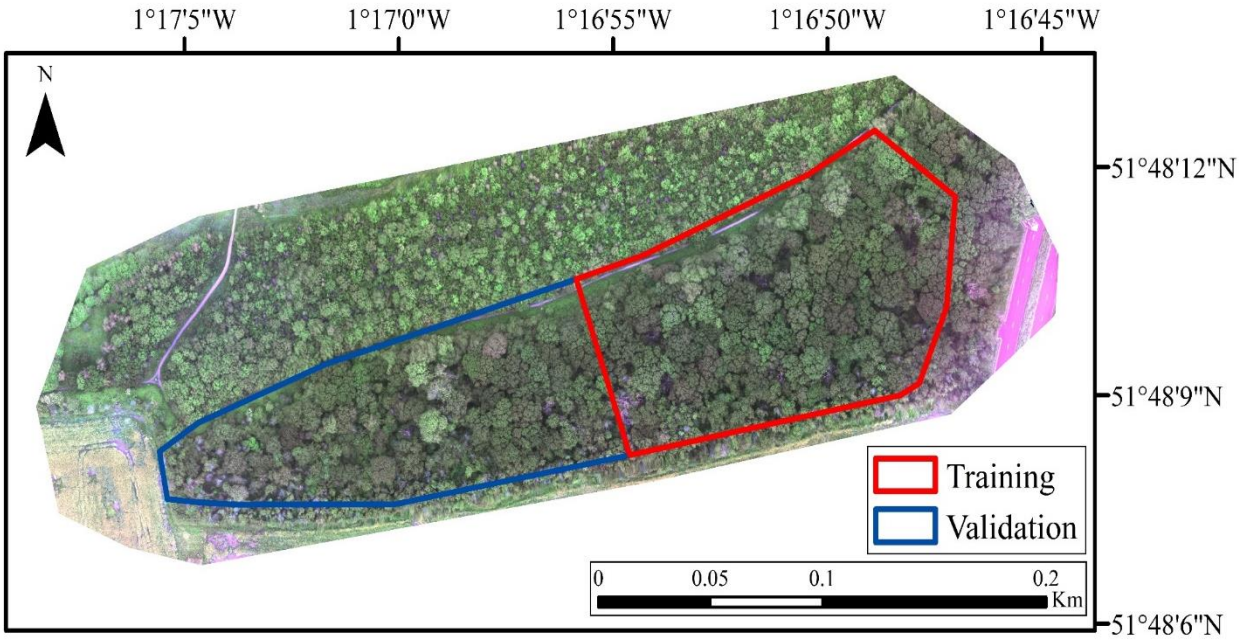

Figure 3.7 – Training and validation areas at the Stratfield Brake mature woodland.

Chapter 4: Individual Tree Crown Delineation from Airborne Laser Scanning for Larch Stands Infected by *Phytophthora ramorum*

The research presented in this chapter has previously been published as:

Barnes, C., Balzter, H., Barrett, K., Eddy, J., Milner, S. and Suárez, J. C. (2017) Individual tree crown delineation from airborne laser scanning for diseased larch forest stands. *Remote Sensing*. **9**, 231.

4.1 Introduction

Although the exact area or extent is unclear, current trends suggest that UK forests and woodlands are subject to a greater threat from exotic phytopathogens than ever previously experienced (Sutherland *et al*., 2008; Potter *et al*., 2011). One particular invasive phytopathogen, *P. ramorum*, has caused large-scale infections of larch (*Larix* spp.) trees in UK forestry, particularly across Southwest England, South Wales and Southwest Scotland (Forestry Commission, 2016). The nature of the infection and its foliar symptoms include discolouration and defoliation (Webber *et al*., 2010), which are currently being used for manual aerial detection by tree-health surveyors during helicopter surveys. This highlights the potential application of remotely sensed datasets for *P. ramorum* assessment in larch across the UK (Medcalf *et al*., 2011).

In recent decades, ALS has been increasingly applied in forestry (Lefsky *et al*., 1999; Lim *et al*., 2003; Wulder *et al*., 2006). The three-dimensional nature of ALS data provides structural information on topography, canopy height, tree density and crown dimensions, which can be used to determine biophysical parameters and inform forest inventories (Popescu *et al*., 2003; Zimble *et al*., 2003; Balzter *et al*., 2007). The high resolution and accuracy associated with ALS enable the extraction of forest parameters associated with ITCs within the forest canopy (Brandtberg *et al*., 2003). The ability to conduct crown-based analysis of remotely sensed data for forest environments provides the opportunity for the detailed study of forest condition and dynamics (Reutebuch *et al*., 2005).

A range of algorithms can be applied for ITC delineation from ALS data, which typically exploit structural differences present among treetops, canopy boundaries and canopy spaces (Chen *et al*., 2006). These algorithms include the region growing (Erikson,

2003; Tiede *et al*., 2005) and watershed segmentations (Chen *et al*., 2006) which often require the prior identification of treetops as seed inputs. From ALS data, treetops are typically located via the detection and filtering of local maxima (Kwak *et al*., 2007; Zhen *et al*., 2014), in CHMs these represent points where neighbouring pixels present equal or lower values in height (Koch *et al*., 2006). The performance of a particular ITC delineation algorithm is dependent on the characteristics of both tree canopies and input datasets, and the subsequent suitability of methods for a specific study should be considered (Pouliot *et al*., 2002; Kaartinen *et al*., 2012). Based on the previous results reported in the scientific literature an overall segmentation accuracy of >70% is used to define a successful ITC segmentation (Wang et al., 2004; Ke and Quackenbush, 2011; Tanhuanpää *et al*., 2016).

In the case of ITC delineation, ALS datasets are typically analysed in raster format as a CHM (Hu *et al*., 2014). A CHM represents the canopy surface elevation and is computed by the subtraction of the DTM from the DSM (Dubayah and Drake, 2000; Ben-Arie *et al*., 2009). The selected pixel size for the CHM, can affect the potential performance of the ITC detection (Chen *et al*., 2006; Khrosravipour *et al*., 2014). In instances where the resolution is too coarse, the ability to distinguish between the boundaries of neighbouring tree crowns can be lost where pixels contain multiple overlapping tree crowns. Conversely, when spatial resolution is too fine, excessive intra-crown height variability may cause an over-segmentation of canopies. Pouliot *et al*. (2002) described the ratio between crown diameter and pixel size in order to address this point. The optimum ratio will vary in accordance with the sensitivity of segmentation algorithms to intra-crown irregularity and the distinction of crown boundaries, but can provide a useful tool in considering the influence of pixel size on ITC delineation success. Nevertheless, the insufficient availability of data regarding the relationship between pixel size and tree crown dimensions makes it difficult to determine specific recommendations for selection (Ke and Quackenbush, 2011). In this chapter the implications of varying CHM pixel size on the performance of ITC delineation will be considered across a range of crown dimensions.

Canopy height anomalies that are present in CHMs are known as data pits and can influence the accuracy of ITC detection (Ben-Arie *et al*., 2009; Khrosravipour *et al*., 2014). Despite the uncertainty surrounding the specific source of these pits, cited causal factors have been acknowledged during the acquisition and processing of ALS datasets

(Ben-Arie *et al*., 2009; Vèga and Durrieu, 2011), these include the penetration of laser beams through the canopy, merging of ALS flight lines (Leckie *et al*., 2003), classification of ground and non-ground points (Kraus and Pfeifer, 1998) and interpolation of point clouds to raster datasets (Axelsson, 1999). To address the problem, many studies have used image smoothing techniques such as Gaussian filtering, to remove intra-canopy elevation artefacts (Brandtberg *et al*., 2003; Koch *et al*., 2006; Kaartinen *et al*., 2012). More recent solutions have introduced the use of pit-filling algorithms (Ben-Arie *et al*., 2009; Zhao *et al*., 2013) and the application of pit-free CHM generation methodologies (Khosravipour *et al*., 2014).

In forests subject to defoliation and dieback as a result of phytopathogens and insect pests, canopy structures are typically more complex and exhibit larger elevation irregularities across the canopy surface (Holdenrieder *et al*., 2004; Larsen *et al*., 2011), causing an increased presence of data pits. Such characteristics can be useful in disease detection (Coops *et al*., 2009; Bright *et al*., 2013; Barnes *et al*., 2017a), but may also provide an added complication with regard to the isolation of ITCs for the assessment of crown deterioration. Consequently, the methodologies employed for ITC delineation in canopies affected by disease require consideration of data pits and their implications for segmentation accuracy.

In the case of phytopathological assessments from remotely sensed datasets, the application of an ITC approach presents several advantages for identifying areas that require phytosanitary interventions (Leckie *et al*., 2016). In the early stages of the disease establishment in the forest stand, the isolation of ITCs, which initially succumb to infection, can enable a rapid response to insect pests and phytopathogens, which present new risks to forest areas (Wulder *et al*., 2006). In studies of diseased forest landscapes, crown-based approaches can also facilitate the detailed study of heterogeneous patterns of infection (Stone and Coops 2004). In addition, the use of ITC delineation techniques alongside species identification (Persson *et al*., 2004; Li *et al*., 2013) can facilitate a targeted assessment of susceptible tree species (Stone and Coops, 2004). This combined approach also presents the potential for the identification of disease resistant individuals, which may prove particularly useful with regard to the breeding of resistant genotypes and the development of resilience in forest stock (Sniezko, 2006). Resultantly, in the case of *P. ramorum*, the application of an ITC-based approach could therefore facilitate a detailed assessment of infected forested areas.

4.2 Objectives

The aim of this research chapter was to:

> *Identify the best approach to the isolation of individual larch crowns affected to Phytophthora ramorum using airborne laser scanning.*

Several key were set out objectives to address the difficulties in conducting ITC segmentation in partially (> 20% defoliation) or wholly defoliated forest canopies and determine the best method for the extraction of ITCs within *P. ramorum* infected larch forests using ALS data. The main objectives of this research chapter are:

1. To determine whether the removal of data pits during CHM generation can improve the accuracy of ITC segmentation in larch stands subject to varying severities of *P. ramorum* infection;
2. To compare the performance of the marker-controlled watershed and region growing segmentation algorithms for the delineation of larch stands subject to varying severities of *P. ramorum* infection; and
3. To assess the performance of CHM pixel size (0.15 m, 0.25 m and 0.5 m) on ITC segmentation for larch forest stands with different canopy characteristics.

4.3 Methods

4.3.1 Ground Data Collection

Across the two established study sites (Ogmore and Radnor Forests) in Wales, UK (Chapter 3; Section 3.1), eight sample plots were established (Chapter 3; Figure 3.4) covering a total area of 0.02 km^2 (Table 4.1). The four plots at Ogmore Forest showed a range of *P. ramorum* infection severities, whilst the four plots at Radnor Forest offered healthy trees for comparison across a similar range of species compositions and stand heights. The rectangular plots were situated along the edge of established forest sub-compartments to facilitate access and aid in recording the geographical position of individual trees. The potential limitation of edge effects associated with this sampling strategy was acknowledged, whereby trees situated along sub-compartment boundaries may be less representative of those situated in the centre. Small variations in plot size (Table 4.1) were incurred as the result of differences in sub-compartment shape and tree

crown size. The severity of the *P. ramorum* infection in each plot was recorded during field visits in 2015 using a simple scale:

- None = no individuals within the plot showed symptoms of *P. ramorum*;
- Light = less than 50% of individuals showed *P. ramorum* symptoms, but these were typically confined to a small portion of the canopy;
- Moderate = more than 50% of individuals demonstrated *P. ramorum* symptoms, a few cases may have resulted in significant discolouration or defoliation of the canopy; and
- Heavy = more than 75% of individuals were infected with *P. ramorum* and many exhibited severe dieback.

In addition, the position of individual trees situated within the established sample plots, which were safely accessible for ground surveying, were also recorded in the field using a handheld Garmin Oregon 550t GPS.

Table 4.1 – Sample plot characteristics. (Tree heights have been calculated using the ALS data (June 2015) and the size, number of trees and *P. ramorum* presence were recorded during field surveys (June, July and August 2015)).

Plot No.	Forest	Species Composition	Max. Height (m)	Min. Height (m)	Mean Height (m)	Plot Size (m^2)	No. Trees*	*P. ramorum* Infection Severity
1	Ogmore	HL, MB, MC	12.6	2.2	8.5	2500	104	Light
2	Ogmore	JL	21.9	8.3	17.4	2500	64	Moderate
3	Ogmore	JL	25.8	8.8	19.7	2500	57	Heavy
4	Ogmore	JL	30.4	19.7	24.6	2500	59	Heavy
5	Radnor	HL, MB, MC	7.1	3.3	5.3	1000	98	None
6	Radnor	JL, MB	19.8	14.3	16.3	1000	72	None
7	Radnor	JL, BE	23.4	9.9	17.8	2500	51	None
8	Radnor	EL, HL, BI, MC	33.8	19.6	29.4	5500	38	None

*Number of trees with complete crowns located within the plot. **Abbreviations**: EL, European Larch; HL, Hybrid Larch; JL, Japanese Larch; BI, Birch; BE, Beech; MB, Mixed Broadleaves; MC, Mixed Conifers.

4.3.2 Airborne Laser Scanning Data Collection

ALS data were acquired by Bluesky International for both study sites via a single aircraft survey utilising the Orion M300 sensor on the 30 June 2015, with an average flight altitude of 1500 m. The scan frequency was 66 Hz, laser pulse repetition frequency was 100 kHz, field-of-view was 8°, beam divergence was 0.25 mrad, sensor range

precision was <8 mm and elevation accuracy was 3–10 cm. Resulting point densities for the Ogmore (infected) and Radnor (control) sites were 20.34 points/m^2 and 27.39 points/m^2, respectively. Small differences in the resulting point densities across the two sites were incurred as a result of slight variations in flight altitude.

4.3.3 Data Processing Overview

To provide an overview of the methodology applied, Figure 4.1 provides a summary of the data processing tasks performed.

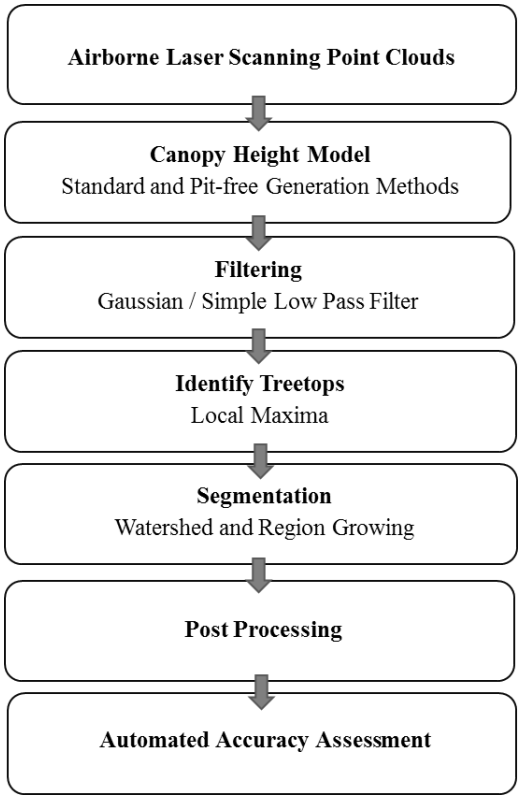

Figure 4. 1 – A summary of the data processing tasks required for the implementation of the ITC segmentation methodology.

4.3.4 Canopy Height Models

CHMs were produced for both study sites using two separate methods. The first approach used a standard normalised digital surface model ($CHM_{standard}$) to represent the relative height of above-ground vegetation (Koch *et al*., 2006). Height normalised ALS points were classified into ground and above-ground returns and following the generation of a triangulated irregular network (TIN) were rasterised to produce a DTM (ground points only) and DSM (maximum of all points). Subsequently, the $CHM_{standard}$ was produced following the subtraction of the DTM from the DSM (Jakubowski *et al*., 2013).

In addition, the pit-free algorithm outlined by Khosravipour *et al*. (2014) was also used to generate CHMs for the study areas ($CHM_{pitfree}$). The method uses height-normalised ALS points for the construction of partial CHMs representing various levels within the canopy (2 m, 5 m, 10 m, 15 m and 20 m). A rasterisation threshold is applied during the triangulation of partial CHMs, to ensure that only triangles within a single crown are rasterised, this threshold was varied based on the pixel size of the CHMs generated (Table 4.2). Partial CHMs are then stacked in height order and the maximum value for each pixel was subsequently extracted for the creation of the pit-free CHM.

Table 4.2 – Rasterisation thresholds for pit-free CHM generation.

Pixel Size (m)	Rasterisation Threshold (m)
0.15	0.45
0.25	0.75
0.5	1.5

The CHM outputs from both methodologies were generated at three different resolutions. Based on the suitable range of crown diameter to pixel size ratios suggested by Pouliot *et al*. (2002) and the CHM resolutions used in previous ITC detection studies (Khosravipour *et al*., 2014; Pitkänen *et al*., 2004; Roberts *et al*., 2005; Solberg *et al*., 2006), pixel sizes of 0.15 m, 0.25 m and 0.5 m were selected. All the processing for both the CHM approaches was implemented using LAStools (LAStools, 2016).

4.3.5 Manual Individual Tree Crown Delineation

A manual tree crown delineation was performed for each sample plot in order to provide information regarding ITC dimensions and a basis for comparing segmentation results (Pouliot *et al*., 2002). The manual delineation was performed using the ALS-derived data, in addition to photographs and GPS positions for ITCs recorded during ground surveys (Brandtberg and Walter, 1998; Fang *et al*., 2016). The resulting reference polygons enabled the extraction of crown area and diameter. In this case, due to the circular nature of coniferous canopies (Fang *et al*., 2016; Popescu and Wynne, 2004), equivalent crown diameter, which represents the diameter of a perfectly circular crown of equal area, was extracted using the diameter equation for a circle (Persson *et al*., 2004; Morsdorf *et al*., 2004).

4.3.6 Filtering

The standard CHMs were smoothed with a Gaussian filter to remove data pits and intra-canopy irregularities as shown in Figure 4.2 (Brandtberg *et al*., 2003; Koch *et al*., 2006; Hyyppä *et al*., 2012; Khosravipour *et al*., 2014). The standard deviation of the Gaussian filter has little impact on the final smoothing of CHMs (Dralle and Rudemo, 1996; Chen *et al*., 2006) and the standard deviation value was set to 2, following preliminary testing (Koch *et al*., 2006). The size (spatial diameter) of the filter applied, however, can have a significant influence on the resulting CHM. Chen *et al*. (2006) acknowledged that filter size should not exceed that of the smallest crown within the canopy of interest. Subsequently, the filter size was varied for each sample plot in accordance with pre-defined maximum canopy height thresholds (Table 4.3). These categories were determined based on the minimum equivalent crown diameter and maximum height for each sample plot. The variation in pixel size was also accounted for, with the size of filter in pixels rounded to the closest multiple for each of the three CHM resolutions (Monnet *et al*., 2010). For implementation over larger areas of larch forest, it is suggested that filtering and segmentation be employed for individual forest stands using the maximum tree height for each stand to define diameter and tailor filtering to stand characteristics.

Table 4.3 – Gaussian and local maxima filter size.

Maximum Tree Height (m)	Filter Diameter (m)	Filter Size in Pixels Based on CHM Resolution (m)		
		0.15	**0.25**	**0.5**
≥15	1	7 × 7	5 × 5	3 × 3
>15 and <30	2	13 × 13	9 × 9	5 × 5
≥30	3	21 × 21	13 × 13	7 × 7

In the case of the pit-free CHMs, a low-pass smoothing filter was applied (Figure 4.2). Preliminary testing was carried out to consider the performance of the pit-free CHMs without smoothing as suggested by Khosravipour *et al*. (2014), however in the majority of plots (Table 4.1) the reduction in intra-canopy variation as a result of the filter prevented the over-segmentation of ITCs. Due to the removal of data pits via the CHM generation methodology, a lower level of filtering was required to smooth the canopy surface in preparation for segmentation. In this case a simple low-pass smoothing filter was selected with a square search mode (Pouliot *et al*., 2002; Kaartinen *et al*., 2012). The filter size was also adjusted in accordance with maximum tree height (Table 4.4), however

it was smaller than that applied for the $CHM_{standard}$, which over-smoothed the data. All filtering undertaken for both CHM generation methodologies was undertaken using SAGA GIS (SAGA GIS, 2016).

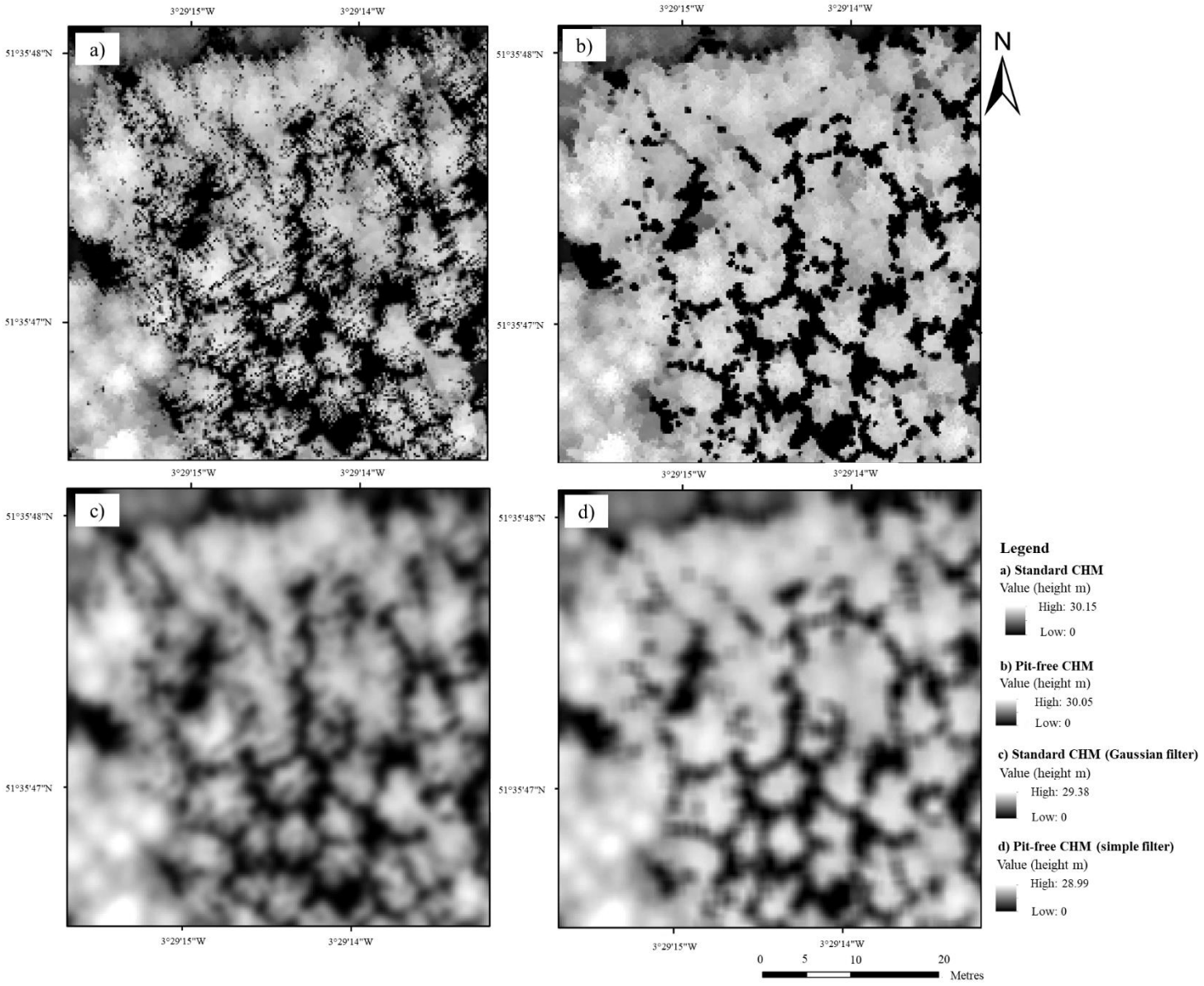

Figure 4.2 – CHMs with 0.25 m resolution for Plot 4 (Ogmore Forest) heavily infected with *P. ramorum*. (a) standard CHM no filter; (b) pit-free CHM no filter; (c) standard CHM with Gaussian filter; and (d) pit-free CHM with simple filter. Legend presents the height (m) for each of the CHM.

Table 4.4 – Simple low-pass filter sizes for pit-free CHMs.

Max Tree Height (m)	Size of Simple Filter in Pixels Based on CHM Resolution (m)		
	0.15	**0.25**	**0.5**
≥15	5 × 5	3 × 3	3 × 3
>15 and <30	7 × 7	5 × 5	3 × 3
≥30	9 × 9	7 × 7	5 × 5

4.3.7 Local Maxima

Prior to the application of the selected segmentation methods (marker-controlled watershed and region growing algorithms), seed points representing treetops within the canopy need to be identified (Wang *et al*., 2004; Tiede *et al*., 2005). Treetops can be located via the identification of local maxima (Palenichka *et al*., 2013), which are detected when neighbouring pixels on the CHM exhibit equal or lower height values (Koch *et al*., 2006). In order to avoid identifying multiple seed points within ITCs, local maxima were extracted from the smoothed standard and pit-free CHMs for each of the three resolutions (Chen *et al*., 2006) using the parameters identified in Table 4.3. Resulting local maxima were then subject to height filtering, removing points with a tree height of less than 2 m, to avoid the detection of understorey vegetation as tree crowns (Hyyppä *et al*., 2012; Duncanson *et al*., 2014).

In addition, minimum distance filters can also be applied to local maxima to reduce the over-estimation of the number of treetops. The size of these filters can be fixed or variable; however, their dimensions are typically informed by the diameter of tree crowns within the forest area of study. Variable filters are typically applied with regard to the relationship between tree height and crown diameter (Chen *et al*., 2006), which in this instance exhibits high levels of variation (Figure 4.3). This is likely to have resulted from the mixture in larch species and the difference in the location of individual trees. A weak relationship between crown diameter and tree height can result in poor estimates of tree crown diameter (Falkowski *et al*., 2006). To detect treetops with smaller crowns, filter size thresholds were used (Koch *et al*., 2006). As with the Gaussian smoothing, filter diameter represented the minimum equivalent crown diameter in relation to the maximum tree height for the sample plots (Table 4.3). This minimal distance point filtering was applied to local maxima points for each sample plot following height filtering, and all

processing was performed in SAGA GIS (SAGA GIS, 2016). Figure 4.4 provides an example of the filtered local maxima generated for Plot 2.

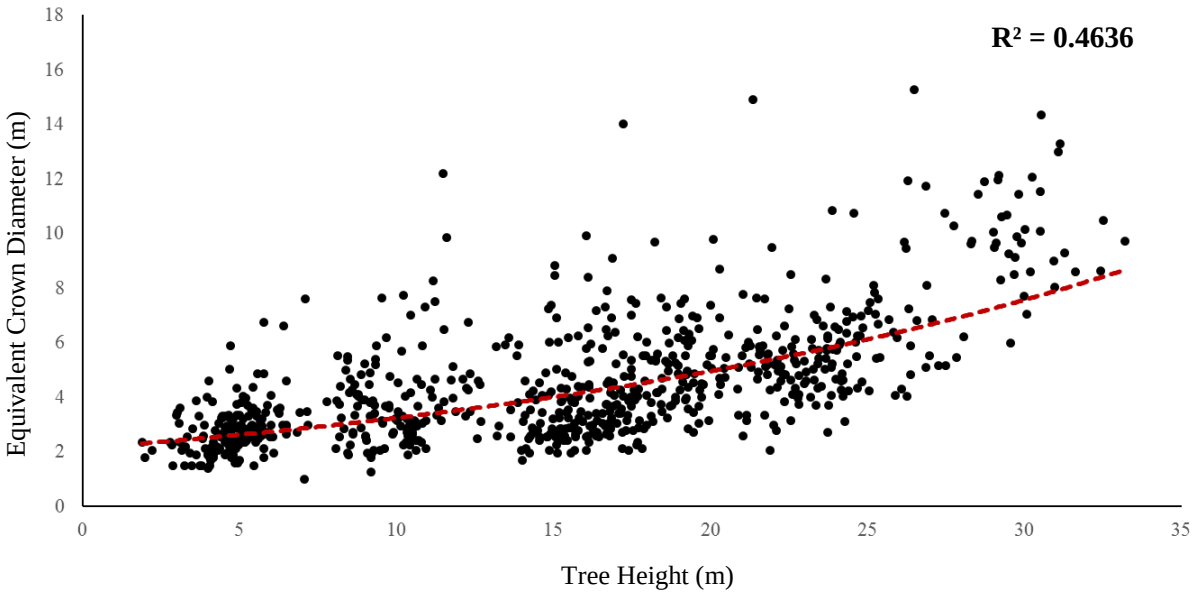

Figure 4.3 – The relationship between equivalent crown diameter and tree height for all individual trees across the eight sample plots. The dashed red line is the exponential regression curve.

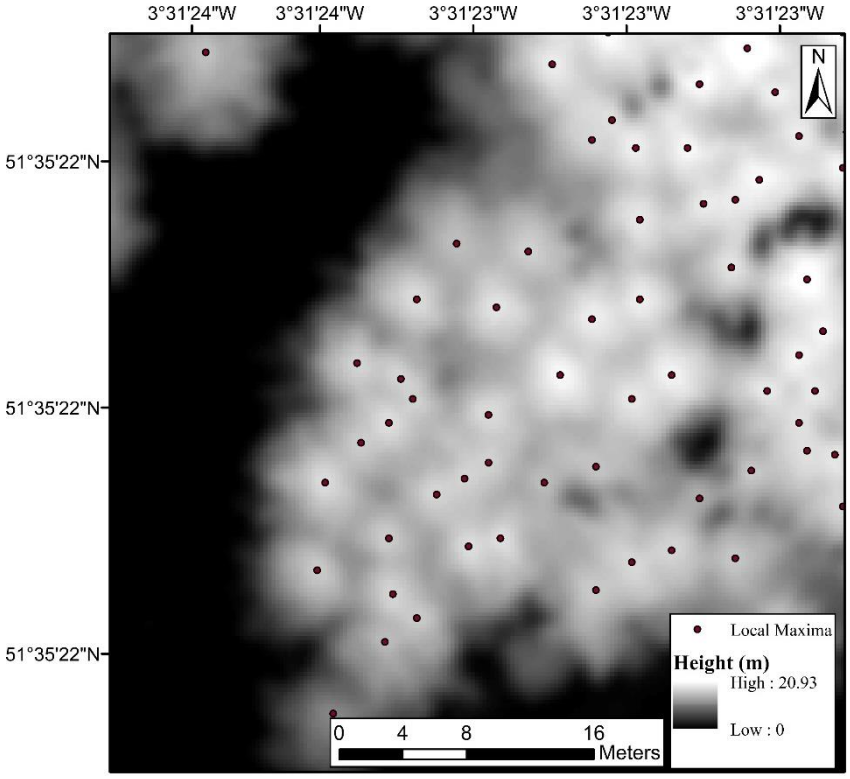

Figure 4.4 – The filtered local maxima points generated for Plot 2 using the Gaussian filtered $CHM_{standard}$.

4.3.8 Segmentation

For CHMs, the marker-controlled watershed and region growing segmentation algorithms have both previously been acknowledged as effective approaches for the delineation of ITCs (Maltamo *et al*., 2004; Chen *et al*., 2006). The marker-controlled watershed algorithm treats the inverted CHM as "valleys", "flooding" each system from points of local minima (markers or seeds) representing treetops within the canopy. Respective boundaries for each tree crown are subsequently delineated by determining the "watershed" for each individual "valley" (Wang *et al*., 2004) (Figure 4.5). The region growing algorithm also requires a seed input to denote the location of treetops, from which neighbouring pixels are compared and merged until some specified threshold criteria is reached (Tiede *et al*., 2005; Böhner *et al*., 2006; Ke and Quackenbush, 2011). In the case of both segmentation methods, filtered local maxima were used as seed inputs and processing was undertaken in SAGA GIS (Böhner *et al*., 2006; Levick and Asner, 2013; Tao *et al*., 2014; Levick *et al*., 2015; Zawawi *et al*., 2015). Additional input parameters for the two segmentation algorithms in SAGA GIS (SAGA GIS, 2016) were subject to preliminary testing, these included a joining threshold for the watershed segmentation and a similarity threshold for the region growing segmentation. Subsequently the marker-controlled watershed segmentation was subject to no additional threshold for joining segments. For the region growing segmentation, the similarity threshold was set to 0.01 and an 8-pixel neighbourhood was applied.

4.3.9 Post-processing

Following the ITC delineations, output segments from both segmentation approaches were labelled with a unique ID (Schardt *et al*., 2002), converted to polygons and joined with tree heights extracted from seed outputs (Koukoulas and Blackburn, 2005). To avoid over-segmentation, polygons with an area below that of the minimum threshold area (Table 4.5), derived as the circular area from the Gaussian and local maxima filter size diameters, were merged with the neighbouring segment exhibiting the longest common border (Weinacker *et al*., 2004; Koch *et al*., 2006).

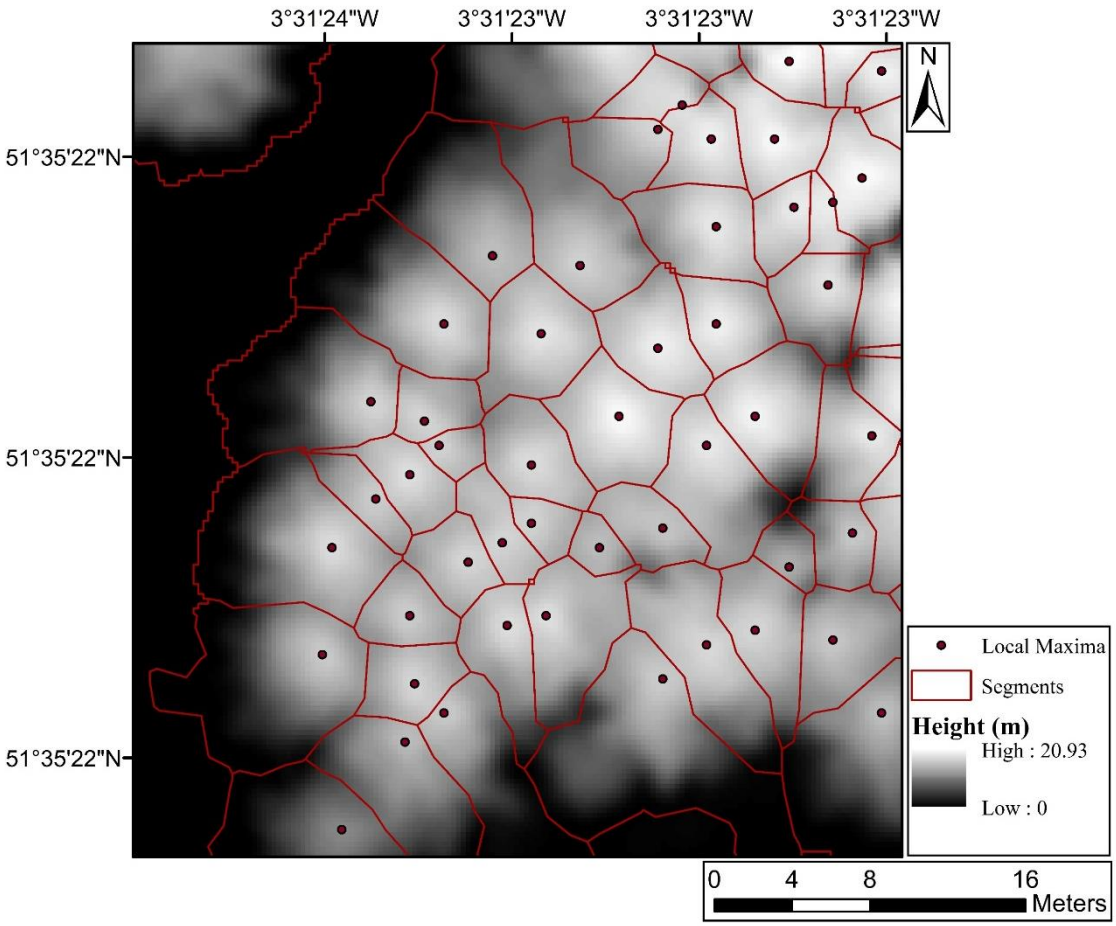

Figure 4.5 – The filtered local maxima points and watershed segments generated for Plot 2 using the Gaussian filtered $CHM_{standard}$.

Table 4.5 – Minimum area thresholds for automatically delineated tree crowns.

Maximum Tree Height Category (m)	Minimum Area Threshold (m^2)
≥15	0.5
>15 and <30	3
≥30	7

4.3.10 Accuracy Assessment

To assess the accuracy of the automated ITC delineations, resulting segments were compared to manual tree crown delineations (reference crowns) via an automated overlap analysis, which determined the percentage of overlap for corresponding polygons. For each reference crown in the plot, the percentage overlap with automated polygons was computed. Subsequently, the two highest percentage overlap values for individual reference crowns were recorded as R1 and R2. In addition, the percentage of the automated polygons which overlapped with the corresponding reference crown were

also determined, the two highest values were reported as A1 and A2. Using these values for each reference tree, percentage overlap criteria were subsequently applied to previously established accuracy assessment categories (Table 4.6) (Leckie *et al*., 2003; Koch *et al*., 2006; Kwak *et al*., 2007; Jing *et al*., 2012; Hu *et al*., 2014; Fang *et al*., 2016). The term successfully delineated segments was used to collectively refer to ITC segmentations classified as correct or satisfactory which were deemed acceptable for the purpose of the study (Kwak *et al*., 2007; Jing *et al*., 2012). Overall accuracy percentages were also calculated using the ratio of successful delineations to the total number of reference tree crowns for each plot (Hu *et al*., 2014).

Table 4.6 – Assessment categories for the tree crown delineation accuracy analysis.

Category	Description	Percentage overlap (%)			
		R1	R2	A1	A2
Correct	Reference crown dominated by one automated crown	≥ 50	< 2	≥ 50	N/C
Satisfactory	Reference crown largely associated with one automated crown	≥50	< 50	≥ 50	< 50
Oversized	Reference crown only accounts for small portion of automated crown	≥ 50	N/C	<50	N/C
Split	Reference crown dominated by more than one automated crown	N/C	N/C	N/C	≥50
Missed	Reference crown has no or poor overlap with automated crowns	<50	N/C	N/C	<50

Abbreviations: N/C = No conditions; R1 = Highest percentage overlap value for reference crown; R2 = Second highest percentage overlap value for reference crown; A1 = Highest percentage overlap value for corresponding automated crown; A2 = Second highest percentage overlap value for corresponding automated crown.

4.3.11 Data Analysis

To evaluate the influence of CHM generation method on delineation accuracy, the non-parametric Wilcoxon signed rank test was used to analyse the difference in the segmentation accuracy percentages produced by the standard and pit-free CHMs for each of the pixel size/segmentation algorithm combinations. The same testing was also applied in the comparison of the two segmentation algorithms (marker-controlled watershed and region growing), for each of the CHM generation method/pixel size combinations. The equivalent parametric paired t-test was not selected in this instance as several datasets did not meet the assumptions of normality (Shapiro–Wilk test $p < 0.05$). To address the additional type 1 error incurred via multiple testing, the Bonferroni-Holm sequential correction was also applied to the results of the statistical testing.

To consider the influence of CHM pixel size on delineation accuracy, the mean and standard deviation values for segmentation accuracy percentages across all study plots were calculated for each CHM generation method/segmentation algorithm

combination. In addition, to assess the relationship between CHM pixel size and tree height, a linear regression model was fitted to the maximum plot tree height (m) and the percentage of successful delineations, for all segmentation algorithms and CHMs tested.

4.4 Results

4.4.1 Overall Segmentation Performance

The ITC delineation results from the marker-controlled watershed and region growing segmentations for all CHMs are displayed in Table 4.7, with the highest percentages for each of the plots in bold. In cases where the highest percentage is tied, those producing the greater percentage of correct delineations (Table 4.6) were selected. Successful delineations exceeding 70% were achieved for all of the sample areas, however no single method or CHM presented optimal results across all sample plots. The most successful delineation method recorded for each of the sample plots is summarised in Table 4.8.

Table 4.7 - Successful delineation percentages for all segmentation algorithm, CHM generation method and CHM pixel size combinations tested for all sample plots.

		0.15 m		0.25 m		0.5 m	
		Standard	Pit-free	Standard	Pit-free	Standard	Pit-free
Plot	Method	Successful (%)	Successful (%)	Successful (%)	Successful (%)	Successful (%)	Successful (%)
1	WS	77.88	74.04	**77.88**	65.38	60.58	53.85
	RG	48.08	44.23	66.35	57.69	36.54	44.23
2	WS	89.06	71.88	82.81	**92.19**	67.19	71.88
	RG	20.31	15.63	54.69	50.00	67.19	78.13
3	WS	63.16	50.88	57.89	**70.18**	61.40	66.67
	RG	10.53	7.02	35.09	33.33	33.33	49.12
4	WS	40.35	37.29	62.71	81.36	76.27	**83.05**
	RG	15.25	5.08	27.12	35.59	57.63	74.58
5	WS	79.59	76.53	79.59	78.57	45.92	20.41
	RG	**80.61**	74.49	73.47	68.37	41.84	11.22
6	WS	**88.89**	84.72	69.44	79.17	50.00	51.39
	RG	61.11	62.50	65.28	79.17	41.67	51.39
7	WS	**84.31**	78.43	68.63	78.43	64.71	64.71
	RG	29.41	23.53	39.22	33.34	43.14	39.22
8	WS	36.84	21.05	71.05	65.79	81.58	**84.21**
	RG	0.00	0.00	2.63	2.63	7.89	78.95

Abbreviations: WS = marker-controlled watershed; RG = region growing.

Table 4.8 - Best performing segmentation algorithm, CHM generation method and pixel size for the individual tree crown segmentation in each of the sample plots.

Plot	*P. ramorum* Infection Severity	Max. Tree Height	No. Trees	Best Delineation Performance			
				Successful Delineation (%)	Segmentation Algorithm	CHM Generation Method	Pixel Size (m)
1	Light	12.6	104	77.88	WS	Standard	0.25
2	Moderate	21.9	64	92.19	WS	Pit-free	0.25
3	Heavy	25.8	57	70.18	WS	Pit-free	0.25
4	Heavy	30.4	59	83.05	WS	Pit-free	0.50
5	None	7.1	98	80.61	RG	Standard	0.15
6	None	19.8	72	88.89	WS	Standard	0.15
7	None	23.4	51	84.31	WS	Standard	0.15
8	None	33.8	38	84.21	WS	Pit-free	0.50

Abbreviations: WS = marker-controlled watershed; RG = region growing.

4.4.2 Canopy Height Model Generation Method

Table 4.8 shows which CHM generation method produced the most successful delineation accuracies. The standard and pit-free methodologies both performed best in four of the eight sample plots. Interestingly, for Plots 2, 3 and 4, which exhibited moderate and heavy severities of *P. ramorum* infection, the pit-free CHM generated the best delineation accuracies. Figure 4.6 displays the difference in successful delineation percentages for the standard and pit-free CHMs, across the three different pixel sizes tested. In the case of the 0.15 m pixel size, the standard CHM produced the best accuracies for all segmentations across the eight sample plots, except one (Plot 6, region growing, 0.15 m). Conversely, for the 0.5 m pixel size, the pit-free CHM generation method resulted in a more successful delineation for the majority of segmentations. At the 0.25 m pixel size however, the CHM generation methods performed similarly. The segmentation algorithms did not influence the success of the two CHM generation methods. The results from the statistical analysis (Table 4.9) demonstrate no significant difference between the delineation accuracy of the two different CHM generation methods, except in the case of the marker-controlled watershed segmentation at the 0.15 m pixel size ($p < 0.10$).

Table 4. 9 - *p* values from the Wilcoxon signed rank test after Bonferroni-Holm correction comparing results from the two CHM generation methods (standard and pit-free). * Denotes values significant at the 90% confidence level ($p < 0.10$).

CHM Pixel Size (m)	Segmentation Algorithm	
	Marker-Controlled Watershed	Region Growing
0.15	0.072*	0.140
0.25	0.789	1.000
0.5	1.000	0.644

4.4.3 Segmentation Algorithm

The marker-controlled watershed approach produced higher delineation accuracies across the sample plots, than the region growing method (Figure 4.7). This result was consistent across the two CHM generation methodologies and three pixel sizes tested. The greatest difference (73.69%) was observed in the case of the $CHM_{standard}$ at the 0.5 m pixel size. In this instance 71% of tree crowns segmented with the region growing algorithm were categorised as missed (Table 4.6). The results from the Wilcoxon signed rank test (Table 4.10) indicated a significant difference, at the 90% confidence level ($p < 0.10$) between the segmentation algorithms across all CHM generation method/pixel size combinations tested.

Table 4.10 - *p* values from the Wilcoxon signed rank test after Bonferroni-Holm correction, comparing results from the two segmentation algorithms (marker-controlled watershed and region growing).

CHM Pixel Size (m)	CHM Generation Method	
	Standard	Pit-free
0.15	0.068 *	0.072 *
0.25	0.072 *	0.054 *
0.5	0.054 *	0.043 *,$

*Denotes values significant at the 90% confidence level ($p < 0.10$). $The *p* value is not significant at the 95% confidence limit because it follows a not significant result in the Bonferroni-Holm sequential correction for a *p* value < 0.05.

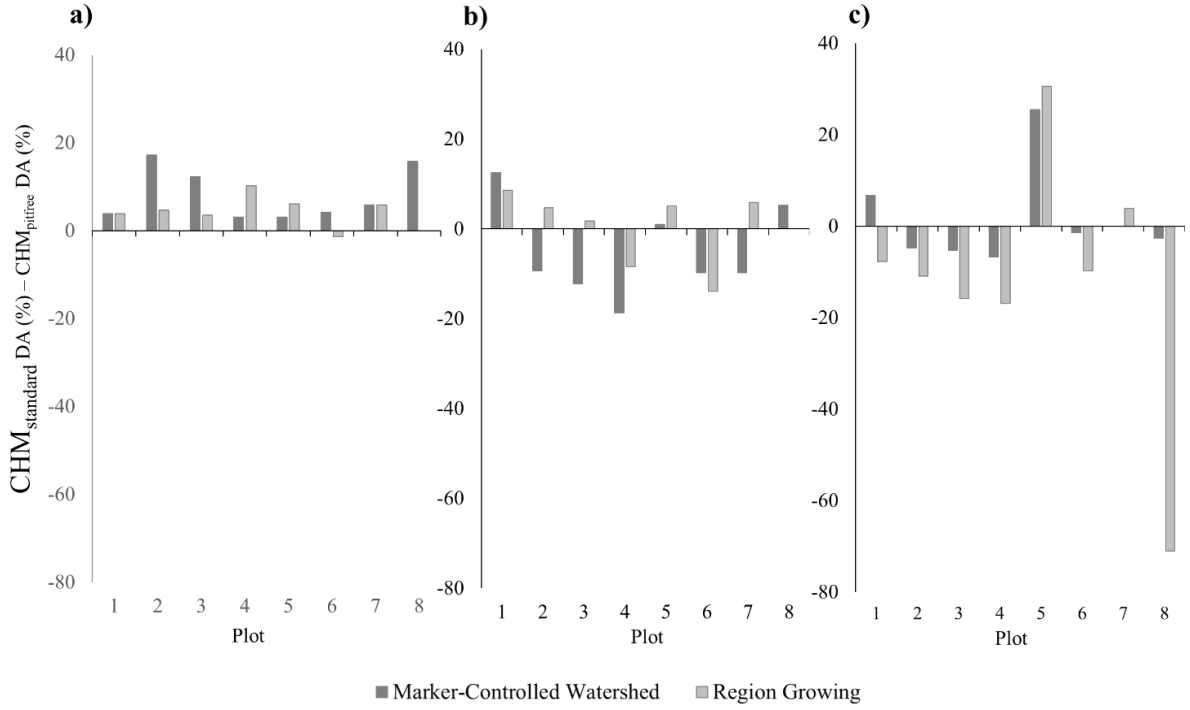

Figure 4.6 – The difference between the $CHM_{standard}$ and $CHM_{pitfree}$ delineation accuracy (DA) percentages for each of the segmentation methods across the (a) 0.15 m; (b) 0.25 m; and (c) 0.5 m pixel sizes.

4.4.4 Canopy Height Model Pixel Size

In relation to CHM pixel size, no single resolution consistently yielded the most successful delineations (Table 4.8). To consider the overall performance of each pixel size, Table 4.11 provides the mean and standard deviation values for the successful delineation percentages from all eight sample plots, for each of the segmentation algorithm and CHM generation methodology combinations tested. The 0.25 m resolution provided the highest mean value in three of the four instances. Additionally, the 0.25 m pixel size also exhibited comparatively low standard deviation values in the case of the two marker-controlled watershed segmentations. The higher standard deviations across all combinations at the 0.15 m and 0.5 m resolutions, in addition to the 0.25 m region growing segmentations, reflect the large disparities in successful delineation percentages across the eight sample plots. To illustrate the influence of CHM pixel size on the

sgementation outputs, Figure 4.8 presents the automated ITC delineations across all three pixel sizes (0.15 m, 0.25m and 0.5 m).

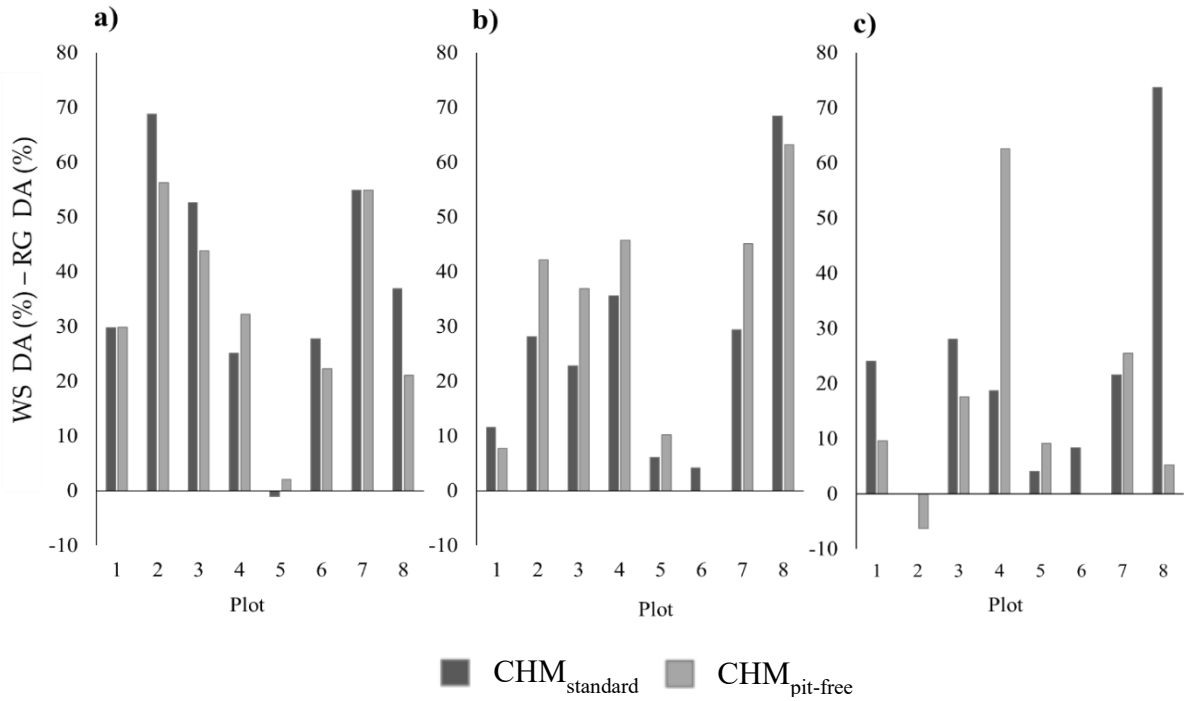

Figure 4.7 – The difference between the marker-controlled watershed (WS) and region growing (RG) segmentation delineation accuracy (DA) percentages for each of the CHM generation methods (standard and pit-free) across the (a) 0.15 m; (b) 0.25 m; and (c) 0.5 m pixel sizes.

Table 4.11 - The mean and standard deviation (σ) values for the successful delineation percentages produced from all sample plots at the three CHM pixel sizes, for each of the segmentation algorithm and CHM generation method combinations.

Segmentation Algorithm	CHM Generation Method	CHM Pixel Size (m)					
		0.15		0.25		0.5	
		Mean	σ	Mean	σ	Mean	σ
WS	Standard	70.01	21.06	71.25	8.53	63.46	12.01
WS	Pit-free	61.85	22.84	76.38	8.97	62.02	20.60
RG	Standard	33.16	27.69	45.48	23.95	41.15	17.50
RG	Pit-free	29.06	28.10	45.02	24.07	53.36	23.30

Abbreviations: WS = marker-controlled watershed; RG = region growing.

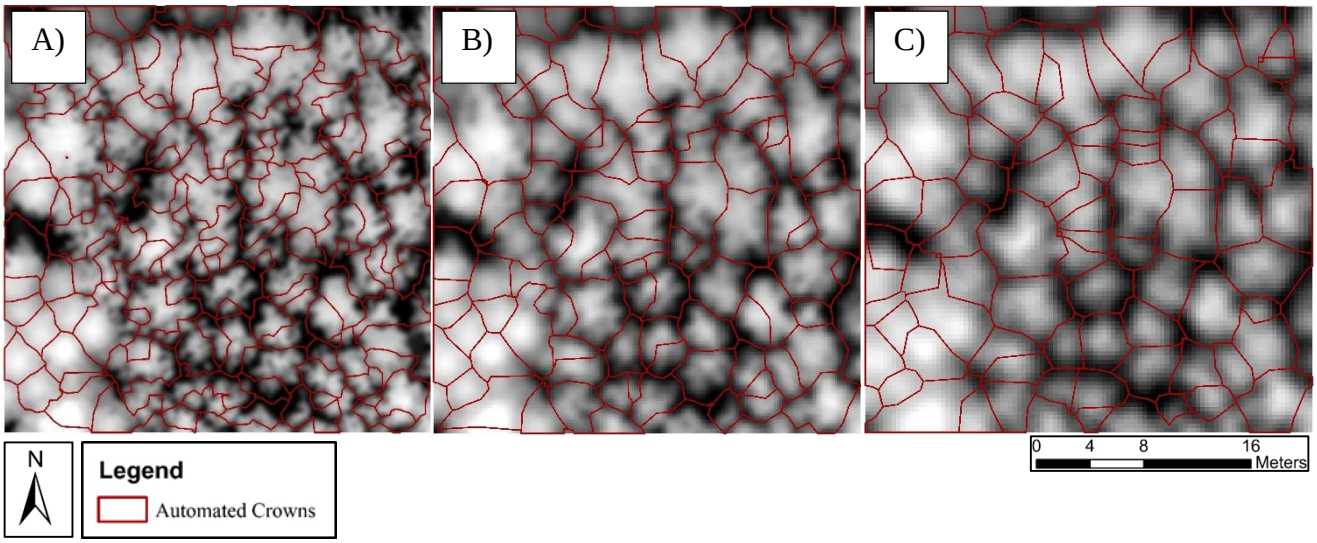

Figure 4.8 – Marker-controlled watershed segmentation outputs for Plot 4 from the $CHM_{standard}$. A) CHM pixel size 0.15 m; B) CHM pixel size 0.25m; C) CHM pixel size 0.5 m.

The segmentation results suggest that the suitability of CHM pixel size for ITC delineation may be governed by crown size and tree height, two correlated variables regarding the structural character of individual trees. Figure 4.9 presents the relationship between tree height and segmentation accuracy for all of the segmentation algorithms and CHMs tested. The linear regressions suggest that the high-resolution CHMs (0.15 m) performed best for plots with a low maximum tree height (<20 m). Conversely, the lowest resolution CHM (0.5 m) was best suited for plots that exhibited a high maximum tree height (>30 m). In the case of the 0.25 m pixel size, the relationship between maximum tree height and successful delineation percentage is less clear, although a negative trend was typically observed.

Each of the scatterplots in Figure 4.9 displays the R^2 values for the fit of the linear regression model between plot maximum tree height per (m) and successful delineation (%), at the three CHM pixel sizes (0.15 m, 0.25 m and 0.5 m) for the different segmentation algorithms and CHM generation methods. For the 0.15 m pixel size, negative trends were consistent across the two segmentation algorithms and CHM generation methods, though more significant in the case of the region growing segmentations (0.82 ($CHM_{standard}$) and 0.78 ($CHM_{pit\text{-}free}$)). At the 0.25 m pixel size, trends were predominantly negative and stronger for segmentations with the region growing algorithm (0.86 ($CHM_{standard}$) and 0.64 ($CHM_{pit\text{-}free}$)). In contrast, segmentations at the 0.5 m pixel size typically exhibited a positive relationship between plot maximum tree height

and delineation success percentage, with stronger correlations produced by the marker-controlled watershed segmentations (0.73 ($CHM_{standard}$) and 0.86 ($CHM_{pit\text{-}free}$).

An additional approach to examine the relationship between pixel size and successful ITC delineation considered the crown diameter to pixel size ratio put forward by Pouliot *et al*. (2002). For each sample plot, the mean equivalent crown diameter was determined in order to produce the crown diameter to pixel ratios for each of the eight sample plots (Table 4.12). The ratios that contributed to the best performance for each of the plots ranged between 10:1 and 35:1. To consider the influence of these ratios on the performance of ITC segmentations, the relationship between the mean equivalent crown diameter to pixel size ratio and the percentage of successful ITC delineations across all sample plots, segmentation approaches and CHMs is shown in Figure 4.10. Segmentations that exceeded 80% success rate exhibited a crown diameter to pixel ratio from 11:1 to 35:1.

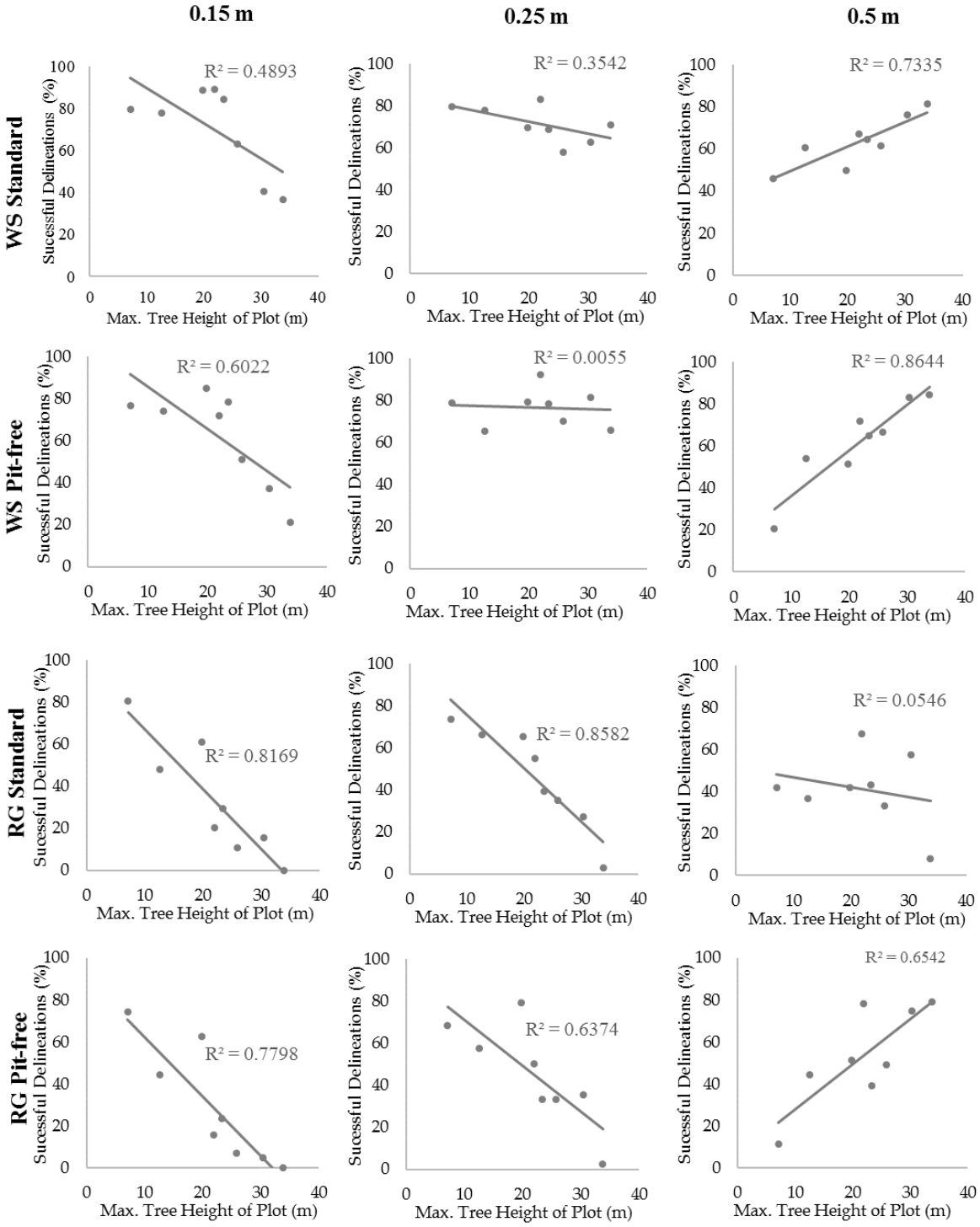

Figure 4.9 – Scatterplots demonstrating the linear regression model fitted between successful tree crown delineations and plot maximum tree height in relation to CHM pixel size (0.15 m, 0.25 m and 0.5 m) and the four segmentation algorithm and CHM generation method combinations (marker-controlled watershed (WS) segmentation for $CHM_{standard}$, marker-controlled watershed segmentation for $CHM_{pit\text{-}free}$, region growing (RG) segmentation for $CHM_{standard}$ and region growing segmentation for $CHM_{pit\text{-}free}$).

Table 4.12 - The mean equivalent crown diameter to pixel ratios for each plot across the three different CHM pixel sizes. The values highlighted in bold demonstrate those associated with the highest successful delineation percentage for the sample plot.

Plot	Study Area	*P. ramorum* Infection Severity	Max. Tree Height (m)	Mean Crown Diameter to Pixel Ratio		
				0.15 m	0.25 m	0.5 m
1	Ogmore	Light	12.6	23:1	**14:1**	7:1
2	Ogmore	Moderate	21.9	31:1	**19:1**	9:1
3	Ogmore	Heavy	25.8	32:1	**19:1**	10:1
4	Ogmore	Heavy	30.4	38:1	23:1	**11:1**
5	Radnor	None	7.1	**17:1**	10:1	5:1
6	Radnor	None	19.8	**21:1**	13:1	6:1
7	Radnor	None	23.4	**35:1**	21:1	11:1
8	Radnor	None	33.8	64:1	38:1	**19:1**

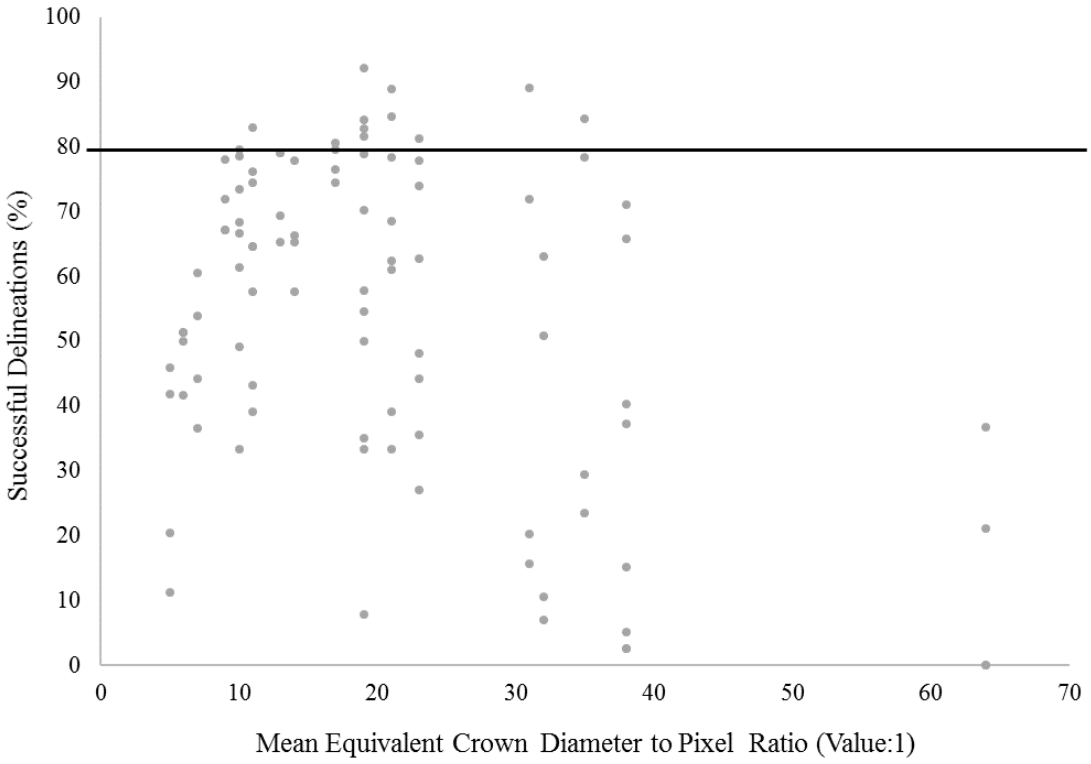

Figure 4.10 – The relationship between mean equivalent crown diameter to pixel size ratio and successful tree crown delineation (%) for all segmentation algorithms (marker-controlled watershed and region growing), CHM generation methods (standard and pit-free) and CHM pixel sizes (0.15 m, 0.25 m, and 0.5 m). The solid black line represents the successful delineations at 80%.

4.5 Discussion

The absence of an optimal method or input CHM for ITC delineation across the study plots highlights the difficulties of utilising a single algorithm and input dataset to segment ITCs in forest environments comprising of mixed stand ages and species (Brandtberg *et al*., 2003; Solberg *et al*., 2006). Nevertheless, the results shown here allow us to infer several key points informing the selection of the most appropriate segmentation approach and CHM input for canopies subject to *P. ramorum* infection.

Neither CHM generation method (standard/pit-free) exhibited a consistently stronger performance, with each outperforming the other for four of the eight sample plots. This is different from the results observed by Khosravipour *et al*. (2014), who documented consistently improved treetop detection accuracy for all pit-free CHM inputs at pixel sizes of 0.15 m and 0.5 m. In our case, it is likely that the weaker performance of the pit-free CHMs in four of the sample plots may stem from the low-pass filtering used to smooth the canopy surface for improved local maxima detection. This was not applied in the study by Khosravipour *et al*. (2014), who instead extracted local maxima with an established variable window for coniferous forests (Popescu and Wynne, 2004). In addition, Khosravipour *et al*. (2014) assessed the accuracy of treetop detection, rather than the segmentation on ITCs. Nevertheless, in the case of the Plots 2, 3 and 4 which were subject to moderate and heavy *P. ramorum* infection, the pit-free CHMs outperformed those generated using the standard CHM. This improved performance is likely to be a result of the data pit filling during the CHM generation, providing a more complete canopy for image segmentation (Figure 4.2).

Between the two segmentation algorithms, the marker-controlled watershed demonstrated a superior performance ($p < 0.10$) compared to the region growing segmentation, for both CHM generation methods and all CHM pixel sizes tested. Since both algorithms were provided with the same input seed points, the difference in performance is due to their ability to delineate crown boundaries in the CHMs. In the case of the region growing segmentation, boundaries are delineated when a specified threshold value is reached. The poor overall performance of this particular segmentation algorithm is likely to have resulted from the inability of the region growing threshold to accommodate the variation in crown size and characteristics across the canopy, as a result of mixed species and tree ages (Fang *et al*., 2016). Although the region growing algorithm

has previously produced satisfactory ITC delineations (Erikson, 2004; Erikson and Olofsson, 2005; Bunting and Lucas, 2006; Ke and Quackenbush, 2011), studies have also noted difficulties and poor performance associated with the algorithm when applied in forest stands comprising of mixed species, multiple canopy layers and high tree densities (Erikson and Olofsson, 2005; Bunting and Lucas, 2006; Ke and Quackenbush, 2011). In comparison, the delineation of crown boundaries by the marker-controlled watershed segmentation directly utilises the height information from the CHMs when delineating watershed boundaries, providing a more informed segmentation (Wang *et al*., 2004). Studies from an array of forest types have noted successful isolation or segmentation of ITCs resulting from the marker-controlled watershed segmentation, examples include commercially thinned conifer forest (75.6%) (Wang *et al*., 2004), savanna woodland (64.1%) (Chen *et al*., 2006) and eucalypts forest (Ali *et al*., 2008). Nevertheless, the delineation accuracies achieved by segmentation algorithms can vary due to a combination of factors including the effectiveness of the algorithm, forest characteristics, and ALS data acquisition and properties (Tao *et al*., 2014). Consequently, the difference between the performance of the marker-controlled watershed and region growing algorithms may change for segmentations performed for other forest environments and ALS datasets.

The results from the study also highlighted that CHM resolution used in the ITC segmentation strongly influences segmentation accuracy. Relationships between the maximum canopy height and optimum CHM pixel size were not unexpected given the strong influence of tree height on crown diameter (Chen *et al*., 2006). The suitability of certain pixel sizes for particular forest canopies has previously been explored in the scientific literature (Pouliot *et al*., 2002). For example, with regard to crown diameter to pixel ratios, Pouliot *et al*. (2002) suggested a lower and upper limit of 3:1 and 19:1 respectively. In comparison, the ratios (mean equivalent crown diameter) that produced the best tree crown delineations across the sample plots were slightly higher, between 10:1 and 35:1. This may be as a result of reduced intra-canopy variation within the CHMs caused by the image smoothing filters applied (Brandtberg *et al*., 2003; Koch *et al*., 2006). In addition, the examples presented by Pouliot *et al*. (2002) were also suggested for optical imagery rather than CHMs produced from ALS. Previous studies have also considered the impact of CHM resolution on segmentation accuracy, Stereńczak *et al*. (2008) for example, noted no significant difference between the ITC segmentation results

from the 0.25 m and 0.5 m resolution CHMs, however a significant reduction in the percentage of recognised ITCs was noted for the 1.0 m CHM. The results from previous research, in addition to those obtained in this study highlight the importance of selecting a suitable CHM pixel size for ITC segmentation. Nevertheless, in many cases the selected resolution of the CHMs utilised for ITC segmentations is governed by ALS point density (Khosravipour *et al*., 2014).

In relation to each of the CHM resolutions, several observed relationships require further discussion. Firstly, the 0.25 m CHM resolution performed consistently well across all sample plots, especially for the marker-controlled watershed segmentations, suggesting that this pixel size may be most suitable for the two study areas as a whole. This implies that at the 0.25 m resolution, enough detail is provided for the majority of ITCs to delineate boundaries without high levels intra-canopy variation resulting in over segmentations. However, in plots which exhibited a large maximum tree height (>30 m), the application of a lower resolution CHM (0.5 m) typically facilitated a greater percentage of successful ITC delineations. Again, the level of intra-crown variation provided in the CHM is likely to be the causal factor for this observation. With regard to the higher resolution CHMs (0.15 m) tested, a relationship between pixel size suitability and maximum tree height was also evident. In this instance, plots characterised by a small maximum tree height (<20 m) in general produced higher percentages of successful ITC delineations.

Nevertheless, it is important to note, that while these criteria explain the characteristic relationship between pixel size, maximum tree height and successful ITC delineation across the sample plots, variability in the observed trend was also evident in the dataset. This suggests that other plot characteristics such as variation in tree size and tree density may also influence the suitability of a particular CHM pixel size for ITC segmentation (Fang *et al*., 2016). Hence, it should be acknowledged that, while crown diameter should be recognised as a dominant variable influencing the suitability of pixel sizes for ITC delineation, consideration should also be given to other forest characteristics. In addition, it should also be recognised that the level of intra-canopy variation is also controlled by the filtering of the CHMs before segmentation (Chen *et al*., 2006). Consequently, relationships between the ITC delineation performance of CHMs at different resolutions and canopy height may be altered for CHMs subject to varying degrees of smoothing.

The research demonstrates that ITCs within larch stands affected by *P. ramorum* can be successfully delineated (>70%) using a pit-free CHM generation methodology, a marker-controlled watershed segmentation and the selection of an appropriate CHM pixel size. Nevertheless, whilst these methods provide successful results at the selected study sites, further testing would be required to consider the performance of these methods for defoliated canopies of other tree species in different forest environments. In addition, preliminary testing was used to identify the most suitable parameters in the filtering and segmentation processes, however such parameters can significantly influence final segmentation results and may not be best suited for other forest environments and ALS datasets (Erikson, 2004; Chen *et al*., 2006). Furthermore, an additional limitation to the study can also be noted with regard to the use of two separate study areas for the comparison between healthy and infected stands. Although larch dominated plots were selected to best match with regard to tree height parameters, variations in tree density and species composition may have also influenced the performance of ITC segmentations across the two sites.

4.6 Conclusions

The results presented in the study highlight that larch canopies partially or wholly defoliated as a result of *P. ramorum* infection can be successfully segmented (>70%). In addition, the research also demonstrates that the selection of segmentation algorithm, CHM generation method and CHM resolution can all impact on the performance of ITC delineations from ALS for larch forests in the UK. The marker-controlled watershed algorithm may provide better successful delineation percentages in comparison to the region growing method in mixed age plantation forests ($p < 0.10$), where the selected threshold value may limit the optimal application of the segmentation across all crowns. In the case of forests subject to moderate and severe defoliation due to *P. ramorum* infection, the application of a pit-free CHM generation method facilitated a greater ITC delineation percentage than segmentations using a standard CHM. With regard to CHM resolution, the results from the research suggest that a 0.25 m pixel size was most suitable for the larch dominated plots of all ages. In the case of the plots which exhibited large (>30 m) or small (<20 m) maximum tree heights, the selection of a lower (0.5 m) or higher (0.15 m) resolution CHM respectively, provided a more successful delineation. Overall, the results demonstrate that despite the increased presence of data pits in defoliated canopies, ITCs subject to infection from phytopathogens can be successfully identified

(> 70%). Whilst the presented methods provide a benchmark for the segmentation of ITCs subject to decline from phytopathogens, in order to consider the performance of this approach in other defoliated tree species and environments further research would be required.

Chapter 5: Airborne Laser Scanning and Tree Crown Fragmentation Metrics for the Assessment of *Phytophthora ramorum* Infected Larch Forest Stands

The research presented in this chapter has previously been published as:

Barnes, C., Balzter, H., Barrett, K., Eddy, J., Milner, S. and Suárez, J. C. (2017) Airborne Laser Scanning and Tree Crown Fragmentation Metrics for the Assessment of *Phytophthora ramorum* infected Larch Forest Stands. *Forest Ecology and Management*. **404**, 294-305.

5.1 Introduction

UK forestry has experienced notable introductions of several significant phytopathogens in recent decades (Brown *et al*., 2003; Brasier, 2008; Webber *et al*., 2008; Mitchell *et al*., 2014). Subsequent to its identification in the UK in 2002 (Lane *et al*., 2003), *P. ramorum* has caused extensive infection of larch (*Larix* spp.) trees, particularly across forests situated in Southwest England, South Wales and Southwest Scotland (Forestry Commission, 2016). The infection which can present both stem and foliar symptoms in affected larch, such as stem bleeds, foliage discolouration and defoliation (Webber *et al*., 2010) has resulted in the felling of over 16,000 ha of larch across the UK, including Japanese (*Larix kaempferi*), European (*Larix decidua*) and hybrid species (*Larix x eurolepis*) (Forestry Commission, 2014).

Current efforts to assess landscape-level patterns of *P. ramorum* infection and identify new outbreaks rely on visual aerial assessment conducted by tree-health surveyors during helicopter surveys. In this instance, foliar symptoms presented by infected larch aid the identification of *P. ramorum*. Figure 5.1 illustrates the foliar changes associated with the progression of *P. ramorum* infection in larch. The use of manual aerial detection highlights an opportunity for the application of remote sensing to detect and assess *P. ramorum* outbreaks in larch stands (Medcalf *et al*., 2011). Despite the increased recognition of remote sensing as a tool for the assessment of forest health and disease, visual surveys continue to dominate in the operational management of insect pests and phytopathogens in the forestry sector (Hall *et al*., 2016; Lausch *et al*., 2017). Commonly cited concerns and barriers to the application of remote sensing techniques for the assessment of forest condition include the perceived insufficient resolution

associated with optical satellite data and the costs associated with data acquisition and processing (Suárez *et al*., 2005; Rullan-Silva *et al*., 2013; Hall *et al*., 2016). Recognising the concerns of end-users is important for implementation of the results from scientific research into forestry management practise (Wulder *et al*., 2006).

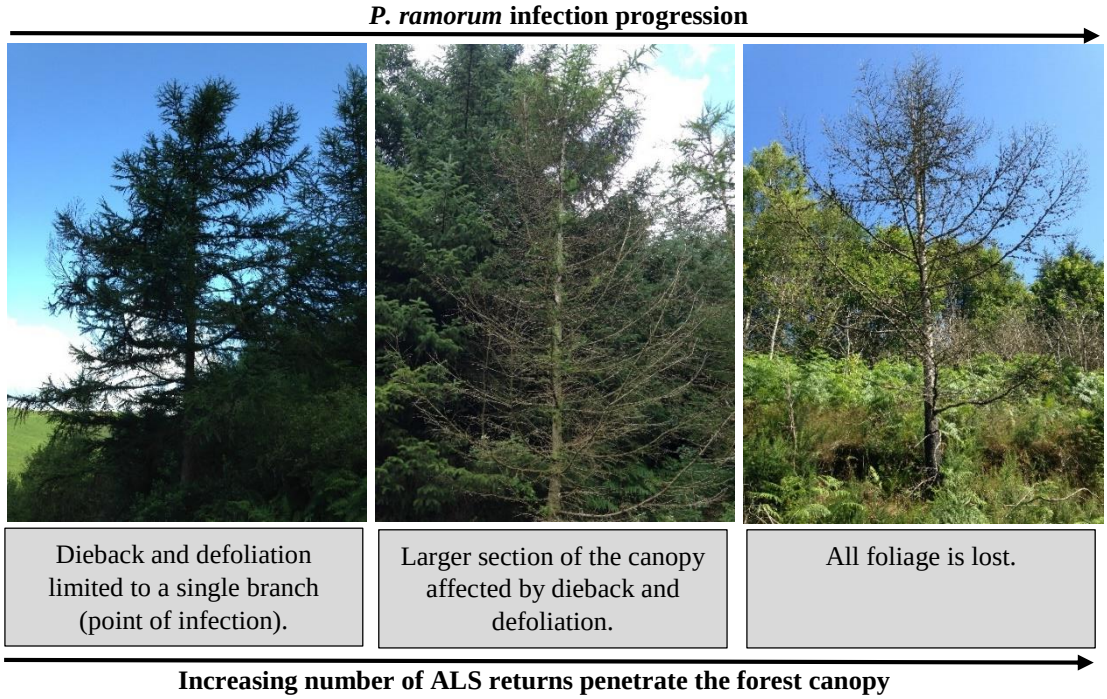

Figure 5.1 – *P. ramorum* disease progression in larch and its implications of ALS characteristics.

In forest research, remote sensing methodologies utilising ALS have been extensively applied to provide information regarding the structural character of vegetation in these landscapes (Lim *et al*., 2003; Wulder *et al*., 2013; Sheridan *et al*., 2015). ALS provides three-dimensional data that have previously been employed to examine biophysical forest parameters (Zimble *et al*., 2003; Balzter *et al*., 2007; Yoga *et al*., 2017). In addition, ALS datasets facilitate the segmentation of individual tree crowns (ITCs) (Brandtberg *et al*., 2003; Barnes *et al*., 2017b), which can subsequently be applied to determine ITC-based metrics such as tree height, crown diameter, canopy cover and species (Popescu *et al*., 2003; Holmgren and Persson, 2004; Reutebuch *et al*., 2005; Breidenbach *et al*., 2010).

One application of ALS for the assessment of crown condition utilises parameters derived from point clouds to assess the three-dimensional structure of trees and their canopies (Kwak *et al*., 2010). Previous studies have utilised height related metrics from ALS point clouds to characterise tree structure and identify crown decline for an array of applications including habitat suitability mapping (Martinuzzi *et al*., 2009; Casas *et al*.,

2016) and assessment of insect pest outbreaks (Bright *et al*., 2013). These metrics can be categorised into three broad categories including height-based metrics and percentiles, distributional metrics and cover metrics. Height-based metrics and percentiles summarise patterns regarding the height of ALS returns. Distributional metrics concern the distribution of returns through the canopy profile, whilst cover metrics typically compare two subsets of points to produce a variety of indices (Coops *et al*., 2009). In addition, ALS point cloud intensity characteristics, which concern the strength of pulse backscattering, have also been applied to the assessment of crown decline, largely with regards to the identification of dead trees (Kim *et al*., 2009; Wing *et al*., 2015; Casas *et al*., 2016).

In the specific context of disease outbreaks in forestry, a series of height related ALS-metrics including the number of canopy returns, maximum height, standard deviation of height, percentage of returns below 10%, 50%, 80% and 90% of total height and gap fraction have all previously been applied to the assessment tree crown condition (Solberg *et al*., 2006; Coops *et al*., 2009; Kantola *et al*., 2010; Vastaranta *et al*., 2013a). In particular, Kantola *et al*. (2010) and Vastaranta *et al*. (2013a) reported accuracies of 80.7% and 84.3% for the respective tree- and plot-level classifications of healthy and defoliated Scots pine (*Pinus sylvestris*) affected by the common pine sawfly *(Diprion pini*). The success of ALS height metrics for the assessment of insect pest defoliation can be attributed to the increased penetration of laser pulses into the forest canopy when foliage is lost (Coops *et al*., 2009; Kantola *et al*., 2010; Vastaranta *et al*., 2013a), as illustrated in Figure 5.1. Nevertheless, the potential use of these ALS-derived height metrics has not previously been considered for disease outbreaks resulting from phytopathogens such as *P. ramorum*.

In addition to the three-dimensional analysis of ALS point clouds, the impacts of dieback and defoliation of tree crowns are also evident in ALS-derived CHMs as increased irregularities in surface elevation across individual crowns (Holdenrieder *et al*., 2004). CHMs are a common raster product derived from ALS datasets to represent the canopy surface, typically computed via the subtraction of the DTM from the DSM which represent the rasterised last and first ALS returns respectively (Dubayah and Drake, 2000; Ben-Arie *et al*., 2009). As a result of increased penetration of ALS pulses through defoliated canopies, crowns subject to disease typically exhibit a patchy appearance when viewed as CHMs (Holdenrieder *et al*., 2004; Barnes *et al*., 2017b). Landscape metrics

traditionally applied to assess habitat fragmentation in the field of landscape ecology provide a means of quantifying the characteristics and spatial distribution of patches (Hargis *et al*., 1998; Kupfer, 2012). Resultantly, this chapter applies this series of metrics to assess the increased patchiness of CHMs for ITCs subject to disease.

Relationships between remotely sensed and ground-based metrics facilitate classifications of tree crown condition, providing a spatial representation of disease or decline throughout forest environments and hence a useful tool for disease management (Shendryk *et al*., 2016). The selection of disease severity category boundaries is particularly important, with difficulties previously noted in the differentiation between classes across the spectrum of moderate disease severity for forest insect pests (Coops *et al*., 2003; Leckie *et al*., 2005). A range of established classifiers including k-nearest neighbour (k-NN) and random forest (RF) have previously been applied to the classification of disease and vegetation structure (McInerney and Nieuwenhuis, 2009; Kantola *et al*., 2010; Bright *et al*., 2013; Ortiz *et al*., 2013), each presenting advantages and limitations, with suitability largely dependent on input data characteristics such as the quantity of training data and class separability (Huang *et al*., 2002; Samaniego *et al*., 2008).

5.2 Objectives

The aim of this research chapter was to:

> *Determine the capability of airborne laser scanning to identify Phytophthora ramorum infection in larch trees.*

To evaluate the applications of ALS point clouds and CHMs for the assessment of *P. ramorum* infection in plantation larch forest several key objectives were constructed. The main objectives for this research chapter are:

1. To evaluate the influence of tree height on ALS point cloud height metrics and CHM fragmentation metrics in healthy larch trees in plantation forest;
2. To assess the ability of ALS point cloud height metrics and CHM fragmentation metrics to discriminate between four categories of *P. ramorum* disease severity in plantation larch trees; and

3. To determine whether automatically segmented larch tree crowns can be correctly classified into *P. ramorum* presence and severity categories using ALS point cloud height metrics and CHM fragmentation metrics.

5.3 Methods

5.3.1 Ground Data Collection

Within the two established study sites, Ogmore Forest and Radnor Forest in Wales, UK outlined in Chapter 3, sixteen sample transects and plots were established (Chapter 3; Figure 3.4). To aid accessibility for ground surveying, a combination of plots and transects were established along sub-compartment edges. Table 5.1 provides a summary of the sample transects from both study sites, variation in transect lengths was incurred due to differences in sub-compartment dimensions. Training and validation datasets were subsequently identified by dividing each sampling area in half. This facilitated an equal spread of tree ages and disease severities across the training and validation datasets.

The 258 trees, 158 at Ogmore Forest and 100 at Radnor Forest, located within selected sampling areas at the two study sites were individually tagged, photographed and surveyed for species and diameter breast height (DBH). The position of each individual was recorded using a handheld Garmin Oregon 550t GPS. In circumstances of poor GPS positional accuracy (>2 m), the distance and bearing of individuals was also noted from a reference point situated outside the forest. Larch species, which formed the majority of surveyed individuals (84%), were subject to additional visual surveying of both the stem and crown to ascertain the overall tree health and the occurrence and severity of *P. ramorum* infection. The presence or absence of cankers, bark stripping and foliage colour change were noted, as well as percentage classes (10% intervals) of deadwood, defoliation, discolouration, wilting and canopy cover. Visual assessments were conducted by the same surveyor throughout the data collection to ensure consistency in recorded observations (Kantola *et al*., 2010; Nutter *et al*., 2010). Surveys were conducted in June, July and August 2015 coinciding with the acquisition of ALS data for both study sites by Bluesky International. At the infected study site, larch trees which exhibited characteristic cankers associated with *P. ramorum* were presumed infected. In circumstances where the presence of *P. ramorum* infection was not definitive from presented symptoms, a lateral flow device (LFD) was used to ascertain the presence of *Phytophthora* spp. in suspect

plant material (Kox *et al*., 2007). A total of three LFD tests were undertaken before a tree was classified as not infected, in order to reduce false negatives.

Table 5.1 – Characteristics of the sample transects and plots. Tree heights have been calculated using the ALS data (June 2015) and the size, number of trees and *P. ramorum* presence were recorded during field surveys (June, July and August 2015).

No.	Forest	Species	Max Height (m)	Min Height (m)	Mean Height (m)	Transect Length (m)* / Plot Size (m^2) $	No. Trees	*P. ramorum* Infection	Proportion of Larch Trees with *P. ramorum* Infection (%)
T1	Ogmore	HL, MB	8.41	4.03	6.01	100*	22	Yes	44
T2	Ogmore	HL, MB	11.54	4.98	8.82	100*	24	Yes	75
P3	Ogmore	JL	18.84	10.90	16.44	900$	22	Yes	75
T4	Ogmore	JL, SS	14.48	6.87	10.00	130*	30	Yes	95
T5	Ogmore	JL	16.64	9.09	13.80	30*	5	Yes	100
T6	Ogmore	JL	20.30	10.18	15.82	130*	9	Yes	100
T7	Ogmore	JL	21.52	11.90	18.87	50*	10	Yes	100
P8	Ogmore	JL	24.59	15.55	21.73	1000$	36	Yes	100
T9	Radnor	JL, MB	21.19	14.61	19.15	60*	11	No	N/A
T10	Radnor	HL, MB, MC	6.88	4.69	5.44	60*	15	No	N/A
T11	Radnor	JL, MB	19.58	13.14	15.65	60*	20	No	N/A
T12	Radnor	JL	32.78	22.69	29.33	60*	7	No	N/A
T13	Radnor	EL, HL	33.04	26.95	30.46	100*	12	No	N/A
T14	Radnor	SS	25.49	21.09	23.84	60*	5	No	N/A
T15	Radnor	JL	18.15	14.67	16.34	100*	9	No	N/A
T16	Radnor	JL	26.79	11.67	21.21	100*	21	No	N/A

Abbreviations: EL, European Larch; HL, Hybrid Larch; JL, Japanese Larch; SS, Sitka Spruce; MB, Mixed Broadleaves; MC, Mixed Conifers; N/A, Not Applicable.

To evaluate the severity of *P. ramorum* infections the scoring system presented in Table 5.2 was used to separately categorise the foliar and stem symptoms for each tree. The overall severity of *P. ramorum* infection was subsequently determined based on the highest value for the foliage and stem scores. In cases where a reliable survey could not be conducted or there were difficulties sampling suspected plant material, the individual was left uncategorised and removed from the analysis (total of 21 individuals). The selected number and boundaries of disease severity classes used in the scoring system for the study, reflects the previously poor performance of remote sensing in the differentiation between classes within the spectrum of moderate disease severity for forest insect pests (Coops *et al*., 2003; Leckie *et al*., 2005). In addition, the management requirements for disease severity data for *P. ramorum* cover two main areas of concern. Firstly, the identification of new infections (category 1) for the issuing of a statutory plant

health notice (Tracy, 2009) and secondly, concerns of public safety regarding trees subject to severe decline (category 3) and the associated reductions in structural integrity (Mistretta, 2002; Forestry Commission, 2014).

Table 5.2 – The scoring system applied to classify *P. ramorum* infections.

Score	Foliage Condition	Stem and Branch Condition
NI: Not Infected	No defoliation, discolouration or wilting.	No evidence of cankers, resin bleeds or deadwood.
1: Light	Defoliation, discolouration or wilting in <20% of the crown.	Cankers may be visible at one or two points on the stem/branches, but a large portion (>80%) of the stem and branches appear healthy.
2: Moderate	Defoliation, discolouration or wilting in 20% to 80% of the crown.	Cankers present and dead branches/portions of the stem may be noted. Between 20% to 80% of the stem/branches affected.
3: Heavy	Defoliation, discolouration or wilting in >80% of the crown.	Significant proportions of the main stem/branches visibly affected by infection (cankers, resin bleeds and deadwood) >80% of the stem and branches affected.

5.3.2 Airborne Laser Scanning Data Collection

The ALS data applied for the study is the same as that described in Chapter 4, Section 4.3.2.

5.3.3 Manual Individual Tree Crown Delineation

To produce reference polygons for each individual tree, ITCs were manually delineated. The manual delineation was performed using the ALS-derived data, in addition to photographs and GPS positions for individual trees recorded during ground surveys (Brandtberg and Walter, 1998; Fang *et al*., 2016). The polygons were applied to the extraction of ALS point cloud and CHM fragmentation metrics from training crowns and used as a basis for determining automated tree crown segmentation accuracy (Pouliot *et al*., 2002).

5.3.4 Metrics from Airborne Laser Scanning Point Cloud Height Values

ALS point clouds for individual trees in the training dataset were isolated using the manually delineated polygons. Subsequently, the lascanopy module within LAStools (LAStools, 2016) was used to derive several metrics based on the properties of ALS return pulses (Table 5.3) from normalised point clouds for each tree (Hopkinson *et al*., 2016; Nevalainen *et al*., 2017). For example, the bicentiles calculated for individual trees represent the proportion of ALS returns located below a specified percent of tree height

(Nevalainen *et al*., 2017). In order to remove the influence of understorey vegetation, height cut-off values, typically between 1 m and 2 m (Andersen, 2009; Hopkinson *et al*., 2016; Zellweger *et al*., 2016), are specified prior to metric calculation. In this study, a static cut-off of 1 m was employed due to the low levels of understorey vegetation across the two study sites. In addition, ALS point cloud metrics were also calculated using a variable cut-off height, set at 50% of tree height, to consider just the characteristics of the upper canopy (Vastaranta *et al*., 2013a). This top portion of the tree canopy is of particular interest for disease detection in the context of the study sites due to the higher vertical position of the live canopy in coniferous plantation environments with limited thinning management (Macdonald *et al*., 2009).

Table 5.3 – Metrics derived from ALS point cloud height values extracted from individual trees in the training dataset.

Metric	Definition
Max Height	Maximum tree height (m).
Skewness	The skewness of ALS returns above the cut-off height.
Bicentiles (B), where N = 10, 20, 30, 40, 50, 60, 70, 80 and 90)	The percentage of ALS returns whose heights are below N% of maximum tree height, after the subtraction of the height cut-off value.
Canopy Cover (CC)	The number of first ALS returns above the cut-off height divided by the total number of first ALS returns.
Canopy Density (CD)	The number of all ALS returns above the cut-off height divided by the total number of ALS returns.

5.3.5 Canopy Height Model Fragmentation Metrics

ALS normalised point clouds were used to construct a DTM (ground points) and DSM (maximum of all points) for the two study sites. CHMs were subsequently constructed by the subtraction of the DTM from the DSM (Jakubowski *et al*., 2013) with a pixel size of 0.15 m. This processing was undertaken in LAStools (LAStools, 2016). For the calculation of fragmentation metrics, CHMs for each individual tree were reclassified based on height. In the two-class reclassification ground and non-ground pixels were distinguished using a threshold value of 0.5 m, this value was selected to minimise the misclassification of ground related pixels. In addition, a three-class

reclassification was also performed to provide more specific consideration to changes in the lower and upper canopy. In this instance the reclassification applied the 1 m static cut-off value to remove understorey vegetation and considered the maximum tree height value extracted from the CHM using the criteria: ≤1 m, >1 m and ≤50% tree height, and > 0% tree height. Following the reclassification of the CHMs, landscape fragmentation metrics were calculated using FRAGSTATS (version 4.2) (McGarigal *et al*., 2012) for each individual tree within the training dataset. This approach defined the individual tree crown as the landscape and the height value categories as classes. Table 5.4 lists all landscape metrics calculated which concern a range of landscape fragmentation measures such as the area-edge relationships, the integrity of core area and the aggregation and diversity of patches within the landscape. Additional information regarding the calculation of metrics can be located in the FRAGSTATS users guide (McGarigal, 2015). An 8-pixel neighbourhood was applied to consider diagonal adjacencies in the definition of patches and in the case of metrics relating to core area a threshold of 1 m was applied.

Table 5.4 – Landscape fragmentation metrics extracted from individual tree crowns in the training dataset.

Metric	Abbrev.	Description
Number of Patches	NP	Number of patches in the landscape.
Patch Density	PD	Number of patches in the landscape divided by total landscape area.
Largest Patch Index	LPI	The percentage of the landscape covered by the largest patch.
Landscape Shape Index	LSI	Standardised measure for the total edge adjusted for the size of landscape.
Total Core Area	TCA	Total core area across the landscape.
Disjunct Core Area Density	DCAD	The number of disjunct core areas divided by total landscape area.
Core Area (Area Weighted Mean)	CORE_AM	Core area for the entire landscape as a percentage of total landscape area.
Euclidean Nearest Neighbour (Area Weighted Mean)	ENN_AM	Measure of patch isolation, area weighted mean of the shortest straight line distance between patches.
Percentage of Like Adjacencies	PLADJ	Sum of like adjacencies divided by the total number of cell adjacencies in the landscape.
Patch Cohesion Index	COHESION	Measure of physical connectedness, using patch perimeter and patch area.
Landscape Division Index	DIVISION	The probability that two randomly selected pixels are not situated in the same patch.
Patch Richness Density	PRD	Number of different patch types in the landscape divided by the total area of the landscape.
Shannon's Diversity Index	SHDI	From the field of ecology, is of indicator or patch diversity in the landscape. More sensitive to rare patch types than Simpson's Index.
Simpson's Diversity Index	SIDI	From the field of ecology, is of indicator or patch diversity in the landscape. More intuitive than the Shannon's Index.
Aggregation Index	AI	The number of like adjacencies with corresponding class divided by maximum possible number of like adjacencies with corresponding class.

5.3.6 Disease Severity Discrimination

Structural variability in ALS point clouds can also arise as a result of differences in stand age (Ørka *et al.*, 2009). Prior to the disease severity discrimination assessment, a linear regression analysis was conducted to determine any relationships present between the metrics (ALS point cloud and CHM fragmentation) and maximum tree height for individuals from the training dataset at the healthy Radnor Forest. Metrics which reported

a significant relationship with tree height were subsequently removed from further analysis and not considered as input variables for the disease severity classification.

To determine the disease severity discrimination potential of the ALS point cloud and CHM fragmentation metrics the Kruskal-Wallis test was applied with Mann-Whitney post hoc tests. The results of the Mann-Whitney post hoc testing were subject to a Bonferroni-Holm correction to limit the overall type I error for multiple testing (Ismail *et al*., 2007). In this instance, the application of the parametric analysis of variance (ANOVA) followed by Tukey's HSD tests (Coops *et al*., 2003; Ismail *et al*., 2007) was not appropriate as several datasets failed to meet the assumptions of normality (Shapiro-Wilk test $p < 0.05$) or homogeneity of variances (Levene's test $p < 0.05$). For the purpose of data analysis all individual trees, from both study sites, without *P. ramorum* have been grouped together to form the not infected (NI) category to be compared with the three disease severity categories (1, 2, and 3) (Table 5.2).

5.3.7 Automated Tree Crown Segmentation

The selected methodology for the automated ITC segmentation of validation crowns at the study sites for the disease presence/absence and severity classifications was based on the finding of Barnes *et al*. (2017b) presented in Chapter 4. A pit-free CHM was generated using the method specified by Khosravipour *et al*., 2014, which requires the construction of partial CHMs (2 m, 5 m, 10 m, 15 m and 20 m) which are then stacked in height order and the maximum value for each pixel is used for the generation of the CHM. CHMs were generated at three pixel sizes (0.15 m, 0.25 m and 0.5 m), with the most suitable pixel size for each plot selected on the basis of maximum tree height (Table 5.5). CHMs were subsequently subject to a low pass smoothing filter followed by the extraction of local maxima (>2 m in height) which were subject to a minimum distance filter, the sizing of both filters was also adjusted in accordance with the maximum tree height of the plot (Table 5.5). Finally, a marker-controlled watershed segmentation (Wang *et al*., 2004) was applied using the smoothed pit-free CHM and the previously extracted local maxima. Segments which failed to meet the minimum area threshold (Table 5.5) were merged with the neighbour of the longest common border (Koch *et al*., 2006). To determine the accuracy of the crown outlines resulting from the ITC segmentation, an automated assessment (Chapter 4; Table 4.6) was conducted to determine the percentage overlap of automated ITCs with the manually delineated reference crowns for the study areas (Barnes *et al*., 2017b) (Chapter 4; Section 4.3.10).

Segments classified in either the correct or satisfactory categories (Chapter 4; Table 4.6) were deemed successful for the purpose of the study and overall accuracy percentages were calculated using the ratio of successfully delineated validation crowns to the total number of validation individuals in sample transects/plots (Hu *et al*., 2014).

Table 5.5 – Parameters for filtering and smoothing prior to ITC segmentation.

Max Tree Height (m)	Local Maxima Distance Filter (m)	Smoothing Filter (Pixels)	Pixel Size (m)	Min Area Threshold (m^2)
≥15	1	5 x 5	0.15	0.5
>15 and <30	2	5 x 5	0.25	3
≥30	3	5 x 5	0.5	7

5.3.8 Classification

Successfully delineated automated ITC polygons for validation trees at the study site were subject to classification. Two sets of classification criteria were tested including presence (not infected and infected) and severity (categories 1, 2, 3 and NI), using ALS point cloud and CHM fragmentation metrics individually. A combination of ALS point cloud and CHM fragmentation metrics as input variables was also considered but this did not yield any improvement in classification. Two distinct classification approaches were used k-nearest neighbour (k-NN) and random forest (RF). For the implementation of the non-parametric pattern recognition classifier k-NN, the *K* value, which represents the number of samples considered for the classification of each feature (Collins *et al*., 2004; Melgani and Bruzzone, 2004; Yu *et al.*, 2006), was established using a grid search cross validation of the training sample testing *K* values ranging from 1 to 30 (Melgani and Bruzzone, 2004; Hsu *et al*., 2003). In the implementation of this classifier input data values were not normalised prior to classification.

The second classification method random forest (RF) (Breiman, 2001), is a non-parametric approach which generates a series of classification trees. Each tree is generated using a bootstrapped set of training samples, with the split at each tree governed by a randomised subset of input variables for each node (Hudak *et al*., 2008; Oliveira *et al*., 2012). The final classification result is subsequently determined based of the highest mean probability estimate across all trees (Belgiu and Drăguţ, 2016). Two important input parameters for the RF classification include the number of regression trees (n_{tree}) and the number of input variables at each split in the tree building process (m_{try}). Following a

preliminary grid search cross validation of the training dataset, the n_{tree} and m_{try} were set to 500 and 2 respectively, similar to the values applied in previous studies (Immitzer *et al*., 2012; Ortiz *et al*., 2013; Shendryk *et al*., 2016). All processing for the two classification methods was undertaken in Python using Scikit-learn (Pedregosa *et al*., 2011). An SVM classifier was also considered, but yielded poor results in preliminary testing.

Classification input variables were selected based on the results of the disease severity discrimination analysis and classification performance was reviewed using the overall accuracy percentage (OA) and Cohen's κ coefficient (Cohen, 1960). Interpretation of κ was based on the following categories: ≤0.20 is poor; >0.20 to ≤0.40 is fair; >0.40 to ≤0.60 is moderate; >0.60 to ≤0.80 is good; and >0.80 to ≤1 is very good (Landis and Koch, 1977). Confusion matrices were also employed to provide a more detailed evaluation of the most successful classifications (Congalton and Green, 1999).

5.4 Results

5.4.1 Tree Height

In the case of the ALS point cloud metrics, significant relationships ($p < 0.05$) were evident between the bicentiles B20, B30 and B50 (1 m cut-off height) and tree height (Table 5.6). As a result, B20, B30 and B50 were therefore removed from further analysis, in addition to B40 which was significant at the 90% confidence level. With regard to the CHM fragmentation metrics (Table 5.7) significant relationships ($p < 0.05$) with tree height were reported for all two-class metrics, excluding ENN_AM. For the three-class approach, seven metrics (NP, LSI, TCA, CORE_AM, ENN_AM, COHESION and PRD) exhibited a significant relationship ($p < 0.05$) with tree height. In light of these results all two-class metrics were removed from the disease severity analysis in addition to the seven significant three-class metrics, to reduce the potential influence of tree height on the disease severity analysis.

Table 5.6 – Coefficient of determination (R^2) and *p* values for the linear regression analysis between the ALS point cloud metrics and tree height (m) for training data from the healthy Radnor Forest. (* = significant $p < 0.05$).

ALS Metric	R^2 value		*p* value	
	1 m CoH	50% CoH	1 m CoH	50% CoH
Skewness	0.07	0.05	0.107	0.167
Canopy Cover	<0.01	<0.01	0.938	0.847
Canopy Density	0.05	0.02	0.174	0.361
B10	0.01	0.03	0.647	0.314
B20	0.11*	0.03	0.040*	0.320
B30	0.15*	<0.01	0.015*	0.747
B40	0.09	<0.01	0.058	0.847
B50	0.11*	0.01	0.043*	0.470
B60	0.06	0.03	0.144	0.280
B70	0.06	0.01	0.120	0.545
B80	0.06	<0.01	0.144	0.701
B90	<0.01	0.02	0.597	0.441

Abbreviations: CoH – Cut-off height

Table 5.7 – Coefficient of determination (R^2) and *p* values for the linear regression analysis between the CHM fragmentation metrics and tree height (m) for training data from the healthy Radnor Forest (* = significant $p < 0.05$).

Fragmentation Metric	R^2 value		*p* value	
	2 Class	3 Class	2 Class	3 Class
NP	0.27*	0.45*	0.001*	0.000*
PD	0.27*	0.10	0.001*	0.058
LPI	0.13*	0.10	0.023*	0.058
LSI	0.20*	0.41*	0.005*	0.000*
TCA	0.37*	0.20*	0.000*	0.004*
DCAD	0.18*	0.04	0.007*	0.236
CORE_AM	0.37*	0.16*	0.000*	0.012*
ENN_AM	0.07	0.20*	0.098	0.005*
PLADJ	0.51*	0.09	0.000*	0.064
COHESION	0.22*	0.42*	0.003*	0.000*
DIVISION	0.13*	0.08	0.025*	0.087
PRD	0.54*	0.59*	0.000*	0.000*
SHDI	0.11*	0.02	0.042*	0.380
SIDI	0.14*	0.06	0.021*	0.150
AI	0.17*	0.01	0.009*	0.535

5.4.2 Disease Severity Discrimination

Figure 5.2 shows the ALS point cloud height profiles and three-class reclassified CHMs for four individual trees across the disease severity categories. The ALS point cloud height profiles demonstrate a larger number of ground or near ground returns for the moderate and heavily infected individuals. In the case of the heavily infected individual, the ALS point cloud profile also demonstrates a greater spread of returns across the height of the tree. In addition, the reclassified (three-class) CHMs from diseased trees exhibit a patchier appearance, with an increased presence of low height values towards the centre of the crown for greater levels of infection. The height related

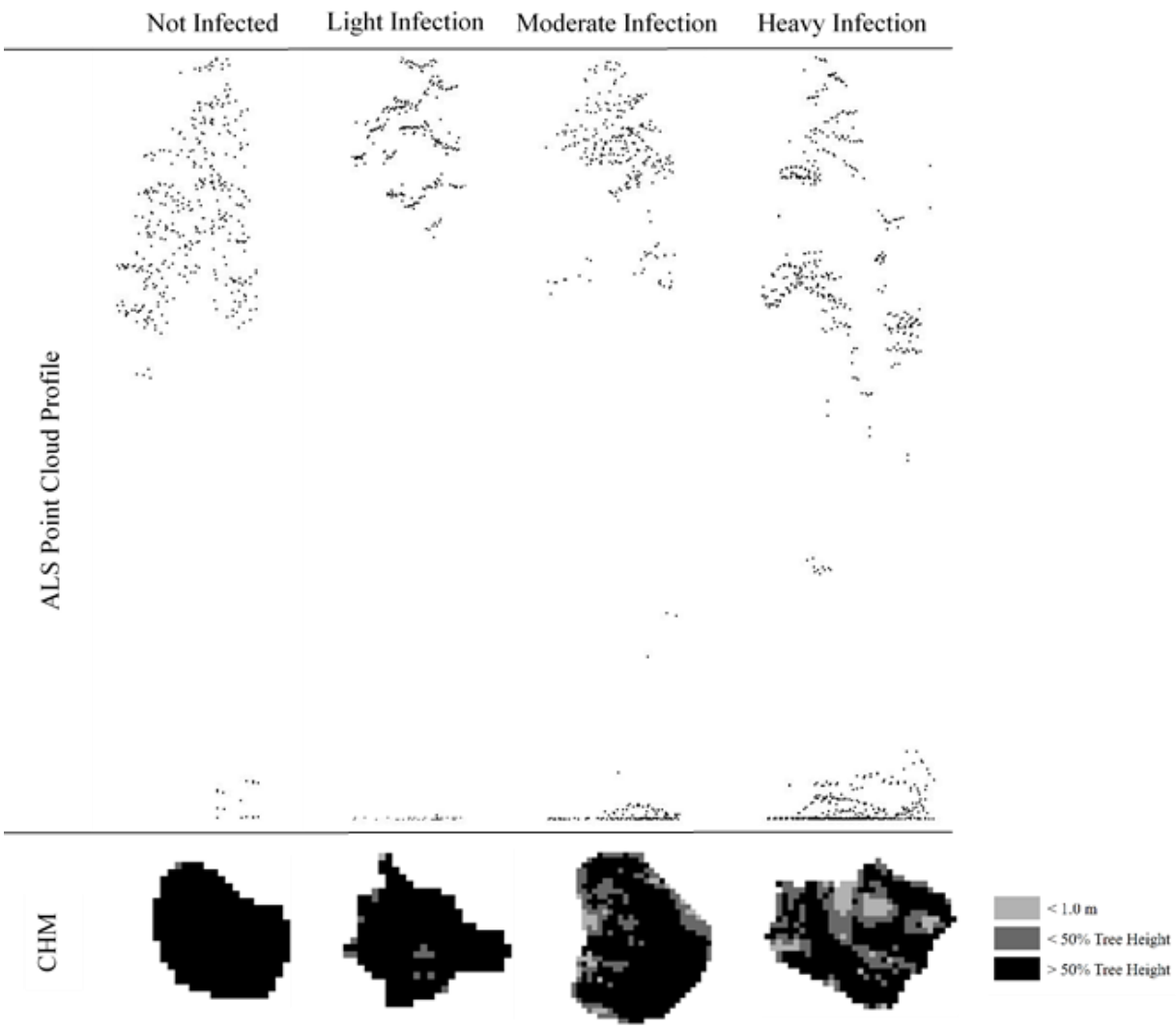

Figure 5.2 – The top four point clouds demonstrate the ALS point cloud vertical profiles for the four disease severity categories. The bottom four images show the horizontal CHM classified into three height categories (<1m; <50% tree height; >50% tree height) for individual trees across the four disease severity categories.

ALS point cloud and CHM fragmentation metrics calculated provide a quantification of these observations across all individual trees within the training dataset.

Tables 5.8 and 5.9 present the *p* values from the Krustal-Wallis test for the disease severity category discrimination for the ALS point cloud metrics and CHM fragmentation metrics respectively. The results from the analysis regarding ALS point cloud metrics demonstrated significant differences in the case of all point cloud metrics at the 50% cut-off height, with the same for the 1m cut-off height except for in the case of B10. In addition, all CHM fragmentation metrics tested also yielded significant differences between disease severity categories.

Table 5.8 - Krustal-Wallis test *p* values for disease severity discrimination from the ALS point cloud metrics (* = significant $p < 0.05$).

ALS Point Cloud Metric	1 m CoH	50% CoH
Skewness	0.002*	0.001*
Canopy Cover	<0.001*	0.002*
Canopy Density	<0.001*	0.006*
B10	0.487	0.005*
B60	0.014*	<0.001*
B70	0.002*	<0.001*
B80	0.001*	<0.001*
B90	<0.001*	<0.001*

Abbreviations: CoH – Cut-off height

Table 5.9 – Krustal-Wallis test *p* values for disease severity discrimination from the three-class CHM fragmentation metrics (* = significant $p < 0.05$).

Fragmentation Metric	*p* value
PD	<0.001*
LPI	0.001*
DCAD	0.001*
PLADJ	<0.001*
DIVISION	0.001*
SHDI	<0.001*
SIDI	0.001*
AI	<0.001*

To assess the difference in ALS point cloud and CHM fragmentation metrics for the four disease severity categories (NI, 1, 2 and 3) in more detail, Mann-Whitney post hoc tests with the Bonferroni-Holm correction for multiple comparisons were conducted. Table 5.10 presents the post hoc test results for the ALS point cloud (1m and 50% cut-off height) and CHM fragmentation metrics. In the case of the ALS point cloud metrics calculated using the static (1 m) and variable (50% of tree height) cut-off heights, significant differences were collectively observed between all disease severity categories excluding not infected (NI) and light infection (1). All ALS point cloud metrics demonstrated a significant difference between at least one set of disease severity categories except for B10 at the 1 m cut-off height. All of the CHM fragmentation metrics demonstrated significant differences between the disease severity category 3 (heavy infection) and all other severity categories (NI, 1 and 2), except for Disjunct Core Area Density (DCAD) which exhibited significant differences between categories 2 and NI, categories 3 and NI, and categories 2 and 3.

5.4.3 Automated Tree Crown Segmentation

The results depicted in Table 5.11 demonstrate the percentage of validation crowns successfully delineated via the automated tree crown segmentation. The large variation in successful delineation percentages across the sample areas is caused by the small number of validation crowns in some of the plots. Figure 5.3 demonstrates the segmentation results for P3 at the Ogmore Forest.

Table 5.10 – Mann-Whitney post hoc test results (with Bonferroni-Holm correction) for the ALS point cloud metrics at the static 1 m cut-off height and variable 50% cut-off height and CHM fragmentation metrics calculated with the three-class reclassification.

		1m CoH				50% CoH					Fragmentation 3 Class			
		1	2	3	NI	1	2	3	NI		1	2	3	NI
1	Skew		****	*	-		****	*	-	PD		-	**	-
2		****		-	*	****		-	*		-		**	
3		*	-		-	*	-		*		**	**		****
NI		-	*	-		-	*	*			-	-	****	
1	CC		-	****	-		-	*	-	LPI		-	***	-
2		-		***	-	-		****	*		-		****	-
3		****	***		****	*	****		**		***	****		****
NI		-	-	****		-	*	**			-	-	****	
1	CD		-	****	-		-	-	-	DCAD		-	-	-
2		-		***	-	-		****	-		-		****	*
3		****	***		****	-	****		**		-	****		**
NI		-	-	****		-	-	**			-	*	**	
1	B10		-	-	-		-	*	-	PLADJ		-	****	-
2		-		-	-	-		-	*		-		***	-
3		-	-		-	*	-		**		****	***		****
NI		-	-	-		-	*	**			-	-	****	
1	B60		*	-	-		***	***	-	DIV.		-	***	-
2		*		-	**	***		-	***		-		****	-
3		-	-		-	***	-		***		***	****		****
NI		-	**	-		-	***	***			-	-	****	
1	B70		***	-	-		***	****	-	SHDI		-	***	-
2		***		-	**	***		-	***		-		****	-
3		-	-		-	****	-		***		***	****		****
NI		-	**	-		-	***	***			-	-	****	
1	B80		***	**	-		***	***	-	SIDI		-	**	-
2		***		-	***	***		-	***		-		****	-
3		**	-		***	***	-		****		**	****		****
NI		-	***	***		-	***	****			-	-	****	
1	B90		**	**	-		-	**	-	AI		-	****	-
2		**		-	****	-		-	***		-		***	-
3		**	-		**	**	-		****		****	***		****
NI		-	****	**		-	***	****			-	-	****	

* $p < 0.10$; ** $p < 0.05$; *** $p < 0.01$; **** $p < 0.001$; - no significant difference. Abbreviations: CoH – Cut-off height; Skew – Skewness; CC – Canopy Cover; CD – Canopy Density; DIV- DIVISION.

Table 5.11 – Percentage of successfully delineated validation tree crowns for each of the sample plots and transects.

No.	Forest	Max Height (m)	Percentage of Test Crowns Successfully Delineated (%)
T1	Ogmore	8.41	63.64
T2	Ogmore	11.54	54.56
P3	Ogmore	18.84	90.91
T4	Ogmore	14.48	42.86
T5	Ogmore	16.64	100
T6	Ogmore	20.30	60
T7	Ogmore	21.52	60
P8	Ogmore	24.59	44.44
T9	Radnor	21.19	80
T10	Radnor	6.88	75
T11	Radnor	19.58	70
T12	Radnor	32.78	100
T13	Radnor	33.04	100
T14	Radnor	25.49	100
T15	Radnor	18.15	25
T16	Radnor	26.79	50

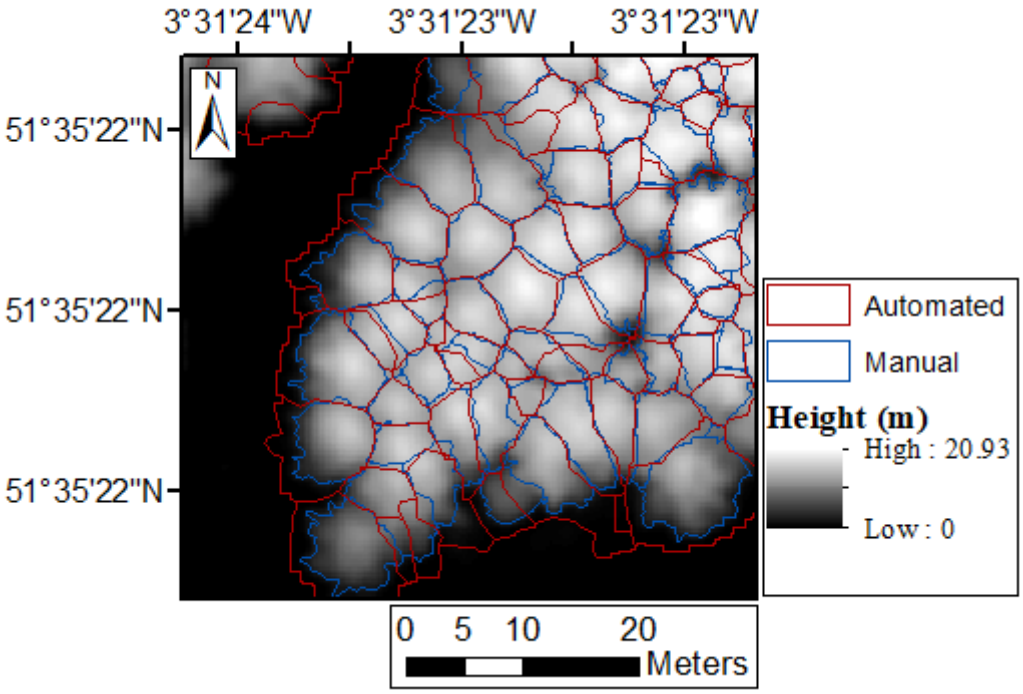

Figure 5.3 – Automated and manual tree crown segmentations for P3, Ogmore Forest

5.4.4 Disease Severity Classification

ALS Point Cloud Metrics

Table 5.12 presents the results from the best k-NN and RF classification of disease presence (infected and not infected) from the ALS point cloud metrics. Overall the best classification was achieved by the k-NN classification of the B80 and B90 (1 m cut-off height). Whilst the resulting κ of 0.32 can be interpreted as a fair classification (Landis and Koch, 1977), the high producer's accuracy (97.78%) for the not infected (NI) class and low number of false positives (1) suggest the classification performs well for healthy individuals, with most confusion resulting from the classification of infected individuals.

Table 5.12 - Confusion matrices for best performing k-NN and RF classification of disease presence (infected/not infected) using ALS point cloud metrics.

		k-NN			**RF**		
		Inputs: 1m cut-off height B80 and B90			**Inputs (Feature Importance)**: 50 % cut-off height Skewness (0.18), CC (0.17), B60 (0.21), B70 (0.23), B80 (0.21)		
		Classified			**Classified**		
		NI	IN	PA	NI	IN	PA
Reference	NI	44	1	97.78	26	19	57.78
	IN	19	8	29.63	10	17	62.96
	UA	69.84	88.88		72.22	47.22	
OA (%)				72.22			59.72
κ				0.32			0.21

Abbreviations: IN – Infected; NI – Not Infected.

The classification results from the k-NN and RF classifiers for disease severity using the ALS point cloud metrics are displayed in Table 5.13. Both performed best using the same input variables (50% cut-off height: skewness, canopy cover, B60, B70 and B80), with the k-NN classifier producing the highest overall accuracy (65.28%) and κ (0.27), which indicates a fair classification (Landis and Koch, 1977). Assessment of the confusion matrix demonstrated that particular difficulties were encountered with the classification of disease categories 1 and 2 which yielded poor user's (28.57%, 40%) and producer's (14.29%, 28.57%) accuracies. To illustrate the difference between the disease presence (2 class) and severity (3 class) classifications conducted, Figure 5.4 presents the classification results for P3 at the Ogmore site.

Table 5.13 - Confusion matrices for k-NN and RF classifications of disease severity categories (1: Light; 2: Moderate; 3: Heavy; NI: Not Infected) using ALS point cloud metrics.

		k-NN					**RF**				
		Inputs: 50% cut-off height Skewness, Canopy Cover, B60, B70, B80					**Inputs (Feature Importance)**: 50% cut-off height Skewness (0.18), CC (0.23), B60 (0.18), B70 (0.23), B80 (0.19).				
		Classified					**Classified**				
		1	2	3	NI	PA	1	2	3	NI	PA
Reference	1	2	0	0	12	14.29	5	0	2	7	35.71
	2	1	2	0	4	28.57	2	1	1	3	14.29
	3	0	2	3	1	50	0	0	5	1	83.33
	NI	4	1	0	40	88.89	6	2	10	27	60
	UA	28.57	40	100	70.18		38.46	33.33	27.78	71.05	
OA (%)						65.28					52.78
κ						0.27					0.23

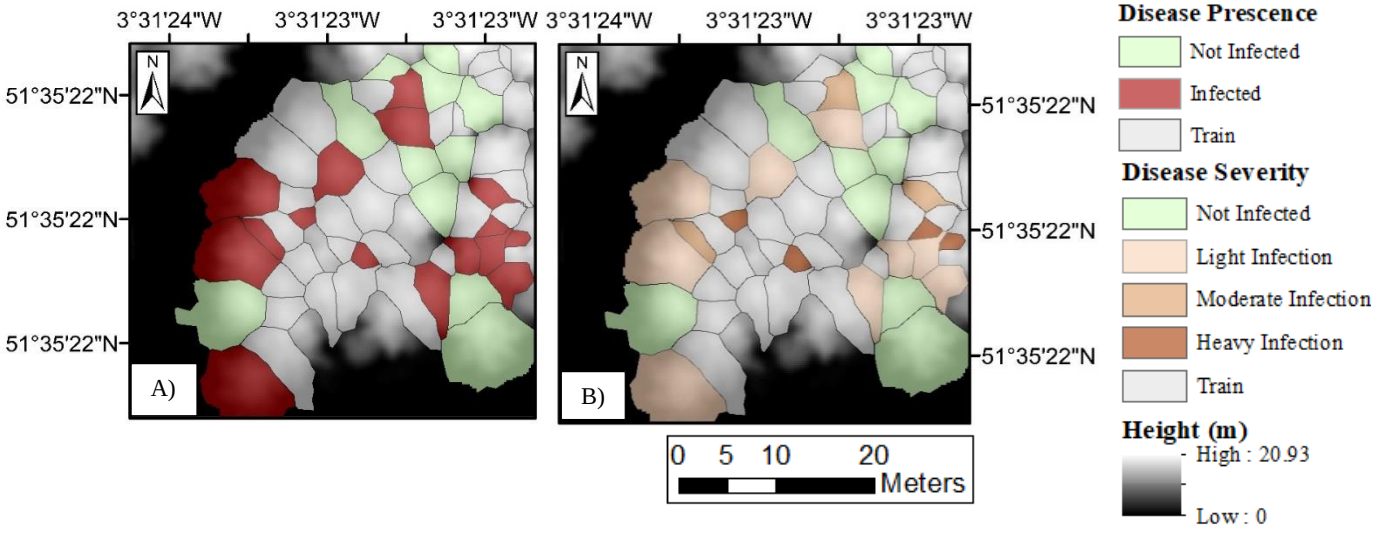

Figure 5.4 – Random Forest classification of A) Disease Presence and B) Disease Severity for P3 at the Ogmore Field Site.

CHM Fragmentation Metrics

The classification results in Tables 5.14 and 5.15 were achieved using all eight three-class CHM fragmentation metrics as input variables. In the case of the disease presence classification (Table 5.14), the k-NN classifier resulted in greatest overall accuracy (65.28%), whilst the RF classifier produced the highest κ at 0.21. The RF confusion matrix exhibited a low number of false negatives, with the majority of

confusion resulting from false positives. In the case of the disease severity classification (Table 5.15), the k-NN classifier was responsible for the best classification (OA = 68.06% and κ = 0.24). Difficulties in identifying categories 1 and 2 were clearly apparent with producer's and user's accuracies for both classes report as 0%. Consideration was given to combing the ALS point cloud and CHM fragmentation metrics but this did not improve the classification accuracies of disease presence or severity.

Table 5.14 – Confusion matrices for k-NN and RF classifications of disease presence (infected/not infected) using all three-class CHM fragmentation metrics.

		k-NN			**RF**		
		Classified			**Classified**		
		NI	IN	PA	NI	IN	PA
Reference	NI	40	5	88.89	19	26	42.22
	IN	20	7	25.93	5	22	81.48
	UA	66.67	58.33		79.17	45.83	
OA (%)				65.28			56.94
κ				0.17			0.21

RF feature importance: PD (0.15), LPI (0.09), DCAD (0.13), PLADJ (0.16), DIV (0.11), SHDI (0.12), SIDI (0.10), AI (0.13); Abbreviations: IN – Infected; NI – Not Infected.

Table 5.15 - Confusion matrices for k-NN and RF classifications of disease severity categories (1: Light; 2: Moderate; 3: Heavy; NI: Not Infected) using all three-class CHM fragmentation metrics.

		k-NN					**RF**				
		Classified					**Classified**				
		1	2	3	NI	PA	1	2	3	NI	PA
Reference	1	0	0	0	14	0	8	1	2	3	57.14
	2	0	0	0	7	0	2	0	2	3	0
	3	0	0	5	1	83.33	1	0	5	0	83.33
	NI	1	0	0	44	97.78	20	0	2	23	51.11
	UA	0	0	100	66.67		25.81	0	45.45	79.31	
OA (%)						68.06					50
κ						0.24					0.23

RF feature importance: PD (0.14), LPI (0.09), DCAD (0.11), PLADJ (0.16), DIV (0.12), SHDI (0.12), SIDI (0.11), AI (0.15).

Classification Limitations

In the case of the disease classifications performed using both the ALS point cloud and CHM fragmentation metrics, several key limitations require acknowledgement. Firstly, the small number of samples from each of the categories, especially in the case of the categories 2 (moderate) and 3 (heavy), fell below the recommended minimum

threshold for a statistically valid assessment (Van Genderen and Lock, 1977; Congalton, 1991), influencing the predictive capabilities of the classifiers (Melgani and Bruzzone, 2004; Belgiu and Drăguţ, 2016). In addition, the number of samples in each of the disease presence and severity categories was also unbalanced, providing potential difficulties in the ability of the classifiers to accurately separate individual classes (Muñoz-Marí *et al*., 2007; Belgiu and Drăguţ, 2016). Furthermore, the use of un-normalised data values in the implementation of the k-NN classifier may have also limited the performance of this particular classifier.

5.5 Discussion

The results highlighted the presence of a linear relationship between some of the ALS point cloud and CHM fragmentation metrics and tree height, demonstrating the influence of tree growth and canopy development on the structure and character of healthy larch crowns. For example, contrasts between crown height and density of foliage in younger and older stands can provide a different signal in metrics calculated from ALS for healthy individuals. The influence of tree height relationships for disease detection purposes in larch can be avoided for the ALS point cloud metrics when a variable cut-off height (50%) based on maximum tree height is applied. However, significant relationships between CHM fragmentation metrics and tree height were evident for both the two- and three-class approaches, although less fragmentation metrics exhibited a significant relationship in the case of the three-class methodology, which was selected for disease discrimination analysis. Resultantly, tree height demonstrates a dominant influence controlling the height-based ALS point cloud and CHM fragmentation metrics produced for individual trees and requires consideration in analysis regarding disease detection and assessment.

The disease severity discrimination analysis revealed that collectively, height-based ALS point cloud metrics exhibited significantly different values for all disease severity categories, except in the case of the not infected (NI) and light infection (1) categories. This highlights that structural canopy changes as the result of *P. ramorum* infection in the later stages of disease progression (categories 2 and 3) can be detected via the application of ALS point cloud metrics at the ITC-scale. This supports the findings of previous research regarding insect pests of coniferous tree species, which noted an increased penetration of ALS pulses through the canopy and a greater portion of ground

returns for canopies subject to defoliation as a result of insect attack (Coops *et al*., 2009; Bright *et al*., 2013). The difficulties noted with regard to the separation of not infected individuals and those in the early stages of infection has also been previously recognised within the scientific literature (Bater *et al*., 2010; Kantola *et al*., 2010). The results from this study indicate that even with high ALS point densities, metrics derived from ALS point clouds are unable to detect the very slight changes in canopy structure which are encountered in the early onset of the *P. ramorum* infection. In addition, discrete return ALS biases the resulting datasets against foliage located in the middle of the tree crown (Lovell *et al*., 2003). As a result, when early stages of infection are not present in the top of the canopy, detection via the application of discrete ALS point cloud metrics may also be more difficult.

The results from the disease severity discrimination analysis for the CHM fragmentation metrics demonstrate the potential applications of this group of metrics for the assessment of severe decline in ITC condition. Whilst significant differences were only consistently noted to provide separation of heavily infected individuals (category 3) with all other severity categories, this is likely to result from the CHMs representation of the canopy surface and the requirement of upper canopy fragmentation for disease detection. Nevertheless, the results indicate the previously untested value of CHM raster data for disease assessment in the absence of the original point cloud. Such results are also of particular interest from the perspective of deadwood mapping in forest environments (Martinuzzi *et al*., 2009; Pasher and King, 2009). The presence of significant results from a range of fragmentation metrics suggests in heavily infected larch trees (category 3) changes in ALS penetration across the upper canopy (Coops *et al*., 2009; Bright *et al*., 2013) can alter resulting height values in CHMs to a large enough extent to increase the fragmentation of height value classes in tree crowns. This effect changes the characteristics of core areas as well as increasing the complexity of height value patches in the tree crown landscape. The contrast in the mosaic of height class patches between heavily infected and healthy tree crowns is sufficient to provide a means of separating these individuals (Du-ning and Xiu-zhen, 1999). Nevertheless, the high point density of the ALS (24 points/m^2) facilitated the generation of the high resolution CHM (0.15 m) applied in this study. Further investigation is subsequently required to determine whether the same level of discrimination can be achieved for CHMs of a lower resolution (>0.15 m).

The results of the disease presence (not infected/infected) classification provided a straightforward indication of the value of ALS datasets for the detection of *P. ramorum* in larch species. The results indicated that the application of a k-NN classifier to ALS point cloud metrics (B80 and B90 1m cut-off height) could provide a fair classification ($\kappa = 0.32$), with an acceptable overall accuracy (72.22%). The greatest limitation of this classification is the poor performance of the infected classification (producer's accuracy 29.63%). Given the results of the disease severity discrimination with the Mann-Whitney post hoc analysis, it is likely that discriminating individuals within the not infected (NI) and light infection (category 1) categories are causing the greatest confusion. Kantola *et al*. (2010) set a defoliation level of 20% or more for their classification of Scots pine (*Pinus sylvestris*) defoliated by the common pine sawfly (*Diprion pini*). Acknowledging the limitations of the approach for the detection of individuals in the early stages of *P. ramorum* infection, a higher threshold of defoliation could be employed for operational use during disease detection. A defoliation threshold was not applied in this study as it was important to assess the overall success of ALS across the spectrum of *P. ramorum* disease severities. With regard to the superior performance of the k-NN in comparison the RF classifier, the less complex application of two input variables (B80 and B90 1m cut-off height) with a cross validated *K* value (Latifi *et al*., 2010) provided a better binary classification of *P. ramorum* infection than the more complex RF (McInerney and Nieuwenhuis, 2009).

The results from the disease severity classification yielded a fair classification ($\kappa = 0.23$ to 0.27), however no classifier or input metrics (ALS point cloud or CHM fragmentation) demonstrated a superior performance over the other. Assessment of the confusion matrices revealed that classification of the infected disease severity classes 1 and 2 were often the most problematic. Whilst classes applied in this study represented key areas of interest during the disease progression, each class exhibits a spectrum of crown conditions, causing difficulty in separating disease severity at specified threshold levels (Coops *et al*., 2003). The use of automated polygons representing tree crowns also results in further complications with regard to the extraction ALS point cloud and CHM fragmentation metrics from the validation crowns for classification. For example, whilst some automated crowns overlap perfectly with reference ITCs, those categorised as satisfactory may incorporate returns from neighbouring vegetation, potentially influencing the calculation of metrics employed as input variables. This effect could be

managed with more restrictive criteria, such as 60% or 70% minimum overlap, for determining successfully delineated automated crowns (Shendryk *et al*., 2016).

The overall classification accuracy of ALS point cloud metrics for discrimination of healthy and *P. ramorum* infected individuals was slightly below the 80.7% achieved for Scots pine (*Pinus sylvestris*) infected by the insect pest the common pine sawfly (*Diprion pini*) (Kantola *et al*., 2010). Nevertheless, the research presents the detection capabilities of ALS across the full spectrum of *P. ramorum* infection, including consideration for individuals in the early stage of infection. In addition, the characteristic impacts of each insect pest and phytopathogen on canopy structure is not uniform and direct comparison does not consider variations in pest- or phytopathogen-host interactions, symptom expression and species crown architecture (Lovett *et al*., 2006).

These results highlight the application of previously untested fragmentation metrics for the quantification the increased patchiness of tree crown CHMs subject to heavy *P. ramorum* infection. Whilst the results indicate the preferable application of ALS point cloud datasets for the assessment of *P. ramorum*, the availability of original datasets, expertise and resources for processing may present barriers in the operational applications of ALS in forestry. Therefore, a range of approaches to the application of ALS to disease assessment provides flexibility for forest management (Suárez *et al*., 2005; Hall *et al*., 2016).

Further consideration for the application of ALS to the detection and assessment of *P. ramorum* infection in larch should take into account the point density of ALS datasets. Whilst point density applied in this instance (24 points/m^2) can be considered high, low density datasets cannot be presumed to provide the same results (Kantola *et al*., 2010). Furthermore, as suggested by Coops *et al*., (2009), further understanding of the impact of disease on ALS point cloud metrics could be established with the application of pre- and post-infection ALS datasets. Such assessment can also be applied in the case of CHMs (Vastaranta *et al*., 2012). To fully assess the potential benefits of an approach based on remote sensing data in comparison to those presently achieved manually by visual assessment, a comparison between the two approaches would also be valuable to provide additional merit to a remote sensing-based method (Pasquarella *et al*., 2017).

5.6 Conclusions

The research demonstrates the successful application of ALS point cloud metrics to isolate ITCs of larch subject to moderate (category 2) and severe (category 3) *P. ramorum* infection based on the impacts of the disease on individual tree crown canopy structure. The results also highlight the merits of CHMs alone for isolating heavily infected individuals (category 3) via the first assessment of fragmentation metrics to quantify the patchiness exhibited by diseased tree crowns. Overall classification of disease presence and severity were best achieved using a k-NN classifier with percentages of 72.22% and 65.28% respectively. κ values for disease presence and severity of 0.32 and 0.27 respectively indicated a fair classification, with low values as a result of poor classification for infected individuals, particularly those within the early stages of infection (category 1). Whilst higher accuracies could be achieved by raising the threshold of symptomatic material for infected individuals, it was important to highlight the performance of ALS across the whole spectrum of *P. ramorum* infection levels. For operational applications regarding disease assessment in larch forests, the limitations of the technique in identifying ITCs subject to the early stages of disease establishment requires acknowledgment.

Chapter 6: Segmentation of Individual Tree Crowns in a Woodland Affected by Acute Oak Decline using an UAV-based Photogrammetric Digital Surface Model

6.1 Introduction

In the UK, the latest episodic incidence of AOD resulting from bacterial phytopathogens, has caused particular concern in recent years due to the rapid deterioration and high levels of mortality in affected individuals (Denman and Webber, 2009; Denman *et al*., 2010). AOD has been documented in native oak species including English oak (*Quercus robur*) and Sessile oak (*Quercus petraea*) as well as the non-native Turkey oak (*Quercus cerris*) (Denman *et al*., 2014). At present the geographic distribution of AOD in the UK extends across southern and midland England and into Wales. AOD affects mature oaks, causing the death of affected trees within as little as 4 years, following the appearance of initial symptoms. The most distinctive symptom associated with AOD is the presence of dark stem bleeds from lesions or vertical cracks between the bark plates. Crown condition also deteriorates as a result of AOD (Brady *et al*., 2010; Denman *et al*., 2010) (Figure 6.1), however the process of infection and

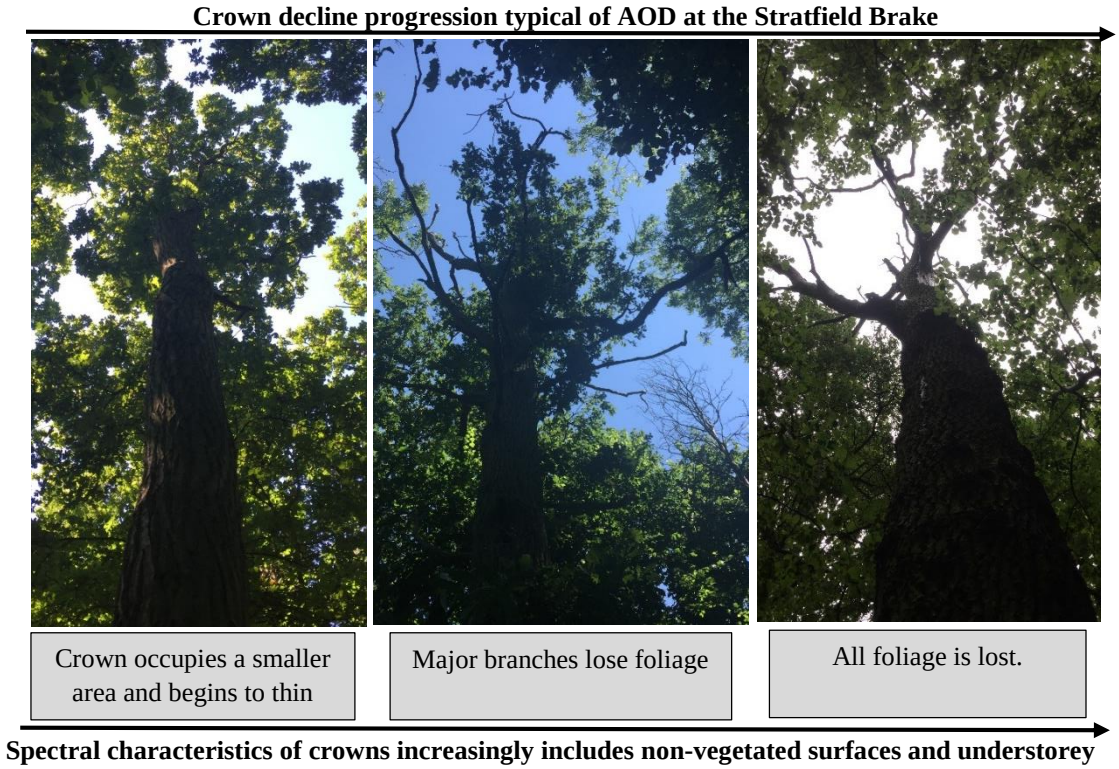

Figure 6.1 – Typical progression of crown decline in mature oak trees at Stratfield Brake and the expected changes in the spectral characteristics of tree crowns.

relationship between stem and foliar symptom severities are still unclear (Denman *et al*., 2014). Stems in the later stages of the decline may also present D-shaped exit holes caused by the opportunistic colonisation of the buprestid beetle (*Agrilus biguttatus*) (Denman *et al.*, 2010; Brown *et al*., 2015).

UAVs have been increasingly utilised in applications concerning environmental monitoring and assessment (Michez *et al*., 2016; Nevalainen *et al*., 2017). Remotely sensed data can be acquired using UAVs via both passive and active sensors and typically provides datasets of higher spatial resolutions than those obtained by other remote sensing platforms, such as aircraft and satellites (Salami *et al*. 2014). This advantage of UAVs, alongside their increased availability and relatively low cost of data acquisition, make the platform an attractive choice for remote sensing studies (Wallace, 2013; Getzin *et al*., 2014), especially for environments of limited spatial extent (Lehmann *et al*., 2015).

With regard to forestry, UAVs also provide a useful platform for the remote sensing of forest environments (Dunford *et al*., 2009; Nex and Remondino, 2014; Salami *et al*., 2014), although the present application of UAVs in this sector is typically experimental (Tang and Shao, 2015; Gambella *et al*., 2016). Key remote sensing products for the management of forests including orthophotographs, DSMs (Aicardi *et al*., 2016), and CHMs (Lisein *et al*., 2013) have all been generated via UAV platforms. These datasets acquired from UAVs have previously been applied to derive information regarding canopy structure (Wallace, 2013), forest gaps (Getzin *et al*., 2014), forest inventories (Wallace *et al*., 2012), forest fire monitoring (Ollero *et al*., 2006) and tree crown detection (Hung *et al*., 2012). The fine resolutions associated with UAV data capture, enables the extraction of biophysical parameters associated with ITCs within the forest canopy. In addition, low operational costs facilitate feasible monitoring programmes consisting of temporal datasets from repeat acquisitions (Aicardi *et al*., 2016).

ITCs can be automatically segmented from remotely sensed datasets representing canopy surface height. For example, ALS-derived CHMs, representing canopy surface elevation have commonly been applied to the segmentation of ITCs (Chen *et al*., 2006; Khosravipour *et al*., 2014). Surface elevation can also be extracted from remotely sensed images via the derivation of photogrammetry point clouds (PPCs). The production of three-dimensional models via photogrammetry requires the presence of illuminated

features in two or more overlapping images. The acquisition of imagery via UAVs can aid in the reduction of errors encountered in photogrammetry from airborne imagery due to increased distance from features, poor image overlap, and obstruction by surrounding features (Lindberg and Holmgren, 2017). PPCs have less commonly been applied than ALS-derived datasets to ITC segmentation (Rahlf *et al*., 2015) and typically provide a poorer characterisation of forest canopies due to the inability of optical sensors to penetrate through the canopy surface (Tanhuanpää *et al*., 2016). Previous research comparing the ITC success of ALS and PPCs has reported comparable or slightly poorer performance of PPCs for coniferous forests (St-Onge *et al*., 2015).

In the application of surface elevation (CHMs and DSMs) for the isolation of ITCs, the pixel size of input raster data influences the intra-crown variability and the performance of the overall segmentation. Resultantly, raster inputs to ITC segmentations can be resampled to provide the most suitable resolution (Ke and Quakenbush, 2011). Previous studies have considered the influence of pixel size on overall segmentation accuracy (Ene *et al*., 2012), acknowledging the influence of crown dimensions on pixel size suitability (Barnes *et al*., 2017b). To account for this, optimal crown diameter to pixel ratios ranging from 3:1 to 19:1 (Pouliot *et al*., 2002) and 10:1 to 35:1 (Barnes *et al*., 2017b) have previously been reported for optical inputs and ALS-derived CHMs respectively. Nevertheless, in the case of deciduous broadleaved crowns the calculation of crown diameter can be complicated by the increased irregularity of crown shape and overlap with surrounding tree crowns (Ke and Quackenbush, 2011; Chang *et al*., 2013).

A range of algorithms can be applied to the segmentation of ITC boundaries, these typically exploit structural differences exhibited by treetops, crown boundaries and canopy spaces (Wang *et al*., 2004; Chen *et al*., 2006). Many methods including the watershed algorithm require the prior identification of treetops within the canopy of interest to act as seed points for segmentation (Wang *et al*., 2004). Treetops are typically identified via the detection of local maxima across surfaces. Local maxima represent pixels in the input raster dataset where neighbouring pixels exhibit equal or lower values in height (Wang *et al*., 2004; Koch *et al*., 2006). Other studies have also applied contouring methods, which create contours at various levels of the forest canopy, to extract treetops from raster datasets of surface elevation (Koukoulas and Blackburn, 2005). The marker-controlled watershed segmentation applies the identified treetops as nodes from which the inverted input raster of “valleys” is “flooded”. The respective

boundaries for each tree crown are then delineated by establishing the "watershed" for each individual "valley" (Wang *et al*., 2004). Previous studies have successfully applied the marker-controlled watershed algorithm to the segmentation of ITCs in a range of forest environments including oak (*Quercus* spp.) savanna woodland (Chen *et al*., 2006), Korean pine (*Pinus koraiensis*), Japanese larch (*Larix leptolepis*) and oak (Quercus spp.) forest (Kwak *et al*., 2007), and diseased larch (*Larix* spp.) forest (Barnes *et al*., 2017b).

Forest structure is an important influencing factor for the success of ITC segmentation (Vauhkonen *et al*., 2012). A large number of ITC delineation studies have focused on coniferous plantation forest, with less emphasis on woodland environments comprising of deciduous broadleaved tree species. For some methods of ITC delineation, the conical shape of conifers makes them more suitable for isolation than deciduous canopies (Ke and Quakenbush, 2011). Additional difficulties in the detection and isolation of ITCs have also been noted with regard to forest environments subject to variable conditions (Tanhuanpää *et al*., 2016). For example, the extraction of local maxima has previously been less successful in forests characterised by high tree density, large variation in crown size and high degrees of tree crown overlap (Mei and Durrieu, 2004).

Further difficulties can be incurred in the segmentation of diseased trees due to the increased presences of canopy surface irregularities caused by defoliation and decline of crowns (Larsen *et al*., 2011; Barnes *et al*., 2017b). Previous research has successfully segmented diseased coniferous forest from ALS-derived CHMs (Barnes *et al*., 2017b) and image-based DSMs (Näsi *et al*., 2015), in addition to the identification of standing deadwood and snags with both ALS and optical datasets (Bütler and Schlaepfer, 2004; Kim *et al*., 2009; Pasher and King, 2009). However, preceding studies have not directly considered the application of photogrammetry-derived surface elevation the for the delineation of defoliated deciduous broadleaved canopies.

6.2 Objectives

The research conducted as part of this chapter aims to:

Consider the most appropriate method for the detection of treetops and segmentation ITCs using a photogrammetry-derived DSM acquired via UAV, for a mature oak-dominated woodland affected by AOD.

The key research objectives for the chapter are:

1. To evaluate the use of photogrammetry-derived DSMs acquired via UAV for the identification of treetops and crown boundaries in mature oak trees at five stages of crown decline;
2. To examine the performance of the local maxima and contour methods for the extraction of individual treetops in a mature oak-dominated woodland affected by AOD; and
3. To determine the influence of DSM pixel size on the performance of treetop detection and crown boundary segmentation in a mature oak-dominated woodland affected by AOD.

6.3 Methods

6.3.1 Ground Data Collection

Within the established field site at Stratfield Brake, Oxfordshire (Chapter 3; Section 3.2) a total of 189 individual trees across the training and validation areas were included in the ground surveys conducted in June 2016. All trees within the sampling areas which exceeded 15 cm in DBH and presented dominance or sub-dominance within the forest canopy were surveyed. Each individual was tagged with a unique ID number and the species and number of stems were noted. The location of each tree was also determined using a handheld Garmin Oregon 550t GPS. In circumstances of poor GPS positional accuracy (>2 m), the distance and bearing of individuals was also noted from a reference point situated outside the forest. The potential limitations of excluding smaller individuals on ITC delineation success and disease assessment was acknowledged, however this could not be achieved with a high degree of accuracy for the study site

Oak trees accounted for 84% of trees in the study area and were also assessed for the severity of crown decline. Crown decline, defined as the percentage of recent mortality within the live crown (Zarnoch *et al*., 2004), was recorded using a categorical scale of crown condition (Table 6.1) (Innes, 1990), previously applied to AOD assessment (Brown *et al*., 2016). The use of this particular categorisation provides a degree of consistency with regard to research conducted for this particular pathogen in oak species. The presence of stem bleeding was recorded, however high temperatures and heavy rainfall during fieldwork both reduced the likelihood of these being visible during

surveys (Denman *et al*., 2010). The occurrence of D-shaped *A. biguttatus* exit holes were also noted when present (Brown *et al*., 2016).

Table 6.1 – Crown decline severity categories (adapted from Innes, 1990).

No.	Category	Criteria
1	Dead	Standing dead tree
2	Severe Decline	Between 80 - 95% canopy missing
3	Moderate Decline	Canopy thinning between 30 - 80% and minor deadwood
4	Minor Decline	Between 10 - 30% of the crown missing
5	Healthy	No decline or deadwood

6.3.2 UAV Data Collection

Multispectral imagery was acquired for the mature woodland at Stratfield Brake on the 13 June 2016 via UAV. The Height Tech HT-8 C180 was used to carry the 150 g MicaSense RedEdge multispectral sensor which obtained imagery consisting of five spectral bands (blue: 465-485nm, green: 550-570nm, red: 663-673nm, red-edge: 712-722nm, near-infrared: 800-880nm). The flight was conducted at a height of 100 m, producing images with a pixel size of 0.06 m. Ground control points (GCPs) located using a real-time kinetic (RTK) GPS (Satlab SL300) were subsequently used to spatially reference the imagery. Pre- and post-flight calibration images were acquired for each of the five bands using a white reference reflectance panel, in order to account for changing light conditions during the flight (Albetis *et al*., 2017) which lasted approximately 15 minutes.

6.3.3 Data Processing

A georeferenced orthoimage was generated using the Pix4D software (Pix4D, 2016), which has been commonly applied for UAV image processing and photogrammetry (Feng *et al*., 2015; Rasmussen *et al*., 2016; Zhang *et al*., 2016; Albetis *et al*., 2017). The three GCPs obtained during data collection were located at the most open areas of the site and used to georeference the images with a spatial accuracy of 0.025 m. The resulting images were mosaicked and cropped to remove distortions present at image edges which occurred as a result of minimal image overlap (Figure 6.2). The orthomosaic was subsequently utilised to generate a photogrammetric point cloud (PPC) (25.2 point/m^2) and DSM with the Pix4D software, using the standard photogrammetry methodology and workflow described in McGlone (2013) which has previously been applied to UAV acquired imagery (Zhang *et al*., 2016).

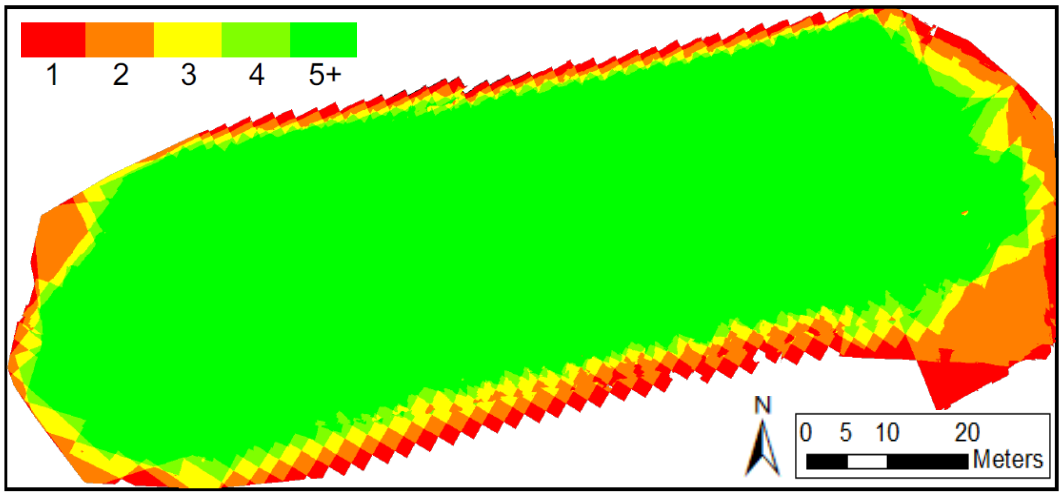

Figure 6.2 – Number of overlapping images from the UAV data collection.

6.3.4 Digital Surface Model

In many previous examples of ITC segmentation, the DSM is normalised via the subtraction of a DTM to create a CHM (Jakubowski *et al*., 2013). As the DSM in this instance was obtained from photogrammetry, as opposed to LiDAR, a DTM cannot be acquired from the UAV dataset (Nevalainen *et al*., 2017). Nevertheless, the ground elevation at the site was considered using an ALS-derived DTM (0.5 m pixel size) from the Environment Agency (UK Government Data, 2016). This demonstrated a ground level variation of 0.004 m. Even with the cited absolute height error of ± 0.15 m (Environment Agency, 2016) and potential overestimates of ground height (0.23 – 0.31

m mean signed error) incurred due to forest cover (Reutebuch *et al*., 2005; Su and Bork, 2006) the site exhibits very low variation in ground elevation. Subsequently it was determined that the DSM alone provided an accurate documentation of the canopy surface for the purpose of the study. The DSM was also resampled using a bilinear interpolation (Brandtberg and Walter, 1998) to pixel sixes of 0.15 m, 0.25 m and 0.5 m. These resolutions were selected based on their previous successful application in ITC studies (Pitkänen *et al*., 2004; Roberts *et al*., 2005; Solberg *et al*., 2006; Khosravipour *et al*., 2014; Barnes *et al*., 2017b) and the PPC point density.

6.3.5 Manual Individual Tree Crown Delineation

ITCs within the study area were manually delineated to provide a means of comparing automated segmentation results and to facilitate the extraction of information regarding tree character (Pouliot *et al*., 2002). In this instance the manual delineation was conducted using the multispectral imagery and DSM, in addition to the GPS positions and photographs recorded during field surveys (Figure 6.3) (Brandtberg and Walter, 1998; Fang *et al*., 2016). Whilst crowns of coniferous trees can be considered relatively circular in nature (Popescu and Wynne, 2004; Fang *et al*., 2016), deciduous broadleaved crowns typically exhibit more complex spatial dimensions (Chang *et al*., 2013). Consequently, inferring the diameter of oak crowns from the area of the crown as a circle (as previously applied for larch trees in Chapter 4; Section 4.3.5), would provide a poor diameter estimate (Ke and Quackenbush, 2011). To provide an indication of ITC spacing in the study area, a proximity analysis was conducted using the manually delineated polygons. Following the conversion of the manually delineated crowns to points located at the central location of each polygon, a proximity analysis was conducted to determine the distance to the closet neighbouring point. Whilst this approach has some limitations, largely the assumption that treetops are located at the centre of manually delineated crowns (Wang *et al*., 2004), it provides an indication of the spacing between treetops within the study area (Table 6.2), which can inform filtering and segmentation parameters (Chen *et al*., 2006; Koch *et al*., 2006). In addition, the area of each of the manually delineated tree crowns was also extracted to identify the minimum crown area for the study site as 2.43m^2. This can inform the threshold specified for merging small automated crowns during the post-processing of segmentation outputs.

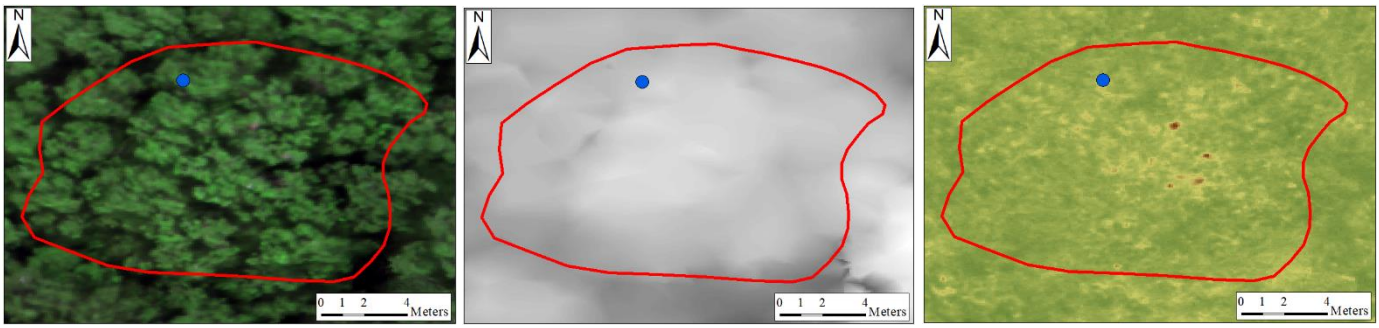

Figure 6.3 – The application of RGB (**Left**), DSM (**Middle**) and NDVI (**Right**) images as well as GPS position (blue point) to manually delineate crown boundaries (red polygon).

Table 6.2 – Proximity analysis results for the distance between the central point of manually delineated tree crowns and the closest neighbour. All values are presented in meters.

Min	P05	P20	Max.	Mean	Median	LQ	UQ
1.77	2.91	5.11	12.73	6.94	7.07	5.58	8.42

Abbreviations: P05 = 5th percentile; P20 = 20th percentile; LQ = Lower Quartile; UQ = Upper Quartile.

6.3.6 Pre-processing

To reduce intra-canopy irregularities across the DSMs, a Gaussian filter was applied to each of the three pixel sizes (0.15 m, 0.25 m and 0.5 m) (Brandtberg *et al.*, 2003; Koch *et al.*, 2006; Hyyppä *et al.*, 2012; Khosravipour *et al.*, 2014). The window size of the Gaussian filter (*d* x *d*) has previously been informed via the dimensions of the smallest crown (Wang *et al.*, 2004). In this instances the smallest distance between treetops was 1.77 m. However, 95% (P05) and 80% (P20) of treetops were >2.91 m and >5.11 m from the closest neighbour respectively (Table 6.2). Preliminary testing was conducted to consider the potential difference in segmentation results when selecting the minimum, P05 and P20 to inform the Gaussian filter size. Resultantly the Gaussian filter size for the study was informed by the P05 (2.91 m) and adjusted in accordance with the three pixel sizes (Monnet *et al.*, 2010) (Table 6.3). The standard deviation (σ), which has previously been noted to have minimal impact on the final smoothing produced by the filter (Dralle and Rudemo, 1996; Chen *et al.*, 2006), was set at 0.2*d* pixels (Jing *et al.*, 2012). In this instance the Gaussian filter was executed using SAGA GIS (SAGA GIS, 2016). Figure 6.4 provides a visual illustration of the impacts of the Gaussian filtering on the DSM.

Table 6.3 – Gaussian filter size (informed by P05 of treetop spacing) in pixels for the DSMs at the three different pixel sizes.

Size of Filter in Pixels Based on DSM Input Resolution (m)		
0.15	**0.25**	**0.5**
19 x 19	11 x 11	5 x 5

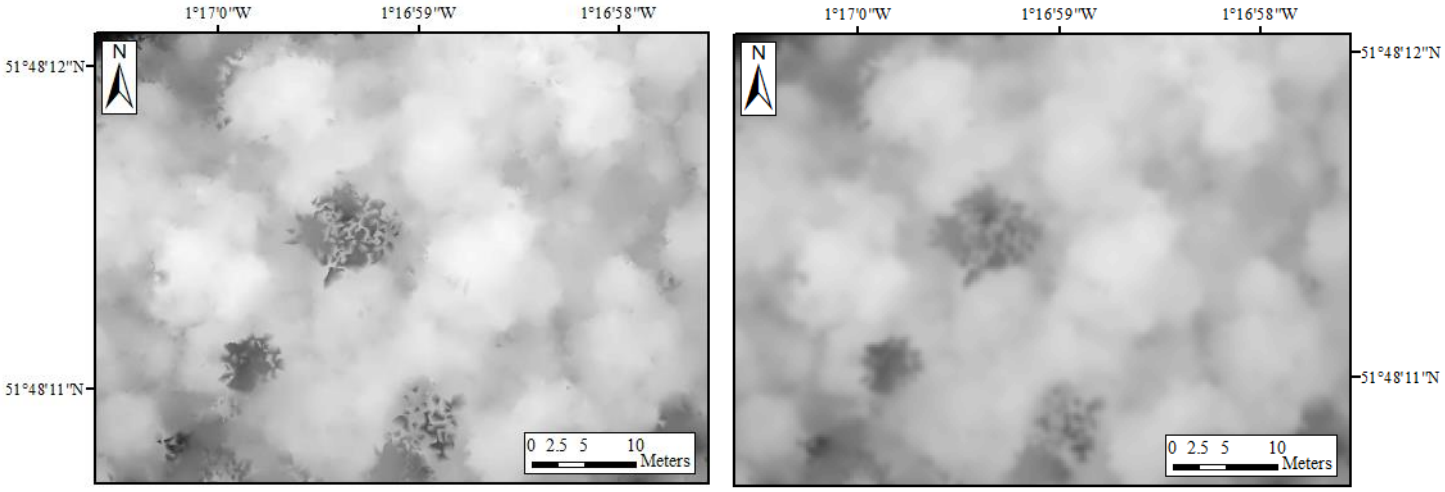

Figure 6.4 – **Left**: DSM (0.25 m) without filtering. **Right**: DSM (2.25) with Gaussian filter.

6.3.7 Local Maxima

One method applied to generate seed inputs for ITC segmentation was to extract point of local maxima from the filtered images. In order to prevent the over-segmentation of tree crowns local maxima are typically selected with minimal distance thresholds informed by crown spacing. As with the Gaussian filter sizes, preliminary tests were conducted to determine the overall performance of local maxima minimal distance thresholds informed by the minimum, P05 and P20 of treetop spacing. Resultantly the minimal distance threshold for the local maxima extraction was informed by the minimum distance (1.77 m) between treetops and rounded to the closest multiple for each of the three pixel sizes (Table 6.4) (Monnet *et al*., 2010). The local maxima extraction was executed in Python using Scikit Image (Van der Walt *et al*., 2014). Figure 6.5 illustrates the filtered local maxima produced for Stratfield Brake.

Table 6.4 – Minimal distance threshold (informed by minimum distance of treetop spacing) in pixels for the DSMs at the three different pixel sizes.

Size of Minimal Distance in Pixels Based on DSM Input Resolution (m).		
0.15	**0.25**	**0.5**
13	7	3

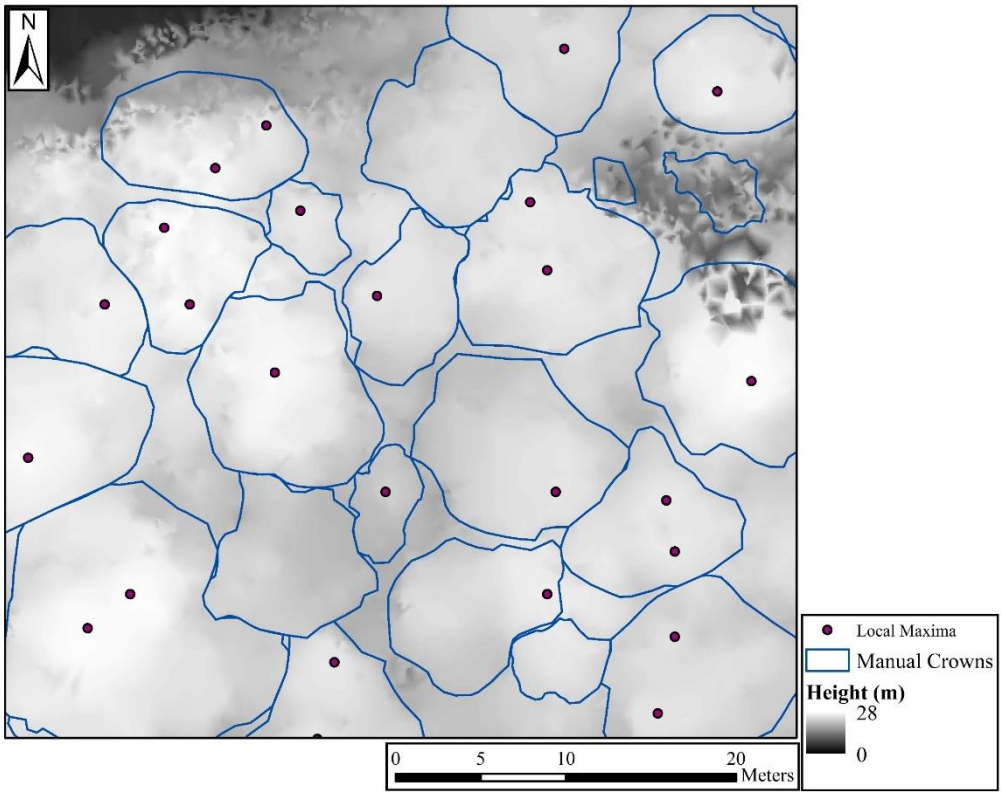

Figure 6.5 – The filtered local maxima points for Stratfield Brake displayed alongside the DSM and the manually delineated tree crowns.

6.3.8 Contour Method

The contour method outlined by Koukoulas and Blackburn (2005) has also previously been applied to the extraction of deciduous treetops in UK forests. In this instance, individual trees are isolated as single polygons through the construction, filtering and dissolving of contours created at various height intervals in the forest canopy (Figure 6.6). Resulting treetops are extracted as the central point from each of the final polygons. Figure 6.7 provides a detailed workflow of each step undertaken in this approach to treetop identification. All processing for the method was undertaken in ArcMap (version 10.5).

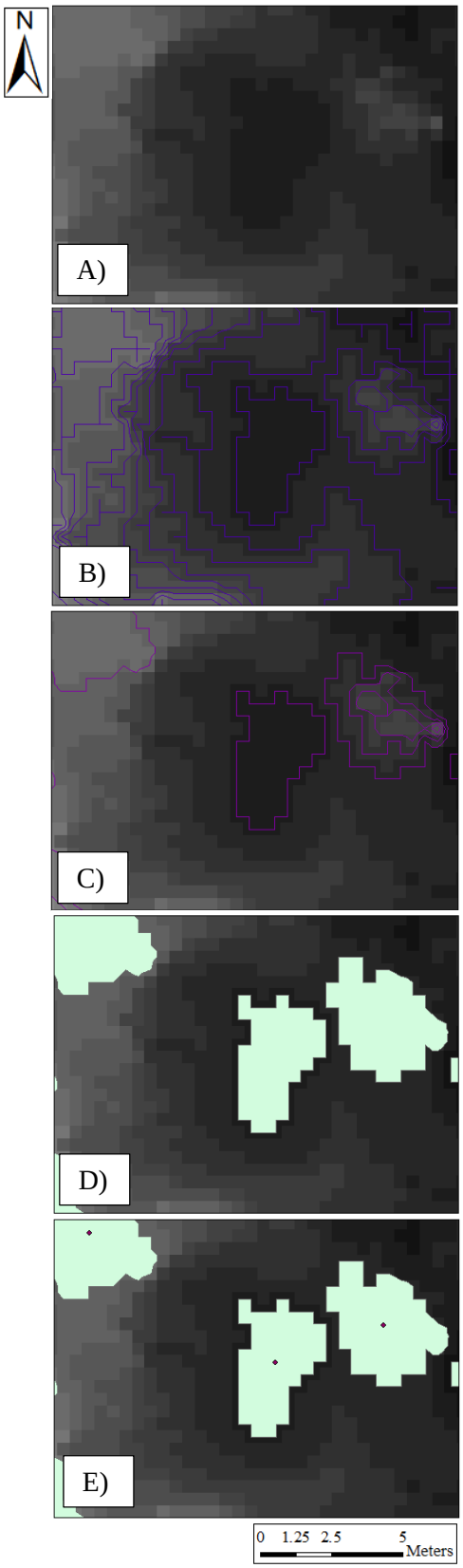

Figure 6.6 – Illustration of the contour method for treetop extraction. A) Reclassify DSM. B) Contour generation. C) Contour length filter. D) Dissolve Polygons. E) Generate treetops at centre of polygon.

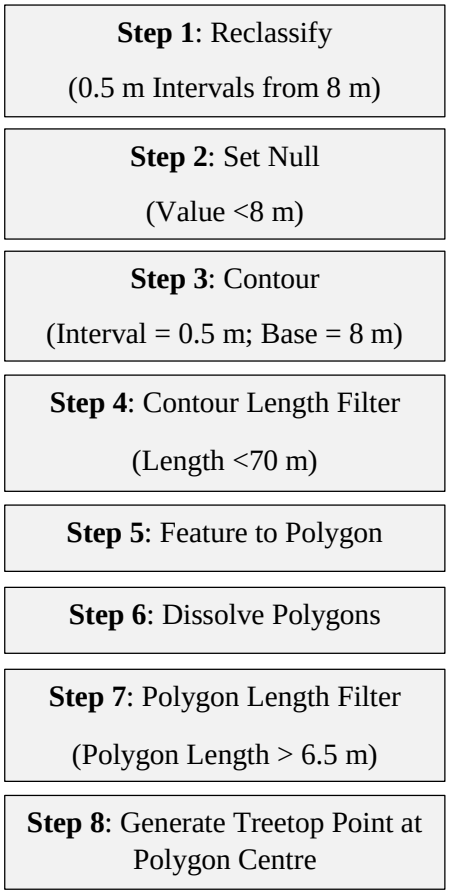

Figure 6.7 – Workflow for the contour approach methodology to treetop extraction.

6.3.9 Individual Tree Crown Segmentation

DSMs across the three pixel sizes were inverted and applied alongside the treetops, from the best overall performing extraction method (local maxima or contour), as inputs for the marker-controlled watershed segmentation, executed in Python using Scikit Image (Van der Walt *et al.*, 2014). Resulting segments were subsequently converted to polygons, those which fell below the minimum area threshold of 2.43 m^2, determined from the manual polygons, were merged with the neighbour of the longest common border (Koch *et al.*, 2006). The application of a region growing algorithm (Chapter 4; Section 4.3.8) was also considered, however preliminary testing yielded poor results for a range of specified threshold values. Figure 6.8 provides an illustration of the automated tree crowns produced for the Stratfield Brake site.

6.3.10 Accuracy Assessment

To provide a comprehensive assessment of the accuracy of the segmentation, treetop points and automated ITC segments were both subject to accuracy assessment. In the case of the treetops, successful detection was determined in instances where a single

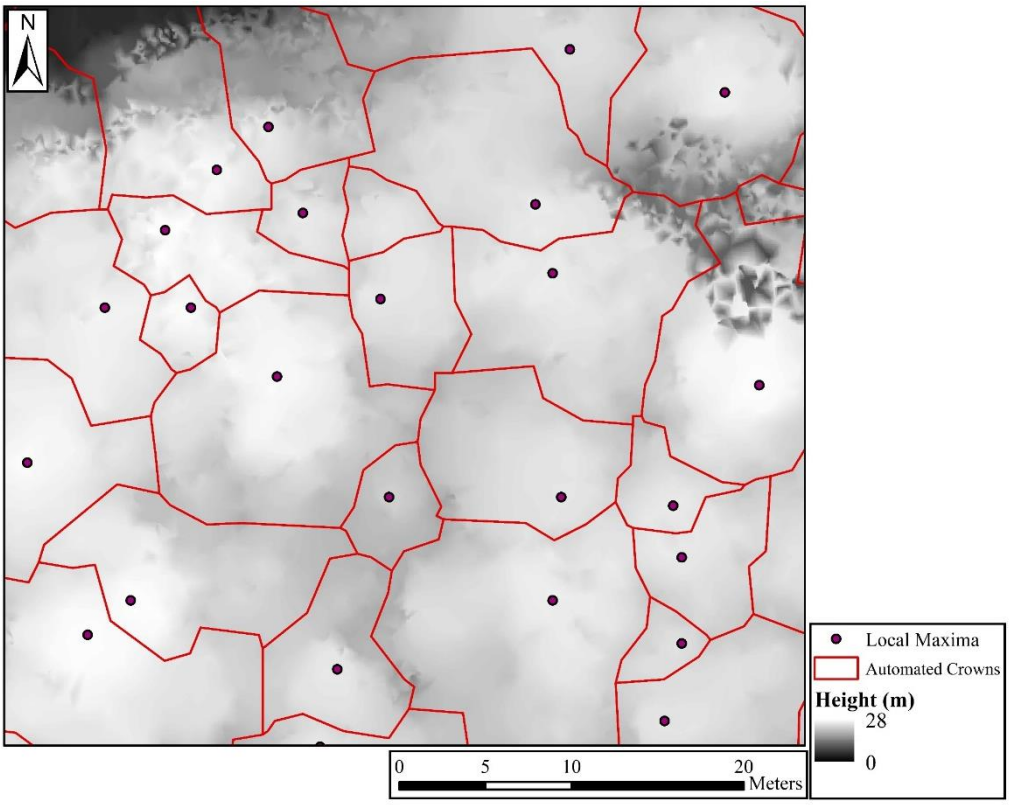

Figure 6.8 – The automated individual tree crowns for Stratfield Brake displayed alongside the local maxima points and DSM.

treetop was associated with one manually delineated tree crown (Ke and Quakenbush, 2011; Khosravipour *et al*., 2014). The overall accuracy for the treetop detection was subsequently calculated using the ratio of successful detected treetops to the total number of trees (Ke and Quackenbush, 2011). In the case of the ITC boundaries, the segmentation performance was determined using the automated accuracy assessment described in Chapter 4, Section 4.3.10. As with the treetops, accuracy percentages were calculated using ratio of successful delineations (Chapter 4; Table 4.6) to the total number of reference tree crowns (Chen *et al*., 2006; Hu *et al*., 2014).

6.3.11 Data Analysis

To evaluate the influence of generation method on treetop detection success, the non-parametric Wilcoxon signed rank test was used to analyse the difference in treetop detection accuracy produced for each of the three DSM pixel sizes. The equivalent parametric paired t-test was not selected as several datasets produced from the contour method did not meet the assumption of normality (Shapiro-Wilk test $p < 0.05$). To address the additional type 1 error incurred via multiple testing, the Bonferroni-Holm sequential correction was also applied to the results of the statistical testing.

6.4 Results

6.4.1 Treetop Generation Method

Table 6.5 presents the treetop detection success percentages for the local maxima and contour methodologies. Overall the local maxima method for treetop generation performed best (59.21 - 63.16%) across all three pixel sizes (0.15m, 0.25m and 0.5m). Nevertheless, the contour method of treetop extraction did perform favourably in the case of categories 1 and 2. The Wilcoxon signed rank test results reported no significant differences between the performance of the two treetop generation methods (Table 6.6). Resultantly, the local maxima treetops were selected as the inputs for the marker-controlled watershed segmentation.

Table 6.5 – Treetop detection results for the local maxima (LM) and contour methods for all five crown decline categories and DSM pixel sizes.

	0.15 m		**0.25 m**		**0.5 m**	
	LM	**Contour**	**LM**	**Contour**	**LM**	**Contour**
Cat 1	23.81	33.33	28.57	33.33	23.81	28.57
Cat 2	50.00	50.00	43.75	56.25	43.75	56.25
Cat 3	75.00	62.50	75.00	61.11	72.22	56.94
Cat 4	71.88	59.38	71.88	59.38	65.63	56.25
Cat 5	54.55	54.55	54.55	54.55	45.45	45.45
Total	63.16	55.92	63.16	55.92	59.21	51.97

Table 6.6 – *p* values for Wilcoxon signed rank test, after Bonferroni-Holm correction, comparing results from the two treetop generation methods (local maxima and contour) across the three DSM pixel sizes.

0.15 m	**0.25 m**	**0.5 m**
0.828	1.000	1.000

6.4.2 Crown Decline Severity Category

Differences in treetop detection (Table 6.5) and ITC segmentation (Table 6.7) accuracy percentages were observed across the five crown decline severity categories. Large variability was observed between the reported results for across the five categories for both treetop detection (28.37 – 51.19%) and ITC segmentation (39.10 – 48.02%), with

categories 1 and 3 consistently yielding the lowest and highest overall accuracy percentages respectively. Figure 6.9 presents the percentage of ITCs classified in each of the five accuracy assessment categories (correct, satisfactory, over-sized, split and missed) (Chapter 4; Table 4.6) for each of the three DSM pixel sizes tested. In the case of all three pixel sizes, the greatest proportion of trees were typically categorised as oversized.

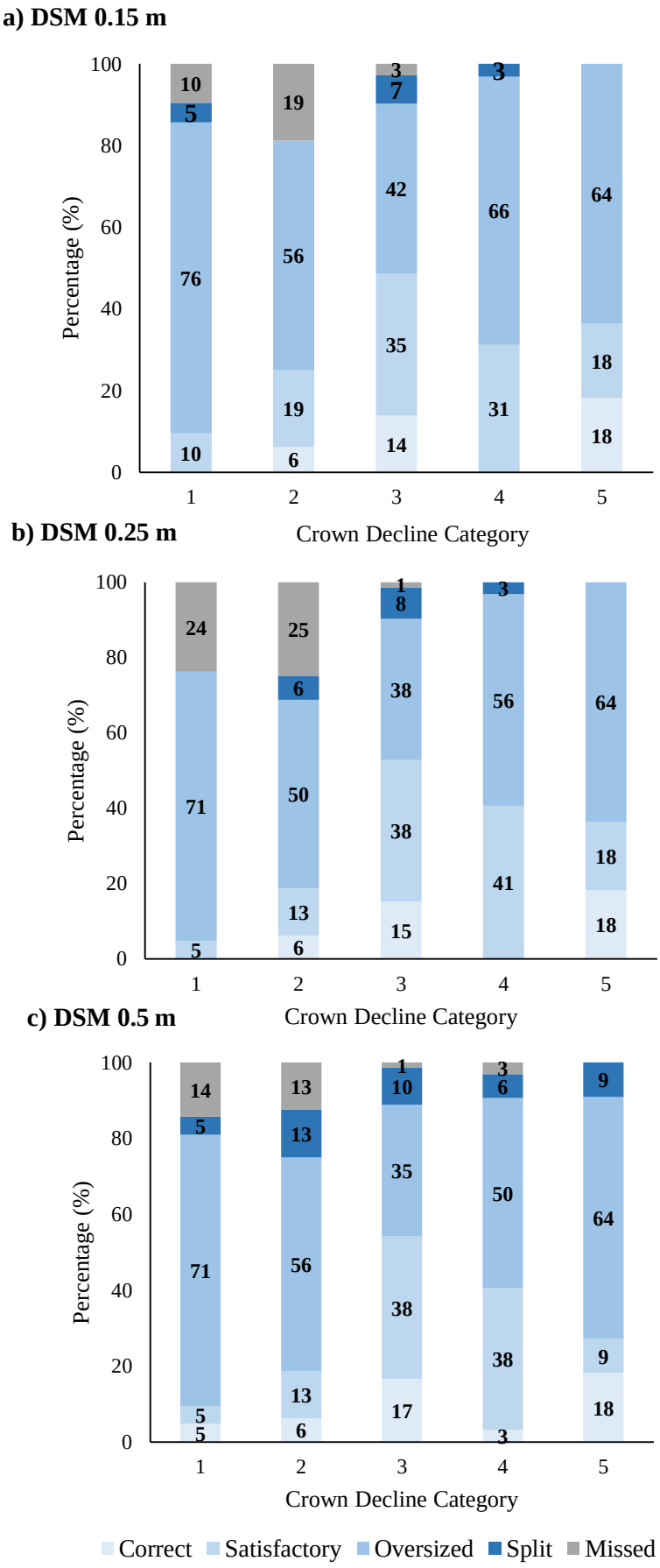

Figure 6.9 – The percentage of trees in each of the five crown decline severity categories classified in the five accuracy assessment categories for ITC segmentations conducted for the 0.15 m (a), 0.25 m (b) and 0.5 m (c) pixel sizes.

Table 6.7 – ITC segmentation results for all five crown decline categories and all three DSM pixel sizes.

	Successful ITC Segmentation (%)		
	DSM Pixel Size (m)		
	0.15	**0.25**	**0.5**
Cat 1	9.52	4.76	9.52
Cat 2	25.00	18.75	18.75
Cat 3	48.62	52.78	54.17
Cat 4	31.25	40.63	40.63
Cat 5	36.36	36.36	27.27
Total	36.18	38.82	39.47

6.4.3 Pixel Size

The variability in total overall accuracies across the three pixel sizes was 3.95% for treetop detection (local maxima method) and 3.29% for ITC segmentation. In the case of treetop detection (local maxima method) the 0.15 m and 0.25 m resolutions performed best (66.16%). However, in contrast, the 0.5 m pixel size yielded the highest total overall accuracy (39.47%) for the ITC segmentation. Figure 6.10 displays the variability in the

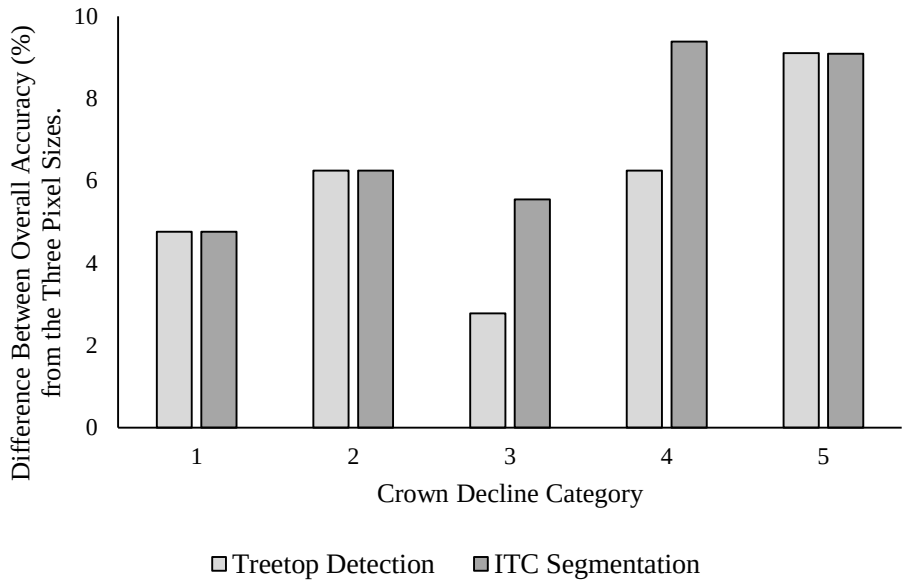

Figure 6.10 – Difference between the highest and lowest overall accuracy values for treetop detection and ITC segmentation reported across the three DSM pixel sizes (0.15 m, 0.25 m and 0.5 m) for each of the crown decline severity classes (1 to 5).

treetop detection and ITC segmentation accuracies across the three DSM pixel sizes for the five crown decline severity classes. Whilst all classes demonstrated low levels of variability (<10%), the highest variation was typically noted in the healthiest trees.

6.5 Discussion

The overall treetop detection accuracies reported for both the local maxima and contour methods (51.97% - 63.16%) yielded inadequate results for operational treetop identification in forest environments. The consistently poorer overall performance of the contour method across the three pixel sizes tested, could be explained by the inability of the user-defined thresholds in the methodology (contour interval and base height, contour length filter, and polygon length filter) (Koukoulas and Blackburn, 2005) to accommodate the variety in crown size and shape experienced across the structurally heterogeneous Stratfield Brake field site. This influencing factor can also be considered in the explanation of the limited performance of the local maxima method (Katoh and Gougeon, 2012), however only one user-defined parameter, minimum distance, is required for this particular approach (Ke and Quackenbush, 2011). In the case of local maxima extraction, previous studies have applied variable minimum distance filters utilising the relationship between crown dimensions and tree height (Chen *et al*., 2006). However, weak relationships between crown diameter and tree height can result in poor estimates of tree crown diameter and the application of inappropriate filter sizes (Falkowski *et al*., 2006). Further difficulties for local maxima extraction in deciduous tree species have also noted with complications as a result of ITCs which are associated with multiple points of local maxima (Koukoulas and Blackburn, 2005).

The total overall accuracies produced by the ITC segmentation (36.18% - 39.47%) can be considered too low to provide a useful method of ITC isolation for forest management. The poor performance of the marker-controlled watershed segmentation was expected given the treetop detection results (59.21% - 63.16%) reported for the input seeds (Wang *et al*., 2004). ITCs not meeting the automated overlap criteria for a successful segmentation were largely classified as oversized, suggesting that automated tree crowns typically overestimated the spatial extent of ITCs at the site. In complex broadleaved forests automated ITC segmentations typically favour individuals dominating the canopy (Lähivaara *et al*., 2014). When coupled with the added difficulty in distinguishing the individual boundaries of overlapping crowns (Poutliot *et al*., 2002;

Koukoulas and Blackburn, 2005) and a complex vertical canopy structure (Wang *et al*., 2016), automated crown boundaries overestimate size and coverage of the existing tree crowns through the merging of subdominant individuals with adjacent dominant tree crowns (Koch *et al*., 2006). Furthermore, the impact of canopy gaps, created from fallen deadwood, across the woodland could also be attributed as a potential causal factor to this oversizing of automated ITCs (Leckie *et al*., 2003).

It was noted that individuals classified as category 1 (dead), presented the greatest treetop detection (23.81% - 28.57%) and segmentation (4.76% - 9.52%) difficulties. These individuals can be shadowed by surrounding canopies and occupy a significantly smaller extent in the canopy due to the loss of foliage and branches (Bater *et al*., 2009). Furthermore, in relation to the photogrammetric process, Nevalainen *et al*. (2017) noted that whilst shorter trees were evident in orthomosaic images, these could not be detected from the resulting point clouds. This affect can be attributed to the limited canopy penetration of passive sensors and the requirement of an xyz location to be visible from at least two viewpoints for the generation of a photogrammetric point (St-Onge *et al*., 2005). It is therefore plausible that detection difficulties noted for category 1 individuals may also be incurred due to the reduced prominence of dead stands in DSMs generated via photogrammetry.

Trees recorded as category 3 (moderate decline) consistently yielded the highest treetop detection and ITC segmentation accuracies. Dispersive broadleaves, such as oak species (*Quercus* spp.), are prone to over-segmentation due to the irregularity of crown shape (Strîmbu and Strîmbu, 2015; Deng *et al*., 2016). It is therefore plausible that the partial dieback of the crowns designated as category 3 (moderate decline) reduced the co-dominance of multiple branches and created a greater distinction of the crown boundary. However, in comparison to trees suffering major decline (category 2), the individuals still exhibited a prominent treetop and sufficient quantities of live foliage to be identified and segmented.

In the case of pixel size, whilst variability was evident between the three tested DSM resolutions, the differences between treetop detection and ITC segmentation accuracies were much smaller than the disparity between crown decline severity categories. Identifying any particular relationship between optimum pixel size and crown characteristics was hindered by difficulties in the calculation of crown diameter for ITCs

in the study area (Ke and Quackenbush, 2011; Chang *et al*., 2013). The 0.5 m DSM exhibited the best performance in the ITC segmentation, despite the poorest treetop detection results, suggesting the reduced intra-crown variability may have resulted in a slight improvement in the delineation of crown boundaries. Given the mature nature of the dominant tree canopy, this would align with the results reported in Barnes *et al*. (2017b) and Chapter 4 which suggested that plantation forest plots with larger maximum tree heights (>30 m) were best segmented from the coarser 0.5 m CHM. Nevertheless, insufficient evidence from this study, along with limited variability between the performance of DSM pixel sizes, prevents the acknowledgment of any conclusions concerning the influence of pixel size on the detection and delineation of ITCs.

Previous studies that have applied photogrammetry-derived surface elevation from UAV imagery for the isolation of individual trees have reported treetop detection success rates of 64 – 95% for boreal stands dominated by pine (*Pinus sylvestris*), spruce (*Picea abies*), birch (*Betula pendula*) and larch (*Larix sibirica*) (Nevalainen *et al*., 2017) and an ITC segmentation success of 74.7% for urban boreal forest dominated by spruce (*Picea abies*) (Näsi *et al*., 2015). By comparison the treetop detection (59.21 - 63.16%) and ITC segmentation results (36.18 – 39.47%) achieved from this study fall below these previously reported accuracies. Nevertheless, contrasts between the studies cause direct comparisons of ITC isolation accuracies to be misleading. For example, variations present in the accuracy assessment methods may result in disparities between reported results (Chen *et al*., 2006; Ke and Quackenbush, 2011; Richardson and Moskal, 2011; Zhen *et al*., 2016). With regard to the Nevalainen *et al*. (2017) study for example, a 2 m radius extending from reference tree crowns was applied for the evaluation of successfully automated treetops. Furthermore, in reference to the Näsi *et al*. (2015) research, only individuals with a DBH exceeding 25 cm were included in the reported accuracy percentage and the exact method of ITC segmentation success assessment was not explicitly specified. Resultantly an objective approach is required for the comparison of accuracy percentages reported for the detection and segmentation of ITCs.

In addition, differences in forest type and character also present further challenges in the comparison of ITC isolation accuracy results (Solberg *et al*., 2006; Zhen *et al*., 2016). In particular, the difficulties in identifying crowns of deciduous tree species has been widely recognised in the scientific literature (Koch *et al*., 2006; Ke and Quackenbush, 2011; Larsen *et al*., 2011), especially in the case of mixed heterogeneous

forest stands (Solberg *et al*., 2006). Cited reasons for the complications in ITC identification in deciduous forest have included the increased irregularity of crown shape (Strîmbu and Strîmbu, 2015), lack of conical crown shape (Ke and Quackenbush, 2011), poor consistency in human interpretation of reference and automated crowns and large discrepancies in segmentation algorithm performance (Larsen *et al*., 2011). The increasing acknowledgement of poor ITC delineation success in deciduous forest from conventional segmentation methods highlights the requirement for further research in this particular forest type (Zhen *et al*., 2016).

Whilst is was not possible to acquire UAV imagery and PPCs for the larch forests applied in the previous chapters (4 and 5). Based on the findings of this research and the results reported by other studies in the literature, the potential performance of the methodology in these environments could be hypothesised. In the case of the healthy larch stands at Radnor forest (Chapter 3; Section 3.1), given the successful results (> 64%) previously reported by Näsi *et al*. (2015) and Nevalainen *et al*. (2017) for boreal forests dominated by conifers, it could be suggested that ITC segmentation accuracies comparable or just below those reported for the ALS in chapter 4 could be achieved (St-Onge *et al*., 2015). Nevertheless, in light of the difficulties reported for the identification of individual oak trees subject to crown decline in this study and the importance of the pit-free CHM generation method for diseased larch segmentation in chapter 4, the performance of photogrammetry-derived DSMs for segmentation of *P. ramorum* affected larch at Ogmore forest is also likely to be poor. However, the conical shape of crowns, regular spacing and presence of one dominate peak in height for commercial plantation larch, may facilitate a slight increase in the ITC segmentation accuracies reported for oak in the mature woodland at Stratfield Brake.

6.6 Conclusions

The results presented in the study highlight the poor performance of treetop detection (59.21 - 63.16%) and ITC segmentation (36.18 – 39.47%) in the AOD affected oak-dominated woodland at Stratfield Brake. Whilst the local maxima approach to treetop extraction outperformed the contour method overall, no significant differences were observed between the results reported by the two techniques. Large variability was observed with regard to the performance of treetop detection and ITC segmentation across the five crown decline severity categories, with categories 1 (dead) and 3 (moderate

decline) consistently producing the lowest and highest accuracy percentages. The selected pixel size of the DSM (0.15 m, 0.25 m and 0.5 m) was noted to result in some small variations in the reported accuracies of treetop detection and ITC segmentation, however no substantial conclusions could be reached with regard to an optimal DSM resolution. The key causal factors for the poor detection and segmentation of ITCs was the irregularity of crown shape and structural canopy complexities caused by the dominance of deciduous trees in the canopy and the variation in crown condition.

Chapter 7: Assessment of Crown Decline in a Woodland Affected by Acute Oak Decline with UAV-based Multispectral Imagery

7.1 Introduction

UAVs have been increasingly utilised in applications concerning environmental monitoring and assessment (Michez *et al*., 2016; Nevalainen *et al*., 2017). Whilst the operational applications of UAVs in the forestry sector are currently experimental (Tang and Shao, 2015; Gambella *et al*., 2016), previous studies have demonstrated the capabilities of the platform for a range of purposes including the assessment of tree species (Michez *et al*., 2016), tree height (Wallace *et al*., 2012), forest fires (Ollero *et al*., 2006) and insect pest damage (Näsi *et al*., 2005). Nevertheless, examples regarding the potential applications of UAVs for the assessment of tree disease is limited (Näsi *et al*., 2015), especially in relation to dieback and mortality events resulting from phytopathogens, such as the current AOD outbreak in the UK (Chapter 6; Section 6.1).

In the case of tree disease assessment, airborne and spaceborne datasets acquired via passive and active sensors have previously been applied in the detection of insect pests and phytopathogens in forest environments (Stone and Coops, 2004; Fraser and Latifovic, 2005; Wulder *et al*., 2006; Coops *et al*., 2009; Barnes *et al*., 2017a). UAVs offer an additional platform for the remote assessment of disease within forests and woodlands (Wallace *et al*., 2012), especially with regard to the recognition of subtle changes in branches and ITCs associated with the early stages of infection (Lehmann *et al*., 2015). Nevertheless, baseline datasets providing information regarding the characteristic structure and spectral signature of a particular tree species are required for healthy canopies (Sims and Gamon, 2002; Turner *et al*., 2003) and those subject to various levels of deterioration as a result of a specific insect pest, phytopathogen or environmental stress (Näsi *et al*. 2015). This information, coupled with an understanding regarding the performance of UAV supported sensors in forest environments, is imperative to the application of this remote sensing platform in the field of forest pathology **(**Nilsson, 1995; Tang and Shao, 2015).

With regard to the remote assessment trees at the ITC-scale, airborne acquired optical imagery typically provides several pixels of spectral information per ITC (Näsi *et al*., 2015). However, in the case of UAV-based imagery, thousands of pixels can represent one ITC (Garcia-Ruiz *et al.*, 2013). The increased data availability improves the potential

application of the imagery for the assessment and monitoring of forest characteristics. Nevertheless, serious challenges are also incurred with regard to the extraction of informative data and the elimination noise, such as pixels associated with shadow. Methodologies previously employed to minimise the extraction of noise affected pixels from tree crowns have included the selection of the brightest pixels within ITCs (Näsi *et al*., 2015), the selection of sunlit portions of the canopy (Leckie and Yuan, 1992) and a halo approach which ignores the brightest central pixels associated with the treetop (Coops *et al*., 2003). Nevertheless, no methodology has been consistently reported to provide the optimal extraction of spectral information from ITCs. Resultantly, further consideration regarding feature extraction for ITCs from UAV-based imagery is still required.

The application of remotely sensed imagery to the assessment of forest health utilises changes in spectral signatures resulting from structural and physiological responses of vegetation subject to stress and disease (Lévesque and King, 2003). Previous studies have noted the particular sensitivity of wavelengths in the green, red and near-infrared regions of the electromagnetic spectrum to infection by insect pests and phytopathogens (Coops *et al*., 2003; Lawrence and Labus, 2003; Leckie *et al*., 2005; Wulder *et al*., 2006). Subsequently, VIs which utilise these sensitive regions of the electromagnetic spectrum, such as NDVI (Rouse *et al*., 1974), NDVI-RE (Gitelson and Merzlyak, 1994; Sims and Gamon, 2002), GNDVI (Gitelson *et al*., 1996) and ARI (Gitelson *et al*., 2001) have also proven effective in the remote assessment of insect pests, phytopathogens and stress in trees and forest environments (Ismail *et al*., 2007; Barry *et al*., 2008; Ortiz *et al*., 2013; Adelabu *et al*., 2014; Murfitt *et al*., 2016).

The classification of tree crown condition from remotely sensed datasets provides a spatial representation of decline across forest areas and provides a useful tool in the management of these of environments (Shendryk *et al*., 2016). Understanding relationships between spectral reflectance and crown condition changes is, however, key to facilitating successful classification outputs (Adelabu *et al*., 2014). A series of established classifiers including support vector machine (SVM) and random forest (RF) have previously been employed for the classification of vegetation condition (Melgani and Bruzzone, 2004; Kantola *et al*., 2010; Rumpf *et al*., 2010; Ortiz *et al*., 2013; Adelabu *et al*., 2014). Each classification approach presents a series of advantages and limitations,

with suitability largely dependent on input data characteristics such as the quantity of training data and class separability (Huang *et al*., 2002; Immitzer *et al*., 2012).

7.2 Objectives

The aim of this research chapter was to:

> *Identify the capability of UAV multispectral imagery in the detection of crown dieback associated with Acute Oak Decline in mature oak trees*.

To consider the applications of UAV-based multispectral imagery for the assessment of crown decline in an AOD affected woodland, a series of specific objectives were constructed. This research chapters' main objectives are:

1. To assess the ability of six vegetation indices (NDVI, NDVI-RE, GRVI, GNDVI, MTCI and ARI) to discriminate between five categories of crown decline, at the ITC-scale, in a woodland environment affected by AOD;
2. To establish whether the calculation of mean vegetation indices for individual oak tree crowns from all pixels, the brightest 80% of pixels or the brightest 20% of pixels influences the discrimination of five crown decline severity classes; and
3. To determine whether oak tree crowns in an AOD affected woodland can be correctly classified into three and five crown decline severity classes based on the mean vegetation index values extracted from UAV-based multispectral imagery.

7.3 Methods

7.3.1 Ground Data Collection

Ground data collection at the Stratfield Brake field site (Chapter 3; Section 3.2) for this research chapter has already been described in Chapter 6, Section 6.3.1.

7.3.2 UAV Data Collection

The methodology for the UAV data collection has already been described in Chapter 6, Section 6.3.2.

7.3.3 Data Processing

The data processing methodology applied in the production of the orthomosaic has already been outlined in Chapter 6, Section 6.3.3.

7.3.4 Manual Individual Tree Crown Delineation

The methodology employed for the manual delineation of ITCs at the Stratfield Brake site has previously been documented in Chapter 6, Section 6.3.5. An automated tree crown segmentation was considered using the DSM acquired via photogrammetry (Chapter 6; Section 6.3.4). However, due to the poor overall accuracies reported for the segmentation of ITCs in the study area in the previous chapter (Chapter 6; Section 6.4.2; Table 6.7), the manually delineated polygons were applied to represent the ITC boundaries.

7.3.5 Vegetation Indices

Six established VIs (NDVI, NDVI-RE, GRVI, GNDVI, MTCI and ARI) were extracted from ITCs (Table 7.1). In the case of the ARI, the green and red-edge bands were selected to represent R_{550} and R_{700} (Table 7.1), as these most closely matched the specified reflectance wavelengths. Across the individual trees within the training area, the average number of pixels associated with each tree crown was 15,974. Three different methods were applied to the extraction of VI values from ITCs, these included the overall mean value from all pixels (Mean_All) (Leckie and Yuan, 1992; Ismail *et al*., 2007), mean value of the brightest 80% of pixels (Mean_80) and mean value of the brightest 20% of pixels (Mean_20). In this particular context, brightness is used to describe the highest VI values. For this selection of VIs, high values are typically associated with dense vegetation. The selection of the brightest pixels aims to remove values of low spectral reflectance associated with shadow (Leckie and Yuan, 1992; Näsi *et al*., 2015).

Table 7.1 – Vegetation indices (VIs) calculated and equations applied.

VIs	Equation	Reference
NDVI	(NIR – Red)/(NIR + Red)	Rouse *et al*. (1974)
NDVI-RE	(NIR – Red-edge)/(NIR + Red-edge)	Gitelson and Merzlyak (1994)
GRVI	(Green – Red)/(Green + Red)	Tucker (1979)
GNDVI	(NIR – Green)/(NIR + Green)	Gitelson *et al*. (1996)
MTCI	(NIR - Red-edge)*(Red-edge - Red)	Dash and Curran (2004)
ARI	$(1/R_{550}) – (1/R_{700})$	Gitelson *et al*. (2001)

Abbreviations: ARI = Anthocyanin Reflectance Index; GNDVI = Green Normalised Difference Vegetation Index; GRVI = Green Red Vegetation Index; MTCI = MERIS Terrestrial Chlorophyll Index;

NDVI = Normalised Difference Vegetation Index; NDVI-RE = Normalised Difference Vegetation Index Red-edge; R = Reflectance.

7.3.6 Crown Decline Category Discrimination

Using the ITCs from the training dataset, the capability of VIs to discriminate between the five crown decline severity classes (Chapter 6; Section 6.3.1; Table 6.1) was analysed. The non-parametric Kruskal-Wallis test was applied with Mann-Whitney post hoc tests, subject to a Bonferroni-Holm correction to account for the type 1 error incurred via multiple testing (Ismail *et al*., 2007). The parametric ANOVA with Tukey's HSD post hoc test (Coops *et al*., 2003) was not appropriate as some datasets failed to meet the assumptions of normality (Shapiro-Wilk test $p < 0.05$) or homogeneity of variances (Levene's test $p < 0.05$).

7.3.7 Classification

Two classification approaches, a SVM and RF, were tested for the classification of oak ITCs into five and three crown decline severity classes using the training and validation areas (Section 3.2; Figure 3.7). The five-class classification reflects the crown decline severity classes (Chapter 6; Section 6.3.1; Table 6.1) applied in the previous discrimination analysis, whilst the three-class approach (Table 7.2) simplifies the classes into healthy, decline and severe decline, three key areas of interest for the management of decline in woodland environments. The SVM classifier (Vapnik, 1998) was employed using a radial basis function (RBF), a kernel commonly employed in cases where datasets are not linearly separable (Fauvel *et al*., 2006; Petropoulos *et al*., 2012). The RBF is parametrised using a simple parameter (σ), determining the decision boundary smoothness. An additional parameter (C) controls the penalisation of error caused by the expectation that some training and validation samples may be assigned the wrong class (Rumpf *et al*., 2010). In the case of this multi-class classification, the one-vs-one decision function was applied (Knerr *et al*., 1990; Pal and Mather, 2005). As minimal guidance regarding kernel-specific parameters is present within the scientific literature (Petropoulos *et al*., 2012), cross-validation of the training sample was used to optimise σ and C prior to classification using a grid search across a range of exponential growing sequences for the two parameters (Hsu *et al*., 2003).

Table 7.2 – Description of classes applied in the three-class classification.

Category	Criteria
Severe Decline	Canopy thinning exceeds 80% and major deadwood present
Decline	Canopy thinning between 10 - 80% and minor deadwood present
Healthy	No decline or deadwood is present

The second classification method is a RF (Breiman, 2001), a non-parametric approach which generates a series of classification trees. Each tree is generated using a bootstrapped set of training samples, with the split at each classification tree governed by a randomised subset of input variables for each node (Hudak *et al*., 2008; Oliveira *et al*., 2012). The final classification result is subsequently determined based of the highest mean probability estimate across all trees (Belgiu and Drăguţ, 2016). Input parameters including the number of regression trees (n_{tree}) and the number of input variables at each split in the tree building process (m_{try}) were set to 500 and 2 respectively, following a preliminary grid search cross-validation of the training dataset (Immitzer *et al*., 2012; Ortiz *et al*., 2013; Shendryk *et al*., 2016). All processing for the two classification methods was undertaken in Python using Scikit-learn (Pedregosa *et al*., 2011). It should be acknowledged that in this instance VI values were not normalised prior to classification.

Classification input variables were selected based on the results of the crown decline severity discrimination analysis and classification performance was reviewed using the overall accuracy percentage (OA) and Cohen's κ coefficient (Cohen, 1960). Interpretation of κ was based on the following categories: ≤0.2 is poor; >0.2 to ≤0.4 is fair; >0.4 to ≤0.6 is moderate; >0.6 to ≤0.8 is good; and >0.8 to ≤1 is very good (Landis and Koch, 1977). Confusion matrices were employed to provide a more detailed evaluation of the most successful classifications (Congalton and Green, 1999).

7.4 Results

7.4.1 Crown Decline Severity Discrimination

Following Kruskal-Wallis tests, all VIs (NDVI, NDVI-RE, GRVI, GNDVI, MTCI and ARI) exhibited significant differences between the five crown decline severity

categories for all three of the extraction methods (Mean_All, Mean_80 and Mean_20) at the 99% confidence level. The results in Table 7.3 demonstrate the outcomes of the Mann-Whitney *a posteriori* tests for ITC decline severity categories. GNDVI (Mean_80) resulted in significant differences (90% confidence) between all crown decline severity categories. NDVI (Mean_All, Mean_80, Mean_20) and GNDVI (Mean_All, Mean_20) produced significant differences (95% confidence) between all categories except 4 and 5, as did NDVI-RE (Mean_20) at the 90% confidence level. Overall, minimal differences were observed between the discrimination performances of the three extraction methods. However, in the case of GNDVI, Mean_80 provided the best performance, whilst for NDVI-RE and MTCI, Mean_20 also improved crown decline severity discrimination. Figure 7.1 provide a visual illustration of the three best performing VIs (NDVI, NDBI-RE and GNDVI) across the five severity categories.

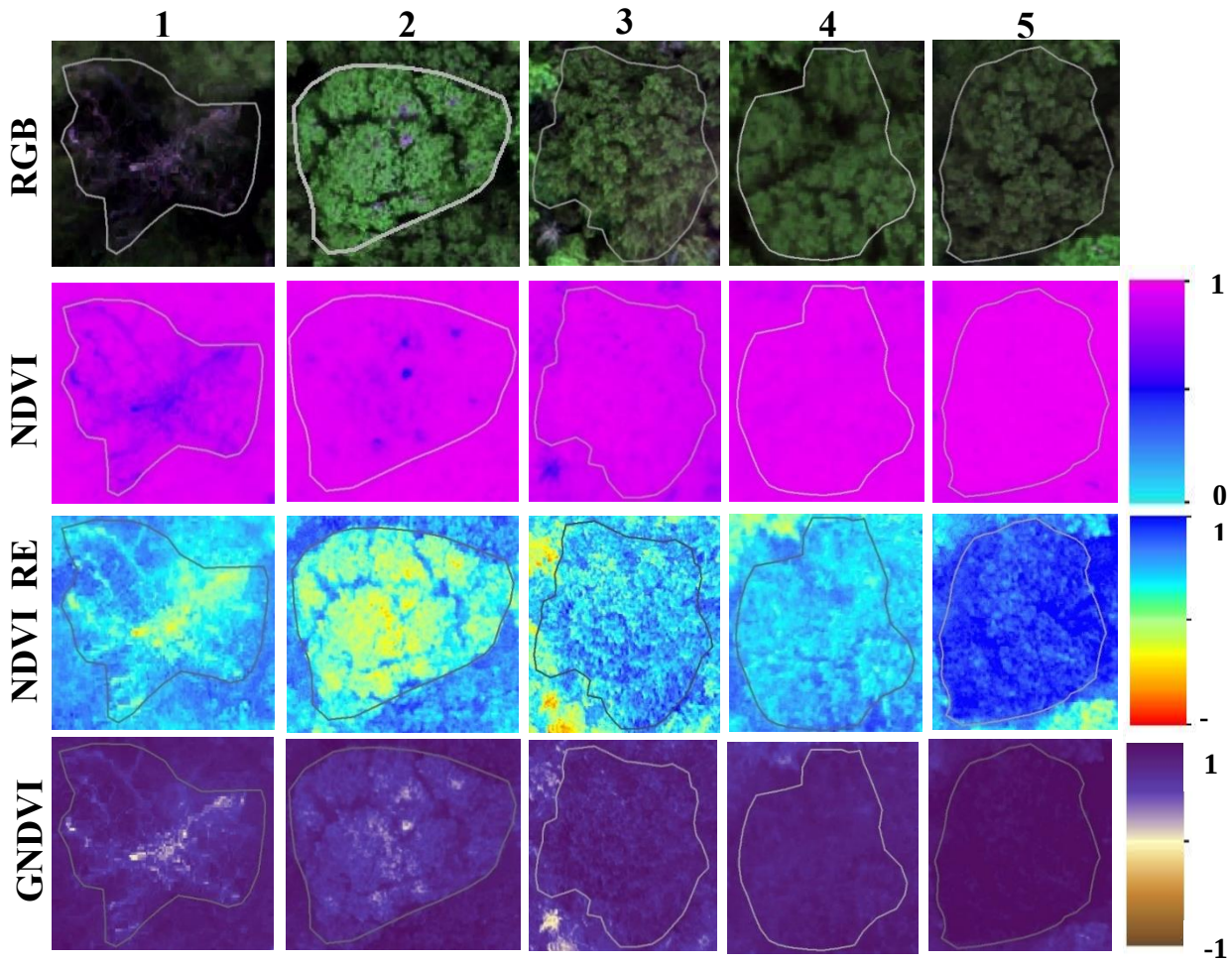

Figure 7.1 – An illustration of the three best performing VIs for the discrimination of crown decline severity categories at the Stratfield Brake site alongside the RGB imagery.

Table 7.3 - Mann-Whitney post hoc test significance results subject to Bonferroni-Holm correction for mean vegetation indices extracted from all pixels (Mean_All), brightest 80% of pixels (Mean_80) and brightest 20% of pixels (Mean_20).

		Mean_All					Mean_80					Mean_20				
		1	2	3	4	5	1	2	3	4	5	1	2	3	4	5
1	NDVI		****	****	****	****		****	****	****	****		****	****	****	****
2		****		***	****	***	****		***	****	***	****		**	****	**
3		****	***		**	**	****	***		**	**	****	**		**	**
4		****	****	**		-	****	****	**		-	****	****	**		-
5		****	***	**	-		****	**	***	-		****	**	**	-	
1	NDVI-RE		-	****	****	****		**	****	****	****		**	****	****	****
2		-		-	****	***	**		-	****	***	**		*	****	***
3		****	-		****	****	****	-		****	****	****	*		****	****
4		****	****	****		-	****	****	****		-	****	****	****		-
5		****	***	****	-		****	***	****	-		****	***	****	-	
1	GRVI		***	****	****	****		****	****	****	****		***	****	****	**
2		***		***	**	-	****		***	**	-	***		*	-	-
3		****	***		-	-	****	***		-	-	****	*		-	-
4		****	**	-		-	****	**	-		-	****	-	-		-
5		****	-	-	-		****	-	-	-		**	-	-	-	
1	GNDVI		****	****	****	****		***	****	****	****		***	****	****	****
2		****		***	****	***	***		**	****	***	***		**	****	***
3		****	***		****	****	****	**		****	****	****	**		***	****
4		****	****	****		-	****	****	****		*	****	****	***		-
5		****	***	****	-		****	***	****	*		****	***	****	-	
1	MTCI		****	****	****	****		****	****	****	****		****	****	****	****
2		****		**	-	-	****		**	-	-	****		***	*	-
3		****	**		-	-	****	**		-	-	****	***		-	-
4		****	-	-		-	****	-	-		-	****	*	-		-
5		****	-	-	-		****	-	-	-		****	-	-	-	
1	ARI		****	****	****	****		****	****	****	****		****	****	****	****
2		****		****	****	***	****		****	****	***	****		****	****	***
3		****	****		-	-	****	****		-	-	****	****		-	-
4		****	****	-		-	****	****	-		-	****	****	-		-
5		****	***	-	-		****	***	-	-		****	***	-	-	

* $p < 0.10$; ** $p < 0.05$; *** $p < 0.01$; **** $p < 0.001$; - no significant difference.

7.4.2 Classification

Table 7.4 presents the best results for the five-class (Chapter 6; Section 6.3.1; Table 6.1) classification of crown decline severity for the SVM and RF classifiers. Both classifiers performed best using the NDVI-RE, NDVI and GNDVI inputs calculated using the mean value from the brightest 80% of pixels (Mean_80). The RF classifier produced a fair classification (Landis and Koch, 1977) and the highest OA = 55.26% and κ = 0.37 values. Assessment of the confusion matrix demonstrated significant difficulties in the classification of healthy trees (category 5), which yielded UA = 20% and PA = 16.67%. Table 7.5 presents the results of the three-class (Table 7.2) classification of crown decline severity. The SVM classifier performed best, resulting in a good classification with OA

Table 7.4 - Confusion matrices for SVM and RF classifications of the validation area for the five crown decline severity categories.

		SVM						**RF**					
		Inputs: NDVI-RE (Mean_80), NDVI(Mean_80), GNDVI (Mean_80)						**Inputs (Feature Importance)**: NDVI-RE (Mean_80) (0.241), NDVI (Mean_80) (0.476), GNDVI (Mean_80) (0.283)					
		Classified						**Classified**					
		1	2	3	4	5	PA	1	2	3	4	5	PA
Reference	1	10	5	0	0	0	66.67	15	0	0	0	0	100
	2	2	1	3	0	0	16.67	1	1	3	1	0	16.67
	3	0	0	28	0	0	100	1	1	19	6	1	67.86
	4	0	0	21	0	0	100	0	0	12	6	3	57.14
	5	0	0	5	0	1	16.67	0	0	5	0	1	16.67
	UA	83.33	16.67	49.12	0	100		88.24	50	48.72	46.15	20	
OA (%)							52.63						55.26
κ							0.31						0.37

Table 7.5 - Confusion matrices for SVM and RF classifications of the validation area for the three crown decline severity categories.

		SVM				**RF**			
		Inputs: NDVI-RE (Mean_80), NDVI(Mean_80), GNDVI (Mean_80)				**Inputs (Feature Importance)**: NDVI-RE (Mean_80) (0.179), NDVI (Mean_80) (0.531), GNDVI (Mean_80) (0.290)			
		Classified				**Classified**			
		Severe Decline	Decline	Healthy	UA	Severe Decline	Decline	Healthy	UA
Reference	Severe Decline	19	2	0	90.48	17	4	0	80.95
	Decline	0	49	0	100	2	44	3	89.78
	Healthy	0	5	1	16.67	0	6	0	0
	PA	100	87.5	100		89.47	81.48	0	
OA (%)					90.79				80.26
κ					0.78				0.58

= 90.79% and κ value = 0.78. Nevertheless, the classification reported a poor performance in the classification of class 3 (healthy) with a UA = 16.67%.

In the case of the three- and five-class decline severity classification, several key limitations require acknowledgement. Firstly, the small number of samples from each of the severity categories, especially in the case of the categories 2 (major decline) and 5 (healthy), fell below the recommended minimum threshold for a statistically valid assessment (Van Genderen and Lock, 1977; Congalton, 1991), influencing the predictive capabilities of the classifiers (Melgani and Bruzzone, 2004; Belgiu and Drăguţ, 2016). In addition, the number of samples in each of the three- and five-class classifications was also unbalanced, providing potential difficulties in the ability of the classifiers to accurately separate individual classes (Muñoz-Marí *et al*., 2007; Belgiu and Drăguţ, 2016). The VI values were not normalised prior to classification, as a result this could have limited the classification performance epically in the case of k_NN.

7.5 Discussion

The VIs which exhibited significant distinctions between four or five of the crown decline severity categories were the GNDVI, NDVI and NDVI-RE, all having in common the use of the NIR band in the VI calculation. Previous studies have noted the particular sensitivity of the NIR region of the electromagnetic spectrum to changes in both leaf and canopy structure (Barry *et al*., 2008; Reynolds *et al*., 2012; Michez *et al*., 2016). This suggests that the NIR band is particularly important with regard to the assessment of crown decline associated with AOD. The GNDVI (Mean_80) outperformed the NDVI and NDVI-RE in the discrimination of categories 4 (minor decline) and 5 (healthy). This implies that using the green band in VI calculation may provide a better distinction between ITCs subject to early stages of crown decline, especially when compared to the red (NDVI) and red-edge (NDVI-RE). The application of green-based VIs for disease severity discrimination has also previously been acknowledged in the scientific literature (Waser *et al*., 2014). In particular, Fassnacht *et al*. (2014) noted the contribution of the green peak (approx. 560 nm) to high classification accuracies of vegetation damage associated with the European bark beetle (*Ips typographus*). In the case of this study, the green peak falls within green band (550-570 nm) applied for GNDVI calculation. In addition, Everritt *et al*. (1999) also reported variation in green band reflectance between dead branches, healthy foliage and diseased foliage in relation to oak wilt disease

(*Ceratocystis fagacearum*) in live oak (*Quercus fusiformis*). An important point to note with regard to operational use of VIs and UAVs is the outperformance of the NDVI-RE by the GNDVI, as it suggests that a multispectral sensor with red-edge capabilities is not an essential requirement for the assessment of oak crown condition.

Overall, the selected extraction method (Mean_All, Mean_80 and Mean_20) exhibited little influence on the crown decline severity discrimination potential of the six VIs. This suggests that whilst the selection of a certain percentage of the brightest pixels may improve the performance of some VIs, the influence of noise pixels on the overall mean value is minimal with regard to crown decline analysis. Nevertheless, the application of the Mean_80 method for the extraction of GNDVI facilitated a significant separation of categories 4 (minor decline) and 5 (healthy), not achieved by the other two extraction methods. This suggests that removing the darkest 20% of pixels can aid the distinction between these two classes, by enhancing subtle differences in spectral reflectance. In relation to disease assessment, Stone and Coops (2004) noted that the presence of shadow increased in forest stands subject to defoliation, resultantly this suggests that the inclusion of noise related pixels may also be of benefit to disease severity discrimination.

The number of classes selected for crown condition classification can impact on the overall accuracies reported (Coops *et al*., 2003; Waser *et al*., 2014; Näsi *et al*., 2015) and this was evident when comparing the classification performance of the five- and three-class classifications. By condensing the classes from five to three, OA and κ both improved to provide a good overall classification (Landis and Koch, 1977) of crown decline. Considering the application of classification output is particularly important for informing the selection of class boundaries. In this instance, woodland management decisions typically require knowledge of the number and location of individual trees affected by decline (Shendryk *et al*., 2016) and information about trees with significant loads of deadwood, which is important for managing structural integrity and public safety (Mistretta, 2002). Resultantly, the broader categories in the three-class classifications provide enough information about crown condition across the woodland environment to fulfil these management objectives.

The performance of the three-class classification reported in this study is comparable with that previously reported from UAV-acquired imagery for insect pests

(Lehman *et al*., 2015; Näsi *et al*., 2015). In this instance the classification was weakest for the classification of healthy ITCs and those subject to decline. Näsi *et al*. (2015) also noted difficulties with the misclassification of healthy and infested classes in the case of a three-class classification (healthy, infested and dead) for the European spruce bark beetle (*Ips typographus*) in Norway spruce (*Picea abies*). In relation to this study, it should also be acknowledged that the disproportionately low number of individuals in the healthy category may have also impacted on the classification performance. In the case of operational forest management, higher decline thresholds for the healthy and declining class boundary could be applied to improve classification accuracy and avoid the misclassification of healthy individuals (Kantola *et al*., 2010).

The limitations associated with the research require consideration prior to the operational application of UAV-based imagery for oak crown decline assessment. For example, whilst surveyed individuals presented a dominant or sub-dominant position in the woodland canopy, no further consideration was given to the potential influence of tree age on the spectral reflectance of oak tree crowns (Waser *et al*., 2014). Whilst AOD typically affects mature oak stands (Denman *et al*., 2010), the potential variability of crown spectral signature with tree age requires further investigation. In addition, due to the deciduous nature of oaks, seasonal variation in crown reflectance may also have significant influences on the assessment of crown condition and requires consideration with regard to both data acquisition and processing (Liu *et al*., 2006).

Whilst the results from the study highlight the disease discrimination potential of UAV-based multispectral imagery for the assessment and management of AOD, a number of additional factors also require attention prior to operational application. For example, the spectral characteristics of other UK oak species such as Sessile (*Q. petraea*) and Turkey (*Q. cerris*) oak require quantification and comparison with the results for English oak (*Q. robur*) presented here. Tree species classification techniques would also be required to provide a comprehensive and targeted assessment of crown decline in heterogeneous mixed woodland environments (Michez *et al*., 2016). In addition, the implementation of an ITC segmentation methodology would also facilitate an entirely automated approach to the assessment of decline in ITCs (Näsi *et al*., 2015). In relation to multiple data acquisitions, consideration should also be given to the implications of illumination conditions on the separability of crown decline severity classes (Näsi *et al*., 2015).

7.6 Conclusions

The research demonstrates that UAV-based multispectral imagery can be used for the separation of five classes of crown decline in oak tress within a woodland affected by AOD. The GNDVI performed best and demonstrated significant differences between all five crown decline classes at the 90% confidence level, when extracted from ITCs using the mean value for the brightest 80% of pixels (Mean_80). The NDVI and NDVI-RE also performed well providing discrimination between all classes except in the case of 4 (minor decline) and 5 (healthy). Across the six VIs tested, none of the extraction methods applied (Mean_All, Mean_80 and Mean_20) consistently outperformed the others. Classification of oak crown decline into three categories (severe decline, decline and healthy) was best achieved with an SVM classifier producing an OA = 90.79% and κ = 0.78. For the operational applications of UAV-based multispectral imagery for the assessment of crown decline associated with AOD further consideration should be given to spectral variations resulting from different species, stand age, time of year and illumination conditions during data acquisition.

Chapter 8: Overall Discussion

8.1 Introduction

This thesis has examined the applications of two contrasting remote sensing approaches for the ITC-scale assessment of phytopathogens in forest environments. The results presented in Chapters 4 and 6 demonstrate conflicting finding regarding the success of automated ITC segmentation across two differing forest environments. However, in the case of phytopathogen detection, ALS (Chapter 5) and UAV-based multispectral imagery (Chapter 7) both demonstrated successful applications in the assessment of crown dieback associated with *P. ramorum* and AOD infections respectively. This chapter will provide an over-arching discussion of all the research findings from the thesis.

In relation to the main scientific question of the research project "How can high resolution remotely sensed datasets be applied to the detection and assessment of phytopathogens in UK forests?" several key conclusions have been highlighted which will be addressed across key areas of this discussion. Firstly, it has been highlighted that when individual tree crowns can be accurately located within the canopy optical and LiDAR data acquired at high resolution can be applied to the detection of disease through spectral and structural changes to the canopy respectively (discussed further in Section 8.2). Nevertheless, the automated identification of ITCs within forest canopies remains a challenging task even with the application of high resolution data (discussed further in Section 8.5.1). In addition, this research only considered two of the pathogens currently impacting UK forestry. Whilst the conclusions from the research concerning *P. ramorum* and AOD can inform the detection of other pests and pathogens they do not provide the detailed understanding of the applications of remote sensing to identify a specific collection of symptoms in particular host species (discussed further in Section 8.5.2).

8.2 Sensor

The type of sensor applied to the acquisition of remotely sensed datasets significantly impacts the dataset characteristics influencing its applications for ITC segmentation (Zhen *et al.*, 2016) and the assessment of forest condition (Lausch *et al.*, 2016; Lausch *et al.*, 2017). The active and passive sensors used to acquire the ALS and multispectral imagery have provided two datasets with contrasting properties. The

suitability of these structural and spectral datasets for ITC segmentation and phytopathogen assessment is discussed in Section 8.2.1.

8.2.1 Individual Tree Crown Segmentation

The ITC segmentations presented in Chapters 4 and 6 both utilised a raster-based input of surface elevation for the isolation of ITCs. However, the CHMs utilised in the larch-dominated forest stands in Chapter 4 were acquired with ALS, whereas the DSMs applied in the case of the oak-dominated forest in Chapter 6 were produced from multi-spectral imagery via the process of photogrammetry. Whilst direct comparison of the results from the two chapters is hindered by differences in forest type (Solberg *et al*., 2006; Larsen *et al*., 2011; Zhen *et al*., 2016), several key differences were observed in the application of surface elevation products for ITC segmentation. Firstly, due to the inability of the passive optical sensor to penetrate the forest canopy (Reitberger *et al*., 2009; Lausch *et al*., 2017), the pit-free CHM generation method (Khosravipour *et al*., 2014) which resulted in an improved segmentation performance of diseased canopies in Chapter 4, was not applicable for the oak-dominated Stratfield Brake site in Chapter 6. As a result, the increased irregularity of canopy surface elevation caused by crown decline (Holdenrieder *et al*., 2004; Larsen *et al*., 2011; Barnes *et al*., 2017b) could only be addressed through the application of a smoothing filter (Khosravipour *et al*., 2014). An area of interest for further study would be to consider the potential improvements in segmentation accuracy at the Stratfield Brake study site (Chapter 6) with the application of a high-density ALS dataset and pit-free CHM generation methodology.

The suitability of a particular ITC segmentation method can also be influenced by input dataset characteristics (Zhen *et al*., 2016). Approaches to treetop detection and ITC segmentation exploit characteristics of the canopy surface topography to identify individual trees (Chen *et al*., 2006). The examples presented in Chapters 4 and 6 both provided surface elevation inputs for ITC segmentation, however these were derived via different remote sensing methods, resulting in slight differences in the representation of the real canopy surface. Whilst previous studies have reported successful applications of photogrammetry-derived DSMs for the delineation of ITCs (Nevalainen *et al*., 2017), the visibility of ITCs can be reduced by view obliquity, especially with regard to closed canopies (St-Onge *et al*., 2015; Wallace *et al*., 2016). To provide an accurate comparison of photogrammetry- and ALS-derived surface elevation inputs for the purpose of ITC

segmentation, both datasets would have to be compared for the same study area (Vastaranta *et al*., 2013b; St-Onge *et al*., 2015), with additional consideration of the performance of different segmentation algorithms (Zhen *et al*., 2016).

8.2.2 Assessment of Phytopathogens

The structural and spectral metrics calculated from the ALS and multispectral imagery both demonstrated disease assessment success in the case of *P. ramorum* (Chapter 5) and AOD (Chapter 7), with both approaches utilising the symptom expression of the infection in the foliage to differentiate between crown decline severity classes. Nevertheless, the VIs applied in the case of AOD provided a significant separation between healthy trees and those subject to minor crown decline, a distinction not evident in the case of the ALS metrics applied for *P. ramorum* assessment. One possible explanation for this contrast could result from the ability of the sensor to identify small-scale changes in the canopy present during the initial stages of infection. For example, if foliage discolouration precedes foliage loss, spectral sensors may exhibit a potential advantage in the detection of disease in the early stages of infection progression. However, to provide a direct comparison of the sensor performance in disease assessment, datasets should be acquired for the same forest environment and phytopathogen outbreak at comparable resolutions (Kantola *et al*., 2010; Lausch *et al*., 2017). Previous research which applied this approach in relation to the common pine sawfly (*Diprion pini*) infestation of Scots pine (*Pinus sylvestris*), noted a slightly improved classification accuracy from image features (87.4%) compared to ALS (80.7%), with the best overall classification of defoliation level (88.1%) achieved through the combination of metrics derived from both sensors (Kantola *et al*., 2010).

Another contrast between ALS and optical sensors which could have potential implications for the assessment of phytopathogens is the section or level of the canopy from which data is acquired. Passive optical sensors only capture information reflected from the canopy surface (Turner *et al*., 2003), in contrast, the capability of ALS to penetrate the forest canopy provides an extra dimension to forest condition assessment, especially with regard to full-waveform ALS sensors (Lausch *et al*., 2017). In certain phytopathogen-host interactions, such as *Dothistroma* needle blight (*Dothistroma septospora*) in pine species (*Pinus* spp.), early symptoms typically manifest in the lower canopy (Coops *et al*., 2003). As a result, the ability of sensors to penetrate the canopy

surface may provide an additional benefit when disease symptoms cannot be viewed from the nadir. Nevertheless, even discrete return ALS applied in Chapter 5, produces a bias against foliage located in the lower- and mid-canopy (Lovell *et al*., 2003). Resultantly the location of phytopathogen infection establishment and symptom development is an important parameter to consider in the selection of remote sensors for disease assessment in forest environments.

8.3 Platform

The greatest contrasts exhibited between remote sensing platforms are typically the spatial extent and resolution of data acquired (Lefsky *et al*., 2002; Boyd and Danson, 2005; Michez *et al*., 2016). The examples presented in the research chapters of this thesis provide a contrast between the airborne and UAV platforms for the segmentation of ITCs and the assessment of phytopathogens.

8.3.1 Individual Tree Crown Segmentation

Despite the expected spatial resolution contrasts in datasets acquired from different platforms (Lefsky *et al*., 2002; Michez *et al*., 2016), the surface elevation inputs applied for the ITC segmentations from the ALS (24 points/m^2) and UAV PPC (25 points/m^2) in chapters 4 and 6 respectively presented a minimal difference in resulting point densities. This facilitated the interpolation of raster-based surface elevation inputs with matching resolutions (0.15 m, 0.25 m and 0.5 m). Resultantly, comparisons concerning spatial resolution differences from the two platforms cannot be conducted in this instance. However, it should be acknowledged that LiDAR systems for the UAV platform can produce point densities up to 62 points/m^2 (Wallace *et al*., 2012) and the increased likelihood of sampling treetops at these resolutions has been noted to improve the detection of ITCs (Wallace *et al*., 2012; Wallace *et al*., 2014). One further consideration, whilst not relevant in the examples presented in the thesis, is the accessibility presented by the UAV platform which presents an opportunity for the assessment of ITCs in forest environments not ordinarily surveyed by more traditional remote sensing approaches (Zhen *et al*., 2016).

8.3.2 Assessment of Phytopathogens

Direct comparison of the two platforms for the assessment of phytopathogens in forest environments is complicated by the difference in sensor used for data acquisition (Lausch *et al*., 2017). Nevertheless, contrasts in spatial resolution and the quantity of data

extracted from ITCs for the assessment of crown condition were evident in the case of Chapter 5 (ALS; 24 points/m^2) and Chapter 7 (6 cm; multispectral-imagery). Spatial resolution differences could be considered as an additional causal factor for the superior performance of the multispectral-imagery in the identification of ITCs subject to the early stages of crown decline (Lehmann *et al*., 2015). In this particular instance the elimination of noise-related pixels was also an important factor for the discrimination of ITCs with minor crown decline from those classified as healthy. Despite the improved disease discrimination performance achieved via the removal of the darkest pixels in mean VI calculation for ITCs, no specific percentage yielded consistently improved results (Chapter 7; Section 7.4.1). As a result, further research is still required to provide an informed recommendation for dealing with noise related pixels in very high resolution imagery for the assessment of crown decline.

Typical spectral datasets collected from the airborne platform are coarser in resolution (0.2 – 2 m) than those acquired via UAV (0.01 – 0.2 m) (Nebiker *et al*., 2008; Matese *et al*., 2015). To facilitate informed decision making with regard to the platform of data acquisition for the assessment of phytopathogens in forestry, spatial resolution thresholds for particular datasets could be determined for the identification of a particular disease or symptom severity in certain forest environments. Further considerations required prior to the acquisition of data should also include the spatial extent of the area of interest. For example, in the case of the 3 ha mature woodland at Stratfield Brake, the application of the UAV platform would provide a more cost-effective approach to data acquisition than airborne remote sensing. Conversely, if the data collection was commissioned as part of a regional scale assessment of AOD, then an airborne platform may present a more financially viable choice (Matese *et al*., 2015).

8.4 Forest Environment

A significant degree of variability is present with regard to forest structure across different forest types. For example, forests can range from structurally simple, such as those present in extensively managed softwood plantations, to very complex, such as those in naturally regenerated mixed deciduous forest environments (Larsen *et al*., 2011; Zhen *et al*., 2016). The examples presented as part of this research, Ogmore and Radnor Forests (Chapter 4) and Stratified Brake (Chapter 6), present a juxtaposition of forest

structure types that facilitate a comparison of ITC-scale phytopathological assessment under differing forest environments.

8.4.1 Individual Tree Crown Segmentation

In the case of heterogeneous forest environments, such as the mature oak-dominated woodland at Stratfield Brake (Chapter 6), tree crowns exhibit greater variability in structural characteristics than those of more homogenous planation environments, such as the Ogmore and Radnor Forests (Chapter 4). The variation present in tree crown size is particularly influential with regard to ITC segmentation success (Brandtberg *et al*., 2003; Larsen *et al*., 2011; Vauhkonen *et al*., 2012; Strîmbu and Strîmbu, 2015). For example, larger trees occupy more space within the canopy shadowing smaller individuals (Brandtberg *et al*., 2003). In addition, clumps of tree crowns exhibiting differing crown shapes and heights can be particularly challenging to separate (Strîmbu and Strîmbu, 2015), especially in circumstances of frequent crown overlap (Zhen *et al*., 2016). Furthermore, the structural characteristics of individual tree species within the forest is also important for the performance of ITC segmentation (Zhen *et al*., 2016). For instance, the irregularity of oak tree crowns and co-dominance of multiple major branches make them more prone to over-segmentation (Strîmbu and Strîmbu, 2015), whilst the conical crown architecture of coniferous tree species results in a single dominant treetop which can improve compatibility with many established segmentation algorithms (Ke and Quackenbush, 2011). The results from the thesis (Chapters 4 and 6), in addition to the findings from previous research (Brandtberg *et al*., 2003; Ke and Quackenbush, 2011; Strîmbu and Strîmbu, 2015; Zhen *et al*., 2016), indicate the significant influence of crown structural characteristics on ITC segmentation success.

In relation to the selection of segmentation parameters such as filter window sizes, difficulties arise in specifying values which capture real tree crowns within the environment whilst filtering out false ones (Wang *et al*., 2004). Defining filter size parameters, including the Gaussian filter for image smoothing and minimal distance filter for treetop detection is also more challenging when large discrepancies are present in crown size (Ke and Quackenbush, 2011). When parameters are too small, large crowns can be misclassified as a crown clusters. Conversely, if defined parameters are too large, smaller crowns will be missed and merged with surrounding trees (Katoh and Gougeon, 2012). In the case of plantation forest, filtering parameters can be adjusted in accordance

with sub-compartment height (Koch *et al*., 2006), as applied in Chapter 4 (Section 4.3.6). Nevertheless, this approach is unfeasible in more irregular forest environments without organised stand planting and management. Previous studies have also applied high resolution imagery to isolate homogenous forest cover types prior to filtering, however this method has only been reported effective in coniferous plantations (Katoh and Gougeon, 2012).

The ITC segmentation at Stratfield Brake (Chapter 6) was further complicated by the crown decline associated with the AOD infection. The pit-free CHM generation method, successfully applied in the case of *P. ramorum* (Chapter 4), was not suitable for the Stratfield Brake woodland as the DSM was derived via photogrammetry not LiDAR. As a result, contrasting levels of crown decline across the site also increased the differences in ITC size, shape and coverage. In the particular instance of Stratfield Brake, trees classified as dead or in major decline provided the greatest segmentation challenges (Chapter 6: Section 6.4.2). To determine whether the pit-free CHM generation method could assist in the improvement of segmentation in diseased deciduous environments further testing and evaluation using LiDAR would be required.

Forest structure attributes can also influence the suitability of the selected pixel size of raster-based surface elevation inputs for ITC segmentation (Ke and Quackenbush, 2011; Barnes *et al*., 2017b). The results presented in Chapter 4 (Section 4.4.4) demonstrated in the case of larch-dominated plantation forest, that ITC success could be improved when an optimal CHM resolution was selected based on the maximum tree height. Whilst this stratified approach can be applied in systematic plantation environments with clearly defined sub-compartment blocks of homogenous forest, such distinct separation is not present in less managed environments, such as the mature oak-dominated woodland at Stratfield Brake (Chapter 3; Section 3.2). In this instance the resolution of DSM inputs could not be optimised via tree height to improve the segmentation of ITCs, due to the disordered nature of ITCs in the forest canopy. Further consideration is subsequently required to provide informed guidance on the selection of pixel size for raster-based surface elevation inputs in heterogeneous deciduous woodland environments.

Previous ITC research has been largely dominated by studies focused on closed softwood stands (40.6%) (Zhen *et al*., 2016). The dominance of these environments in

the scientific literature was explained by Ke and Quackenbush (2011) by the large number of studies conducted at high latitudes and the abundance of conifer forest in this geographical region, in addition to the suitability of the conical shape of conifer tree species to the majority of ITC segmentation algorithms. Zhen *et al*. (2016) acknowledged the limited availability of research concerning the isolation of deciduous tree crowns, in addition to poorer segmentation accuracies associated with mixed deciduous forest and the overall difficulties associated with ITC delineation in these environments. These concerns are supported by the results of this thesis and demonstrate a clear requirement for further research.

8.4.2 Assessment of Phytopathogens

The most direct influence of forest environment on phytopathogen establishment is the occurrence of host species (Holdenrieder *et al*., 2004; Brasier, 2008). In studies concerned with the identification of a particular phytopathogen, the prior identification of recognised susceptible host species has been common practise (Näsi *et al*., 2015). In the case of the disease detection examples presented for *P. ramorum* (Chapter 5) and AOD (Chapter 7) the respective host species of larch and oak were manually differentiated and isolated from other tree species in the forest environments. Previous studies however, have automated this process and applied species identification techniques prior to disease assessment (Michez *et al*., 2016). Nevertheless, difficulties can arise when structural and spectral properties applied to discriminate between tree species are subsequently altered by the deterioration of crown condition as a result of disease outbreaks (Michez *et al*., 2016).

8.5 Operational Application of Remote Sensing for Phytopathogen Assessment in Forestry

The outputs from the four research chapters have yielded a series of conclusions with interesting implications for the management of *P. ramorum,* AOD, and other phytopathogens. It is therefore important to consider the results of the thesis with regard to the operational management of phytopathogens in forest environments (Wulder *et al*., 2006).

8.5.1 Individual Tree Crown Segmentation

The results presented in Chapter 4 demonstrate a successful methodology for the isolation of individual larch crowns in a plantation forest environment. The presented

approach could be applied alongside the National Forest Inventory to tailor ITC segmentation in sub-compartments of publically managed commercial larch forest. From this perspective, ITCs in plantation environments could be individually segmented and resulting polygons employed as part of operational forest management and monitoring. In contrast, the poor results achieved in Chapter 6 for the mature oak-dominated woodland at Stratfield Brake demonstrate the potential difficulties in automating the isolation of ITCs in less structured forest environments. From this viewpoint, operational segmentation of ITCs for ITC-based assessment from remote sensing cannot be achieved without further research, development and refinement of methodologies. This requirement has previously been identified by Lausch *et al*. (2017) who acknowledged that ITC detection research is still in development.

The novel automated overlap approach to ITC segmentation evaluation outlined and applied in Chapters 4 and 6, demonstrates the opportunity for objective comparison between reported segmentation accuracy percentages (Barnes *et al*., 2017b). This presents a useful tool in the development of ITC segmentation methodologies for particular datasets and forest environments as it provides a quantitative approach to produce overall accuracies and facilitates the robust comparison of results (Zhen *et al*., 2016). In addition, the numerically defined overlap criteria can be altered in order to increase or reduce the quantity of overlap required between automated and manual ITCs for successful delineation. This may be of particular importance in disease detection or classification when a high level of overlap is required to ensure extracted metrics represent the condition of the real tree crown (Shendryk *et al*., 2016).

8.5.2 Assessment of Phytopathogens

The phytopathogen-host interaction is a complex and unique relationship which influences the physical expression and virulence of symptoms following infection (Lovett *et al*., 2006). Whilst the broad symptoms of discolouration, defoliation and death of canopies can be common across disease outbreaks (Innes, 1990), the specificity of symptom development and the variability in crown architecture and spectral properties across tree species requires the evaluation of remote sensing applicability for individual phytopathogen outbreaks (Lovett *et al*., 2006). As a result, prior to the operational deployment of a remote sensing approach for phytopathogen assessment, preliminary studies concerning the ability of sensors to detect a particular disease outbreak is

imperative. This research project has provided the baseline understanding for the remote assessment of crown decline and dieback associated with *P. ramorum* and AOD.

With regard to symptom expression, crown condition is often just one symptom of phytopathogen infection in trees. In the case of both *P. ramorum* in larch and AOD, stem symptoms such as resin bleeds can be additional confirmation that deterioration in tree health has resulted from a specific phytopathogen infection (Brasier and Webber, 2010; Denman *et al*., 2014). Such symptoms cannot be observed from remotely sensed datasets acquired from above the forest canopy. Furthermore, with reference to AOD, the relationship between crown decline and stem symptom severity is still unclear, with no clear observable trend presently acknowledged (Denman *et al*., 2014). In addition, biological testing in the field or laboratory is often required to determine the presence of a specific phytopathogen in new disease outbreaks (Potter *et al*., 2011). For example, in the case of *P. ramorum* and larch disease in the UK, confirmation of the phytopathogen is essential for the issue of a statutory plant health notice (Tracy, 2009). As a result, from an operational perspective, remote sensing cannot provide a diagnostic tool for the confirmation of specific infections in forest environments (Lehman *et al*., 2015). Nevertheless, the technology provides an objective means to monitor known disease outbreaks and identify, with great precision, the locations of ITCs subject to a deterioration in crown condition for further investigation (Fassnacht *et al*., 2014).

The operational requirements for the quantity of information required regarding the severity of crown decline is also an important consideration (Coops *et al*., 2003; Wulder *et al*., 2006). The results from both the *P. ramorum* (Chapter 5; Section 5.4.4) and AOD (Chapter 7; Section 7.4.2) classifications demonstrate the higher overall accuracies obtained in instances of lower class numbers, corresponding with previous findings from the scientific literature (Coops *et al*., 2003; Näsi *et al*., 2015). In addition to the number of categories, the specified class boundaries are also important with regard to classification success. For example, in the application of ALS point cloud metrics for the detection of *P. ramorum* (Chapter 5; Section 5.4.2), no statistically significant difference was observed between individuals classified as healthy and those with light levels of infection (<20 % of crown or stem affected). If this limitation of the approach is recognised prior to operational implementation, then class boundaries can be adjusted and classification and mapping accuracies improved (Kantola *et al*., 2010). Alternatively, if detection of individuals in the early stages of disease progression is an essential

requirement for forest management, other platforms and sensors could subsequently be explored (Wulder *et al*., 2006).

Small-scale site specific studies have clearly presented the assessment and detection capabilities of spectral and structural indicators derived from remote sensing in the case of insect pests and phytopathogens (Coops *et al*., 2009; Kantola *et al*., 2010; Vastaranta *et al*., 2013a; Nielsen *et al*., 2014; Waser *et al*., 2014; Näsi *et al*., 2015) (Chapters 5 and 7). However, the capabilities of remote sensing techniques to assist national programmes of phytopathogen and insect pest monitoring requires further research and development for the technology to provide a more significant large-scale operational role (Lausch *et al*., 2017). Furthermore, whilst a remote sensing approach offers an array of advantages in the objective detection and precise location of crown decline (Fassnacht *et al*., 2014; Reid *et al*., 2016), the technology presents one input into a multi-disciplinary approach in the overall management of phytopathogens in forest environments (Pautasso *et al*., 2012).

Chapter 9: Conclusions, Research Contributions and Outlook

9.1 Thesis Conclusions

To present the overall findings of the research conducted for the thesis, the conclusions have been presented for each research chapter in relation the original research questions outlined in Chapter 1, Section 1.3. Several key conclusions were also reached with regard to the overarching science questions for the research:

> **SQ**: The research demonstrated that high resolution ALS and imagery can be applied to the detection of larch disease and AOD in ITCs. However, the automated segmentation of ITCs remains challenging, especially in mixed deciduous forest.

In **Chapter 4**, the segmentation results for the delineation of individual larch crowns infected with *P. ramorum* from ALS-derived CHMs are reported. Several key findings were acknowledged in response to the initial research questions (RQs 1-3):

> **RQ1**: Compared to the standard CHM, the application of a pit-free CHM generation method improved the segmentation of ITCs in forest stands subject to moderate and severe defoliation resulting from *P. ramorum* infection. However, with regard to segmentation performance in plots comprised of healthy larch forest or light *P. ramorum* infection, the standard approach to CHM generation typically reported higher segmentation accuracies.
>
> **RQ2**: The selected CHM pixel size was acknowledged to influence the overall ITC segmentation accuracy. The application of a 0.25 m CHM pixel size was reported to be most suitable for the larch dominated plots of all ages. However, in instances where the reported maximum plot height was large (>30 m) or small (<20 m), the selection of a coarser (0.5 m) or finer (0.15 m) CHM respectively improved the overall segmentation accuracy.
>
> **RQ3**: The segmentation algorithm applied to the delineation of ITCs was also acknowledged to influence the overall accuracies reported for the larch dominated plots. In particular, the marker-controlled watershed algorithm provided a more successful segmentation of ITCs than the region growing algorithm ($p < 0.10$) in a mixed age planation larch forest. This conclusion was irrespective of *P. ramorum* infection severities.

In **Chapter 5**, the evaluation of ALS for the detection and assessment of *P. ramorum* infection in individual larch trees yielded several informative conclusions with regard to the application of the active sensor for disease assessment. The specific results acknowledged in relation to the initial research questions (RQs 4-6) are outlined below:

RQ4: In the case of the ALS point clouds metrics tested, no significant relationships were evident between maximum tree height and metrics derived using a variable cut-off height (50% of tree height). However, bicentiles B20, B30, B40 and B50 demonstrated a significant linear regression ($p < 0.10$) with maximum tree height when calculated using the static (1 m) cut-off height. Significant relationships with maximum tree height were also evident for CHM fragmentation metrics. For the two-class CHM reclassification (ground/non-ground), all tested fragmentation metrics, excluding ENN_AM, demonstrated a statistically significant linear regression ($p < 0.05$) with maximum tree height. When CHMs were subject to the three-class reclassification, separating the lower and upper canopy, seven of the fifteen fragmentation metrics produced a significant linear regression ($p < 0.05$) with tree height. The analysis demonstrated the requirement to consider the influence of maximum tree height on metric variability prior to their application for disease assessment.

RQ5: In the case of the ALS point cloud and CHM fragmentation metrics, all metrics, excluding the B10 static (1 m) cut-off, demonstrated significant differences ($p < 0.05$) between four *P. ramorum* infection severity categories (not infected, light infection, moderate infection, and heavy infection). However, the more specific post-hoc evaluation of class differences yielded more contrasting results between the ALS point cloud and CHM fragmentation metrics. Collectively, the ALS height point cloud metrics presented significant discrimination between all four disease severity categories, except in the case of the not infected and light infection classes. Conversely, CHM fragmentation metrics only provided consistently significant discrimination between heavily infected larch trees and all other categories.

RQ6: The classification of automated individual tree crowns was conducted for disease presence (infected/not infected) and severity (not infected, light infection, moderate infection, and heavy infection). In both cases, the ALS point cloud

metrics produced the best classifications, with the k-NN classifier yielding overall accuracies of 72.22% (presence) and 65.28% (severity). The k-NN classification performed using the CHM fragmentation metrics resulted in overall accuracies of 65.28% (presence) and 68.06% (severity), with particular difficulties noted in the classification of light and moderate infection levels.

In **Chapter 6**, the automated segmentation of ITCs in a mature oak-dominated woodland environment was assessed with the application of a photogrammetry-derived DSM acquired via UAV. The concluding remarks for this particular study are addressed below in relation to the initial research questions (RQs 7-9) for the chapter:

RQ7: With regard to the impact of crown decline on ITC detection and segmentation, accuracy percentages were calculated for each of the five severity categories (dead, severe decline, moderate decline, minor decline, and healthy). It was noted that the poorest results for treetop detection (23.81% – 28.57%) and ITC segmentation (4.76% – 9.52%) were consistently reported for the individuals classified as dead. In contrast, ITCs classified as moderate decline consistently reported the highest accuracies for treetop detection (72.22% - 75.00%) and segmentation (48.62% – 54.17%). Nevertheless, total accuracies for treetop detection (59.21% - 63.16%) and ITC segmentation (36.18% - 39.47%) demonstrated a poor overall performance for the isolation of ITCs at the Stratfield Brake study site.

RQ8: The extraction of treetops from the study areas was best achieved overall with the application of the local maxima approach (59.21% - 63.16%). The contour methodology also trialled as part of the research, produced improved detection of treetops belonging to individuals classified as dead or in major decline, but overall produced a poorer performance (51.97% - 55.92%). Nevertheless, statistical comparison of results reported for the two treetop extraction methodologies concluded no significant differences in the reported accuracy percentages.

RQ9: The selected pixel size for the photogrammetry-derived DSM inputs was noted to result in minimal variation in accuracy percentages for both treetop detection (3.95%) and ITC segmentation (3.29%). Contrasting resolutions were noted to produce the highest overall accuracies for treetop detection (0.15 m and

0.25 m = 66.16%) and ITC segmentation (0.5 m = 39.47%). Resultantly, no specific conclusions or recommendations could be produced with regard to the optimal DSM pixel size for the isolation of ITCs at the Stratfield Brake site.

In **Chapter 7**, the application of VIs derived for ITCs from UAV-based multispectral imagery was evaluated for the assessment of crown decline associated with AOD in a mature oak-dominated woodland. The outputs from the conducted research are concluded below with specific relation to the initial research questions (RQs 10-12):

RQ10: All five disease severity categories demonstrated significant differences between all other categories ($p < 0.10$) in the GNDVI values extracted from ITCs using the mean value of the brightest 80% of pixels (Mean_80). The VIs NDVI and NDVI-RE were also noted to provide significant distinction ($p < 0.05$) between all disease severity classes, except in the case of individuals classified as healthy or in minor decline. The other VIs tested GRVI, MTCI and ARI exhibited significant differences ($p < 0.01$) between categories, however the specific distinction between individual categories were reported in fewer cases.

RQ11: The evaluation of VI extraction methods, which considered the percentage of the brightest pixels applied in mean VI extraction (Mean_All, Mean_80 and Mean_20) demonstrated no optimum or superior approach to VI calculation. The performance of each approach varied slightly between the six VIs, however no single method could be selectively recommended for further studies.

RQ12: The classifications of crown decline severity for manually delineated individual oak crowns demonstrated improved overall accuracies when the five severity classes (dead, severe decline, moderate decline, minor decline, and healthy) (52.63% - 55.26%) were condensed into three (severe decline, decline, and healthy) (80.26% - 90.79%).

9.2 Research Contributions

The research conducted as part of this thesis has provided several notable contributions to the field of ITC segmentation. Firstly, the research has provided the first direct assessment of ITC segmentation performance in defoliated forest canopies (Chapter 4) (Barnes *et al.*, 2017b). The results also demonstrated the successful segmentation (> 70%) of partially and wholly defoliated larch ITCs via the application of

a pit-free CHM generation methodology, an approach previously untested for diseased forest. Furthermore, the automated overlap assessment developed and applied as part of the research (Chapters 4; Section 4.3.10 and Chapter 6; Section 6.3.10), presents a more objective approach to the evaluation of ITC segmentation success. The method combines the established overlap categories previously applied in visual assessments, but provides quantified class boundaries for a robust comparison of automated and manually delineated ITCs. Resultantly, the ITC segmentation success accuracies reported from different study sites and plots can be reviewed without the influence of interpreter's error on the assignment of overlap categories.

With regard to phytopathogen assessment in forest environments the work conducted as part of this thesis also presents a selection of research contributions. In the case of Chapter 5, which concerned the phytopathogen *P. ramorum* and larch disease, two key research contributions can be identified. Firstly, the disease detection capabilities of ALS point cloud metrics for the assessment of *P. ramorum* infection in larch trees has been established. The research findings demonstrated the application of height-based ALS point cloud metrics for the discrimination of ITCs subject to moderate and heavy defoliation. In addition, the research also presents the first assessment of landscape fragmentation metrics from the field of ecology, for the quantification of upper crown fragmentation in CHMs of diseased trees. The results highlight the applications of these metrics in the assessment of individual larch tree crowns subject to severe defoliation as a result of *P. ramorum* infection. Overall, this research has presented the first example for the application of ALS in the assessment of phytopathogens in forested environments.

In the case of crown decline associated with AOD, the research presented in Chapter 7 provides another notable contribution to the assessment of this particular disease. The results from the research have demonstrated the first successful application of UAV-based multispectral imagery for the discrimination of decline severity categories in mature oak trees affected by AOD ($p < 0.10$). Furthermore, the research stands alongside a limited number of previous studies concerned with insect pests to present the potential applications of the UAV remote sensing platform for disease assessment in forest environments.

9.3 Outlook and Opportunities for Further Research

As a result of the research outputs and analysis of the current scientific literature, several themes and avenues for further research have been identified. In the field of ITC segmentation, a number of unanswered scientific questions were acknowledged. Firstly, the limited success of the ITC segmentation for the mature oak-dominated woodland presented in Chapter 6, in addition to low previously reported segmentation accuracies for deciduous forest, has demonstrated the requirement for further research into the performance of established segmentation methodologies in these environments. This further work may also entail the development of new approaches to identify ITCs within these heterogeneous forest canopies. In the case of raster-based segmentation methods, consideration is also required to provide pixel size recommendations for deciduous forest of varying characteristics. For forests subject to dieback and decline, further research is required to determine whether the pit-free CHM generation methodology, which facilitated the successful segmentation (>70%) of partially and wholly defoliated larch canopies, could also improve the isolation of deciduous oak canopies subject to varying severities of crown decline. This research would require the application of LiDAR to a study area such as Stratfield Brake, as opposed to the photogrammetry-derived DSM applied in Chapter 6. Comparing the performance of LiDAR acquired via aircraft and UAV and the performance of LiDAR and photogrammetry-derived surface elevation for the segmentation of diseased ITCs in varying forest environments would also be of benefit to inform operational forestry decisions.

Whilst the ALS utilised in Chapter 5 provided successful detection of ITCs subject to moderate and severe *P. ramorum* infection, the average point density of 24 points/m^2 demonstrates a high resolution dataset. In many cases ALS surveys commissioned for operational forestry applications may exhibit a much lower density of ALS points. Resultantly, in order to provide clear recommendations with regard to ALS data acquisition requirements and spatial resolution thresholds for disease detection, further research is required to determine the disease discrimination potential of ALS across a range of point densities. As an initial starting point for this investigation, point thinning could be applied to the existing ALS datasets for the Ogmore and Radnor Forests.

With regard to the application of very high resolution UAV-based imagery, the results presented in Chapter 7 demonstrated an inconclusive result in relation to the best

practise for eliminating noise related pixels. Whilst calculating VIs from only the brightest percent of pixels (80% and 20%) improved crown decline category discrimination in some cases, performance was not consistent. Subsequently, further research is required to evaluate methods for the elimination of noise related pixels in very high resolution UAV imagery for decline and disease detection conducted at the ITC-level. Such information is of particular importance for providing clear recommendations for the operational applications of UAVs in the assessment of phytopathogens in forest environments.

Whilst the research presented in Chapters 5 and 7 presents the successful assessment of *P. ramorum* in larch and AOD, these studies are confined to specific locations where the presence of the respective phytopathogen infections had previously been identified. The results from these chapters demonstrate the proof of concept for the application of ALS and UAV-based multispectral imagery for the assessment of these specific phytopathogens in the particular forest environments. However, further research is required to consider the applications of remote sensing technologies for the detection of new outbreaks at regional and national scales. To consider the remote sensing applications for phytopathogen assessment across larger geographical extents research is required over larger spatial scales. With regard to the isolation of ITCs at the national scale, UK based remote sensing company Bluesky International, who acquired the ALS for the research, have previously produced a National Tree Map for England and Wales employing a range of segmentation techniques to identify ITCs (Bluesky, 2017). Such type of product could be employed to provide the basis for conducting larger-scale assessment of tree disease. In addition, with regard to publically managed commercial forestry in the UK, the National Forest Inventory (Forestry Commission, 2017) which provides detailed information of tree species and ages within designated sub-compartments, could be applied to facilitate a targeted assessment of phytopathogens and their known hosts. Furthermore, in the case of *P. ramorum* in larch species, conducting a regional scale trial alongside the current approach of performing visual inspections via helicopter survey would also facilitate an informative comparison of the two approaches for disease detection.

Reference List

Adelabu, S., Mutanga, O. and Adam, E. (2014) Evaluating the impact of red-edge band from Rapideye image for classifying insect defoliation levels. *ISPRS Journal of Photogrammetry and Remote Sensing*. **95**, 24-41.

Aicardi, I., Dabove, P., Lingua, A. M. and Piras, M. (2016) Integration between TLS and UAV photogrammetry techniques for forestry applications. *iForest – Biogeosciences and Forestry*. **10** (1), 41.

Albetis, J., Duthoit, S., Guttler, F., Jacquin, A., Goulard, M., Poilvé, H., Féret, J. B. and Dedieu, G. (2017) Detection of flavescence dorée grapevine disease using unmanned aerial vehicle (UAV) multispectral imagery. *Remote Sensing*. **9** (4), 308.

Alexander, J. and Lee, C. A. (2010) Lessons learned from a decade of sudden oak death in California: evaluating local management. *Environmental Management*. **46**, 315-328.

Ali, S. S., Dare, P. and Jones, S. D. (2008) Fusion of remotely sensed multispectral imagery and lidar data for forest structure assessment at the tree level. *International Archives of Photogrammetry and Remote Sensing*. **37** (2), 1089-1094.

Andersen, H. E. (2009) Using airborne light detection and ranging (LIDAR) to characterize forest stand condition on the Kenai Peninsula of Alaska. *Western Journal of Applied Forestry*. **24** (2), 95-102.

Axelsson, P. (1999) Processing of laser scanner data—algorithms and applications. *ISPRS Journal of Photogrammetry and Remote Sensing*. **54** (2), 138-147.

Balzter, H., Luckman, A., Skinner, L., Rowland, C. and Dawson, T. (2007) Observations of forest stand top height and mean height from interferometric SAR and LiDAR over a conifer plantation at Thetford Forest, UK. *International Journal of Remote Sensing*. **28** (6), 1173-1197.

Baral, H. O., Queloz, V. and Hosoya, T. (2014) *Hymenoscyphus fraxineus*, the correct scientific name for the fungus causing ash dieback in Europe. *IMA Fungus*. **5** (1), 79-80.

Barnes, C., Balzter, H., Barrett, K., Eddy, J., Milner, S. and Suárez, J. C. (2017a) Airborne laser scanning and tree crown fragmentation metrics for the assessment of *Phytophthora ramorum* infected larch forest stands. *Forest Ecology and Management*. **404**, 294-305.

Barnes, C., Balzter, H., Barrett, K., Eddy, J., Milner, S. and Suárez, J. C. (2017b) Individual tree crown delineation from airborne laser scanning for diseased larch forest stands. *Remote Sensing*. **9**, 231.

Barry, K. M., Stone, C. and Mohammed, C. L. (2008) Crown-scale evaluation of spectral indices for defoliated and discoloured eucalypts. *International Journal of Remote Sensing*. **29** (1), 47-49.

Bater, C. W., Coops, N. C., Gergel, S. E., LeMay, V. and Collins, D. (2009) Estimation of standing dead tree class distributions in northwest coastal forests using lidar remote sensing. *Canadian Journal of Forest Research*. **39** (6), 1080-1091.

Bater, C. W., Wulder, M. A., White, J. C. and Coops, N. C. (2010) Integration of LIDAR and digital aerial imagery for detailed estimates of lodgepole pine (*Pinus contorta*) volume killed by mountain pine beetle (*Dendroctonus ponderosae*). *Journal of Forestry*. **108** (3), 111-119.

Belgiu, M. and Drăguţ, L. (2016) Random forest in remote sensing: a review of applications and future directions. *ISPRS Journal of Photogrammetry and Remote Sensing*. **114**, 24-31.

Ben-Arie, J. R., Hay, G. J., Powers, R. P., Castilla, G. and St-Onge, B. (2009) Development of a pit filling algorithm for LiDAR canopy height models. *Computers & Geosciences*. **35**, 1940-1949.

Berni, J. A., Zarco-Tejada, P. J., Suárez, L. and Fereres, E. (2009) Thermal and narrowband multispectral remote sensing for vegetation monitoring from an unmanned aerial vehicle. *IEEE Transactions on Geoscience and Remote Sensing*. **47** (3), 722-738.

Bigler, C., Bräker, O. U., Bugmann, H., Dobbertin, M. and Rigling, A. (2006) Drought as an inciting mortality factor in Scots pine stands of the Valais, Switzerland. *Ecosystems*. **9** (3), 330-343.

Birth, S. G. and McVey, R. G. (1968) Measuring the colour of growing turf with a reflectance spectrophotometer. *Agronomy Journal*. **60** (6), 640-643.

Blackburn, G. A. (2007) Hyperspectral remote sensing of plant pigments. *Journal of Experimental Botany*. **58** (4), 855-867.

Blaschke, T. (2010) Object based image analysis for remote sensing. *ISPRS Journal of Photogrammetry and Remote Sensing*. **65** (1), 2-16.

Bluesky (2017) *National Tree Map*. [online] <https://www.blueskymapshop.com/products/national-tree-map> [Accessed on 01/09/17].

Böhner, J., Selige, T. and Ringeler, A. (2006) Image segmentation using representativeness analysis and region growing. *Gottinger Geographischne Abhandlungen*. **115**, 29-38.

Boyd, D. S. and Danson, F. M. (2005) Satellite remote sensing of forest resources: three decades of research development. *Progress in Physical Geography*. **29** (1), 1-26.

Boyd, I. L., Freer-Smith, P. H., Gilligan, C. A. and Godfray, C. J. (2013) The consequence of tree pests and diseases for ecosystem services. *Science*. **342**, 823.

Brady, C., Denman, S., Kirk, S., Venter, S., Rodríguez-Palenzuela, P. and Coutinho, T. (2010) Description of *Gibbsiella quercinecans* gen. nov., sp. nov., associated with acute oak decline. *Systematic and Applied Microbiology*. **33**, 444-450.

Brady, C., Allainguillaume, J., Denman, S. and Arnold, D. (2016) Rapid identification of bacteria associated with Acute Oak Decline by high-resolution melt analysis. *Letters in Applied Microbiology*. **63** (2), 89-95.

Brandtberg, T. and Walter, F. (1998) Automated delineation of individual tree crowns in high spatial resolution aerial images by multiple-scale analysis. *Machine Vision and Applications*. **11**, 64-73.

Brandtberg, T., Warner, T. A., Landenberger, R. E. and McGraw, J. B. (2003) Detection and analysis of individual leaf-off tree crowns in small footprint, high sampling density lidar data from the eastern deciduous forest in North America. *Remote Sensing of Environment*. **85**, 290-303.

Brasier, C. M. (2008) The biosecurity threat to the UK and global environment from international trade in plants. *Plant Pathology*. **57**, 792-808.

Brasier, C. M., Denman, S., Rose, J., Kirk, S. A., Hughes, K. J. D., Griffin, R. L., Lane, C. R., Inman, A. J. and Webber, J. F. (2004) First report of ramorum bleeding canker on *Quercus falcata*, caused by *Phytophthora ramorum*. *Plant Pathology*. **53**, 804.

Brasier, C. M. and Webber, J. F. (2010) Sudden larch death. *Nature*. **466**, 824-825.

Brasier, C. M., Vettraino, A. M., Chang, T. T. and Vannini, A. (2010) *Phytophthora lateralis* discovered in an old growth *Chamaecyparis* forest in Taiwan. *Plant Pathology*. **59**, 595-603.

Breidenbach, J., Naesset, E., Lien, V., Gobakken, T. and Solberg, S. (2010) Prediction of species specific forest inventory attributes using a nonparametric semi-individual tree crown approach based on fused airborne laser scanning and multispectral data. *Remote Sensing of Environment*. **114** (4), 911-924.

Breiman, L. (2001) Random forests. *Machine Learning*. **45**, 5-32.

Bright, B. C., Hudak, A. T., McGaughey, R., Andersen, H. E. and Negrón, J. (2013) Predicting live and dead tree basal area of bark beetle affected forests from discrete-return lidar. *Canadian Journal of Remote Sensing*. **39**, S1-S13.

Brown, A. V., Rose, D. R. and Webber, J. F. (2003) *Red Band Needle Blight of Pine*. Edinburgh, UK: Forestry Commission: Forest Research Information Note 49.

Brown, N., Inward, D. J. G., Jeger, M. and Denman, S. (2015) A review of *Agrilus biguttatus* in UK forests and its relationship with acute oak decline. *Forestry*. **88**, 53-63.

Brown, N., Jeger, M., Kirk, S., Xu, X. and Denman, S. (2016) Spatial and temporal patterns in symptom expression within eight woodlands affected by acute oak decline. *Forest Ecology and Management*. **360**, 97-109.

Bunting, P. and Lucas, R. (2006) The delineation of tree crowns in Australian mixed species forests using hyperspectral Compact Airborne Spectrographic Imager (CASI) data. *Remote Sensing of Environment*. **101** (2), 230-248.

Bütler, R. and Schlaepfer, R. (2004) Spruce snag quantification by coupling colour infrared aerial photos and a GIS. *Forest Ecology and Management*. **195** (3), 325-339.

Carleer, A. and Wolff, E. (2004) Exploitation of very high resolution satellite data for tree species identification. *Photogrammetric Engineering & Remote Sensing*. **70** (1), 135-140.

Carter, G. A., Cibula, W. G. and Miller, R. L. (1996) Narrow-band reflectance imagery compared with thermal imagery for early detection of plant stress. *Journal of Plant Physiology*. **148** (5), 515-522.

Casas, A., García, M., Siegel, R. B., Koltunov, A., Ramírez, C. and Ustin, S. (2016) Burned forest characterization at single-tree level with airborne laser scanning for assessing wildlife habitat. *Remote Sensing of Environment*. **175**, 231-241.

Castillejo-González, I. L., López-Granados, F., García-Ferrer, A., Peña-Barragán, J. M., Jurado-Expósito, M., de la Orden, M. S. and González-Audicana, M. (2009) Object-and pixel-based analysis for mapping crops and their agro-environmental associated measures using QuickBird imagery. *Computers and Electronics in Agriculture*. **68** (2), 207-215.

Chadfield, V. and Pautasso, M. (2012) *Phytophthora ramorum* in England and Wales: which environmental variables predict county disease incidence. *Forest Pathology*. **42**, 150-159.

Chang, A., Eo, Y., Kim, Y. and Kim, Y. (2013) Identification of individual tree crowns from LiDAR data using a circle fitting algorithm with local maxima and minima filtering. *Remote Sensing Letters*. **4** (1), 29-37.

Chen, B., Wang, K., Li, S., Xiao, C., Chen, J. and Jin, X. (2011) Estimating severity level of cotton infected verticillium wilt based on spectral indices of TM image. *Sensor Letters*. **9** (3), 1157-163.

Chen, Q., Baldocchi, D., Gong, P. and Kelly, M. (2006) Isolating individual trees in a savanna woodland using small footprint lidar data. *Photogrammetric Engineering & Remote Sensing*. **72** (8), 923-932.

Cobb, R. C. and Metz, M. R. (2017) Tree diseases as a cause and consequence of interacting forest disturbances. *Forests*. **8** (5), 147.

Cohen, J. (1960) A coefficient of agreement for nominal scales. *Educational and Psychological Measurement*. **20** (1), 37-46.

Collins, M. J., Dymond, C. and Johnson, E. A. (2004) Mapping subalpine forest types using networks of nearest neighbour classifiers. *International Journal of Remote Sensing*. **25** (9), 1701-1721.

Colomina, I. and Molina, P. (2014) Unmanned aerial systems for photogrammetry and remote sensing: a review. *ISPRS Journal of Photogrammetry and Remote Sensing*. **92**, 79-97.

Condeso, T. E. and Meentemeyer, R. K. (2007) Effects of landscape heterogeneity on the emerging forest disease sudden oak death. *Journal of Ecology*. **95** (2), 364-375.

Congalton, R. G. (1991) A review of assessing the accuracy of classifications of remotely sensed data. *Remote Sensing of Environment*. **37**, 35-46.

Congalton, R. and Green, K. (1999) *Assessing the Accuracy of Remotely Sensed Data: Principles and Practises*. Boca Raton, FL: CRC/Lewis Press. 137.pp.

Conyers, S., Somerwill, K., Ramwell, C., Hughes, J., Laybourn, R. and Jones, N. (2011) *Review of the known potential biodiversity impacts of Phytophthora and the likely impact on ecosystem services*. [pdf] York: Food and Environment Research. <https://www.gov.uk/government/organisations/department-for-environment-food-rural-affairs> [Accessed on 22/08/16].

Coops, N. C., Hilker, T., Wulder, M. A., St-Onge, B., Newnham, G., Siggins, A. and Trofymow, J. T. (2007) Estimating canopy structure of Douglas-fir forest stands from discrete-return LiDAR. *Trees*. **21** (3), 295.

Coops, N. C., Johnson, M., Wulder, M. A. and White, J. C. (2006) Assessment of QuickBird high spatial resolution imagery to detect red attack damage due to mountain pine beetle infestation. *Remote Sensing of Environment*. **103**, 67-80.

Coops, N. C., Stanford, M., Old, K., Dudzinski, M., Culvenor, D. and Stone, C. (2003) Assessment of Dorthistroma needle blight of *Pinus radiata* using airborne hyperspectral imagery. *Ecology and Epidemiology*. **93** (12), 1524-1532.

Coops, N. C., Varhola, A., Bater, C. W., Teti, P., Boon, S., Goodwin, N. and Weiler, M. (2009) Assessing differences in tree and stand structure following beetle infestation using lidar data. *Canadian Journal of Remote Sensing*. **35** (6), 497-508.

Cover, T. and Hart, P. (1967). Nearest neighbor pattern classification. *IEEE Transactions on Information Theory*. **13** (1), 21–7.

Curran, P. J., Dungan, J. L. and Gholz, H. L. (1990) Exploring the relationship between reflectance red edge and chlorophyll content in slash pine. *Tree Physiology*. **7**, 33-48.

Dash, J. and Curran, P. J. (2004) The MERIS terrestrial chlorophyll index. *International Journal of Remote Sensing*. **25** (23), 5403-5413.

Dash, J. and Ogutu, B. (2016) Recent advances in space-borne optical remote sensing systems for monitoring global terrestrial ecosystems. *Progress in Physical Geography*. **40** (2), 322-351.

Davidson, J. M., Wickland, A. C., Patterson, H. A., Falk, K. R. and Rizzo, D. M. (2005) Transmission of *Phytophthora ramorum* in mixed-evergreen forest in California. *Ecology and Epidemiology*. **95** (5), 587-596.

de Beurs, K. M. and Townsend, P. A. (2008) Estimating the effect of gypsy moth defoliation using MODIS. *Remote Sensing of Environment*. **112**, 3983-3990.

DEFRA (2016) *UK Plant Health Risk Register*. [Excel Workbook] <https://secure.fera.defra.gov.uk/phiw/riskRegister/> [Accessed on 02/12/16].

Deng, S., Katoh, M., Yu, X., Hyyppä, J. and Gao, T. (2016) Comparison of tree species classifications at the individual tree level by combining ALS data and RGB images using different algorithms. *Remote Sensing*. **8** (12), 1034.

Denman, S., Brady, C., Kirk, S., Cleenwerck, I., Venter, S., Coutinho, T. and De Vos, P. (2012) *Brenneria goodwinii* sp. nov., associated with acute oak decline in the UK. *International Journal of Systematic and Evolutionary Microbiology*. **62**, 2451-2456.

Denman, S., Brown, N., Kirk, S., Jeger, M. and Webber, J. (2014) A description of acute oak decline in Britain and a comparative review on causes of similar disorders on oak in Europe. *Forestry*. **87**, 535-551.

Denman, S., Kirk, S. A. and Webber, J. F. (2010) *Managing Acute Oak Decline*. Forestry Commission Practise Note 15. Forestry Commission: Edinburgh, UK.

Denman, S., Plummer, S., Kirk, S., Peace, A. and McDonald, J. E. (2016) Isolation studies reveal a shift in the cultivable microbiome of oak affected with acute oak decline. *Systematic and Applied Microbiology*. **39** (7), 484-490.

Denman, S. and Webber, J. (2009) Oak declines: new definitions and new episodes in Britain. *Quarterly Journal of Forestry*. **103** (4), 285-290.

Devadas, R., Lamb, D. W., Simpfendorfer, S. and Backhouse, D. (2009) Evaluating ten spectral vegetation indices for identifying rust infection in individual wheat leaves. *Precision Agriculture*. **10** (6), 459-470.

Di Gennaro, S. F., Battiston, E., Di Marco, S., Facini, O., Matese, A., Nocentini, M., Palliotti, A. and Mugnai, L. (2016) Unmanned aerial vehicle (UAV)-based remote sensing to monitor grapevine leaf stripe disease within a vineyard affected by esca complex. *Photopathologia Mediterranea*. **55** (2), 262.

Dralle, K. and Rudemo, M. (1996) Stem number estimation by kernel smoothing of aerial photos. *Canadian Journal of Forest Research*. **26**, 1228-1236.

Du-ning, X. and Xiu-zhen, L. (1999) Core concepts of landscape ecology. *Journal of Environmental Sciences*. **11** (2), 131-135.

Dubayah, R. O. and Drake, J. B. (2000) Lidar remote sensing for forestry. *Journal of Forestry*. **98** (6), 44-46.

Duncanson, L. I., Cook, B. D., Hurtt, G. C. and Dubayah, R. O. (2014) An efficient, multi-layered crown delineation algorithm for mapping individual tree structure across multiple ecosystems. *Remote Sensing of Environment*. **154**, 378-386.

Dunford, R., Michel, K., Gagnage, M., Piégay, H. and Trémelo, M. L. (2009) Potential and constraints of unmanned aerial vehicle technology for the characterization of Mediterranean riparian forest. *International Journal of Remote Sensing*. **30**, 4915-4935.

Ene, L., Næsset, E. and Gobakken, T. (2012) Single tree detection in heterogeneous boreal forests using airborne laser scanning and area-based stem number estimates. *International Journal of Remote Sensing*. **33** (16), 5171-5193.

Environment Agency (2016) Environment Agency LIDAR Data, Technical Note. [pdf] <http://www.geostore.com/environment-agency/docs/Environment_Agency_LIDAR_Open_Data_FAQ_v5.pdf> [Accessed on 21/02/17].

Erikson, M. (2003) Segmentation of individual tree crowns in colour aerial photographs using region growing supported by fuzzy rules. *Canadian Journal of Forest Research*. **33** (8), 1557-1563.

Erikson, M. (2004) Species classification of individually segmented tree crowns in high-resolution aerial images using radiometric and morphologic image measures. *Remote Sensing of Environment*. **91** (3), 469-477.

Erikson, M. and Olofsson, K. (2005) Comparison of three individual tree crown detection methods. *Machine Vision and Applications*. **16** (4), 258-265.

Everitt, J. H., Escobar, D. E., Appel, D. N., Riggs, W. G. and Davis, M. R. (1999) Using airborne digital imagery for detecting oak wilt disease. *Plant disease*. **83** (6), 502-505.

Falkowski, M. J., Smith, A. M., Hudak, A. T., Gessler, P. E., Vierling, L. A. and Crookston, N. L. (2006) Automated estimation of individual conifer tree height and crown diameter via two-dimensional spatial wavelet analysis of lidar data. *Canadian Journal of Remote Sensing*. **32** (2), 153-161.

Fang, F., Im, J., Lee, J. and Kim, K. (2016) An improved tree crown delineation method based on live crown ratios from airborne LiDAR data. *GIScience & Remote Sensing*. **53** (3), 402-419.

Fassnacht, F. E., Latifi, H., Ghosh, A., Joshi, P. K. and Koch, B. (2014) Assessing the potential of hyperspectral imagery to map bark beetle-induced tree mortality. *Remote Sensing of Environment*. **140**, 533-548.

Fauvel, M., Chanussot, J. and Benediktsson, J. A. (2006) *Evaluation of kernels for multiclass classification of hyperspectral remote sensing data*. In: Proceedings IEEE International Conference on Acoustics, Speech and Signal Processing, ICASSP. Toulouse, France.

Feng, Q., Liu, J. and Gong, J. (2015) UAV remote sensing for urban vegetation mapping using random forest and texture analysis. *Remote Sensing*. **7**, 1074-1094.

Ferris, R., Peace, A. J., Humphrey, J. W. and Broome, A. C. (2000) Relationships between vegetation, site type and stand structure in coniferous plantations in Britain. *Forest Ecology and Management*. **136** (1-3), 35-51.

Filipe, J. A. N., Cobb, R. C., Meentemeyer, R. K., Lee, C. A., Valachovic, Y. S., Cook, A. R., Rizzo, D. M. and Gilligan, C. A. (2012) Landscape epidemiology and control of pathogens with cryptic and long-distance dispersal: sudden oak death in northern Californian forests. *PLoS Computational Biology*. **8** (1), e1002328.

Forestry Commission (2014) *Tree pests and diseases* [online]. Available at <http://www.forestry.gov.uk/forestry/INFD-6ABL5V> [Accessed on 17/03/15].

Forestry Commission (2016) *Phytophthora ramorum outbreak and risk zones maps* [online]. <http://www.forestry.gov.uk/forestry/infd-86ajqa> [Accessed on 11/03/16].

Forestry Commission (2017) *Datasets* [online]. < https://www.forestry.gov.uk/datasets> [Accessed on 01/09/17].

Foster, A. C., Walter, J. A., Shugart, H. H., Sibold, J. and Negron, J. (2017) Spectral evidence of early-stage spruce bark beetle infestation in Engelmann spruce. *Forest Ecology and Managemen*t. **384**, 347-357.

Fraser, R. H. and Latifovic, R. (2005) Mapping insect-induced tree defoliation and mortality using coarse spatial resolution satellite imagery. *International Journal of Remote Sensing*. **26** (1), 193-200.

Gambella, F., Sistu, L., Piccirilli, D., Corposanto, S., Caria, M., Arcangeletti, E., Proto, A. R., Chessa, G. and Pazzona, A. (2016) Forest and UAV: a bibliometric review. *Contemporary Engineering Sciences*. **9** (28), 1359-1370.

Garcia-Ruiz, F., Sankaran, S., Maja, J. M., Lee, W. S., Rasmussen, J. and Ehsani, R. (2013) Comparison of two aerial imaging platforms for identification of Huanglongbing-infected citrus trees. *Computers and Electronics in Agriculture*. **91**, 106-115.

Garrity, S. R., Allen, C. D., Brumby, S. P., Gangodagamage, C., McDowell, N. G. and Cai, D. M. (2013) Quantifying tree mortality in a mixed species woodland using multitemporal high spatial resolution satellite imagery. *Remote Sensing of Environment*. **129**, 54-65.

Getzin, S., Nutske, R. S. and Wiegand, K. (2014) Using unmanned aerial vehicles (UAV) to quantify spatial gap patterns in forests. *Remote Sensing*. **6**, 6988-7004.

Gitelson, A., Kaufman, Y. J. and Merzlyak, M. N. (1996) Use of a green channel in remote sensing of global vegetation from EOS-MODIS. *Remote Sensing of Environment*. **58** (3), 289-298.

Gitelson, A. and Merzlyak, M. N. (1994) Spectral reflectance changes associated with autumn senescence of *Aesculus hippocastanum* L. and *Acer platanoides* L. leaves. Spectral features and relation to chlorophyll estimation. *Journal of Plant Physiology*. **143**, 286-292.

Gitelson, A., Merzlyak, M. N. and Chivkunova, O. B. (2001) Optical properties and non-destructive estimation of anthocyanin content in plant leaves. *Photochemistry and Photobiology*. **74** (1), 38-45.

Goetz, A. F. H. (2009) Three decades of hyperspectral remote sensing of the Earth: a personal view. *Remote Sensing of Environment*. **113**, S5-S16.

Gower, S. T. and Richards, J. H. (1990) Larches: deciduous conifers in an evergreen world. *Biosceince*. **40** (11), 818-826.

Grenzdörffer, G. J., Engel, A. and Teichert, B. (2008) The photogrammetric potential of low-cost UAVs in forestry and agriculture. *The International Archives of the Photogrammetry, Remote Sensing and Spatial Information Sciences*. **31** (B3), 1207-1214.

Hall, R. J., Castilla, G., White, J. C., Cooke, B. J. and Skakun, R. S. (2016) Remote sensing of forest pest damage: a review and lessons learned from a Canadian perspective. *The Canadian Entomologist.* **148**, S296-S356.

Hanavan, R. P., Pontius, J. and Hallett, R. (2015) A 10-Year assessment of hemlock decline in the catskill mountain region of New York state using hyperspectral remote sensing techniques. *Journal of Economic Entomology*. **108** (1), 339-349.

Hansen, E. M. and Goheen, E. M. (2000) *Phellinuas weirii* and other native root pathogens as determinants of forest structure and process in western North America. *Annual Review of Phytopathology*. **38** (1), 515-539.

Hargis, C. D., Bissonette, J. A. and David, J. L. (1998) The behaviour of landscape metrics commonly used in the study of habitat fragmentation. *Landscape Ecology*. **13**, 167-186.

Harris, A. R. and Webber, J. F. (2016) Sporulation potential, symptom expression and detection of *Phytophthora ramorum* on larch needles and other foliar hosts. *Plant Pathology*. **65**, 1441-1451.

Hatala, J. A., Crabtree, R. L., Halligan, K. Q. and Moorcroft, P. R. (2010) Landscape-scale patterns of forest pest and pathogen damage in the Greater Yellowstone Ecosystem. *Remote Sensing of Environment*. **114** (2), 375-384.

Hay, G. J., Marceau, D. J., Dube, P. and Bouchard, A. (2001) A multiscale framework for landscape analysis: object-specific analysis and upscaling. *Landscape Ecology*. **16** (6), 471-490.

Heurich, M., Ochs, T., Andresen, T. and Schneider, T. (2010) Object-orientated image analysis for the semi-automatic detection of dead trees following a spruce bark beetle (*Ips typographus*) outbreak. *European Journal of Forest Research*. **129** (3), 313-324.

Holdenrieder, O., Pautasso, M., Weisberg, P. J. and Lonsdale, D. (2004) Tree diseases and landscape processes: the challenge of landscape pathology. *TRENDS in Ecology and Evolution*. **19** (8), 446-452.

Holmgren, J. and Persson, A. (2004) Identifying species of individual trees using airborne laser scanner. *Remote Sensing of Environment*. **90** (4), 415-423.

Hopkinson, C., Chasmer, L., Gynan, C., Mahoney, C. and Sitar, M. (2016) Multisensor and multispectral lidar characterization and classification of a forest environment. *Canadian Journal of Remote Sensing*. **42** (5), 501-520.

Hsu, C. W., Chang, C. C. and Lin, C. J. (2003) *A practical guide to support vector classification*. Technical Report, Department of Computer Science, National Taiwan University, Taipei 106, Taiwan.

Hu, B., Li, J., Jing, L. and Judah, A. (2014) Improving the efficiency and accuracy of individual tree crown delineation from high-density LiDAR data. *International Journal of Applied Earth Observation and Geoformation*. **26**, 145-155.

Huang, C., Davis, L. S. and Townshend, J. R. G. (2002) An assessment of support vector machines for land cover classification. *International Journal of Remote Sensing*. **23** (4), 725-749.

Hudak, A. T., Crookston, N. L., Evans, J. S., Hall, D. E. and Falkowski, M. J. (2008) Nearest neighbour imputation of species-level, plot-scale forest structure attributes from LiDAR data. *Remote Sensing of Environment*. **112**, 2232-2245.

Huete, A. R. (2012) Vegetation indices, remote sensing and forest monitoring. *Geography Compass*. **6** (9), 513-532.

Hung, C., Bryson, M. and Sukkarieh, S. (2012) Multi-class predictive template for tree crown detection. *ISPRS Journal of Photogrammetry and Remote Sensing*. **68**, 170-183.

Hyun, I. H. and Choi, W. (2014) *Phytophthora* species, new threats to the plant health in Korea. *The Plant Pathology Journal*. **30** (4), 331-342.

Hyyppä, J., Hyyppä, H., Inkinen, M., Engdahl, M., Linko, S. and Zhu, Y. H. (2000) Accuracy comparison of various remote sensing data sources in the retrieval of forest stand attributes. *Forest Ecology and Management*. **128**, 109-120.

Hyyppä, J., Yu, X., Hyyppä, H., Vastaranta, M., Holopainen, M., Kukko, A., Kaartinen, H., Jakayla, A., Vaaja, M., Koskinen, J. and Alho, P. (2012) Advances in forest inventory using airborne laser scanning. *Remote Sensing*. **4** (5), 1190-1207.

Immitzer, M., Atzberger, C. and Koukal, T. (2012) Tree species classification with random forest using very high spatial resolution 8-band WorldView-2 satellite data. *Remote Sensing*. **4** (9), 2661-2693.

Innes, J. L. (1990) *Forestry Commission Field Book 12: Assessment of Tree Condition*. London: HMSO.

Ismail, R., Mutanga, O. and Bob, U. (2007) Forest health and vitality: the detection and monitoring of *Pinus patula* trees infected by *Sirex noctilio* using digital multispectral imagery. *Southern Hemisphere Forestry Journal*. **69** (1), 39-47.

Ivors, K., Garbelotto, M., Vries, D. E., Ruyter-Spira, B., Hekkert, B. T. E., Rosenzweig, N. and Bonants, P. (2006) Microsatellite markers identify three lineages of *Phytophthora ramorum* in US nurseries, yet single lineages in US forest and European nursery populations. *Molecular Ecology*. **15**, 1493-1505.

Ivors, K., Hayden, K. J., Bonants, P. J. M., Rizzo, D. M. and Garbelotto, M. (2004) AFLP and phylogenetic analyses of North America and European populations of *Phytophthora ramorum*. *Mycological Research*. **108** (4), 378-392.

Jakubowski, M. K., Li, W., Guo, Q. and Kelly, M. (2013) Delineating individual trees from lidar data: a comparison of vector- and raster-based segmentation approaches. *Remote Sensing*. **5** (9), 4163-4186.

Jing, L., Hu, B., Noland, T. and Li, J. (2012) An individual tree crown delineation method based on multi-scale segmentation of imagery. *ISPRS Journal of Photogrammetry and Remote Sensing*. **70**, 88-98.

Johnson, B. A., Tateishi, R. and Hoan, N. T. (2013) A hybrid pansharpening approach and multiscale object-based image analysis for mapping diseased pine and oak trees. *International Journal of Remote Sensing*. **34** (20), 6969-6982.

Jones, D. R. and Baker, R. H. A. (2007) Introductions of non-native plant pathogens into Great Britain, 1970-2004. *Plat Pathology*. **56**, 891-910.

Jones, H. G. and Vaughan, R. A. (2010) *Remote Sensing of Vegetation Principles, Techniques and Applications*. New York: Oxford University Press.

Kaartinen, H., Hyyppä, J., Yu, X., Vastaranta, M., Hyyppä, H., Kukko, A., Holopainen, M., Heipke, C., Hirschmugl, M., Morsdorf, F., Naesset, E., Pitkänen, J., Popescu, S., Solberg, S., Wolf, B. M. and Wu, J. C. (2012) An international comparison of individual tree detection and extraction using airborne laser scanning. *Remote Sensing*. **4**, 950-974.

Kantola, T., Vastaranta, M., Yu, X., Lyytikainen-Saarenmaa, P., Holopainen, M., Talvitie, M., Kaasalainen, S., Solberg, S. and Hyyppä, J. (2010) Classification of defoliated trees using tree-level airborne laser scanning data combined with aerial images. *Remote Sensing*. **2** (12), 2665-2679.

Katoh, M. and Gougeon, F. A. (2012) Improving the precision of tree counting by combining tree detection with crown delineation and classification on homogeneity guided smoothed high resolution (50 cm) multispectral airborne digital data. *Remote Sensing*. **4** (5), 1411-1424.

Ke, Y. and Quakenbush, L. J. (2011) A review of methods for automatic individual tree-crown detection and delineation from passive remote sensing. *International Journal of Remote Sensing*. **32** (17), 4725-4747.

Ke, Y., Quakenbush, L. J. and Im, J. (2010) Synergistic use of QuickBird multispectral imagery and LIDAR data for object-based forest species classification. *Remote Sensing of Environment*. **114** (6), 1141-1154.

Kelly, N. M. and Liu, D. (2004) Mapping diseased oak trees using ADAR imagery. *Geocarto International*. **19** (1), 57-64.

Khosravipour, A., Skidmore, A. K., Isenburg, M., Wang, T. and Hussin, Y. A. (2014) Generating pit-free canopy height models from airborne lidar. *Photogrammetric Engineering and Remote Sensing*. **80** (9), 863-872.

Kim, Y., Yang, Z., Cohen, W. B., Pflugmacher, D., Lauver, C. L. and Vankat, J. L. (2009) Distinguishing between live and dead standing tree biomass on the north rim of Grand Canyon National Park, USA using small-footprint lidar data. *Remote Sensing of Environment*. **113** (11), 2499-2510.

King, K. M., Harris, A. R. and Webber, J. F. (2015) *In planta* detection used to define the distribution of the European lineages of *Phytophthora ramorum* on larch (*Larix*) in the UK. *Plant Pathology*. **64**, 1168-1175.

Koch, B. (2010) Status and future of laser scanning, synthetic aperture radar and hyperspectral remote sensing data for forest biomass assessment. *ISPRS Journal of Photogrammetry and Remote Sensing*. **65**, 581-590.

Koch, B., Heyder, U. and Weinacker, H. (2006) Detection of individual tree crowns in airborne lidar data. *Photogrammetric Engineering and Remote Sensing*. **72** (4), 357-363.

Kotsiantis, S. B. (2007) Supervised machine learning: a review of classification techniques. *Informatica*. **31**, 249-268.

Koukoulas, S. and Blackburn, G. A. (2005) Mapping individual tree location, height and species in broadleaved deciduous forest using airborne LIDAR and multi-spectral remotely sensed data. *International Journal of Remote Sensing*. **26** (3), 431-455.

Kox, L. F. F., Brouwershaven, I. V., Vossenberg, B. V. D., Beld, H. V. D., Bonants, P. J. M. and Gruyter, J. D. (2007) Diagnostic values and utility of immunological, morphological, and molecular methods for in planta detection of *Phytophthora ramorum*. *Phytopathology*. **97** (9), 1119-1129.

Knerr, S., Personnaz, L. and Dreyfus, G. (1990) Single-layer learning revisited: a stepwise procedure for building and training a neural network. In. *Neurocomputing*. Berlin: Springer. pp. 41-50.

Kraus, K. and Pfeifer, N. (1998) Determination of terrain models in wooded areas with airborne laser scanner data. *ISPRS Journal of Photogrammetry and Remote Sensing*. **53** (4), 193-203.

Kupfer, J. A. (2012) Landscape ecology and biogeography: rethinking landscape metrics in a post-FRAGSTATS landscape. *Progress in Physical Geography*. **36** (3), 400-420.

Kwak, D. A., Chung, J., Lee, W, K., Kafatos, M., Lee, S. Y., Cho, H. K. and Lee, S. H. (2010) Evaluation for damaged degree of vegetation by forest fire using Lidar and a digital aerial photograph. *Photogrammetric Engineering & Remote Sensing*. **76** (3), 277-287.

Kwak, D. A., Lee, W. K., Lee, J. H., Biging, G. S. and Gong, P. (2007) Detection of individual trees and estimation of tree height using LIDAR data. *Journal of Forest Research*. **12** (6), 425-434.

Lähivaara, T., Seppänen, A., Kaipio, J. P., Vauhkonen, J., Korhonen, L., Tokola, T. and Maltamo, M. (2014) Bayesian approach to tree detection based on airborne laser scanning data. *IEEE Transactions on Geoscience and Remote Sensing*. **52** (5), 2690-2699.

Lane, C. R., Beales, P. A., Hughes, K. J. D., Griffin, R. L., Munro, D., Brasier, C. M. and Webber, J. F. (2003) First outbreak of *Phytophthora ramorum* in England, on *Viburnum tinus*. *Plant Pathology*. **52**, 414.

Landis, J. R. and Koch, G. G. (1977) The measurement of observer agreement for categorical data. *Biometrics*. **33**, 159-174.

Larsen, M., Eriksson, M., Descombes, X., Perrin, G., Brandtberg, T. and Gougeon, F. A. (2011) Comparison of six individual tree crown detection algorithms evaluated under varying forest conditions. *International Journal of Remote Sensing*. **32** (20), 5827-5852.

LAStools (2016) *LAStools* [online]. <https://rapidlasso.com/lastools/> [Accessed on 01/06/16].

Latifi, H., Nothdurft, A. and Koch, B. (2010) Non-parametric prediction and mapping of standing timber volume and biomass in a temperate forest: application of multiple optical/LiDAR-derived predictors. *Forestry*. **83** (4), 395-407.

Lausch, A., Erasmi, S., King, D. J., Magdon, P. and Heurich, M. (2016) Understanding forest health with remote sensing – part I – a review of spectral traits, processes and remote-sensing characteristics. *Remote Sensing*. **8**, 1029.

Lausch, A., Erasmi, S., King, D. J., Magdon, P. and Heurich, M. (2017) Understanding forest health with remote sensing - part II - a review of approaches and data models. *Remote Sensing*. **9** (2), 129.

Lawrence, R. and Labus, M. (2003) Early detection of Douglas-fir beetle infestation with subcanopy resolution hyperspectral imagery. *Western Journal of Applied Forestry*. **18** (3), 202-206.

Leckie, D. G., Cloney, E. and Joyce, S. P. (2005) Automated detection and mapping of crown discolouration caused by jack pine budworm with 2.5m resolution multispectral imagery. *International Journal of Applied Earth Observation and Geoinformation*. **7**, 61-77.

Leckie, D., Gougeon, F., Hill, D., Quinn, R., Armstrong, L. and Shreenan, R. (2003) Combined high-density lidar and multispectral imagery for individual tree crown analysis. *Canadian Journal of Remote Sensing*. **29** (5), 633-649.

Leckie, D. G., Walsworth, N. and Gougeon, F. A. (2016) Identifying tree crown delineation shapes and need for remediation on high resolution imagery using an evidence based approach. *ISPRS Journal of Photogrammetry and Remote Sensing*. **114**, 206-227.

Leckie, D. G. and Yuan, X. (1992) Analysis of high resolution multispectral MEIS imagery for spruce budworm damage assessment on a single tree basis. *Remote Sensing of Environment*. **40** (2), 125-136.

Lee, A. C. and Lucas, R. M. (2007) A lidar-derived canopy density model for tree stem and crown mapping in Australian forests. *Remote Sensing of Environment*. **111**, 493-518.

Lefsky, M. A., Cohen, W. B., Acker, S. A., Parker, G. G., Spies, T. A. and Harding, D. (1999) Lidar remote sensing of the canopy structure and biophysical properties of Douglas-fir western hemlock forests. *Remote Sensing of Environment*. **70** (3), 339-361.

Lefsky, M. A., Cohen, W. B., Parker, G. G. and Harding, D. J. (2002) Lidar remote sensing for ecosystem studies: lidar, an emerging remote sensing technology that directly measures the three-dimensional distribution of plant canopies, can accurately estimate vegetation structural attributes and should be of particular interest to forest, landscape, and global ecologists. *BioScience*. **52** (1), 19-30.

Lehmann, J. R. K., Nieberding, F., Prinz, T. and Knoth, C. (2015) Analysis of unmanned aerial system-based CIR images in forestry - a new perspective to monitor pest infestation levels. *Forests*. **6** (3), 594-612.

Lentile, L. B., Holden, Z. A., Smith, A. M. A., Falkowski, M. J. and Hudak, A. T. (2006) Remote sensing techniques to assess active fire characteristics and post-fire effects. *International Journal of Wildland Fire*. **15**, 319-345.

Lévesque, J. and King, D. J. (2003) Spatial analysis of radiometric fractions from high-resolution multispectral imagery for modelling individual tree crown and forest canopy structure and health. *Remote Sensing of Environment*. **84**, 589-602.

Levick, S. R. and Asner, G. P. (2013) The rate and spatial pattern of treefall in a savanna landscape. *Biological Conservation*. **157**, 121-127.

Levick, S. R., Baldeck, C. A. and Asner, G. P. (2015) Demographic legacies of fire history in an African savanna. *Functional Ecology*. **29** (1), 131-139.

Li, J., Hu, B. and Noland, T. L. (2013) Classification of tree species based on structural features derived from high density LiDAR data. *Agricultural and Forest Meteorology*. **171-172**, 104-114.

Li, W., Guo, Q., Jakubowski, M. K. and Kelly, M. (2012) A new method for segmenting individual trees from the lidar point cloud. *Photogrammetric Engineering & Remote Sensing*. **78** (1), 75-84.

Liebhold, A. M., Macdonald, W. L., Bergdahl, D. and Mastro, V. C. (1995) Invasion by exotic forest pests: a threat to forest ecosystems. *Forest Science Monographs*. **30**, 49.

Lim, K., Treitz, P., Wulder, M., St-Onge, B. and Flood, M. (2003) LiDAR remote sensing of forest structure. *Progress in Physical Geography*. **27** (1), 88-106.

Lindberg, E. and Holmgren, J. (2017) Individual tree crown methods for 3D data from remote sensing. *Current Forestry Reports*. **3** (1), 19-31.

Lisein, J., Pierrot-Deseilligny, M., Bonnet, S. and Lejeune, P. (2013) A photogrammetric workflow for the creation of a forest canopy height model from small unmanned aerial system imagery. *Forests*. **4**, 922-944.

Liu, D., Kelly, M. and Gong, P. (2006) A spatial–temporal approach to monitoring forest disease spread using multi-temporal high spatial resolution imagery. *Remote Sensing of Environment*. **101** (2), 167-180.

Loo, J. A. (2009) Ecological impacts of non-indigenous invasive fungi as forest pathogens. *Biological Invasions*. **11**, 81-96.

Lovell, J. L., Jupp, D. L., Culvenor, D. S. and Coops, N. C. (2003) Using airborne and ground-based ranging lidar to measure canopy structure in Australian forests. *Canadian Journal of Remote Sensing*. **29** (5), 607-622.

Lovett, G. M., Canham, C. D., Arthur, M. A., Weathers, K. C. and Fitzhugh, R. D. (2006) Forest ecosystem responses to exotic pests and pathogens in Eastern North America. *BioScience*. **56** (5), 395-405.

Macdonald, E., Gardiner, B. and Mason, W. (2009) The effects of transformation of even-aged stands to continuous cover forestry on conifer log quality and wood properties in the UK. *Forestry*. **83** (1), 1-16.

MacLeod, A., Pautasso, M., Jeger, M. J. and Haines-Young, R. (2010) Evolution of international regulation of plant pests and challenges for future plant health. *Food Security*. **2**, 49-70.

Mahlein, A. K., Steiner, U., Dehne, H. W. and Oerke, E. C. (2010) Spectral signature of sugar beet leaves for the detection and differentiation of diseases. *Precision Agriculture*. **11**, 413-431.

Maltamo, M., Mustonen, K., Hyyppä, J., Pikänen, J. and Yu, X. (2004) The accuracy of estimating individual tree variables with airborne laser scanning in a boreal nature reserve. *Remote Sensing of Environment*. **90** (3), 319-330.

Martinuzzi, S., Vierling, L. A., Gould, W. A., Falkowski, M. J., Evans, J. S., Hudak, A. T. and Vierling, K. T. (2009) Mapping snags and understory shrubs for a LiDAR-based assessment of wildlife habitat suitability. *Remote Sensing of Environment*. **113** (12), 2533-2546.

Matese, A., Toscano, P., Di Gennaro, S. F., Genesio, L., Vaccari, F. P., Primicerio, J., Belli, C., Zaldei, A., Bianconi, R. and Gioli, B. (2015) Intercomparison of UAV, aircraft and satellite remote sensing platforms for precision viticulture. *Remote Sensing*. **7** (3), 2971-2990.

McGarigal, K. (2015) *FRAGSTATS Help* [pdf]. Available at <https://www.umass.edu/landeco/research/fragstats/documents/fragstats.help.4.2.pdf> [Accessed on 01/12/16].

McGarigal, K., Cushman, S. A. and Ene, E. (2012) *FRAGSTATS v4: Spatial Pattern Analysis Program for Categorical and Continuous Maps*. Computer software program produced by the authors at the University of Massachusetts, Amherst. Available at <http://www.umass.edu/landeco/research/fragstats/fragstats.html> [Accessed on 01/12/16].

McGlone, J. C. (2013) *Manual of Photogrammetry*. Bethesda: American Society for Photogrammetry and Remote Sensing.

McInerney, D. O. and Nieuwenhuis, M. (2009) A comparative analysis of k NN and decision tree methods for the Irish National Forest Inventory. *International Journal of Remote Sensing*. **30** (19), 4937-4955.

Medcalf, K. A., Bodevin, N., Cameron, I., Webber, J. and Turton, N. (2011) *Assessing the potential of using remote sensing in support of current Phytophthora work.* Report to FERA. <http://www.envsys.co.uk/wp-content/uploads/2015/02/Remote_Sensing_Phytophthora.pdf> [Accessed on 08/03/16].

Mei, C. and Durrieu, S. (2004) Tree crown delineation from digital elevation models and high resolution imagery. In M. Thies, B. Koch, H. Spiecker, and H. Weinacker (Eds.), Proceedings of the ISPRS working group VIII/2 Laser scanners for forest and landscape assessment. Frieburg, Germany, Vol. XXXVI Part 8/W2.

Melgani, F. and Bruzzone, L. (2004) Classification of hyperspectral remote sensing images with support vector machines. *IEEE Transactions on Geoscience and Remote Sensing*. **42** (8), 1778-1790.

Michez, A., Piégay, H., Lisein, J., Claessens, H. and Lejeune, P. (2016) Classification of riparian forest species and health condition using multi-temporal and hyperspectral imagery from unmanned aerial system. *Environmental Monitoring and Assessment*. **188** (3), 1-19.

Millers, I., Lachance, D., Burkman, W. G. and Allen, D. C. (1991) *North American sugar maple decline project, organisation and field methods*. Radnor, Pennsylvania: General Technical Report. NE-154. USDA Forest Service.

Mirik, M., Ansley, R. J., Michels, G. J. and Elliott, N. C. (2012) Spectral vegetation indices selected for quantifying Russian wheat aphis (*Diuraphis noxia*) feeding damage in wheat (*Triticum aestivum* L.). *Precision Agriculture*. **13** (4), 501-516.

Mistretta, P. A. (2002) Southern forest resource assessment highlights: managing for forest health. *Journal of Forestry*. **100** (7), 24-27.

Mitchell, R. J., Beaton, J. K., Bellamy, P. E., Broome, A., Chetcuti, J., Eaton, S., Ellis, C. J., Gimona, A., Harmer, R., Hester, A. J., Hewison, R. L., Hodgetts, N. G., Iason, G. R., Kerr, G., Littlewood, N. A., Newey, S., Potts, J. M., Pozsgai, G., Ray, D., Sim, D. A., Stockan, J. A., Taylor, A. F. S. and Woodward, S. (2014) Ash dieback in the UK: a review of the ecological and conservation implications and potential management options. *Biological Conservation*. **175**, 95-109.

Monnet, J. M., Mermin, E., Chanussot, J. and Berger, F. (2010) Tree top detection using local maxima filtering: a parameter sensitivity analysis. In *10th International Conference on LiDAR Applications for Assessing Forest Ecosystems (Silvilaser 2010)*, pp. 9.

Morsdorf, F., Meier, E., Kötz, B., Itten, K. I., Dobbertin, M. and Allgöwer, B. (2004) LIDAR-based geometric reconstruction of boreal type forest stands at single tree level for forest and wildland fire management. *Remote Sensing of Environment*. **92**, 353-363.

Muñoz-Marí, J., Bruzzone, L. and Camps-Valls, G. (2007) A support vector domain description approach to supervised classification of remote sensing images. *IEEE Transactions on Geoscience and Remote Sensing*. **45** (8), 2683-2692.

Murfitt, J., He, Y., Yang, J., Mui, A. and De Mille, K. (2016) Ash decline assessment in emerald ash borer infested natural forests using high spatial resolution images. *Remote Sensing*. **8** (3), 256.

Nagendra, H., Lucas, R., Honrado, J. P., Jongman, R. H., Tarantino, C., Adamo, M. and Mairota, P. (2013) Remote sensing for conservation monitoring: assessing protected areas, habitat extent, habitat condition, species diversity and threats. *Ecological Indicators*. **33**, 45-59.

Nainanayake, A. D., Gunathilake, J., Kumarathunga, M. D. P., Gunawardena, P. M. and Wijesekara, H. T. R. (2016) Limitation in the use of spectral analysis to detect Weligama coconut leaf wilt affected palms in Southern Sri Lanka. *COCOS*. **22** (1), 13-24.

Näsi, R., Honkavaara, E., Lyytikäinen-Saarenmaa, P., Blomqvist, M., Litkey, P., Hakala, T., Viljanen, N., Kantola, T., Tanhuanpää, T. and Holopainen, M. (2015) Using UAV-based photogrammetry and hyperspectral imaging for mapping bark beetle damage at tree-level. *Remote Sensing*. **7**, 15467-15493.

National Assembly for Wales (2016) *Phytophthora ramorum* [pdf]. <http://www.assembly.wales/research> [Accessed on 02/12/16].

Needham, J., Merow, C., Butt, N., Malhi, Y., Marthews, T. R., Morecroft, M. and McMahon, S. M. (2016) Forest community response to invasive pathogens: the case of ash dieback in a British woodland. *Journal of Ecology*. **104**, 315-330.

Nebiker, S., Annen, A., Scherrer, M. and Oesch, D. (2008) A light-weight multispectral sensor for micro UAV – opportunities for very high resolution airborne remote sensing. The *International Archives of the Photogrammetry, Remote Sensing and Spatial Information Sciences*. **XXXVII**, Part B1. Beijing.

Nevalainen, O., Honkavaara, E., Tuominen, S., Viljanen, N., Hakala, T., Yu, X., Hyyppä, J., Saari, H., Pölönen, I., Imai, N. N. and Tommaselli, A. M. G. (2017) Individual tree detection and classification with UAV-based photogrammetric point clouds and hyperspectral imaging. *Remote Sensing*. **9** (3), 185.

Nex, F. and Remondino, F. (2014) UAV for 3D mapping applications: a review. *Applied Geomatics*. **6**, 1-15.

Nielsen, M. M., Heurich, M., Malmberg, B. and Brun, A. (2014) Automatic mapping of standing deadwood after an insect outbreak using the window independent context segmentation method. *Journal of Forestry*. **112** (6), 564-571.

Nijland, W., de Jong, R., de Jong, S. M., Wulder, M. A., Bater, C. W. and Coops, N. C. (2014) Monitoring plant conditions and phenology using infrared sensitive consumer grade digital cameras. *Agricultural and Forest Meteorology*. **184**, 98-106.

Nilsson, H. E. (1995) Remote sensing and image analysis in plant pathology. *Annual Review of Phytopathology*. **15**, 489-527.

Nutter, F., van Rij, N., Eggenberger, S. K. and Holi, N. (2010) Spatial and temporal dynamics of plant pathogens. In: E. C. Oerke, R. Gerhards, G. Menz and R. A. Sikora (eds), *Precision crop protection the challenge and use of heterogeneity*. Dordrecht: Springer: Chapter 3.

Oliveira, S., Oehler, F., San-Miguel-Ayanz, J., Camia, A. and Pereira, J. M. (2012) Modeling spatial patterns of fire occurrence in Mediterranean Europe using Multiple Regression and Random Forest. *Forest Ecology and Management*. **275**, 117-129.

Ollero, A. and Merino, L. (2006) Unmanned aerial vehicles as tools for forest-fire fighting. *Forest Ecology and Management*. **234** (1), S263.

Ørka, H. O., Dalponte, M., Gobakken, T., Naesset, E. and Ene, L. T. (2013) Characterizing forest species composition using multiple remote sensing data sources and inventory approaches. *Scandinavian Journal of Forest Research*. **28** (7), 677-688.

Ørka, H. O., Næsset, E. and Bollandsås, O. M. (2009) Classifying species of individual trees by intensity and structure features derived from airborne laser scanner data. *Remote Sensing of Environment*. **113** (6), 1163-1174.

Ortiz, S. M., Breidenbach, J. and Kändler, G. (2013) Early detection of bark beetle green attack using TerraSAR-X and RapidEye data. *Remote Sensing*. **5** (4), 1912-1931.

Pal, M. and Mather, P. M. (2005) Support vector machines classification in remote sensing. *International Journal of Remote Sensing*. **26** (5), 1007-1011.

Palenichka, R., Doyon, F., Lakhssassi, A. and Zaremba, M. B. (2013) Multi-scale segmentation of forest areas and tree detection in LiDAR images by the attentive vision method. *IEEE Journal of Selected Topics in Applied Earth Observations and Remote Sensing*. **6** (3), 1313-1323.

Pasher, J. and King, D. J. (2009) Mapping dead wood distribution in a temperate hardwood forest using high resolution airborne imagery. *Forest Ecology and Management*. **258**, 1536-1548.

Pasquarella, V. J., Bradley, B. A. and Woodcock, C. E. (2017) Near-real-time monitoring of insect defoliation using Landsat time series. *Forests*. **8** (8), 275.

Pautasso, M., Döring, T. F., Garbelotto, M., Pellis, L. and Jeger, M. J. (2012) Impacts of climate change on plant diseases – opinions and trends. *European Journal of Plant Pathology*. **133**, 295-313.

Pedregosa, F., Varoquaux, G., Gramfort, A., Michel, V., Thirion, B., Grisel, O., Blondel, M., Prettenhofer, P., Weiss, R., Dubourg, V. and Vanderplas, J. (2011) Scikit-learn: machine learning in python. *Journal of Machine Learning Research*. **12**, 2825-2830.

Persson, Å., Holmgren, J., Söderman, U. and Olsson, H. (2004) Tree species classification of individual trees in Sweden by combining high resolution laser data with high resolution near-infrared digital images. *International Archives of Photogrammetry, Remote Sensing and Spatial Information Sciences*. **36** (8), 204-207.

Petropoulos, G. P., Kalaitzidis, C. and Vadrevu, K. P. (2012) Support vector machines and object-based classification for obtaining land-use/cover cartography from Hyperion hyperspectral imagery. *Computers & Geoscience*. **41**, 99-107.

Pitkänen, J., Maltamo, M., Hyyppä, J. and Yu, X. (2004) Adaptive methods for individual tree detection on airborne laser based canopy height model. *International Archives of Photogrammetry, Remote Sensing and Spatial Information Sciences*. **36** (8), 187-191.

Pix4D (2016) *Pix4D* [online]. <https://pix4d.com> [Accessed on 01/07/16]

Pontius, J., Martin, M., Plourde, L. and Hallett, R. (2008) Ash decline assessment in emerald ash borer-infested regions: a test of tree-level, hyperspectral technologies. *Remote Sensing of Environment*. **112** (5), 2665-2676.

Poona, N. K. and Ismail, R. (2013) Discriminating the occurrence of pitch canker fungus in *Pinus radiate* trees using Quickbird imagery and artificial neural networks. *Southern Forests: A Journal of Forest Science*. **75** (1), 29-40.

Popescu, S. C. and Wynne, R. H. (2004) Seeing the trees in the forest: using lidar and multispectral data fusion with local filtering and variable window size for estimating tree height. *Photogrammetric Engineering & Remote Sensing*. **70** (5), 589-604.

Popescu, S. C., Wynne, R. H. and Nelson, R. F. (2003) Measuring individual tree crown diameter with lidar and assessing its influence on estimating forest volume and biomass. *Canadian Journal of Remote Sensing*. **29** (5), 564-577.

Potter, C., Harwood, T., Knight, J. and Tomlinson, I. (2011) Learning from history, predicting the future: the UK Dutch elm disease outbreak in relation to contemporary tree disease threats. *Philosophical Transactions of the Royal Society B*. **366**, 1966-1974.

Potter, C. and Urquhart, J. (2017) Tree disease and pest epidemics in the Anthropocene: a review of the drivers, impacts and policy responses in the UK. *Forest Policy and Economics*. **79**, 61-68.

Pouliot, D. A., King, D. J., Bell, F. W. and Pitt, D. G. (2002) Automated tree crown detection and delineation in high-resolution digital camera imagery of coniferous forest regeneration. *Remote Sensing of Environment*. **82**, 322-324.

Pu, R., Kelly, M., Anderson, G. L. and Gong, P. (2008) Using CASI hyperspectral imagery to detect mortality and vegetation stress associated with a new hardwood forest disease. *Photogrammetric Engineering & Remote Sensing*. **74** (1), 65-75.

Rahlf, J., Breidenbach, J., Solberg, S. and Astrup, R. (2015) Forest parameter prediction using an image-based point cloud: a comparison of semi-ITC with ABA. *Forests*. **6** (11), 4059-4071.

Ranjitha, G., Srinivasan, M. R. and Rajesh, A. (2014) Detection and estimation of damage caused by thrips *Thrips tabaci* (lind) of cotton using hyperspectral radiometer. *Agrotechnology*. **3** (1), 1-5.

Rasmussen, J., Ntakos, G., Nielsen, J., Svensgaard, J., Poulsen, R. N. and Christensen, S. (2016) Are vegetation indices derived from consumer-grade cameras mounted on UAVs sufficiently reliable for assessing experimental plots? *European Journal of Agronomy*. **74**, 75-92.

Reid, A. M., Chapman, W. K., Prescott, C. E. and Nijland, W. (2016) Using excess greenness and green chromatic coordinate colour indices from aerial images to assess

lodgepole pine vigour, mortality and disease. *Forest Ecology and Management*. **374**, 146-153.

Reitberger, J., Schnörr, C., Krzystek, P. and Stilla, U. (2009) 3D segmentation of single trees exploiting full waveform LIDAR data. *ISPRS Journal of Photogrammetry and Remote Sensing*. **64**, 561-574.

Reutebuch, S. E., Andersen, H. E. and McGaughey, R. J. (2005) Light detection and ranging (LIDAR): an emerging tool for multiple resource inventory. *Journal of Forestry*. **103** (6), 286-292.

Reynolds, G. J., Windels, C. E., MacRae, I. V. and Laguette, S. (2012) Remote sensing for assessing Rhizoctonia crown and root tot severity in sugar beet. *Plant Disease*. **96**, 497-505.

Richards, J. A. and Jia, X. (2006) *Remote Sensing Digital Image Analysis: An Introduction*. 4th ed. Berlin: Springer-Verlag.

Richardson, J. J. and Moskal, L. M. (2011) Strengths and limitations of assessing forest density and spatial configuration with aerial LiDAR. *Remote Sensing of Environment*. **115** (10), 2640-2651.

Riutta, T., Slade, E. M., Morecroft, M. D., Bebber, D. P. and Malhi, Y. (2014) Living on the edge: quantifying the structure of a fragmented forest landscape in England. *Landscape Ecology*. **29** (6), 949-961.

Rizzo, D. M., Garbelotto, M., Davidson, J. M., Slaughter, G. W. and Koike, S. T. (2002) *Phytophthora ramorum* as the cause of extensive mortality of *Quercus* spp. and *Lithocarpus densiflorus* in California. *Plant Disease*. **86**, 205-214.

Roberts, S. D., Dean, T. J., Evans, D. L., McCombs, J. W., Harrington, R. L. and Glass, P. A. (2005) Estimating individual tree leaf area in loblolly pine plantations using LiDAR-derived measurements of height and crown dimensions. *Forest Ecology and Management*. **213**, 54-70.

Rouse, J. W. J., Haas, H. R., Schell, A. J. and Deering, W. D. (1974) Monitoring vegetation systems in the Great Plains with ERTS. In *NASA Special Publication*. **1**, 309-317.

Rullan-Silva, C. D., Olthoff, A. E., Delgado de la Mata, J. A. and Pajares-Alonso, J. A. (2013) Remote monitoring of forest insect defoliation: a review. *Forest Systems*. **22** (3), 377-391.

Rumpf, T., Mahlein, A. K., Steiner, U., Oerke, E. C., Dehne, H. W. and Plümer, L. (2010) Early detection and classification of plant disease with support vector machines based on hyperspectral reflectance. *Computers and Electronics in Agriculture*. **74** (1), 91-99.

SAGA GIS (2016) *System for Automated Geoscientific Analyses* [online]. <http://www.saga-gis.org> [Accessed on 30/03/16].

Salami, E., Barrado, C. and Pastor, E. (2014) UAV flight experiments applied to the remote sensing of vegetated areas. *Remote Sensing*. **6**, 11051-11081.

Samaniego, L., Bárdossy, A. and Schulz, K. (2008) Supervised classification of remotely sensed imagery using a modified k-NN technique. *IEEE Transactions on Geoscience and Remote Sensing*. **46** (7), 2112-2125.

Sankaran, S., Ehsani, R., Inch, S. A. and Ploetz, R. C. (2012) Evaluation of visible near infrared reflectance spectra of avocado leaves as a non-destructive sensing tool for detection of laurel wilt. *Plant Disease*. **96**, 1683-1689.

Sapp, M., Lewis, E., Moss, S., Barrett, B., Kirk, S., Elphinstone, J. G. and Denman, S. (2016) Metabarcoding of bacteria associated with the Acute Oak Decline syndrome in England. *Forests*. **7**, 95-115.

Schardt, M., Ziegler, M., Wimmer, A., Wack, R. and Hyyppä, J. (2002) Assessment of forest parameters by means of laser scanning. *International Archives of Photogrammetry Remote Sensing and Spatial Information Sciences*. **34** (3/A), 302-309.

Schomaker, M. E., Zarnoch, S. J., Bechtold, W. A., Latelle, D. J., Burkman, W. G. and Cox, S. M. (2007) *Crown Condition Classification: A Guide to Data Collection and Analysis*. Fort Collins, CO: USDA Forest Service, Southern Research Station.

Schowengerdt, R. A. (2007) *Remote Sensing: Models and Methods for Image Processing*. 3rd ed. San Diego: Academic Press.

Shendryk, I., Broich, M., Tulbure, M. G., McGrath, A., Keith, D. and Alexandrov, S. V. (2016) Mapping individual tree health using full-waveform airborne laser scans and

imaging spectroscopy: a case study for floodplain eucalypt forest. *Remote Sensing of Environment*. **187**, 202-217.

Sheremet, O., Healey, J. R., Quine, C. P. and Hanley, N. (2017) Public preferences and willingness to pay for forest disease control in the UK. *Journal of Agricultural Economics*. **68** (3), 781-800.

Sheridan, R. D., Popescu, S. C., Gatziolis, D., Morgan, C. L. S. and Ku, N. W. (2015) Modeling forest aboveground biomass and volume using airborne LiDAR metrics and forest inventory and analysis data in the Pacific Northwest. *Remote Sensing*. **7** (1), 229-255.

Sims, D. A. and Gamon, J. A. (2002) Relationships between leaf pigment content and spectral reflectance across a wide range of species, leaf structures and developmental stages. *Remote Sensing of Environment*. **81**, 337-354.

Sniezko, R. A. (2006) Resistant breeding against non-native pathogens in forest trees – current successes in North America. *Canadian Journal of Plant Pathology*. **28** (1), S270-S279.

Soille, P. (1999) *Morphological Image Analysis*. Berlin: Springer.

Solberg, S., Naesset, E. and Bollandsas, O. M. (2006) Single tree segmentation using airborne laser scanner data in a structurally heterogeneous spruce forest. *Photogrammetric Engineering & Remote Sensing*. **72** (12), 1369-1378.

Song, C. (2012) Optical remote sensing of forest leaf area index and biomass. *Progress in Physical Geography*. **37** (1), 98-113.

Sripada, R. P., Heiniger, R. W., White, J. G. and Meijer, A. D. (2006) Aerial color infrared photography for determining early in-season nitrogen requirements in corn. *Agronomy Journal*. **98** (4), 968-977.

St-Onge, B., Audet, F. A. and Bégin, J. (2015) Characterizing the height structure and composition of a boreal forest using and individual tree crown approach applied to photogrammetric point clouds. *Forests*. **6** (11), 3899-3922.

Steddom, K., Heidel, G., Jones, D. and Rush, M. (2003) Remote detection of rhizomania in sugar beets. *Phytopathology*. **93** (6), 720-226.

Stereńczak, K., Będkowski, K. and Weinacker, H. (2008) Accuracy of crown segmentation and estimation of selected trees and forest stand parameters in order to resolution of used DSM and nDSM models generated from dense small footprint LIDAR data. *The International Archives of the Photogrammetry, Remote Sensing and Spatial Information Sciences*. **38**, 27-33.

Stone, C. and Coops, N. C. (2004) Assessment and monitoring of damage from insects in Australians eucalypt forests and commercial plantations. *Australian Journal of Entomology*. **43**, 283-292.

Stone, C., Turner, R. and Verbesselt, J. (2008) Integrating plantation health surveillance and wood resource inventory systems using remote sensing. *Australian Forestry*. **71** (3), 245-253.

Strîmbu, V. F. and Strîmbu, B. M. (2015) A graph-based segmentation algorithm for tree crown extraction using airborne LiDAR data. *ISPRS Journal of Photogrammetry and Remote Sensing*. **104**, 30-43.

Sturrock, R. N., Frankel, S. J., Brown, A. V., Hennon, P. E., Kliejunas, J. T., Lewis, K. J., Worrall, J. J. and Woods, A. J. (2011) Climate change and forest diseases. *Plant Pathology*. **60**, 133-146.

Su, J. and Bork, E. (2006) Influence of vegetation, slope, and lidar sampling angle on DEM accuracy. *Photogrammetric Engineering & Remote Sensing*. **72** (11), 1265-1274.

Suárez, J. C., Ontiveros, C., Smith, S. and Snape, S. (2005) Use of airborne LiDAR and aerial photography in the estimation of individual tree heights in forestry. *Computers & Geoscience*. **31** (2), 253-262.

Sutherland, W. J., Bailey, M. J., Bainbridge, I. P., Brereton, T., Dick, J. T. A., Drewitt, J., Dulvy, N. K., Dusic, N. R., Freckleton, R. P., Gatson, K. J., Gilder, P. M., Green, R. E., Heathwaite, A. L., Johnson, S. M., Macdonald, D. W., Mitchell, R., Osborn, D., Owen, R. P., Pretty, J., Prior, S. V., Prosser, H., Pullin, A. S., Rose, P., Stott, A., Tew, T., Thomas, C. D., Thompson, D. B. A., Vickery, J. A., Walker, M., Walmsley, C., Warrington, S., Watkinson, A. R., Williams, R. J., Woodroffe, R. and Woodroof, H. J. (2008) Future novel threats and opportunities facing UK biodiversity identified by horizon scanning. *Journal of* Applied *Ecology*. **45** (3), 821-833.

Tang, L. and Shao, G. (2015) Drone remote sensing for forestry research and practises. *Journal of Forestry Research*. **26**, 791-797.

Tanhuanpää, T., Saarinen, N., Kankare, V., Nurminen, K., Vastaranta, M., Honkavaara, E., Karjalainen, M., Yu, X., Holopainen, M. and Hyyppä, J. (2016) Evaluating the performance of high-altitude aerial image-based digital surface models in detecting individual tree crowns in mature boreal forests. *Forests*. **7**, 143.

Tao, S., Guo, Q., Li, L., Xue, B., Kelly, M., Li, W., Xu, G. and Su, Y. (2014) Airborne lidar-derived volume metrics for aboveground biomass estimation: a comparative assessment of conifer stands. *Agricultural and Forest Meteorology*. **198**, 24-32.

Taylor, J. A., Mowat, A. D., Bollen, A. F. and Whelan, B. M. (2014) Early season detection and mapping of Pseudomonas syringae pv. actinidae infected kiwifruit (Actinidia sp.) orchards. *New Zealand Journal of Crop and Horticultural Science*. **42** (4), 303-311.

Thomas, F. M., Blank, R. and Hartmann, G. (2002) Abiotic and biotic factors and their interactions as causes of oak decline in Central Europe. *Forest Pathology*. **32** (4-5), 277-307.

Thomas, J. R. and Gausman, H. W. (1977) Leaf reflectance vs. leaf chlorophyll and carotenoid concentrations of eight crops. *Agronomy Journal*. **69** (5), 799-802.

Tiede, D., Hochleitner, G. and Blaschke, T. (2005) A full GIS-based workflow for tree identification and tree crown delineation using laser scanning. In: *ISPRS Workshop CMRT*, Vol. 5, No. 2930.08, pp. 2005.

Torresan, C., Berton, A., Carotenuto, F., Di Gennaro, S. F., Gioli, B., Matese, A., Miglietta, F., Vagnoli, C., Zaldei, A. and Wallace, L. (2016) Forestry applications of UAVs in Europe: a review. *International Journal of Remote Sensing*. **38**, 2427-2447.

Tracy, D. R. (2009) *Phytophthora ramorum* and *Phytophthora kernoviae*: the woodland perspective. *EPPO Bulletin*. **39** (2), 161-167.

Tubby, K. V. and Webber, J. F. (2010) Pests and diseases threatening urban trees under a changing climate. *Forestry*. **83** (4), 451-459.

Tucker, C. J. (1979) Red and photographic infrared linear combinations for monitoring vegetation. *Remote Sensing of Environment*. **8**, 127-150.

Turner, W., Spector, S., Gardiner, N., Fladeland, M., Sterling, E. and Steininger, M. (2003) Remote sensing for biodiversity science and conservation. TRENDS in Ecology and Evolution. **18** (6), 306-314.

UK Government Data (2016) *Survey Open Data* [online]. <http://environment.data.gov.uk/ds/survey/index.jsp#/survey> [Accessed on 01/12/16].

Van der Walt, S., Schönberger, J. L., Nunez-Iglesias, J., Boulogne, F., Warner, J. D., Yager, N., Gouillart, E. and Yu, T. (2014) Scikit-image: image processing in Python. *PeerJ*. **2**, e453.

Van Genderen, J. L. and Lock, B. F. (1977) Testing land-use map accuracy. *Photogrammetric Engineering and Remote Sensing*. **43** (9), 1135-1137.

Van Leeuwen, M., Coops, N. C. and Wulder, M. A. (2010) Canopy surface reconstruction from a LiDAR point cloud using Hough transform. *Remote Sensing Letters*. **1** (3), 125-132.

Van Leeuwen, M. and Nieuwenhuis, M. (2010) Retrieval of forest structural parameters using LiDAR remote sensing. *European Journal of Forest Research*. **129** (4), 749-770.

Van Poucke, K., Franceschini, S., Webber, J. F., Vercauteren, A., Turner, J. A., McCracken, A. R., Heungens, K. and Brasier, C. M. (2012) Discovery of a fourth evolutionary lineage of *Phytophthora ramorum*: EU2. *Fungal Biology*. **116**, 1178-1191.

Vapnik, V. N. (1998) *Statistical learning theory* (Vol. 1). New York: Wiley.

Vastaranta, M., Kantola, T., Lyytikäinen-Saarenmaa, P., Holopainen, M., Kankare, V., Wulder, M. A., Hyyppä, J. and Hyyppä, H. (2013a) Area-based mapping of defoliation of Scots pine stands using airborne scanning LiDAR. *Remote Sensing*. **5** (3), 1220-1234.

Vastaranta, M., Wulder, M. A., White, J. C., Pekkarinen, A., Tuominen, S., Ginzler, C., Kankare, V., Holopainen, M., Hyyppä, J. and Hyyppä, H. (2013b) Airborne laser scanning and digital stereo imagery measures of forest structure: comparative results and implications to forest mapping and inventory update. *Canadian Journal of Remote Sensing*. **39** (5), 382-395.

Vastaranta, M., Korpela, I., Uotila, A., Hovi, A. and Holopainen, M. (2012) Mapping of snow-damaged trees based on bitemporal airborne LiDAR data. *European Journal of Forest Research*. **131** (4), 1217-1228.

Vauhkonen, J., Ene, L., Gupta, S., Heinzel, J., Holmgren, J., Pitkänen, J., Solberg, S., Wang, Y., Weinacker, H., Hauglin, K. M. and Lien, V. (2012) Comparative testing of single-tree detection algorithms under different types of forest. *Forestry*. **85** (1), 27-40.

Vèga, C. and Durrieu, S. (2011) Multi-level filtering segmentation to measure individual tree parameters based on Lidar data: application to a mountainous forest with heterogeneous stands. *International Journal of Applied Earth Observation and Geoinformation*. **13** (4), 646-656.

Waage, J. K. and Mumford, J. D. (2008) Agricultural biosecurity. *Philosophical Transactions of the Royal Society B: Biological Sciences*. **363** (1492), 863-876.

Wallace, L. (2013). Assessing the stability of canopy maps produced from UAV-LiDAR data. In *International Geoscience and Remote Sensing Symposium*, 21-26 July 2013, Melbourne, VIC (IEEE), pp. 3879-3882.

Wallace, L., Lucieer, A., Malenovský, Z., Turner, D. and Vopěnka, P. (2016) Assessment of forest structure using two UAV techniques: a comparison of airborne laser scanning and structure from motion (SfM) point clouds. *Forests*. **7** (3), 62.

Wallace, L., Lucieer, A., Watson, C. and Turner, D. (2012) Development of a UAV-LiDAR system with application to forest inventory. *Remote Sensing*. **4**, 1519-1543.

Wallace, L., Lucieer, A. and Watson, C. S. (2014) Evaluating tree detection and segmentation routines on very high resolution UAV LiDAR data. *IEEE Transactions on Geoscience and Remote Sensing*. **52** (12), 7619-7628.

Wang, L., Gong, P. and Biging, G. S. (2004) Individual tree-crown delineation and treetop detection in high-spatial-resolution aerial imagery. *Photogrammetric Engineering & Remote Sensing*. **70** (3), 351-357.

Wang, H., Pu, R., Zhu, Q., Ren, L. and Zhang, Z. (2015) Mapping health levels of *Robinia pseudoacacia* forests in the Yellow River delta, China, using IKONOS and Landsat 8 OLI imagery. *International Journal of Remote Sensing*. **36** (4), 1114-1135.

Wang, Y., Hyyppä, J., Liang, X., Kaartinen, H., Yu, X., Lindberg, E., Holmgren, J., Qin, Y., Mallet, C., Ferraz, A., Torabzadeh, H., Morsdorf, F., Zhu, L., Liu, J. and Alho, P. (2016) International benchmarking of the individual tree detection methods for modeling 3-D canopy structure for silviculture and forest ecology using airborne laser scanning. *IEEE Transactions on Geoscience and Remote Sensing*. **54** (9), 5011-5027.

Waser, L. T., Küchler, M., Jütte, K. and Stampfer, T. (2014) Evaluating the potential of WorldView-2 data to classify tree species and different levels of ash mortality. *Remote Sensing*. **6** (5), 4515-4545.

Webber, J. (2008) Status of *Phytophthora ramorum* and *P. kernoviae* in Europe. In: Frankel, S. J., Kliejuna, J. T., Palmieri, K. M., eds. *Proceedings of the Sudden Oak Death Third Science Symposium*. Albany, California, USA: US Department of Agriculture, Forest Service, Pacific Southwest Research Station: General Technical Report PSW-GTR-214, 19-26.

Webber, J. F., Mullett, M. and Brasier, C. M. (2010) Dieback and mortality of plantation Japanese larch *(Larix kaempferi*) associated with infection by *Phytophthora ramorum*. *New Disease Reports*. **22**, 19.

Webber, J. F., Parkinson, N. M., Rose, J., Stanford, H., Cook, R. T. A. and Elphinstone, J. G. (2008) Isolation and identification of *Pseudomonas syringae pv. aesculi* causing bleeding canker of horse chestnut in the UK. *Plant Pathology*. **57** (2), 368-368.

Weinacker, H., Koch, B., Heyder, U. and Weinacker, R. (2004) Development of filtering, segmentation and modelling modules for lidar and multispectral data as a fundament of an automatic forest inventory system. *International Archives of Photogrammetry, Remote Sensing and Spatial Information Sciences*, 36 (Part 8), W2.

Werres, S., Marwitz, R., Man In't Veld, W. A., De Cock, A. W. A. M., Bonants, P. J. M., De Weerdt, M., Themann, K., Ilieva, E. and Baayen, R. P. (2001) *Phytophthora ramorum* sp. Nov., a new pathogen on *Rhododendron* and *Viburnum*. *Mycological Research*. **105** (10), 1155-1165.

Winder, R. S. and Shamoun, S. F. (2006) Forest pathogens: friend or foe to biodiversity? *Canadian Journal of Plant Pathology*. **28** (1), 221-227.

Wing, B. M., Ritchie, M. W., Boston, K., Cohen, W. B. and Oslen, M. J. (2015) Individual snag detection using neighbourhood attribute filtered airborne lidar data. *Remote Sensing of Environment*. **163**, 165-179.

Wulder, M. (1998) Optical remote-sensing techniques for the assessment of forest inventory and biophysical parameters. *Progress in Physical Geography*. **22** (4), 449-476.

Wulder, M. A., Coops, N. C., Hudak, A. T., Morsdorf, F., Nelson, R., Newnham, G. and Vastaranta, M. (2013) Status and prospects for LiDAR remote sensing of forested ecosystems. *Canadian Journal of Remote Sensing*. **39**, S1-S5.

Wulder, M. A., Dymond, C. C., White, J. C., Leckie, D. G. and Carroll, A. L. (2006) Surveying mountain pine beetle damage of forests: a review of remote sensing opportunities. *Forest Ecology and Management*. **221**, 27-41.

Wulder, M. A. and Franklin, S. E. (2003) Remote sensing of forest environments, introduction. The transition from theory to information. In: M. A. Wulder and S. E. Franklin (eds), *Remote Sensing of Forest Environments Concepts and Case Studies*. New York: Springer, Chapter 1.

Wulder, M. A., White, J. C., Coggins, S., Ortlepp, S. M., Coops, N. C., Heath, J. and Mora, B. (2012) Digital high spatial resolution aerial imagery to support forest health monitoring: the mountain pine beetle context. *Journal of Applied Remote Sensing*. **6** (1), 062527-1.

Wulder, M. A., White, J. C., Niemann, K. O. and Nelson, T. (2004) Comparison of airborne and satellite high spatial resolution data for the identification of individual trees with local maxima filtering. *International Journal of Remote Sensing*. **25** (11), 2225-2232.

Xie, Y., Sha, Z. and Yu, M. (2008) Remote sensing imagery in vegetation mapping: a review. *Journal of Plant Ecology*. **1** (1), 9-23.

Xu, X., Harwood, T. D., Pautasso, M. and Jeger, M. J. (2009) Spatio-temporal analysis of an invasive plant pathogen (*Phytophthora ramorum*) in England and Wales. *Ecograph*y. **32**, 504-516.

Yoga, S., Bégin, J., St-Onge, B. and Gatziolis, D. (2017) Lidar and multispectral imagery classifications of balsam fir tree status for accurate predictions of merchantable volume. *Forests*. **8**, 253.

Yu, Q., Gong, P., Clinton, N., Biging, G., Kelly, M. and Schirokauer, D. (2006) Object-based detailed vegetation classification with airborne high spatial resolution remote sensing imagery. *Photogrammetric Engineering & Remote Sensing*. **72** (7), 799-811.

Yuan, L., Huang, Y., Loraamm, R. W., Nie, C., Wang, J. and Zhang, J. (2014) Spectral analysis of winter wheat leaves for detection and differentiation of diseases and insects. *Field Crop Research*. **156**, 199-207.

Zarco-Tejada, P. J., Berjón, A., López-Lozano, R., Miller, J. R., Martín, P., Cachorro, V., González, M. R. and De Frutos, A. (2005) Assessing vineyard condition with hyperspectral indices: leaf and canopy reflectance simulation in a row-structured discontinuous canopy. *Remote Sensing of Environment*. **99** (3), 271-287.

Zarnoch, S. J., Bechtold, W. A. and Stoke, K. W. (2004) Using crown condition variables as indicators of forest health. *Canadian Journal of Forest Research*. **34** (5), 1057-1070.

Zawawi, A. A., Shiba, M. and Jemali, N. J. N. (2015) Accuracy of LiDAR-based tree height estimation and crown recognition in a subtropical evergreen broad-leaved forest in Okinawa, Japan. *Forest Systems*. **24** (1), 002.

Zellweger, F., Baltensweiler, A., Ginzler, C., Roth, T., Braunisch, V., Bugmann, H. and Bollmann, K. (2016) Environmental predictors of species richness in forest landscapes: abiotic factors versus vegetation structure. *Journal of Biogeography*. **43** (6), 1080-1090.

Zhang, J., Hu, J., Lian, J., Fan, Z., Ouyang, X. and Ye, W. (2016) Seeing the forest from drones: testing the potential of lightweight drones as a tool for long-term forest monitoring. *Biological Conservation*. **198**, 60-69.

Zhao, D., Pang, Y., Li, Z. and Sung, G. (2013) Filling invalid values in a lidar-derived canopy height model with morphological crown control. *International Journal of Remote Sensing*. **34** (13), 4636-4654.

Zhen, Z., Quackenbush, L. J. and Zhang, L. (2014) Impact of tree-orientated growth order in marker-controlled region growing for individual tree crown delineation using airborne laser scanner (ALS) data. *Remote Sensing*. **6**, 555-579.

Zhen, Z., Quackenbush, L. J. and Zhang, L. (2016) Trends in automatic individual tree crown detection and delineation - evolution of LiDAR data. *Remote Sensing*. **8** (4), 333.

Zimble, D. A., Evans, D. L., Carlson, G. C., Parker, R. C., Grado, S. C. and Gerard, P. D. (2003) Characterizing vertical forest structure using small-footprint airborne LiDAR. *Remote Sensing of Environment*. **87**, 171-182.

Zwally, H. J., Schutz, B., Abdalati, W., Abshire, J., Bentley, C., Brenner, A., Bufton, J., Dezio, J., Hancock, D., Harding, D., Herring, T., Minster, B., Quinn, K., Palm, S., Spinhirne, J. and Thomas, R. (2002) ICESat's laser measurements of polar ice, atmosphere, ocean, and land. *Journal of Geodynamics*. **34** (3-4), 405-445.